論文 / 著書情報
Article / Book Information

題目(和文)	サンドイッチ型希土類ポリ酸分子・結晶へのキラリティ付与およびその構造・分光化学的研究
Title(English)	Studies on sanduichi-type lanthanide-containing polyoxotungstates : structure, spectroscopy, and molecular chirality
著者(和文)	飯島淳
Author(English)	Jun Iijima
出典(和文)	学位:博士(理学), 学位授与機関:東京工業大学, 報告番号:甲第8500号, 授与年月日:2011年9月25日, 学位の種別:課程博士, 審査員:成毛 治朗
Citation(English)	Degree:Doctor (Science), Conferring organization: Tokyo Institute of Technology, Report number:甲第8500号, Conferred date:2011/9/25, Degree Type:Course doctor, Examiner:
学位種別(和文)	博士論文
Type(English)	Doctoral Thesis

Studies on Sandwich-type Lanthanide-containing Polyoxotungstates — Structure, Spectroscopy, and Molecular Chirality

Jun Iijima

A dissertation for the degree of Doctor of Science

Tokyo Institute of Technology

July, 2011

Contents

Chapter 1 General Introduction

1-1 Structures and properties of lacunary polyoxometalate

Polyoxometalates (POMs) are metal oxide clusters in which metal atoms such as Mo, V, Nb, Ta, and W, and oxygen atoms are regularly arranged in discrete molecules. From structural point of view, POMs generally consist of metal-centered tetrahedra or octahedra as basic units, where oxygen atoms are located in their vertex positions. These polyhedral units are mutually connected by sharing their edges and vertexes. A variety of metal elements and connection modes of the polyhedra results in formations of various kinds of POMs that exhibit a broad spectrum in physicochemical properties. In general, POMs and their crystals are known to have characteristic chemical properties; high solubility to various kinds of polar solvents, inclusion of many crystal waters, easy substitution of a part of metals to different ones, controllable molecular size and structure [1-4]. POMs can be categorized into isopolyoxometalates and heteropolyoxometalates; the former is composed of the only one kind of metals, and the latter is composed of more than two kinds of elements including the parent metal. Since POMs are usually anionic, they are also referred to as ‘polyanions’, ‘isopolyanions’, and ‘heteropolyanions’. So-called Keggin [5], Wells-Dawson [6], Lindqvist [7], and Anderson [8] type POMs are the typical species in POM chemistry (**Fig. 1-1**). Removals of one or more WO_6 octahedral units (stoichiometrically, {WO} units) from these POMs yield a series of vacant species so-called “lacunary” POMs. The structural isomers and properties of the parent Keggin, Wells-Dawson, and Lindqvist type POMs and their lacunary derivatives will be discussed below.

1-1-1 Isomerism of Keggin structure and lacunary species

The most fundamental structure in Keggin type polyanion $[XM_{12}O_{40}]^{n-}$ is the α-type structure. As shown in **Fig. 1-2 (above)**, this structure is the polyhedral assembly composed of one XO_4 and four M_3O_{13} triads, whose triads are got together from the apical direction of tetrahedron. Successive rotations of one, two, three, and all of the four M_3O_{13} triads by 60º from the plenary α-Keggin structure yield four β, γ, δ, and ε isomers as shown in **Fig. 1-2 (below)**. Based on these plenary isomers, mono, di and tri-lacunary structures are derived by removals of one, two, and three MO_6 octahedra, respectively. In the case of mono-lacunary β-Keggin structure, β_1, β_2, and β_3 are generated by removing WO_6 octahedron from bottom, belt, and top site (**Fig. 1-3**). In reality, mono-lacunary $[\alpha\text{-}PW_{11}O_{39}]^{7-}$, $[\beta_1\text{-}SiW_{11}O_{39}]^{8-}$, $[\beta_2\text{-}SiW_{11}O_{39}]^{8-}$, and $[\beta_3\text{-}SiW_{11}O_{39}]^{8-}$ have been synthesized and utilized for building blocks in larger polyanions [9-11]. For the di-lacunary species, $[\alpha\text{-}PW_{10}O_{36}]^{7-}$, $[\gamma\text{-}SiW_{10}O_{37}]^{8-}$, and isostructural $[\gamma\text{-}GeW_{10}O_{37}]^{8-}$ have been prepared (**Fig. 1-4**), and used for precursors of metal-substituted tungstophosphates, $[\gamma\text{-}PV_2W_{10}O_{40}]^{5-}$ and $[\gamma\text{-}SiW_{10}Fe_2O_{38}]^{6-}$ – these are catalyses for CH_4 oxidation reaction – and a giant cluster $[Ce_{20}Ge_{10}W_{100}O_{376}(OH)_4(H_2O)_{30}]^{56-}$, respectively [9, 12-16]. Polyanions of $[PW_9O_{34}]^{9-}$, $[SiW_9O_{34}]^{10-}$, $[GeW_9O_{34}]^{10-}$, $[AsW_9O_{33}]^{n-}$, $[SbW_9O_{33}]^{n-}$, and $[BiW_9O_{33}]^{n-}$ are popular in the tri-lacunary species, which exhibit two types of structural isomers defined by positions of the vacancies. A removal of three corner-shared MO_6 octahedra from parent α-Keggin gives 'A-type', while a removal of three edge-shared octahedra gives 'B-type' tri-lacunary species (**Fig. 1-5**). Each of these two types has α and β derivatives in the same manner as the parent Keggin isomers. A compound $Na_{8.5}H_{1.5}[A\text{-}GeW_9O_{34}]\cdot 20H_2O$, which contains both A-α and A-β isomers with disordering, is active in SHG (Second

Harmonic Generation) due to a presence of noncentrosymmetric center [9, 17-22]. It is known that lone pairs of the hetero X atoms in the $[XW_9O_{33}]^{9-}$ (X = As^{III}, Sb^{III}, Bi^{III}) units largely affect the structures and physicochemical properties of their derivatives. For example, $[M_6(H_2O)_2(AsW_9O_{34})_2(AsW_6O_{26})]^{17-}$ (M^{2+} = Mn^{2+}, Co^{2+}, Zn^{2+}), $[(VO)_3(Sb/BiW_9O_{33})_2]^{11-/12-}$, and $[(MCl)_6(As/SbW_9O_{33})_2]^{12-}$ (M^{2+} = Cu^{2+}, Mn^{2+}) have been reported to display interesting magnetic behavior like a single molecular magnet [23-25]. In their structure, since the lone pairs in hetero X atoms prevail in the vacant site of $[XW_9O_{33}]^{9-}$, the linear sandwich-type structures like vanadium tri-nuclear cluster of $[(VO)_3(Sb/BiW_9O_{33})_2]^{11-/12-}$ are favored to their steric repulsion.

1-1-2 Isomerism of Wells-Dawson structure and lacunary species

The structure of Wells-Dawson type polyanion $[X_2M_{18}O_{62}]^{n-}$ is considered as a dimer of tri-lacunary Keggin-type $[A\text{-}\alpha\text{-}XM_9O_{34}]^{n-}$ polyanion sharing ring-shaped six O atoms (**Fig. 1-6**). Formally, the β isomer is possible by 60°-rotation of edge-shared apical M_3O_{13} group in the plenary Wells-Dawson structure. However, only the α isomer has been structurally characterized (**Fig. 1-6**). Mono-lacunary $[\alpha_1\text{-}X_2W_{17}O_{61}]^{n-}$ and $[\alpha_2\text{-}X_2W_{17}O_{61}]^{n-}$ polyanions have vacant sites at the 'apical' and 'belt' positions, respectively (**Figs. 1-6** and **1-7**). A tri-lacunary $[\alpha\text{-}X_2M_{15}O_{56}]^{n-}$ polyanion lacks a M_3O_{13} triad on the apical position (**Fig. 1-7**). These mono and tri-vacant polyanions are known as useful building blocks for preparing larger clusters [26-28]. However, di-lacunary species have never been reported to date.

1-1-3 Lindqvist structure and lacunary species

The Lindqvist structure has a high (O_h) symmetry and is composed of edge-shared

six MO_6 octahedra, forming a larger octahedron. The plenary species, $[W_6O_{19}]^{2-}$, $[Mo_6O_{19}]^{2-}$, $[Nb_6O_{19}]^{8-}$, and $[Ta_6O_{19}]^{8-}$ have been isolated by Lemeur, Walton, Stucky, and Aronsson, respectively [29-32], while no lacunary species have been isolated to date. However, a few number of the compounds containing plenary, mono-lacunary, and mono-substituted units, such as $[Ln_6O_2(OH)_6Al_2(Nb_6O_{19})_5]^{26-}$, $[Ln(W_5O_{18})_2]^{n-}$, and $[Mo_5O_{13}(OMe)_4(NO)\{Na(MeOH)\}]^{2-}$ have been reported, respectively [33, 34, 35].

1-2 Polyoxometalate containing lanthanide metal ions (Polyoxometallolanthanoate)

The elements with atomic numbers from 57 to 71 in the periodic table are called lanthanide (Ln). Generally, it is known that a trivalent Ln^{3+} is easily formed. The electronic configuration of Ln^{3+} is represented to be $[Xe]4f^n$ (n = 0-14). Their valence electron configuration is the same throughout Ln, and the electrons are filled in only the 4f orbital, meaning that a series of Ln exhibits a similar chemical behavior. The space distribution for the 4f, 5s, 5p, 6s orbitals are presented in **Fig. 1-8**. It shows that the $4f^n$ electrons are shielded by both $5s^2$ and $5p^6$ electrons. Thus, the 4f-4f electronic transition is hardly influenced by the coordination and ligand field, giving UV-Vis absorption and luminescent bands with narrow width.

Recently, POMs containing lanthanide (Ln) ions, referred to as “polyoxometallolanthanoates” (Ln-POMs), have been intensively studied by many inorganic chemists. The Ln-POMs can be considered as clusters composed of lacunary and/or non-lacunary POM units as building blocks which are connected together by Ln ions as linkers. There were only a few examples of Ln-POMs until the work by Peacock and Weakley published in 1971 [35]. They first established a systematic preparation

method to construct Ln-POMs by complexation between Ln and lacunary POMs. The details will be described in the next Section 1-3. A decatungstatolanthanoate $[Ln(W_5O_{18})_2]^{n-}$ (**Fig. 1-9 (e)**) has the simplest structure in Ln-POMs, where Ln ion is sandwiched by two tetradentate mono-lacunary Lindqvist $[W_5O_{18}]^{6-}$ units, and compounds with Ln = Ce, Pr, Nd, Sm, Gd, Eu, Tb, Dy, Er, have been isolated and structurally characterized [36-40]. Peacock and Weakley also reported $[Ln(XM_{11}O_{39})_2]^{n-}$ and $[Ln(X_2M_{17}O_{61})_2]^{n-}$ polyanions, in which Ln are sandwiched by two mono-lacunary Keggin and Wells-Dawson units, respectively. These three polyanions, $[Ln(W_5O_{18})_2]^{n-}$, $[Ln(XM_{11}O_{39})_2]^{n-}$ and $[Ln(X_2M_{17}O_{61})_2]^{n-}$, are categorized in "Peacock-Weakley type". In Ln-POMs, Ln ions play a key role in connecting POM units because of their high oxophilicity and coordination flexibility, and these allow to form a various kinds of structures. For example, large polyanion clusters, $[Ce_{20}Ge_{10}W_{100}O_{376}(OH)_4(H_2O)_{30}]^{56-}$ and $[Ce_{16}(H_2O)_{36}(WO_2)_4(W_2O_6)_8(W_5O_{18})_4(\alpha\text{-}AsW_9O_{33})_{12}]^{76-}$ (**Fig. 1-9 (g)**), bear $[GeW_{10}O_{37}]^{8-}$ and $[AsW_9O_{33}]^{n-}$ as building blocks which are interlinked by Ce^{3+} cations [16, 41]. Other examples, $[K\subset\{Eu(H_2O)_2(\alpha\text{-}AsW_9O_{33})\}_6]^{35-}$ and $[Cs\subset\{Eu(H_2O)_2(\alpha\text{-}AsW_9O_{33})\}_4]^{23-}$ reported by Yamase, indicate cation-dependent structures whose Ln ions link six and four $[AsW_9O_{33}]^{9-}$ units respectively, to yield windmill-shaped clusters (**Figs. 1-9 (a), (b)**) [42]. Thus, Ln-POMs have high potentials to evolve to giant structured supramolecules and novel functional materials with useful magnetic and luminescent properties derived from characteristic $4f^n$ configuration of the Ln ions. In our Naruke (also the former Professor Yamase) laboratory, syntheses, structures, and magnetic and luminescence properties of novel Ln-POMs have been studied (**Figs. 1-9 (a)-(c)**, and **(f)**).

1-3 Ln-POMs bearing one and two mono-lacunary Keggin/Wells-Dawson units

As briefly stated in Section 1-2, Ln ion frequently adopts an eight-fold coordination mode in Ln-POMs. There are two kinds of Ln-POMs composed of single Ln centers and mono-lacunary POM units. The first is a 1:1 complex between an Ln ion and one mono-lacunary Keggin, Wells-Dawson, or Lindqvist unit, so-called as "mono-substituted type". The second is a 1:2 complex between Ln and two mono-lacunary units, so-called as "sandwich-type". The Peacock-Weakley type Ln-POMs belong to the latter category.

1-3-1 The mono-substituted type Ln-POM bearing *one* Ln and *one* mono-lacunary Keggin/Wells-Dawson unit.

All of the mono-substituted Ln-POMs are tungstates, and corresponding molybdate frameworks have never been reported to date. A number of studies about the lanthanide mono-substituted Keggin-type $[\alpha\text{-Ln}(H_2O)_4(PW_{11}O_{39})]^{4-}$ (Ln = Nd, Eu, Gd) [43, 44], $[\alpha\text{-Ln}(H_2O)_4(SiW_{11}O_{39})]^{5-}$ (Ln = La, Ce, Yb) [45, 46], and $[\alpha\text{-Ln}(H_2O)_4(GeW_{11}O_{39})]^{5-}$ (Ln = Nd, Sm, Eu, Tb, Dy, Yb) [47-49] has been developed from the viewpoint of magnetism and luminescence (**Fig. 1-10(a)**), of which some complexes have polymeric structures. In contrast, a fewer number of the mono-substituted Wells-Dawson type $[Ln(H_2O)_4(P_2W_{17}O_{61})]^{7-}$ (Ln = Ce, Nd, Eu, Tb, Lu) (**Figs. 1-10(b), (c)**) has been reported by Pope, Kortz, Krebs, and Francesconi groups [50-54]. The rarity of the latter type comes from a difficulty in the synthesis of the free mono-lacunary Wells-Dawson $[P_2W_{17}O_{61}]^{10-}$ unit. Some polyanions of this type show interesting Lewis-acid catalytic activity [55] and redox behavior [56].

1-3-2 The sandwich-type Ln-POM bearing *one* Ln and *two* mono-lacunary Keggin/Wells-Dawson units.

1-3-2-1 The sandwich-type Ln-POM containing the mono-lacunary Keggin structure

For the sandwich-type Ln-POMs coordinated by two mon-lacunary Keggin units, only $[Ln(\alpha\text{-}XM_{11}O_{39})_2]^{n-}$ and $[Ln(\beta_2\text{-}XM_{11}O_{39})_2]^{n-}$ have been reported to date (**Fig. 1-11**) [35, 57]. More specifically, several conformations are possible for the former $[Ln(\alpha\text{-}XM_{11}O_{39})_2]^{n-}$ polyanion depending on relative rotation of the $[\alpha\text{-}XM_{11}O_{39}]^{n-}$ units. The rotation results in three molecular configurations with chiral C_2 and achiral C_{2v} and C_{2h} symmetries (details will be described in Chapter 3). Until now, $[Ln(\alpha\text{-}PW_{11}O_{39})_2]^{11-}$ (Ln = Pr, Eu, Gd), $[Ln(\alpha\text{-}PMo_{11}O_{39})_2]^{11-}$ (Ln = all lanthanides), $[Ln(\alpha\text{-}SiW_{11}O_{39})_2]^{13-}$ (Ln = Ce, Pr), $[Ln(\alpha\text{-}SiMo_{11}O_{39})_2]^{13-}$ (Ln = Pr, Dy), $[Ln(\alpha\text{-}GeW_{11}O_{39})_2]^{13-}$ (Ln = Pr), and $[Ln(\alpha\text{-}GeMo_{11}O_{39})_2]^{13-}$ (Ln = Nd) have been isolated as crystalline salts and structurally characterized [44, 58-66], in which all of the polyanions have the identical structure with C_2 symmetry (**Fig. 1-11(b)**). On the other hand, structural studies of a series of $[Ln(\alpha\text{-}PW_{11}O_{39})_2]^{11-}$ using ^{183}W-NMR spectroscopy [67] revealed that the symmetry is variable in aqueous solutions, exhibiting C_{2v} or C_{2h} symmetry for early La-Eu, and C_2 for late Tb-Lu in the Ln series. The polyanion $[Ln(\beta_2\text{-}SiW_{11}O_{39})_2]^{13-}$ was prepared recently by Kortz et al. for the first time (**Fig. 1-11(a)**) [57]. This polyanion has more structural complexity due to a presence of chirality in the $[\beta_2\text{-}SiW_{11}O_{39}]^{8-}$ moiety and combination of the two chiral units. Theoretical approach has been carried out for $[M(\alpha\text{-}PMo_{11}O_{39})_2]^{10-}$ (M = Ce^{IV}, Th^{IV}) to evaluate M—O coordination, and concluded that Ce—O bond strength is greater than Th—O strength [68].

1-3-2-2 The sandwich-type Ln-POM containing the mono-lacunary Wells-Dawson structure

For the sandwich-type Ln-POM coordinated by two mono-lacunary Wells-Dawson units, three types, $[Ln(\alpha_1\text{-}X_2M_{17}O_{61})_2]^{n-}$ (α_1-α_1 type), $[Ln(\alpha_2\text{-}X_2M_{17}O_{61})_2]^{n-}$ (α_2-α_2 type), and $[Ln(\alpha_1\text{-}X_2M_{17}O_{61})(\alpha_2\text{-}X_2M_{17}O_{61})]^{n-}$ (α_1-α_2 type), have been isolated and structurally characterized (**Fig. 1-12**). The α_2-α_2 type has two equivalent $[\alpha_2\text{-}X_2M_{17}O_{61}]^{n-}$ units coordinating to the Ln center. In the same manner as for $[Ln(\alpha\text{-}XM_{11}O_{39})_2]^{n-}$, several coordination modes depending on a rotation of the $[\alpha_2\text{-}X_2M_{17}O_{61}]^{n-}$ units are possible for the α_2-α_2 type, affording chiral C_2 and achiral C_{2v} and C_{2h} symmetry. Still, only C_2-symmetric polyanions have been reported until now [59, 69, 70]. For the α_1-α_1 type isomer, La-analogue has been isolated and structurally characterized [69]. In the case of the α_1-α_2 type, an uranium(IV)-centered analogue has been prepared by Pope in 2003 [71]. This $[U(\alpha_1\text{-}P_2W_{17}O_{61})(\alpha_2\text{-}P_2W_{17}O_{61})]^{16-}$ polyanion is an unique example that bears different isomers of the mono-lacunary Wells-Dawson units. Since the mono-lacunary Wells-Dawson $[P_2W_{17}O_{61}]^{10-}$ has larger size and higher anionic valence than corresponding Keggin or Lindqvist ones, steric repulsion between lacunary units would be larger when forming a sandwich-type Ln-POM. Thus, structural chemistry of the mono-lacunary Wells-Dawson sandwich-type Ln-POM $[Ln(X_2M_{17}O_{61})_2]^{n-}$ is an interesting target of study, because it would show somewhat different behavior from $[Ln(\alpha\text{-}XM_{11}O_{39})_2]^{n-}$.

1-3-2-3 Conformation, isomers, and chirality of mono-lacunary Keggin/Wells-Dawson sandwich-type polyanions

Here, the relation between coordination mode of the Ln center and overall

symmetry of $[Ln(\alpha\text{-}XM_{11}O_{39})_2]^{n-}$ is described in detail. **Fig. 1-11(b) (left)** shows the structure of $[Ln(\alpha\text{-}XM_{11}O_{39})_2]^{n-}$ which has been observed in crystals. Each mono-lacunary $[\alpha\text{-}XM_{11}O_{39}]^{n-}$ unit has a point symmetry of C_s; a mirror plane which halves this unit exists as represented in **Fig. 1-11(b) (middle)**. An expected dihedral angle (ϕ) between the two mirror planes in $[Ln(\alpha\text{-}XM_{11}O_{39})_2]^{n-}$ is 45º when the central Ln has an ideal square-antiprismatic coordination. The ϕ value is considered as the "twist angle" between the two $[\alpha\text{-}XM_{11}O_{39}]^{n-}$ units. The chiral C_2 symmetry of the $[Ln(\alpha\text{-}XM_{11}O_{39})_2]^{n-}$ polyanion occurs when $0º<\phi<180º$. Two enantiomers of the chiral $[Ln(\alpha\text{-}XM_{11}O_{39})_2]^{n-}$ polyanion are displayed in **Fig. 1-13(a)**, where the left polyanion (L-form) is identical to the mirror image of the right polyanion (D-form), and *vice versa*. In the cases of $\phi = 0º$ and 180º, the two mirrors are aligned in-plane, resulting in cubic coordination of the Ln center and non-chiral C_{2v} and C_{2h} symmetries for the $[Ln(\alpha\text{-}XM_{11}O_{39})_2]^{n-}$ polyanions, respectively (structures not shown). The cubic octa-coordination of Ln is quite rare and is achieved for the first time in Chapter 3. Thus, ϕ is the important parameter that defines the ligand-field of Ln and overall molecular symmetry and chirality.

In the same manner, the "twist angle" ϕ is defined in the mono-lacunary Wells-Dawson sandwich-type $[Ln(\alpha_2\text{-}X_2M_{17}O_{61})_2]^{n-}$ polyanion because of C_s symmetry for the $[\alpha_2\text{-}X_2M_{17}O_{61}]^{n-}$ unit, and afford rotational-isomers with chiral C_2 and non-chiral C_{2v} and C_{2h} symmetries. Two enantiomers of the chiral C_2 symmetric $[Ln(\alpha_2\text{-}X_2M_{17}O_{61})_2]^{n-}$ polyanion are displayed in **Fig. 1-13(b)**.

1-4 Chemical and physical properties of Ln-POMs

As shown in the previous sections, the sandwich-type Ln-POMs containing Ln ions

coordinated by two mono-lacunary Keggin and Wells-Dawson units have interesting structures from the viewpoint of coordination chemistry. As well as $[Ln(W_5O_{18})_2]^{n-}$, these polyanions have relatively simple structures in the diverse structures of Ln-POMs. These polyanions have gathered continuous interests due to their photophysical and magnetic properties arising from $4f^n$ electrons in Ln^{3+}. For example, a $[Eu(XW_{11}O_{39})_2]^{n-}$ (X = B, Si, P) polyanion exhibits intense photoluminescence at low temperature (< 77 K) by excitation into O→W ligand-to-metal charge-transfer (LMCT) band (< 300 nm) of the $[XW_{11}O_{39}]^{n-}$ unit as a result of intramolecular energy transfer into the Eu^{3+} emitting center [72-75]. At room temperature, the luminescence is almost quenched by non-radiative deactivation of the $[XW_{11}O_{39}]^{n-}$ unit. Thus, the mono-lacunary unit acts as a temperature-switched photosensitizer of the Ln^{3+}. Also, $[Pr(\alpha\text{-}GeW_{11}O_{39})_2]^{13-}$ and $[Er(W_5O_{18})_2]^{9-}$ express magnetic behavior like a single molecule magnet [40, 65]. These luminescence and magnetic properties of these Ln-POMs, which are expected to be applied to molecular devices in the next generation, are largely governed by composition and structure of POM units and ligand-field of $Ln^{3+/4+}$, i.e. the twist angle ϕ. Furthermore, the ligand-field of $Ln^{3+/4+}$ directs also the chirality, which would open a new window in their functional property. It has been expected and partially evidenced that chiral POMs (including Ln-POMs) in enantiopure forms have activities in asymmetric synthesis, chiral sensing, and biological and photophysical effects. Recently, spontaneous resolution of $[M(\alpha\text{-}PW_{11}O_{39})_2]^{10-}$ (M = Zr^{IV} and Hf^{IV}), which is isostructural with $[Ln(\alpha\text{-}XM_{11}O_{39})_2]^{n-}$, was achieved without using chiral agents, and circular dichiroism (CD) spectra of the LMCT band of their enantiomers were separately measured [76, 77]. If chiral resolution of Ln-POMs becomes successful, CD activity for 4f-4f absorptions of Ln^{3+} is expected. Additionally, for a photoluminescent

Ln^{3+} ions, circularly polarized luminescence (CPL) would occur. The chiral Ln-POMs with such optical and luminescence properties have potential application to optical memory, display material, and chiral sensing in biological field. However, unfortunately, most of the chiral Ln-POMs are racemized and isolated as crystals consisting of both enantiomers, and few enantiopure forms have been obtained so far.

1-5 Research motivation and objectives

As described in above sections, mono-lacunary Keggin and Wells-Dawson sandwich-type Ln-POMs, $[Ln(\alpha\text{-}XM_{11}O_{39})_2]^{n-}$ and $[Ln(\alpha_2\text{-}X_2M_{17}O_{61})_2]^{n-}$ respectively, possess attractive structural chemistry and physicochemical properties. Their structural studies in aqueous solutions and in the solid states have been developed by means of ^{31}P- and ^{183}W-NMR spectroscopy and single crystal X-ray diffraction. However, in fundamental and application research on Ln-POMs, several uncertainties and problems to be overcome still remain. In solid crystals, all the coordination environment of Ln ion in mono-lacunary sandwich-type Ln-POMs is square-antiprism regardless of the kind of POM units. In aqueous solutions, however, cubic coordination of Ln has been presumed for large-sized Ln^{3+} ions, and square-antiprismatic coordination for smaller-sized Ln^{3+} ions in both $[Ln(\alpha\text{-}XM_{11}O_{39})_2]^{n-}$ (X = Si, P) and $[Ln(\alpha_2\text{-}P_2W_{17}O_{61})_2]^{n-}$ from ^{183}W-NMR spectroscopy [67, 78]. The preference of cubic form for larger Ln^{3+} species has been explained as a smaller “barrier” to the rotation of POM units [79]. However, this assumption would be effective only in aqueous solutions. Thus, details on what regulates the coordination geometry of Ln and conformation of polyanion (i.e. the twist angle ϕ) in crystalline solids are still unclear. As for the chirality of $[Ln(\alpha\text{-}XM_{11}O_{39})_2]^{n-}$ and $[Ln(\alpha_2\text{-}P_2W_{17}O_{61})_2]^{n-}$, ϕ is again a definitive parameter, because the two

enantiomers can be described as $\phi \sim 45^{o}$ and $\sim -45^{o}$. Thus, elucidation of what controls the parameter ϕ is crucial in fundamental and applied studies of these polyanions.

I have fixed the goals of this study to stereochemical control and induction of chirality in the sandwich-type Ln-POMs of $[Ln(\alpha\text{-}PW_{11}O_{39})_2]^{n-}$ and $[Ln(\alpha_2\text{-}P_2W_{17}O_{61})_2]^{n-}$. There are three reasons why these polyanions are focused among a numerous kinds of POMs. The first one is that the central Ln ion acts as a chiral center, and its characteristic 4f-4f transitional absorption circular dichroism (CD) which would be available for detecting the chirality with a high sensitivity. The second one is that these anions have simple structures in chiral Ln-POMs and are easy to synthesize and characterize. The third one is that a number of applications is expected by chiral POMs [80]. The research strategies are to investigate the polyanion structure and chirality expression by controlling not only the charge and size of the central $Ln^{3+/4+}$ ions but also the cationic environment of the polyanion and co-existing structure directing molecules. In concrete, effects of (i) symmetry, arrangement, and chirality of counter cations or co-existing molecule and (ii) ionic radius of $Ln^{3+/4+}$ due to the lanthanide contraction are investigated in detail and discussed from the spectrochemical and stereochemical points of view.

1-6 Outline of this thesis

This dissertation mainly studies on the molecular conformation and chirality of the Ln-POM. It comprises seven chapters. Chapter 1 briefly introduces the background of POM chemistry, and our research objectives and strategy. Chapter 2 describes the synthesis and single crystal X-ray diffraction analysis of $[Ce^{III/IV}(\alpha\text{-}PW_{11}O_{39})_2]^{11-/10-}$; spontaneous resolution of the DMA salts for Ce^{IV} containing polyanion was achieved

with no chiral auxiliaries on crystallization. In Chapter 3, a sandwich-type Ln-POM $[Ln(\alpha\text{-}PW_{11}O_{39})_2]^{11-}$ (Ln = La, Ce) with a cubic coordination, which has only been confirmed by ^{183}W-NMR spectroscopy in aqueous solution, was successfully isolated as a tetramethylammonium salt and characterized by single crystal X-ray diffraction analysis. The results of this Chapter allowed to discuss an influence of anion–cation interaction on the conformation of $[Ln(\alpha\text{-}PW_{11}O_{39})_2]^{11-}$. In Chapter 4, enantioselective synthesis of sandwich-type Ln-POM $[Ln(\alpha\text{-}PW_{11}O_{39})_2]^{11-}$ was successfully completed by using L- and D-proline as chiral inducers, and the chirality of the polyanion both in aqueous solution and in the solid state was addressed. In Chapter 5, enantioselective synthesis of sandwich-type Ln-POM $[Ln(\alpha_2\text{-}P_2W_{17}O_{61})_2]^{17-}$ was also successfully accomplished by using L- and D-proline, and the chirality of the polyanion both in aqueous solution and in the solid state was presented. In Chapter 6, structural chemistry of the sandwich-type Ln-POM $[M(\alpha\text{-}PW_{11}O_{39})_2]^{n-}$ and $[M(\alpha_2\text{-}P_2W_{17}O_{61})_2]^{17-}$ was elucidated in detail by evaluating ϕ and intramolecular repulsion between the mono-lacunary units. Finally, the dissertation is summarized in Chapter 7.

1-7 References

[1] M. T. Pope, *Heteropoly and Isopoly Oxometalates*, Springer, Berlin, 1983.

[2] C. L. Hill (Ed.), *Chem. Rev.* **98**, 1 (1998).

[3] J. M. Clemente-Juan, M. Clemente-León, E. Coronado, J.R. Galán-mascarós, C. Giménez-Saiz and C. J. Gómez-Garcia, *C. R. Acad. Sci., Serie II c,* **1**, 305 (1998).

[4] *Polyoxometalate Chemistry for Nano-composite Design*, Kluwer Academic/Plenum Publishers, 2002.

[5] J. F. Keggin, *Nature*, **131**, 908 (1933).

[6] B. Dawson, *Acta Crystallogr.*, **6**, 113 (1953).

[7] I. Lindqvist, *Arkiv. Kemi.*, **5**, 247 (1952).

[8] J. S. Anderson, *Nature*, **150**, 850 (1937).

[9] A. P. Ginsburg, *Inorg. Synth.*, **27**, 96 (1990).

[10] J. Fuchs, A. Thiele, R. Palm, *Zeitschrift fuer Naturforschung*, Teil B, **36**, 544 (1981).

[11] K. Matsumono, Y. Sasaki, *Bull. Chem. Soc. Jpn.*, **49**, 156 (1976).

[12] W. H. Knoth, R. L. Harlow, *J. Am. Chem. Soc.*, **103**, 1865 (1981).

[13] J. Canny, A. Teze, R. Thouvenot, G. Herve, *Inorg. Chem.*, **25**, 2114 (1986).

[14] N. Nsouli, B. S. Bassil, M. H. Dickman, U. Kortz, B, Keita, L. Nadjo, *Inorg. Chem.*, **45**, 3858 (2006).

[15] N. Mizuno, *Catal. Surv. from Japan*, **4**, 149 (2001).

[16] B. S. Bassil, M. H. Dickman, I. Rőmer, B. kammer, U. Kortz, *Angew. Chem. Int. ed.*, **46**, 6192 (2007).

[17] F. Robert, A. Teze, *Acta Crystallogr B*, **37**, 318 (1981).

[18] V. Hubert, H. Hartl, *Zeitschrift fuer Naturforschung*, Teil B, **51**, 969 (1996).

[19] X. Cao, H. Naruke, T. Yamase, *Acta Crystallogr.*, **E59,** i116 (2003).

[20] C. Tourné, A. Reve, G. Tourné, M. Vendrell, *C. R. Acad. Sci., Serie C*, **277**, 643

[21] M. Bösing, I. Loose, H. Pohlmann, B. Krebs, *Chem.Eur. J.*, **3**, 1232 (1997).

[22] B. Botar, T. Yamase, E. Ishikawa, *Inorg. Chem. Commun.*, **3**, 579 (2000).

[23] T. Yamase, K. Fukaya, E. Ishikawa, H. Nojiri, T. Taniguchi, and T. Atake, *Inorg. Chem* ., **43**, 8150 (2004).

[24] T. Yamase, K. Fukaya, H. Nojiri, and Y. Ohshima, *Inorg. Chem.*, **45**, 7698 (2006).

[25] K. Fukaya, T. Yamase, *Bull. Chem. Soc. Jpn.,* **80**, 178 (2007).

[26] Y. Lu, Y. Xu, Y. Li, E. Wang, X. Xu, Y. Ma, *Inorg. Chem.*, **45**, 2055 (2006).

[27] J. Y. niu, D. J. Guo, J. P. Wang, J. W. Zhao, *Crystal Growth & Design*, **4**, 241 (2004)

[28] T. M. Anderson, X. Zhang, K. I. Hardcastle, C. L. Hill, *Inorg. Chem.*, **41**, 2477 (2002)

[29] M. Boyer, B. Lemeur, *C. R. Hebd. Seances Cad. Sci., Ser C*, **281**, 59 (1975).

[30] W. Clegg, G. M. Sheldrick, C. D. Garner, I. B. Walton, *Acta Crystallogr., Sect B*, **38**, 2906 (1982).

[31] C. M. Flynn. Jr, G. D. Stucky, *Inorg. Chem.,* **8**, 332 (1969).

[32] I. Lindqvist, B. Aronsson, *Ark. Kemi*, **7**, 49 (1954).

[33] H. Naruke, T. Yamase., *Acta Crystallogr.*, **C52**, 2655, (1996).

[34] P. Gouzerch, Y. Jeannin, F. Robert, A. Proust, *Angew. Chem. Int. Ed.,* **28**, 1363 (1989).

[35] R. D. Peacock, T. J. R. Weakley, *J. Chem. Soc.*, **A**, 1836 (1971).

[36] G. Xue, B. Lin, W. Wang, Q. Li, H. Li, *Hua Hsueh Hsueh Pao,* **60**, 2022 (2002).

[37] C. Rosu, T. J. R. Weakley, *Acta Crystallogr.,* **C54**, 2 (1998).

[38] T. Ozeki, T. Yamase, *Acta Crystallogr.*, **B50**, 128, (1994).

[39] M. Sugeta, T. Yamase, *Bull. Chem. Soc. Jpn.,* **66**, 444 (1993).

[40] M. A. AlDamen, S. Cardona-Serra, J. M. Clemente-Juan, E. Coronado, A. Gaita-Ariño, C. Martí-Gastaldo, F. Luis, O. Montero, *Inorg. Chem.,* **48**, 3467 (2009).

[41] K. Wassermann, M. H. Dickman, M. T. Pope, *Angew. Chem. Int. ed.,* **39**, 2914 (1997).

[42] K. Fukaya, T. Yamase, *Angew. Chem. Int. ed.*, **42**, 654 (2003).

[43] J. Niu, K. Wang, H. Chen, J. Zhao, P. Ma, J. Wang, M. Li, Y. Bai, D. Dang, *Crystal Growth & Design* **9**, 4362 (2009).

[44] C. Zhang, R. C. Howell, K. B. Scotland, F. G. Perez, L. Todaro, L. C. Francesconi, *Inorg. Chem.,* **43**, 7691 (2004).

[45] M. Sadakane, M. H. Dickman, M. T. Pope, *Angew. Chem. Int. ed.*, **39**, 2914 (2000).

[46] P. Mialane, L. Lipard, A. Mallard, J. Marrot, E. Antic-Fidancev, P. Aschehoug, D. Vivien, F. Secheresse, *Inorg. Chem.,* **42**, 2102 (2003).

[47] J. Wang, Q. Yan, X. Du, X. Duan, J. Niu, *Inorg. Chim. Acta*, 361, 2701 (2008).

[48] J. Wang, Q. Yan, X. Du, X. Duan, J. Niu, *Chin. J. Chem.,* **26**, 1239 (2008).

[49] J. Wang, Q. Yan, X. Du, X. Duan, J. Niu, *Crystal Growth & Design* **6**, 2266 (2006).

[50] M. Sadakane, A. Ostuni, M. T. Pope, *J. Chem. Soc., Dalton Trans.*, 63 (2002)

[51] U. Kortz, *J. Cluster Sci.,* **14**, 205 (2003).

[52] Q.-H. Luo, R. C. Howell, J. Bartis, M. Dankova, W. D. jr. Horrocks, A. L. Rheingold, L. C. Francesconi, *Inorg. Chem.,* **41**, 6112 (2002).

[53] D. Drewes, B. Krebs, *Zeitschrift fuer Naturforschung*, Teil B, **61**, 637 (2006).

[54] Q.-H. Luo, R. C. Howell, J. Bartis, C. W. Williams, W. D. jr. Horrocks, V. G. jr, Young, A. L. Rheingold, L. C. Francesconi, M. R. Antonio, *Inorg. Chem.*, 40, 1894 (2001).

[55] C. Boglio, G. Lemière, B. Hasenknopf, S. Thorimbert, E. Lacôte, M. Malacria, *Angew. Chem. Int. Ed,* **45**, 3324 (2006).

[56] J. Jing, B. P. Burton-Pye, L. C. Francesconi, M. R. Antonio, *Inorg. Chem.,* **47**,

6889 (2008).

[57] B. S. Bassil, M. H. Dickman, B. Kammer, U. Kortz, *Inorg. Chem.*, **46**, 2452 (2007).

[58] L. Fan, L. Xu, C. Zhang, F. Li, Z. Li, X. Liu, Structural Chemistry, **18**, 917 (2007).

[59] Y. H. Liu, G. L. guo, J. P. Wang, *J.Coord.Chem.*, **61**, 2428 (2008).

[60] R. Copping, A. J. Gaunt, I. May, M. J. Sarsfield, D. Collison, M. Helliwell, I. S. Denniss, D. C. Apperley, *Dalton Trans.*, 1256 (2005).

[61] R.-Q. Sun, H.-H Zhang, S.-L. Zhao, C.-C. Huang, X.-L. Zheng, *Jiegon Huaxue*, **20**, 413 (2001).

[62] P. Mialane, A. Dovecq, E. Riviere, J. Marrot, F. Secheresse, *Eur. J. Inorg. Chem.*, 33, 33 (2004).

[63] Y.-K. Shan, Z.-X. Liu, Z.-S. Jin, G.-C. Wei, Y.-S. Liu, E.-B. Wang, *Science in China.* B34, 513 (1991).

[64] Y.-K. Shan, Z.-X. Liu, E.-B. Wang, Z.-S. Jin, G.-C. Wei, Y.-S. Liu, *Jiegon Huaxue*, **9** 159 (1990).

[65] N. Jian, L. Xu, F. Li, G. Gao, L. Fan, *Inorg. Chem. Comm.*, **11**, 24 (2008).

[66] Y.-K. Shan, Z.-X. Liu, Z.-S. Jin, G.-C. Wei, *Hua Hsueh Hsueh Pao*, **50**, 357 (1992).

[67] M. A. Fedotov, B. Z. Pertsikov, D. K. Danovich, *Polyhedron*, **9**, 1249 (1990).

[68] R. Copping, L. Jonasson, A. J. Gaunt, D. Drennan, D. Collison, M. Helliwell, R. J. Pirttijarvi, C. J. Jones, A. Huguet, D. C. Apperley, N. Kaltsoyannis, I. May, *Inorg. Chem.*, **47**, 5787 (2008).

[69] C. Zhang, R. C. Howell, Q.-H. luo, H. L. Fieselmann, J. Todaro, L. C.

Francesconi, *Inorg. Chem.*, **44**, 3569 (2005).

[70] J.-Y. Niu, J. Zhao, D. Guo, J.-P. Wang, *J. Mol. Struct.*, **692**, 223 (2004).

[71] A. Ostuni, R. E. Bachman, M. T. Pope, *J. Cluster Sci.*, **43**, 431 (2003).

[72] R. D. Peacock, T. J. R. Weakley, *J. Chem. Soc.*, **A**, 1937 (1971).

[73] M. J. Stillman, A. J. Thomson, *J. Chem. Soc., Dalton Trans.*, 1138 (1976).

[74] G. Blasse, G. J. Dirksen, F. Zonnevijlle, *J. Inorg. Nucl. Chem.*, **43**, 2847 (1981).

[75] R. Ballardini, E. Chiorboli, V. Balzani, *Inorg. Chim. Acta*, **95**, 323 (1984).

[76] Y. Hou, X. Fang, C. L. Hill, *Chem. Eur. J.*, **13**, 9442 (2007).

[77] L. Cai, Y. Li, C. Yu, H. Ji, Y. Liu, S. Liu, *Inorg. Chim. Acta,* **362** 2895 (2009).

[78] J. Bartis, S. Sukal, M. Dankova, E. Kraft, R. Kronzon, M. Blumenstein, L. C. Francesconi, *J. Chem. Soc., Dalton Trans.*, 1937 (1997).

[79] A. Müller, F. Peters, M. T. Pope, D. Gatteschi, *Chem. Rev.*, **98**, 239 (1998).

[80] B. Hasenknopf, K. Micoine, E. Lacôte, S. Thorimbert, M. Malacria, R. Thouvenot, *Eur. J. Inorg. Chem.*, 5001 (2008).

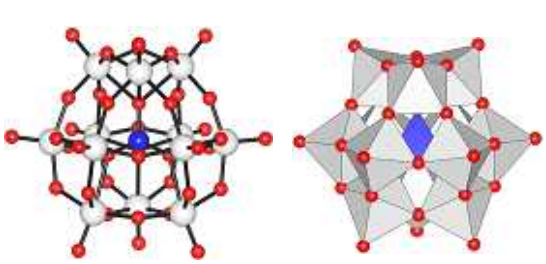

(**a**) Keggin

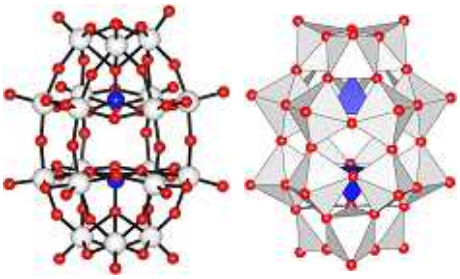

(**b**) Wells-Dawson

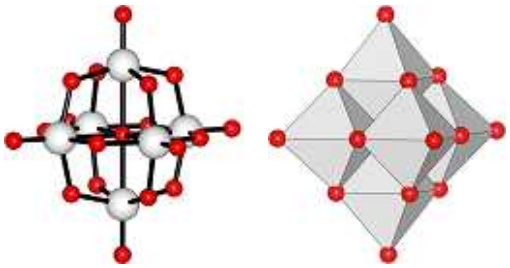

(**c**) Lindqvist

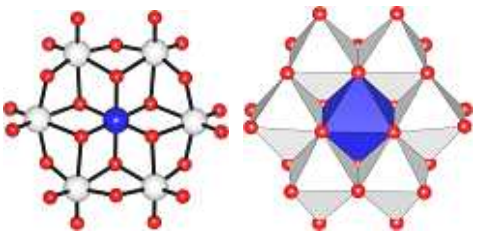

(**d**) Anderson

Figure 1-1. Typical polyoxometalates; (**a**) Keggin, (**b**) Wells-Dawson, (**c**) Lindqvist, (**d**) Anderson. The structures are drawn with both ball-and-stick and polyhedral models.

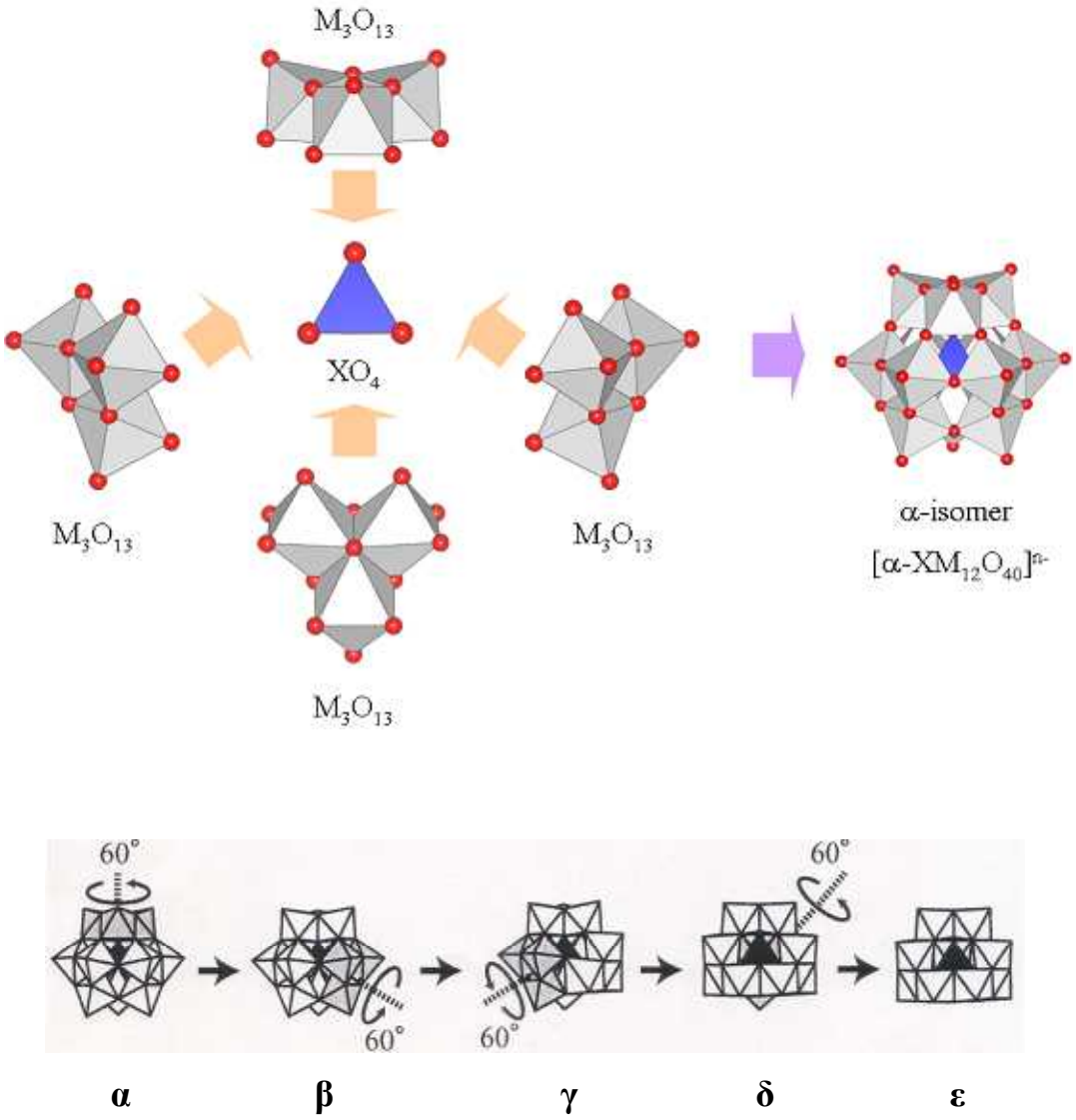

Figure 1-2. The formation components of Keggin type $[\alpha\text{-}XM_{12}O_{40}]^{n-}$ polyanion (above) and isomerism (α-ε) (below) of Keggin structure.

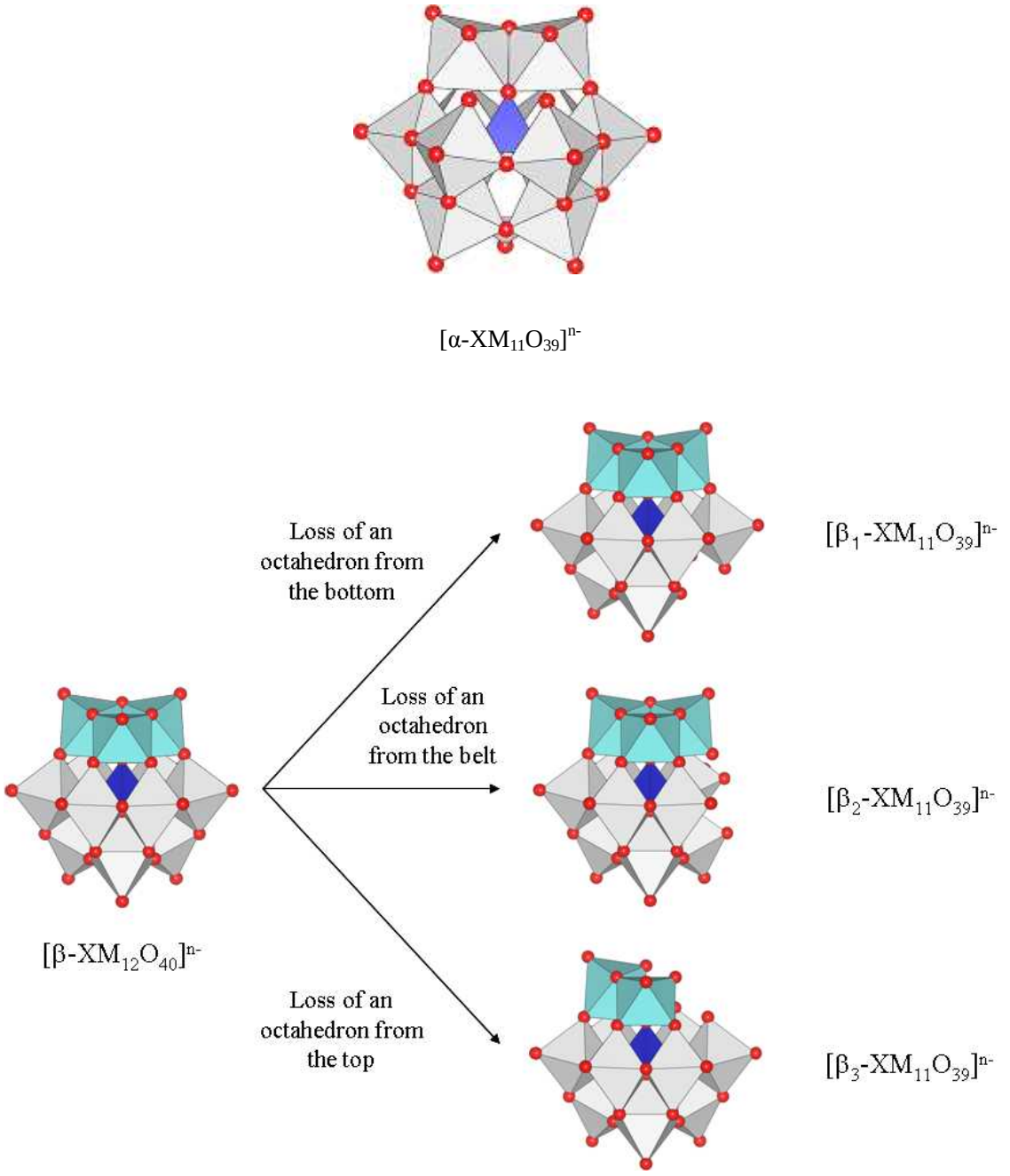

Figure 1-3. Typical mono-lacunary Keggin structures.

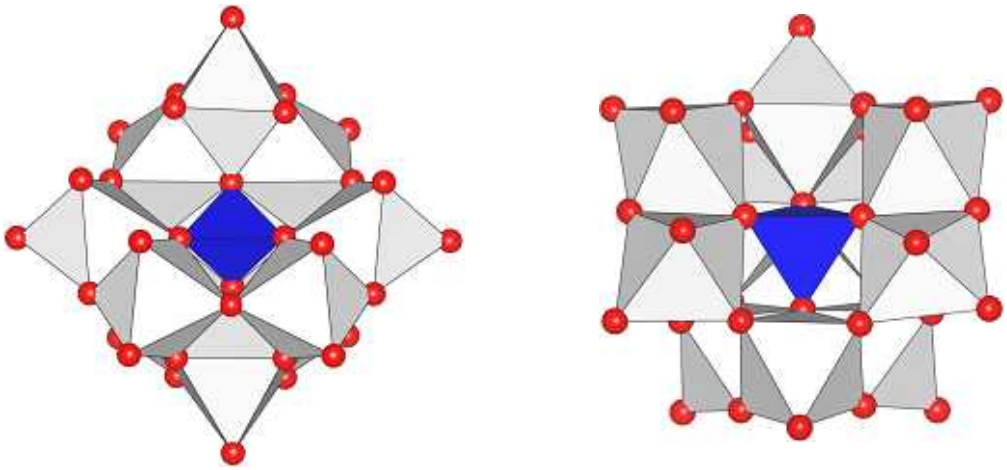

$[\alpha\text{-}XM_{10}O_{36}]^{n-}$ $[\gamma\text{-}XM_{10}O_{36}]^{n-}$

Figure 1-4. Typical di-lacunary Keggin structures.

(a) $[A\text{-}\alpha\text{-}XM_9O_{34}]^{n-}$ (b) $[A\text{-}\beta\text{-}XM_9O_{34}]^{n-}$

(c) $[B\text{-}\alpha\text{-}XM_9O_{34}]^{n-}$ (d) $[B\text{-}\beta\text{-}XM_9O_{34}]^{n-}$

Figure 1-5. Typical tri-lacunary Keggin structures; (a) $[A\text{-}\alpha\text{-}XM_9O_{34}]^{n-}$, (b) $[A\text{-}\beta\text{-}XM_9O_{34}]^{n-}$, (c) $[B\text{-}\alpha\text{-}XM_9O_{34}]^{n-}$, (d) $[B\text{-}\beta\text{-}XM_9O_{34}]^{n-}$.

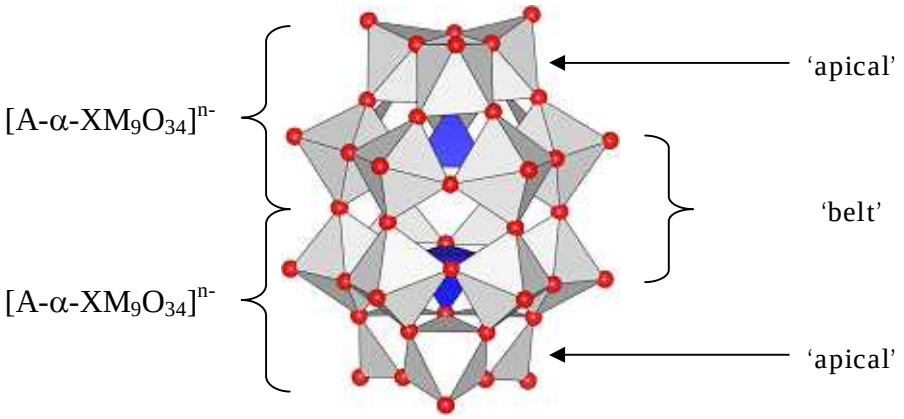

Figure 1-6. Structure of the α-type Wells-Dawson polyanion.

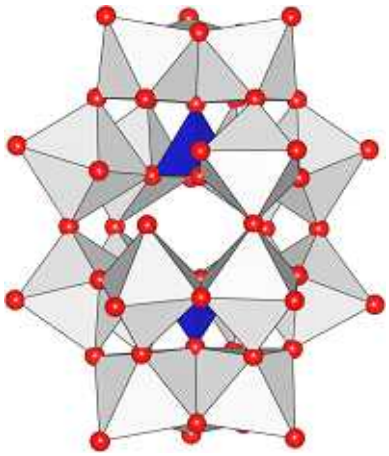

(a) $[\alpha_1\text{-}X_2M_{17}O_{61}]^{n-}$

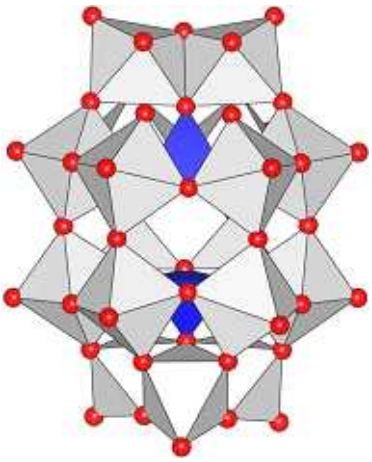

(b) $[\alpha_2\text{-}X_2M_{17}O_{61}]^{n-}$

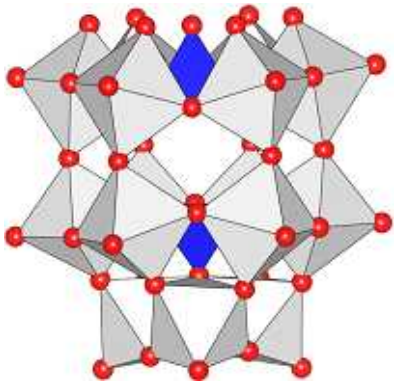

(c) $[\alpha\text{-}X_2M_{15}O_{56}]^{n-}$

Figure 1-7. Typical lacunary Wells-Dawson structures; (a) mono-lacunary $[\alpha_1\text{-}X_2M_{17}O_{61}]^{n-}$, (b) mono-lacunary $[\alpha_2\text{-}X_2M_{17}O_{61}]^{n-}$, (c) tri-lacunary $[\alpha\text{-}X_2M_{15}O_{56}]^{n-}$.

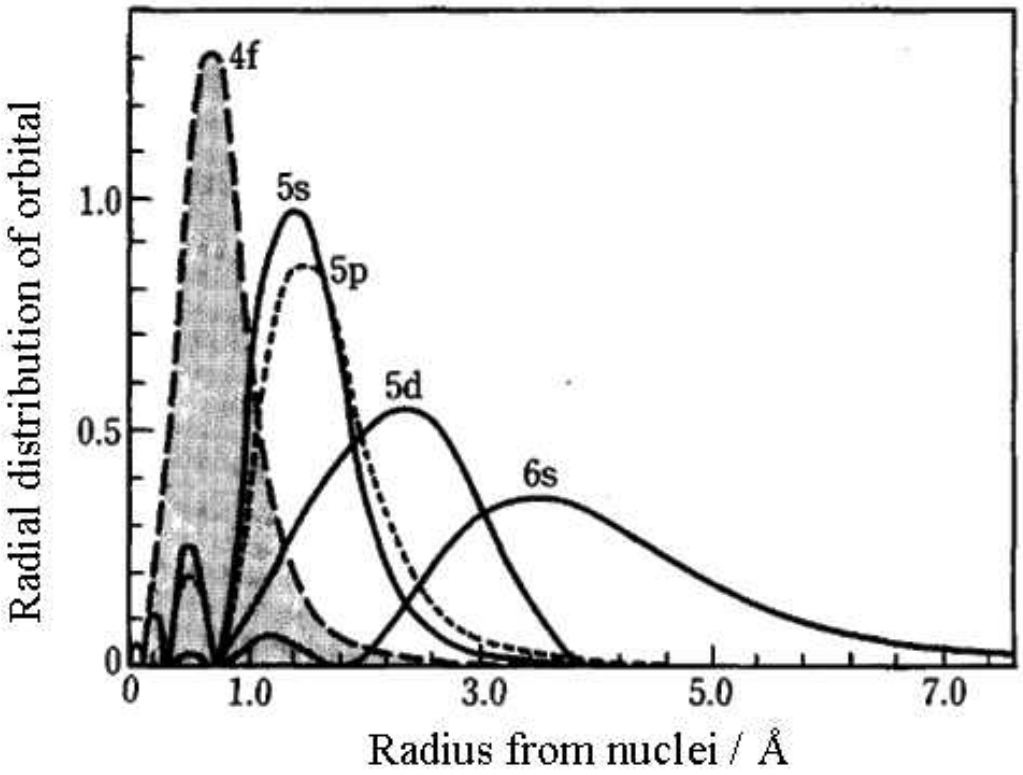

Figure 1-8. The space distribution of 4f, 5s, 5p, and 6s orbitals.

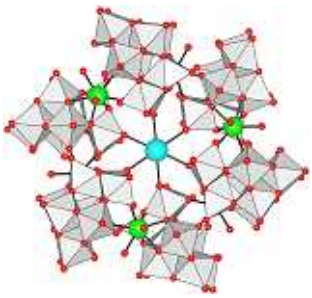

(a) $[K\subset\{Eu(H_2o)_2(\alpha\text{-}AsW_9O_{33})\}_6]^{35-}$

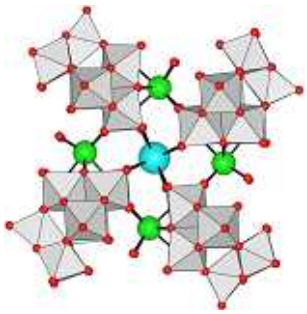

(b) $[Cs\subset\{Eu(H_2o)_2(\alpha\text{-}AsW_9O_{33})\}_4]^{23-}$

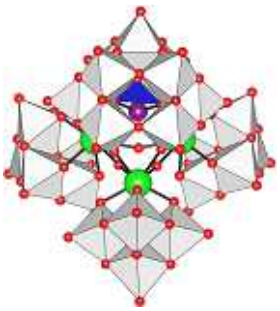

(c) $[Eu_3(CO_3)(SbW_9O_{33})(W_5O_{18})_3]^{20-}$

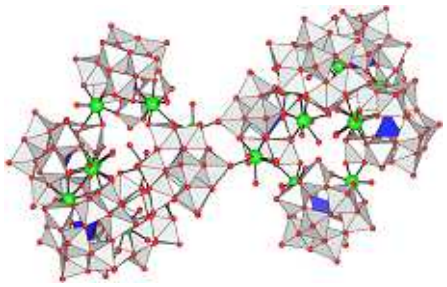

(d) $[Ce_{20}Ge_{10}W_{100}O_{376}(OH)_4(H_2O)_{30}]^{56-}$

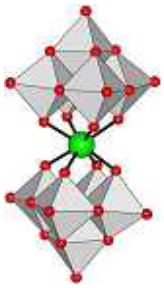

(e) $[Ln(W_5O_{18})_2]^{n-}$

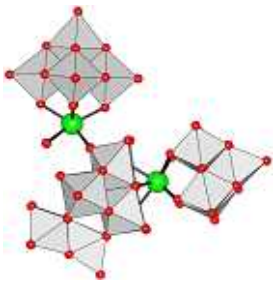

(f) $[Er_2(H_2O)_2(SbW_9O_{33})(W_5O_{18})_2]^{15-}$

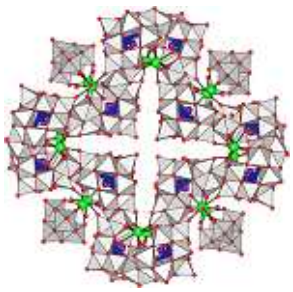

(g) $[Ce_{16}(H_2O)_{36}(WO_2)_4(W_2O_6)_8(W_5O_{18})_4(\alpha\text{-}AsW_9O_{33})_{12}]^{76-}$

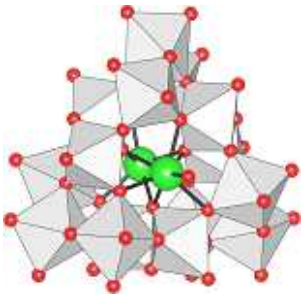

(h) $[H_6Ce_2(H_2O)ClW_{15}O_{54}]^{7-}$

Figure 1-9. Structures of the polyoxometallolanthanoate; (a) $[K\subset\{Eu(H_2o)_2(\alpha\text{-}AsW_9O_{33})\}_6]^{35-}$, (b) $[Cs\subset\{Eu(H_2o)_2(\alpha\text{-}AsW_9O_{33})\}_4]^{23-}$, (c) $[Eu_3(CO_3)(SbW_9O_{33})(W_5O_{18})_3]^{20-}$, (d) $[Ln(W_5O_{18})_2]^{n-}$, (e) $[Ce_{20}Ge_{10}W_{100}O_{376}(OH)_4(H_2O)_{30}]^{56-}$, (f) $[Er_2(H_2O)_2(SbW_9O_{33})(W_5O_{18})_2]^{15-}$, (g) $[Ce_{16}(H_2O)_{36}(WO_2)_4(W_2O_6)_8(W_5O_{18})_4(\alpha\text{-}AsW_9O_{33})_{12}]^{76-}$, (h) $[H_6Ce_2(H_2O)ClW_{15}O_{54}]^{7-}$.

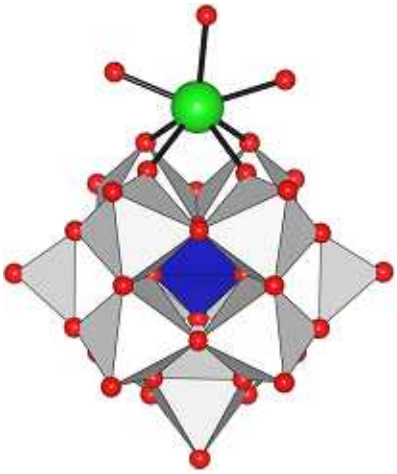

(a) $[Ln(H_2O)_3(\alpha\text{-}XM_{11}O_{39})_2]^{n-}$

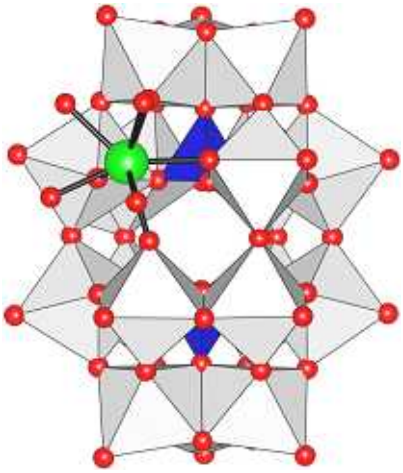

(b) $[Ln(H_2O)_4(\alpha_1\text{-}X_2M_{17}O_{61})]^{n-}$

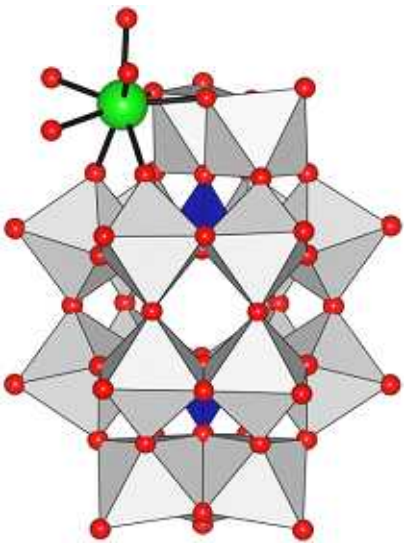

(c) $[Ln(H_2O)_4(\alpha_2\text{-}X_2M_{17}O_{61})]^{n-}$

Figure 1-10. Structures of the Ln mono-substituted Keggin and Wells-Dawson polyoxometallolanthanoates. (a) $[Ln(H_2O)_3(\alpha\text{-}XM_{11}O_{39})]^{n-}$, (b) $[Ln(H_2O)_4(\alpha_1\text{-}X_2M_{17}O_{61})]^{n-}$ (c) $[Ln(H_2O)_4(\alpha_2\text{-}X_2M_{17}O_{61})]^{n-}$.

(**a**) $[Ln(\beta_2\text{-}XM_{11}O_{39})_2]^{n-}$

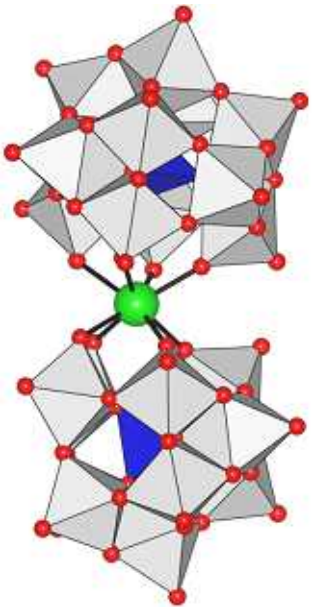

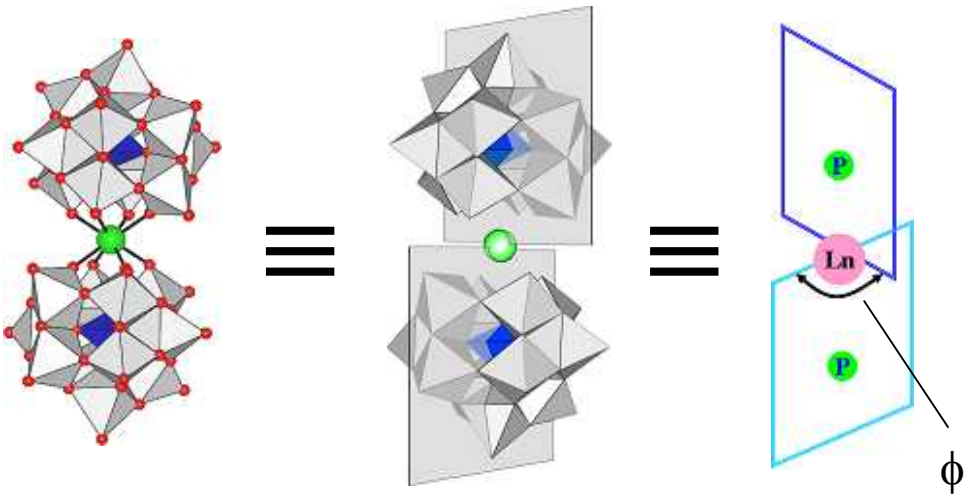

(**b**) $[Ln(\alpha\text{-}XM_{11}O_{39})_2]^{n-}$

Figure 1-11. Structures of the mono-lacunary Keggin sandwich-type polyoxometallolanthanoates; (a) $[Ln(\beta_2\text{-}XM_{11}O_{39})_2]^{n-}$, (b) $[Ln(\alpha\text{-}XM_{11}O_{39})_2]^{n-}$.

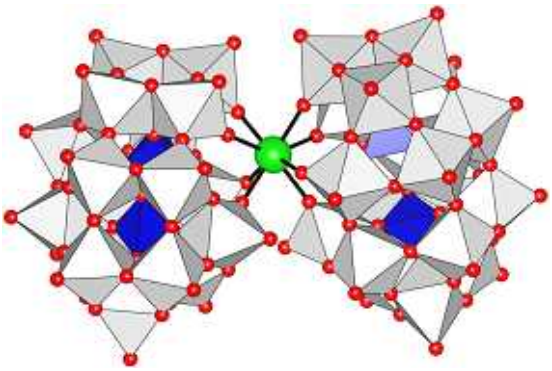

(a) $[Ln(\alpha_1\text{-}X_2M_{17}O_{61})_2]^{n-}$

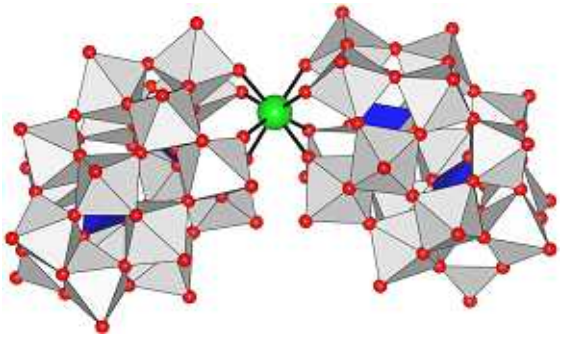

(b) $[Ln(\alpha_2\text{-}X_2M_{17}O_{61})_2]^{n-}$

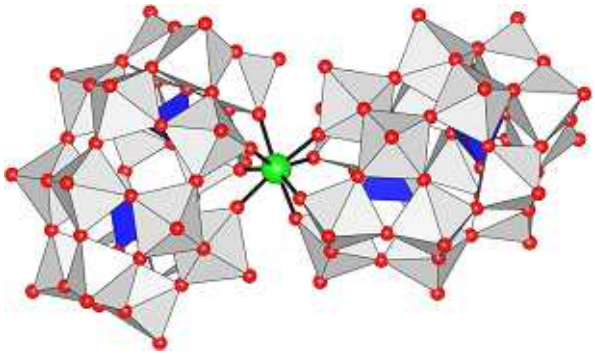

(c) $[Ln(\alpha_1\text{-}X_2M_{17}O_{61})(\alpha_2\text{-}X_2M_{17}O_{61})]^{n-}$

Figure 1-12. Structures of the mono-lacunary Wells-Dawson sandwich-type polyoxometallolanthanoates; (a) $[Ln(\alpha_1\text{-}X_2M_{17}O_{61})_2]^{n-}$, (b) $[Ln(\alpha_2\text{-}X_2M_{17}O_{61})_2]^{n-}$ (c) $[Ln(\alpha_1\text{-}X_2M_{17}O_{61})(\alpha_2\text{-}X_2M_{17}O_{61})]^{n-}$.

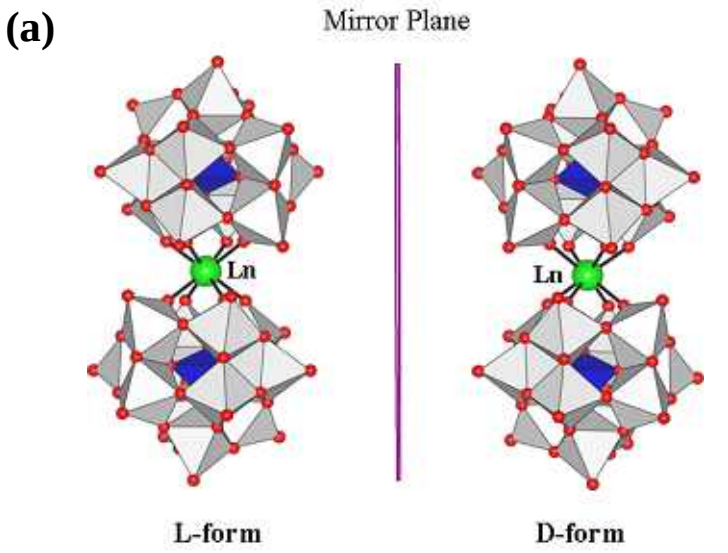

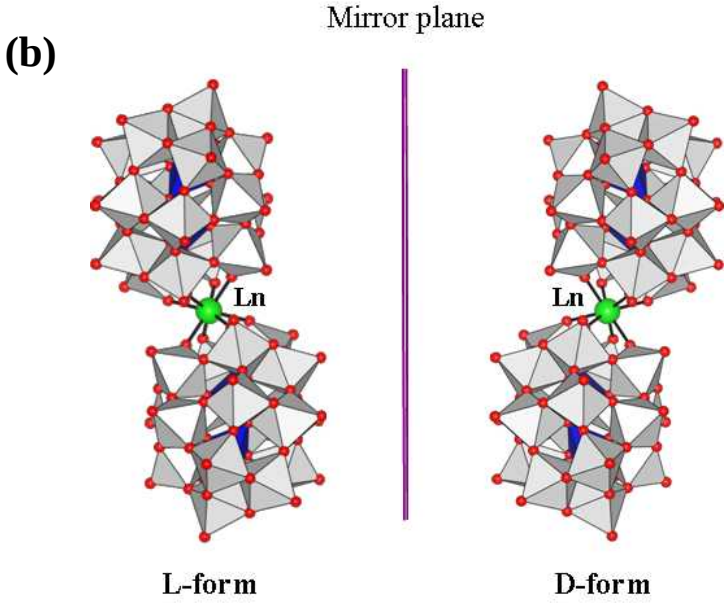

Figure 1-13. Enantiomers of $[Ln(\alpha\text{-}XM_{11}O_{39})_2]^{n-}$ (a) and $[Ln(\alpha_2\text{-}X_2M_{17}O_{61})_2]^{n-}$ (b).

Chapter 2 Synthesis and spontaneous resolution of the dimethylammonium (DMA) salts of sandwich-type $[Ce^{III/IV}(\alpha\text{-}PW_{11}O_{39})_2]^{11-/10-}$ polyanion

2-1 Introduction

Ongoing research on structure-sensitive molecular and crystal functions of polyoxometalates (POMs) has prompted us to develop and design rational synthesis methods. In this context, the selective synthesis and/or enantiomeric resolution of chiral POMs are expected and desired, but this is yet to be achieved. Development of this technology would expand the usability of chiral POMs [1] into chiral synthesis, sensing, and resolution of various organic and inorganic molecules in combination with existing functions of POMs such as homogeneous/heterogeneous catalytic and photocatalytic activities, redox, and sorption behavior. In particular, enantiomerically pure POMs are key materials in biological studies, especially on structure-activity relationship of POMs and their potential application to inorganic medicine.

Lanthanide ions ($Ln^{3+/4+}$) possessing a flexible mode of ligand coordination react with complete or lacunary POMs to form a series of Ln-POM complexes [2, 3]. As described in Chapter 1, the sandwich-type $[Ln(\alpha\text{-}XW_{11}O_{39})_2]^{n-}$ and $[Ln(\alpha_2\text{-}P_2W_{17}O_{61})_2]^{n-}$ polyanions are well-known species composed of $Ln^{3+/4+}$ chelated by two mono-lacunary Keggin $[\alpha\text{-}XW_{11}O_{39}]^{n-}$ and Wells-Dawson $[\alpha_2\text{-}P_2W_{17}O_{61}]^{10-}$ units acting as tetradentate O-donor ligands. Chirality of the $[Ln(\alpha\text{-}XW_{11}O_{39})_2]^{n-}$ polyanions with C_2 symmetry occurs from a twist angle $\phi \sim 45°$ of the two mono-lacunary groups (**Fig. 2-1(a)**), which is originated from the square-antiprismatic coordination of O atoms to the $Ln^{3+/4+}$ center

(for details, see Chapter 1). Interests have been focused on the absolute structures of $[Ln(\alpha\text{-}XW_{11}O_{39})_2]^{n-}$ polyanions [4, 5] and the isomeric derivative $[Ln(\beta_2\text{-}XW_{11}O_{39})_2]^{n-}$ [6], but they usually crystallize as racemates that include both enantiomers and no substantive chiral resolution or synthesis has been successful. Recently, a spontaneous resolution of $[M(\alpha\text{-}PW_{11}O_{39})_2]^{10-}$ ($M = Hf^{IV}$, Zr^{IV}) isostructural with $[Ln(\alpha\text{-}XW_{11}O_{39})_2]^{n-}$ was achieved by crystallization with achiral dimethylammonium ($Me_2NH_2^+$) cations [7, 8]. This topic inspired us to attempt chiral resolution of the $[Ln(\alpha\text{-}PW_{11}O_{39})_2]^{n-}$ species using $Ln = Ce^{IV}$.

In this Chapter, the synthesis and crystal structures of $[Me_2NH_2]_{10}[Ce^{IV}(\alpha\text{-}PW_{11}O_{39})_2]\cdot 14H_2O$ (**Ce-IV**) is described, which is the first example of spontaneously resolved sandwich-type Ln-POM complex. Moreover, corresponding Ce^{III} complex, $[Me_2NH_2]_{11}[Ce^{III}(\alpha\text{-}PW_{11}O_{39})_2]\cdot 14H_2O$ (**Ce-III**), is also prepared to study the influences of the anion charge (**Ce-III**: 10-; **Ce-IV**: 11-) on the structure and resolution.

2-2 Experimental

2-2-1 Materials

All chemicals were commercially available and used without further purification. $Na_9[A\text{-}\alpha\text{-}PW_9O_{34}]\cdot 16H_2O$ was prepared according to the previous report and identified by IR spectroscopy [9].

2-2-2 Measurements

Elemental analysis of C, H, and N were performed on a Yanaco MT5 CHN CORDER. The contents of Ce, P, and W were determined by inductively coupled

plasma (ICP) atomic emission spectroscopy on an ICPS-8100 spectrometer. These two measurements were requested to the Center for Advanced Analysis of the Tokyo Institute of Technology. IR (4000-400 cm^{-1}) spectra were recorded on a JASCO FT/IR-410 spectrometer using KBr disc method. Thermogravimetric and differential thermal analyses (TG-DTA) were conducted with a ULVAC MTS9000 + TGD9600 system. Magic angle spinning nuclear magnetic resonance (MAS-NMR) spectroscopy for ^{31}P was carried out on a JEOL JNM-ECA 400 at a frequency of 161.51 MHz with spinning at 5.44 kHz. The H_3PO_4 was used as a reference. Solution ^{31}P-NMR spectra were measured on JEOL JNM-500 spectrometer at a frequency of 202.47 MHz and Bruker Biospin AVANCE III at a frequency of 161.98 MHz using 85 % H_3PO_4 as an external reference.

2-2-3 Syntheses

2-2-3-1 $[Me_2NH_2]_{11}[Ce^{III}(\alpha\text{-}PW_{11}O_{39})_2]\cdot 14H_2O$ (**Ce-III**)

$Ce(NO_3)_3\cdot 6H_2O$ (0.44 g, 1.00 mmol) was dissolved in 15 ml of H_2O, and the pH was adjusted to 1.5 with 1M HCl. $Na_9[A\text{-}\alpha\text{-}PW_9O_{34}]\cdot 16H_2O$ (2.44 g, 1.00 mmol) dissolved in 15 ml of H_2O was added dropwise, and the solution was heated to 60 ºC for 1h with stirring and then cooled to room temperature. After the addition of an aqueous solution of $Me_2NH\cdot HCl$ (0.82 g, 10 mmol dissolved in 7 ml of H_2O), the solution was further heated at 60 ºC for 30 min with stirring and then allowed to cool to room temperature. Residual powders were filtered out, and the reddish orange filtrate was kept for a few months at room temperature. Reddish-orange needle-like crystals of (**Ce-III**) were obtained (yield, 0.96 g, 38.0% based on W). Found: C, 4.30; H, 1.72; N, 2.58; P, 1.03; W, 64.6; Ce, 2.33; H_2O, 4.2 wt %. Calcd for $C_{22}H_{116}N_{11}O_{92}P_2CeW_{22}$: C,

4.23; H, 1.87; N, 2.46; P, 0.99; W, 64.7; Ce, 2.24; H_2O, 4.03 wt %. IR (KBr disk): 1624m, 1465m, 1384m, 1092m, 1047m, 1019w, 952vs, 882m, 827s, 766vs, 730s, 593w.

2-2-3-2 $[Me_2NH_2]_{10}[Ce^{IV}(\alpha\text{-}PW_{11}O_{39})_2]\cdot 14H_2O$ (**Ce-IV**)

$(NH_4)_4Ce(SO_4)_4\cdot 4H_2O$ (1.33 g, 2.00 mmol) was dissolved in 15 ml of H_2O, and the pH was adjusted to 1.5 with 1M HCl. $Na_9[A\text{-}\alpha\text{-}PW_9O_{34}]\cdot 16H_2O$ (4.87 g, 2.00 mmol) in 10 ml of H_2O was dropped into the solution, which was heated to 60 ºC for 1h with stirring and then cooled to room temperature. $Me_2NH\cdot HCl$ (1.63 g, 20 mmol) in 6 ml of H_2O was added and further heated at 60 ºC for 30 min with stirring. After cooling to room temperature, the residual powders were filtered out, and the filtrate was kept for a few days. Yellow needle-like crystals of **Ce-IV** were obtained (yield, 2.10 g, 41.3% based on W). Found: C, 3.83; H, 1.47; N, 2.26; P, 0.96; W, 62.5; Ce, 2.20; H_2O, 4.0 wt %. Calcd for $C_{20}H_{108}N_{10}O_{92}P_2CeW_{22}$: C, 3.87; H, 1.47; N, 2.26; P, 0.96; W, 65.2; Ce, 2.26; H_2O, 4.06 wt %. IR (KBr disk): 1623m, 1464m, 1413w, 1102m, 1053m, 1018w, 956vs, 884m, 806s, 737s, 593w, 516m.

2-2-4 X-ray crystallography

Single crystal X-ray diffraction analysis of **Ce-III** was carried out on a Rigaku Saturn AFC8 diffractometer with graphite monochromatized MoK_α radiation (λ = 0.7107 Å) at 173 K. The structure was solved by the direct method SIR92 [10] and refined by the full-matrix least-squares on F^2 using CrystalStructure, which is a crystallographic software package [11]. The reflection data for the single crystal X-ray diffraction analysis of **Ce-IV** were collected on a Rigaku RAXIS-RAPID imaging plate diffractometer with graphite monochromatized MoK_α radiation (λ = 0.7107 Å) at 173 K.

The structure was solved by the direct method SHELXS-97 [12] and refined by the full-matrix least-squares [13] on F^2 using the CrystalStructure [11]. For both compounds, the W, Ce, and P atoms were refined anisotropically, and the other atoms isotropically. The H atoms were not included in the refinements. The Flack parameter (0.009(14)) for **Ce-IV** indicates the correct absolute configuration. The crystallographic data and the results of structure refinement are summarized in **Table 2-1**. The final atomic coordinates with thermal parameters ($B_{eq/iso}$) for **Ce-III** and **Ce-IV** are also summarized in **Table 2-2**.

2-3 Results and discussion

2-3-1 Preparation and molecular structures of $[Ce^{III}(\alpha\text{-}PW_{11}O_{39})_2]^{11-}$ (**Ce-III**) and $[Ce^{IV}(\alpha\text{-}PW_{11}O_{39})_2]^{10-}$ (**Ce-IV**)

Both compounds were synthesized using the conventional solution method by the reaction between tri-lacunary Keggin $[A\text{-}\alpha\text{-}PW_9O_{34}]^{9-}$ and $Ce^{3+/4+}$ in a 1:1 ratio in aqueous media according to the previous reports by Hill and Liu [7, 8]. The both crystals are composed of the $[Ln(\alpha\text{-}PW_{11}O_{39})_2]^{n-}$ polyanion, $[Me_2NH_2]^+$ (DMA), and lattice waters. In the synthesis of **Ce-III**, the common reagent $Ce(NO_3)_3{\cdot}6H_2O$ was used as the Ce^{3+} source. On the other hand, $(NH_4)Ce(SO_4)_4{\cdot}4H_2O$ was adopted in the synthesis of **Ce-IV**. Use of $(NH_4)_2Ce(NO_3)_6$ or $Ce(SO_4)_2{\cdot}nH_2O$ for synthesis of **Ce-IV** resulted in formations of only unidentified solids with poor crystallinity. Therefore, the choice of Ce^{4+} sources is important in successful preparation of **Ce-IV**.

The polyanion $[Ce^{III}(\alpha\text{-}PW_{11}O_{39})_2]^{11-}$ in **Ce-III** is constructed from two mono-lacunary Keggin $[\alpha\text{-}PW_{11}O_{39}]^{7-}$ units sandwiching the central Ce^{3+} ions in a square-antiprismatic (SA) coordination environment (**Fig. 2-1**). The bond lengths of Ce-O are in the range of

2.38(1)-2.52(1) Å (average 2.461 Å), which are comparable to those in $[Ce^{III}(W_5O_{18})_2]^{9-}$ (2.43(2)-2.55(2) Å, average 2.473 Å) [14] and $[Ce^{III}(W_5O_{18})(BW_{11}O_{39})]^{12-}$ (2.39(4)-2.54(3) Å, average 2.469 Å) [15]. The bond valence sums (BVSs) [16] calculated from the observed bond lengths are 5.4-6.6 for W, 4.7-5.1 for P, and 3.5 for Ce, which are reasonably consistent with their formal valences of W^{6+}, P^{5+}, and Ce^{3+}.

The polyanion $[Ce^{IV}(\alpha\text{-}PW_{11}O_{39})_2]^{10-}$ in **Ce-IV** are also constructed from two mono-lacunary Keggin $[\alpha\text{-}PW_{11}O_{39}]^{7-}$ units sandwiching the central Ce^{4+} ions in a SA coordination environment (**Fig. 2-1**). The bond lengths of Ce-O are in the range of 2.30(2)-2.38(2) Å (average 2.357 Å), which are comparable to those in $[Ce^{IV}(W_5O_{18})_2]^{8-}$ (2.34(1)-2.38(1) Å, average 2.3625 Å) [17] and $[Ce^{IV}(\alpha\text{-}PW_{11}O_{39})_2]^{10-}$ (2.448(10)-2.500(8) Å, average, 2.476 Å) [18]. The BVSs [16] calculated from the observed bond lengths are 5.8-6.2 for W, 5.0 for P, and 3.8 for Ce, which are reasonably consistent with their formal valences of W^{6+}, P^{5+}, Ce^{4+}.

2-3-2 Crystal structures and comparison with the other chiral analogues

The twist angle (ϕ) of the two mono-lacunary units due to the square-antiprismatic CeO_8 coordination results in the chiral C_2 symmetry of the polyanion (**Fig. 2-1(a)**). Here, the two enantiomeric polyanions are defined as D- and L-forms (**Fig. 2-1(b)**). Due to the achiral space group ($P2_1/n$) for **Ce-III**, the unit cell accommodates four polyanions as a racemate, i.e., two D- and two L-form polyanions (**Fig. 2-2(left)**). On the other hand, the unit cell for **Ce-IV** contains two polyanions, both of which are L-form (**Fig. 2-2(right)**); this demonstrates that spontaneous resolution occurred without chiral auxiliaries.

In 2007, Hill et al. reported that $[Me_2NH_2]_{10}[Hf^{IV}(\alpha\text{-}PW_{11}O_{39})_2]\cdot 8H_2O$ showed a

spontaneous resolution [7]. This compound has similar unit cell dimensions and crystal packing to those of **Ce-IV**, however, crystallized in orthorhombic space group $P2_12_12$ with highly disordered DMA cations. In the Hf analogue, the polyanion's C_2 axis is strictly defined as a crystallographic C_2 axis parallel to the c axis, whereas the polyanion's C_2 axis in **Ce-IV** slightly tilts (nonparallel) with respect to the c axis (**Fig. 2-3**). The symmetry reduction from $P2_12_12$ to $P2_1$ resulted in elimination of the disordering of DMA; the positions of all DMA could be determined in **Ce-IV**. The lower crystal symmetry for **Ce-IV** was confirmed by ^{31}P-MAS NMR spectroscopy (**Fig. 2-4**). The spectrogram showed adjacent two peaks at -12.81 and -13.07 ppm with an approximate 1:1 ratio for **Ce-IV**, while the Hf analogue exhibited a single peak at -15.6 ppm [7]. This observation was reflected by the decrease of number for crystallographic P site in the asymmetric unit from one to two due to the symmetry reduction from $P2_12_12$ to $P2_1$. In 2009, Liu et al. reported a Zr analogue obtained in spontaneous resolution [8]. This compound crystallized in the same space group as **Ce-IV**, however, a part of the DMA cations was not determined probably due to poor crystal quality.

The crystal packings viewed along the *a* axes of **Ce-III** and **Ce-IV** show extended hydrogen bondings (d(X···O) < 3.3 Å; X = N or O) involving DMA and lattice water molecules (**Fig. 2-5**). For **Ce-III**, two enantiomeric polyanions are linked via two DMA to yield a dimeric structure, while the polyanions in **Ce-IV** are linked to form a linear right-handed helical chain structure. The similar helix structure has been observed for the Hf and Zr analogues [7, 8].

2-3-3 ^{31}P-NMR spectroscopy of **Ce-III** and **Ce-IV** in aqueous solutions

The behavior of **Ce-III** and **Ce-IV** in aqueous solutions was examined by ^{31}P-NMR

spectroscopy. **Fig. 2-6** showed single resonances at -18.19 ppm for **Ce-III** and –12.84 ppm for **Ce-IV**, respectively. This observation shows that the structures of the polyanion in both **Ce-III** and **Ce-IV** are maintained in aqueous solutions. On the other hand, Zr analogues with the same space group $P2_1$ showed adjacent two peaks at -14.31 and -14.40 ppm, one of which is assigned to a protonation isomer [8]. No such protonation species seems to be present for **Ce-III** and **Ce-IV** in aqueous solutions.

2-4 Conclusion

In the series of sandwich-type $[Ln(XM_{11}O_{39})_2]^{n-}$, spontaneous resolution of $[Ce^{IV}(\alpha\text{-}PW_{11}O_{39})_2]^{10-}$ as a DMA salt was achieved for the first time without any chiral auxiliaries. The spontaneous resolution on crystallization was first discovered by L. Pasteur in 1849 in observation of left and right-handed single crystals of tartaric acid. However, its mechanism and methodology is generally complicated and still unclear; a lot of factors such as week intermolecular interaction on packing procedure when crystallization, crystal seeding, and stirred and unstirred history of solution, may contribute to the resolution [20]. In the case of **Ce-IV**, the DMA^+ cation and the charge (-10) of the polyanion are probably major factors for chiral resolution, because all of the analog polyanions with $M^{IV} = Hf^{IV}$ [7], Zr^{IV} [8], and Ce^{IV} (**Ce-IV** in this study) obtained by spontaneous resolution have the same cation and charge. In fact, combinations of DMA^+–$[M^{III}(\alpha\text{-}PW_{11}O_{39})_2]^{11-}$ (**Ce-III** in this study), $Et_2NH_2^+$– $[M^{IV}(\alpha\text{-}PW_{11}O_{39})_2]^{10-}$ [19], and $(NH_4/Me_4N/Na)^+$–$[M^{IV}(\alpha\text{-}PW_{11}O_{39})_2]^{10-}$ [18] produced racemete crystals with achiral space groups. Unfortunately, the solid-state CD (Circular dichroism) spectrum for the resolved crystals of **Ce-IV** could not be obtained because their crystal size was too small to measure.

2-5 References

[1] B. Hasenknopf, K. Micoine, E. Lacôte, S. Thorimbert, M. Malacria, R. Thouvenot, *Eur. J. Inorg. Chem.*, 5001 (2008).

[2] T. Yamase, H. Naruke, *Coord. Chem. Rev.*, **111**, 83 (1991).

[3] A. Müller, F. Peters, M.T. Pope, D. Gatteschi, *Chem. Rev.*, **98**, 239 (1998).

[4] J. Bartis, S. Sukal, M. Dankova, E. Kraft, R. Kronzon, M. Blumenstein, L.C. Francesconi, *J. Chem. Soc., Dalton Trans.*, 1937 (1997).

[5] M.A. Fedotov, B.Z. Pertsikov, D.K. Danovich, *Polyhedron*, **9**, 1249 (1990).

[6] B.S. Bassil, M.H. Dickman, B. von der Kammer, U. Kortz, *Inorg. Chem.*, **46**, 2452 (2007).

[7] Y. Hou, X. Fang, C.L. Hill, *Chem. Eur. J.*, **13**, 9442 (2007).

[8] L. Cai, Y. Li, C. Yu, H. Ji, Y. Liu, S. Liu, *Inorg. Chim. Acta*, **362** 2895 (2009).

[9] A. P. Ginsburg, *Inorg. Synth.*, **27**, 96 (1990).

[10] A. Altomare, G. Cascarano, C. Giacovazzo, A. Guagliardi, M. Buria, G. Polidori, M. Camalli, *J. Appl. Cryst.*, **27**, 435 (1994).

[11] J. R. Carruthers, J. S. Rollet, P. W. Betteridge, D. Kinna, L. Pearce, A. Larsen, E. Gabe, Chemical Crystallography Laboratory, Oxford, UK. (1999).

[12] G. M. Sheldrick, SHELXS-97, Program for Crystal Structure Solution, University of Gettingen, Germany, 1997.

[13] G. M. Sheldrick, SHELXL-97, Program for Crystal Structure Refinement, University of Gettingen, Germany, 1997.

[14] G. Xue, B. Liu, W. Wang, Q. Li, H. Li, *Acta Chim. Sin.*, **60**, 2022 (2002).

[15] H. Naruke, T. Yamase, *Bull. Chem. Soc. Jpn.*, **73** 375 (2000).

[16] I. D. Brown, “Structure and Bonding in Crystals,” ed by M. O’keeffe, A.

Navrotsky, Academic Press, New York **Vol. II**, 1 (1980).

[17] C. Rosu, T. J. R. Weakley, *Acta Crystallogr.,* **C54**, 2 (1998).

[18] L. Fan, L. Xu, G. Gao, F. Li, Y. Qiu, *Inorg. Chem. Commun.,* **9** 1308 (2006).

[19] C. N. Kato, A. Shinohara, K. Hayashi, K. Nomiya, *Inorg. Chem.,* **45**, 8108 (2006).

[20] W. A. Bonner, *Origins of Life and Evolution of the Biosphere*, **21**, 59 (1991).

Table 2-1. Crystallographic data and refinement results of **Ce-III** and **Ce-IV**.

	Ce-III	**Ce-IV**
Empirical formula	$C_{22}H_{116}N_{11}O_{92}P_2W_{22}Ce$	$C_{20}H_{108}N_{10}O_{92}P_2W_{22}Ce$
Formula weight	6253.94	6207.85
Crystal system	monoclinic	monoclinic
Space group	$P2_1/n$	$P2_1$
a (Å)	12.111(5)	12.157(1)
b (Å)	20.100(8)	20.527(1)
c (Å)	45.519(19)	20.938(1)
β (°)	95.370(6)	90.452(1)
V (Å^3)	11032(8)	5225.0(5)
Z	4	2
θ range (°)	3.0-31.0	3.1-27.4
Limiting indices reflections	-17≦h≦17	-14≦h≦15
	-29≦k≦28	-26≦k≦26
	-65≦l≦64	-27≦l≦27
Crystal size (mm^3)	0.30 × 0.10 × 0.05	0.45 × 0.05 × 0.04
D_c (g cm^{-3})	3.765	3.945
F(000)	10868	5500
μ (mm^{-1})	23.400	24.702
Todal data collected	72639	50489
Unique data	25119	23410
[$R_{(int)}$]	0.078	0.102
Goodness-of-fit (GOF)	0.987	1.045
R_1 [$I > 2\sigma(I)$][a]	0.0998	0.0629
wR_2[b]	0.2732	0.1351
Flack parameter	----------	0.009(14)

[a] $R_1 = (\Sigma||F_0|-|F_c||)/(\Sigma|F_c|)$.

[b] $wR_2 = \Sigma[w(F_0^2-F_c^2)^2]/\Sigma[w(F_0^2)^2]^{1/2}$.

w (for **1**) = $1/[0.0075F_0^2 + 1.5000\sigma(F_0^2) + 0.1200]/(4F_0^2)$

w (for **2**) = $1/[\sigma^2(F_0^2) + (0.0289\cdot P)^2 + 195.7301\cdot P]$, where $P = (\mathrm{Max}(F_0^2,0) + 2F_c^2)/3$

Table 2-2. Atomic coordinates and B_{eq} ($Å^2$) of **Ce-III**.

atom	x	y	z	Beq	occ
W(1)	0.62656(6)	0.99231(4)	0.177380(10)	1.460(15)	1
W(2)	0.50327(6)	0.82391(4)	0.191000(10)	1.442(15)	1
W(3)	0.34561(6)	0.95105(4)	0.143500(10)	1.419(15)	1
W(4)	0.73106(6)	0.75176(4)	0.16702(2)	1.707(16)	1
W(5)	0.85279(6)	0.91922(4)	0.15189(2)	1.723(16)	1
W(6)	0.69813(7)	1.03297(4)	0.10852(2)	1.821(17)	1
W(7)	0.41761(7)	0.98728(4)	0.074590(10)	1.866(17)	1
W(8)	0.31075(6)	0.82893(4)	0.089660(10)	1.605(15)	1
W(9)	0.81390(7)	0.79389(5)	0.09254(2)	2.251(18)	1
W(10)	0.66543(7)	0.90653(5)	0.04848(2)	2.289(18)	1
W(11)	0.55204(7)	0.74979(5)	0.06297(2)	2.056(17)	1
W(12)	0.05512(6)	0.41256(4)	0.166030(10)	1.507(15)	1
W(13)	0.17514(6)	0.58638(4)	0.170140(10)	1.500(15)	1
W(14)	0.04554(6)	0.51682(4)	0.099030(10)	1.536(15)	1
W(15)	0.28647(6)	0.55687(4)	0.068670(10)	1.611(15)	1
W(16)	0.17532(7)	0.39533(4)	0.062810(10)	1.779(16)	1
W(17)	0.18790(6)	0.28980(4)	0.130370(10)	1.646(16)	1
W(18)	0.30377(6)	0.35097(4)	0.196720(10)	1.607(16)	1
W(19)	0.42155(6)	0.52565(4)	0.200180(10)	1.602(15)	1
W(20)	0.55064(6)	0.49154(4)	0.100670(10)	1.505(15)	1
W(21)	0.44608(6)	0.32929(4)	0.095230(10)	1.696(16)	1
W(22)	0.55945(6)	0.38853(4)	0.161680(10)	1.606(16)	1
Ce(1)	0.44224(8)	0.66627(6)	0.13793(2)	1.50(2)	1
P(1)	0.5833(3)	0.8705(2)	0.12150(8)	1.33(9)	1
P(2)	0.3007(3)	0.4547(2)	0.13352(9)	1.26(9)	1
O(1)	0.6226(9)	1.0450(6)	0.2071(2)	1.6(2)	1
O(2)	0.4590(10)	0.8297(7)	0.2261(2)	2.1(2)	1
O(3)	0.2446(10)	0.9868(6)	0.1614(2)	2.0(2)	1
O(4)	0.8382(10)	0.7082(7)	0.1872(2)	2.2(2)	1
O(5)	0.9882(10)	0.9277(6)	0.1648(2)	2.1(2)	1
O(6)	0.7513(13)	1.1108(9)	0.0955(3)	4.4(3)	1
O(7)	0.3625(10)	1.0521(6)	0.0513(2)	1.9(2)	1
O(8)	0.1850(11)	0.8016(7)	0.0717(2)	2.9(2)	1
O(9)	0.9389(11)	0.7613(7)	0.0863(2)	2.7(2)	1
O(10)	0.6965(11)	0.9371(7)	0.0168(2)	2.9(2)	1
O(11)	0.5238(12)	0.6980(8)	0.0332(3)	3.3(2)	1
O(12)	-0.0718(9)	0.4102(6)	0.1793(2)	1.8(2)	1
O(13)	0.0783(11)	0.6333(7)	0.1874(2)	2.7(2)	1
O(14)	-0.0790(12)	0.5497(8)	0.0897(3)	3.6(3)	1
O(15)	0.3043(10)	0.6036(6)	0.0373(2)	2.0(2)	1
O(16)	0.1248(11)	0.3525(7)	0.0325(2)	2.7(2)	1
O(17)	0.1477(10)	0.2114(7)	0.1218(2)	2.3(2)	1
O(18)	0.3326(10)	0.3057(7)	0.2293(2)	2.2(2)	1
O(19)	0.4820(9)	0.5321(6)	0.2359(2)	1.6(2)	1
O(20)	0.6627(10)	0.5164(6)	0.0813(2)	1.8(2)	1

O(21)	0.4910(10)	0.2637(6)	0.0762(2)	1.9(2)	1
O(22)	0.6724(10)	0.3571(6)	0.1832(2)	2.0(2)	1
O(23)	0.5788(8)	0.8162(5)	0.1457(2)	0.96(17)	1
O(24)	0.6502(11)	0.9276(7)	0.1344(2)	2.9(2)	1
O(25)	0.4659(9)	0.8984(6)	0.1126(2)	1.34(19)	1
O(26)	0.6354(10)	0.8423(7)	0.0943(2)	2.2(2)	1
O(27)	0.3111(9)	0.5161(6)	0.1534(2)	1.7(2)	1
O(28)	0.2384(9)	0.3987(6)	0.1492(2)	1.20(18)	1
O(29)	0.2305(11)	0.4726(7)	0.1034(2)	2.5(2)	1
O(30)	0.4169(9)	0.4297(6)	0.1260(2)	1.30(19)	1
O(31)	0.4362(9)	0.7500(6)	0.1791(2)	1.7(2)	1
O(32)	0.3448(9)	0.7638(6)	0.1159(2)	1.8(2)	1
O(33)	0.5330(11)	0.7057(7)	0.0970(2)	2.8(2)	1
O(34)	0.6344(11)	0.6846(7)	0.1580(2)	2.7(2)	1
O(35)	0.3224(10)	0.6141(6)	0.0987(2)	2.0(2)	1
O(36)	0.5316(9)	0.5613(6)	0.1229(2)	1.18(18)	1
O(37)	0.4769(10)	0.6008(7)	0.1834(2)	2.4(2)	1
O(38)	0.2587(11)	0.6534(7)	0.1580(3)	3.0(2)	1
O(39)	0.3895(10)	0.8774(6)	0.1700(2)	1.8(2)	1
O(40)	0.5924(10)	0.9102(6)	0.1930(2)	1.8(2)	1
O(41)	0.4722(9)	0.9965(6)	0.1598(2)	1.6(2)	1
O(42)	0.0151(8)	0.4490(5)	0.1284(2)	0.95(17)	1
O(43)	0.1007(8)	0.5683(5)	0.1328(2)	0.81(16)	1
O(44)	0.1047(9)	0.4955(6)	0.1780(2)	1.44(19)	1
O(45)	0.6494(10)	0.7846(6)	0.1992(2)	1.7(2)	1
O(46)	0.7856(9)	0.9729(6)	0.1807(2)	1.50(19)	1
O(47)	0.6680(10)	1.0571(7)	0.1466(2)	2.2(2)	1
O(48)	0.3430(9)	1.0059(6)	0.1099(2)	1.51(19)	1
O(49)	0.2603(10)	0.8885(6)	0.1200(2)	1.9(2)	1
O(50)	0.2779(8)	0.5630(5)	0.2040(2)	0.89(17)	1
O(51)	0.1497(11)	0.3693(7)	0.1979(2)	2.5(2)	1
O(52)	0.0594(11)	0.3263(7)	0.1457(2)	2.8(2)	1
O(53)	0.0467(9)	0.4420(6)	0.0711(2)	1.7(2)	1
O(54)	0.1247(10)	0.5688(7)	0.0729(2)	2.3(2)	1
O(55)	0.3165(9)	0.9187(6)	0.0672(2)	1.9(2)	1
O(56)	0.5396(10)	1.0340(6)	0.0957(2)	1.9(2)	1
O(57)	0.8359(10)	1.0002(7)	0.1272(2)	2.4(2)	1
O(58)	0.8129(10)	0.8434(7)	0.1683(2)	2.3(2)	1
O(59)	0.3477(10)	0.4386(7)	0.2060(2)	2.2(2)	1
O(60)	0.2552(10)	0.2765(7)	0.1700(2)	2.4(2)	1
O(61)	0.1393(11)	0.3364(7)	0.0946(2)	2.8(2)	1
O(62)	0.2329(10)	0.4717(7)	0.0464(2)	2.3(2)	1
O(63)	0.4173(9)	0.7984(6)	0.0643(2)	1.41(19)	1
O(64)	0.5294(11)	0.9455(7)	0.0518(2)	2.8(2)	1
O(65)	0.7206(9)	0.9699(6)	0.0772(2)	1.7(2)	1
O(66)	0.8689(10)	0.8668(7)	0.1169(2)	2.4(2)	1
O(67)	0.7812(10)	0.7574(7)	0.1279(2)	2.2(2)	1
O(68)	0.5227(10)	0.4638(7)	0.1833(2)	2.4(2)	1

O(69)	0.4443(9)	0.3439(6)	0.1799(2)	1.6(2)	1
O(70)	0.3354(10)	0.2906(7)	0.1189(2)	2.2(2)	1
O(71)	0.3236(12)	0.3628(8)	0.0707(3)	3.3(2)	1
O(72)	0.4288(10)	0.5084(7)	0.0725(2)	2.2(2)	1
O(73)	0.5927(9)	0.8301(6)	0.0364(2)	1.6(2)	1
O(74)	0.7990(9)	0.8542(6)	0.0610(2)	1.6(2)	1
O(75)	0.7136(11)	0.7392(7)	0.0700(2)	2.9(2)	1
O(76)	0.6291(9)	0.4446(6)	0.1346(2)	1.19(18)	1
O(77)	0.5446(9)	0.3216(6)	0.1316(2)	1.6(2)	1
O(78)	0.5384(9)	0.4003(6)	0.0837(2)	1.7(2)	1

Table 2-2 (Continued). Atomic coordinates and B_{eq} ($Å^2$) of **Ce-IV**.

atom	x	y	z	Beq	occ
W(1)	0.07405(8)	0.45993(5)	0.38817(5)	1.335(15)	1
W(2)	0.19037(8)	0.62985(5)	0.39909(5)	1.331(15)	1
W(3)	0.33786(8)	0.49813(5)	0.31057(5)	1.320(15)	1
W(4)	-0.04404(8)	0.69170(4)	0.33825(5)	1.274(15)	1
W(5)	-0.16343(8)	0.52344(5)	0.32588(5)	1.234(15)	1
W(6)	-0.02177(8)	0.40628(5)	0.24255(5)	1.289(15)	1
W(7)	0.24378(8)	0.44687(5)	0.16556(5)	1.396(15)	1
W(8)	0.34659(8)	0.60375(5)	0.18171(5)	1.223(15)	1
W(9)	-0.15628(8)	0.63045(5)	0.18389(5)	1.364(15)	1
W(10)	-0.01754(8)	0.51555(5)	0.10070(5)	1.405(15)	1
W(11)	0.09144(8)	0.67066(5)	0.11786(5)	1.249(15)	1
W(12)	0.63058(8)	1.00864(5)	0.28119(5)	1.364(15)	1
W(13)	0.50482(8)	0.84744(5)	0.32487(5)	1.247(15)	1
W(14)	0.61372(8)	0.87660(5)	0.16196(5)	1.424(16)	1
W(15)	0.36111(8)	0.82836(5)	0.10408(5)	1.374(15)	1
W(16)	0.47423(8)	0.97708(5)	0.05979(5)	1.519(16)	1
W(17)	0.48734(8)	1.10988(5)	0.18004(5)	1.498(16)	1
W(18)	0.39648(8)	1.08323(5)	0.33263(5)	1.380(15)	1
W(19)	0.27123(8)	0.92054(5)	0.37315(5)	1.219(15)	1
W(20)	0.11174(8)	0.90870(5)	0.15697(5)	1.345(15)	1
W(21)	0.21786(8)	1.05862(5)	0.11148(5)	1.547(16)	1
W(22)	0.12671(8)	1.03651(5)	0.26332(5)	1.346(15)	1
Ce(1)	0.22894(11)	0.76350(6)	0.26866(7)	1.22(2)	1
P(1)	0.0884(5)	0.5660(2)	0.2539(3)	1.10(9)	1
P(2)	0.3725(4)	0.9556(3)	0.2199(3)	1.11(9)	1
O(1)	0.0907(14)	0.4164(8)	0.4587(8)	2.0(3)	1
O(2)	0.2470(13)	0.6348(8)	0.4763(8)	1.6(2)	1
O(3)	0.4447(13)	0.4680(8)	0.3529(8)	1.8(2)	1
O(4)	-0.1406(13)	0.7362(8)	0.3735(8)	1.8(2)	1
O(5)	-0.2923(12)	0.5186(7)	0.3571(7)	1.2(2)	1
O(6)	-0.0670(12)	0.3287(8)	0.2198(7)	1.5(2)	1
O(7)	0.2896(13)	0.3836(8)	0.1194(8)	1.8(2)	1
O(8)	0.4577(13)	0.6306(8)	0.1446(7)	1.5(2)	1
O(9)	-0.2831(14)	0.6629(9)	0.1666(8)	2.2(3)	1
O(10)	-0.0573(12)	0.4737(8)	0.0355(7)	1.5(2)	1
O(11)	0.1112(16)	0.7211(10)	0.0537(9)	2.8(3)	1
O(12)	0.7597(14)	1.0180(9)	0.3112(8)	2.1(3)	1
O(13)	0.5989(13)	0.8066(8)	0.3697(7)	1.5(2)	1
O(14)	0.7363(14)	0.8409(8)	0.1500(8)	2.0(3)	1
O(15)	0.3384(15)	0.7675(9)	0.0502(9)	2.3(3)	1
O(16)	0.5172(15)	1.0036(9)	-0.0112(9)	2.4(3)	1
O(17)	0.5304(14)	1.1829(9)	0.1476(9)	2.2(3)	1
O(18)	0.3836(15)	1.1395(9)	0.3909(9)	2.4(3)	1
O(19)	0.2235(14)	0.9289(9)	0.4469(8)	2.2(3)	1
O(20)	-0.0010(14)	0.8761(9)	0.1217(9)	2.3(3)	1

O(21)	0.1722(13)	1.1135(8)	0.0580(7)	1.5(2)	1
O(22)	0.0242(14)	1.0773(8)	0.3004(8)	2.0(3)	1
O(23)	0.0973(12)	0.6240(7)	0.2994(7)	1.2(2)	1
O(24)	0.0234(12)	0.5089(7)	0.2867(7)	1.1(2)	1
O(25)	0.2017(12)	0.5410(7)	0.2370(7)	1.4(2)	1
O(26)	0.0285(12)	0.5858(7)	0.1920(7)	1.3(2)	1
O(27)	0.3626(12)	0.9070(8)	0.2748(7)	1.5(2)	1
O(28)	0.4410(14)	1.0148(8)	0.2413(8)	2.0(3)	1
O(29)	0.4289(12)	0.9234(7)	0.1624(7)	1.1(2)	1
O(30)	0.2584(11)	0.9797(6)	0.1993(6)	0.7(2)	1
O(31)	0.2514(14)	0.6988(8)	0.3615(8)	2.0(3)	1
O(32)	0.3151(13)	0.6690(8)	0.2375(8)	1.7(2)	1
O(33)	0.1227(13)	0.7190(8)	0.1845(8)	1.7(2)	1
O(34)	0.0500(12)	0.7536(7)	0.3109(7)	1.1(2)	1
O(35)	0.3324(12)	0.7953(7)	0.1792(7)	1.3(2)	1
O(36)	0.1456(12)	0.8539(7)	0.2188(7)	1.3(2)	1
O(37)	0.2129(13)	0.8437(8)	0.3492(8)	1.7(2)	1
O(38)	0.4093(13)	0.7823(8)	0.3101(8)	1.7(2)	1
O(39)	0.2970(15)	0.5742(9)	0.3619(9)	2.4(3)	1
O(40)	0.1063(13)	0.5444(8)	0.4117(7)	1.6(2)	1
O(41)	0.2143(13)	0.4558(8)	0.3496(8)	1.7(2)	1
O(42)	0.6538(12)	0.9536(8)	0.2081(7)	1.5(2)	1
O(43)	0.5718(13)	0.8434(8)	0.2431(8)	2.0(3)	1
O(44)	0.5751(13)	0.9353(8)	0.3259(8)	1.9(3)	1
O(45)	0.0488(13)	0.6693(8)	0.4081(8)	1.8(2)	1
O(46)	-0.0790(13)	0.4810(8)	0.3921(8)	1.6(2)	1
O(47)	0.0277(13)	0.3907(8)	0.3298(8)	1.6(2)	1
O(48)	0.3292(12)	0.4366(7)	0.2426(7)	1.4(2)	1
O(49)	0.4114(15)	0.5546(9)	0.2537(9)	2.3(3)	1
O(50)	0.4151(12)	0.8825(7)	0.3921(7)	1.4(2)	1
O(51)	0.5505(13)	1.0619(8)	0.3393(8)	1.9(3)	1
O(52)	0.6205(12)	1.0813(8)	0.2219(7)	1.5(2)	1
O(53)	0.6037(13)	0.9341(8)	0.0883(8)	1.6(2)	1
O(54)	0.5213(13)	0.8172(8)	0.1160(8)	1.8(3)	1
O(55)	0.3386(12)	0.5142(7)	0.1421(7)	1.3(2)	1
O(56)	0.1248(14)	0.4071(9)	0.2127(8)	2.3(3)	1
O(57)	-0.1562(14)	0.4395(9)	0.2813(9)	2.3(3)	1
O(58)	-0.1150(11)	0.6033(7)	0.3561(7)	1.0(2)	1
O(59)	0.3589(14)	1.0074(8)	0.3685(8)	2.1(3)	1
O(60)	0.4394(14)	1.1406(8)	0.2605(8)	2.0(3)	1
O(61)	0.5224(13)	1.0487(8)	0.1128(8)	1.8(2)	1
O(62)	0.4116(12)	0.8989(7)	0.0392(7)	1.1(2)	1
O(63)	0.2288(12)	0.6240(7)	0.1254(7)	1.1(2)	1
O(64)	0.1291(12)	0.4803(7)	0.1150(7)	1.1(2)	1
O(65)	-0.0593(13)	0.4547(8)	0.1698(7)	1.5(2)	1
O(66)	-0.1913(12)	0.5630(8)	0.2458(7)	1.5(2)	1
O(67)	-0.1109(13)	0.6805(8)	0.2541(8)	1.6(2)	1
O(68)	0.1680(12)	0.9718(7)	0.3257(7)	1.2(2)	1

O(69)	0.2529(13)	1.0846(8)	0.2928(8)	1.5(2)	1
O(70)	0.3418(12)	1.1056(7)	0.1530(7)	1.4(2)	1
O(71)	0.3302(13)	1.0145(8)	0.0663(7)	1.6(2)	1
O(72)	0.2249(13)	0.8760(8)	0.1023(8)	1.5(2)	1
O(73)	0.0436(13)	0.5910(8)	0.0679(8)	1.6(2)	1
O(74)	-0.1486(14)	0.5632(8)	0.1208(8)	2.0(3)	1
O(75)	-0.0664(12)	0.6804(7)	0.1286(7)	1.2(2)	1
O(76)	0.0448(12)	0.9713(7)	0.2177(7)	1.1(2)	1
O(77)	0.1347(14)	1.0848(8)	0.1862(8)	2.0(3)	1
O(78)	0.1212(12)	0.9914(7)	0.1005(7)	1.1(2)	1

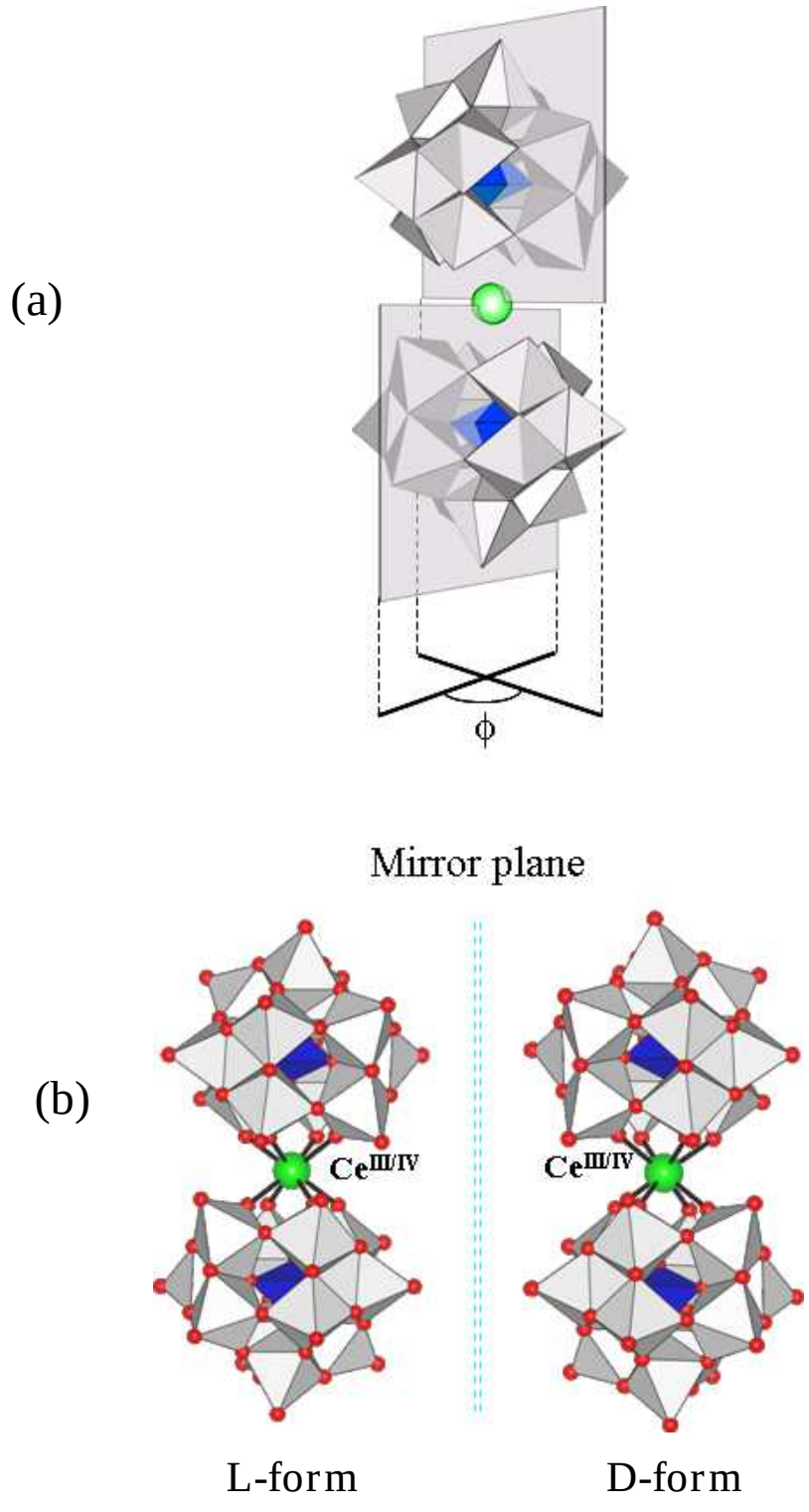

Figure 2-1. (a) Definition of the twist angle ϕ in an $[Ln(\alpha\text{-}PW_{11}O_{39})_2]n$- anion (see text). (b) Combined polyhedral and ball-and-stick representation of two enantiomers of the $[Ce^{III/IV}(\alpha\text{-}PW_{11}O_{39})_2]^{11-/10-}$ anion viewed along the molecular C_2 axies. Left: L-form, Right: D-form. (WO_6: white octahedron, PO_4: blue tetrahedron, O atom: red sphere, $Ce^{III/IV}$ atom: green sphere).

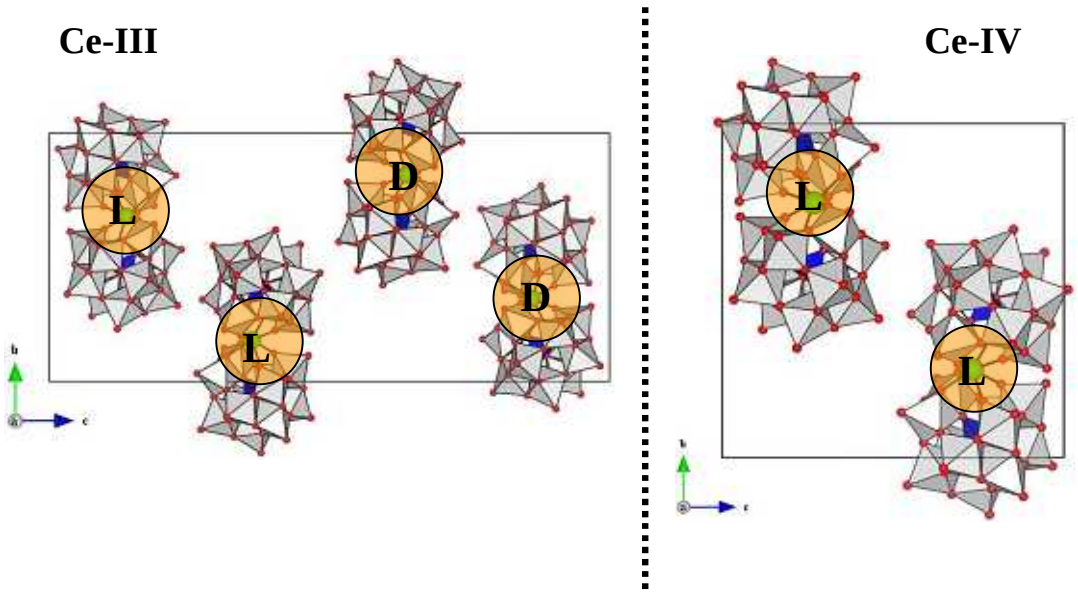

Figure 2-2. The unit cell packing of the $[Ce^{III/IV}(\alpha\text{-}PW_{11}O_{39})_2]^{11-/10-}$ anions in **Ce-III** (left) and **Ce-IV** (right) projected on the *bc* plane. The DMA cations and water molecules are omitted for clarity. Color codes are denoted in the caption of **Figure 2-1**. The "L" and "D" marked on the anions represent the anions to have the L- and D-forms, respectively.

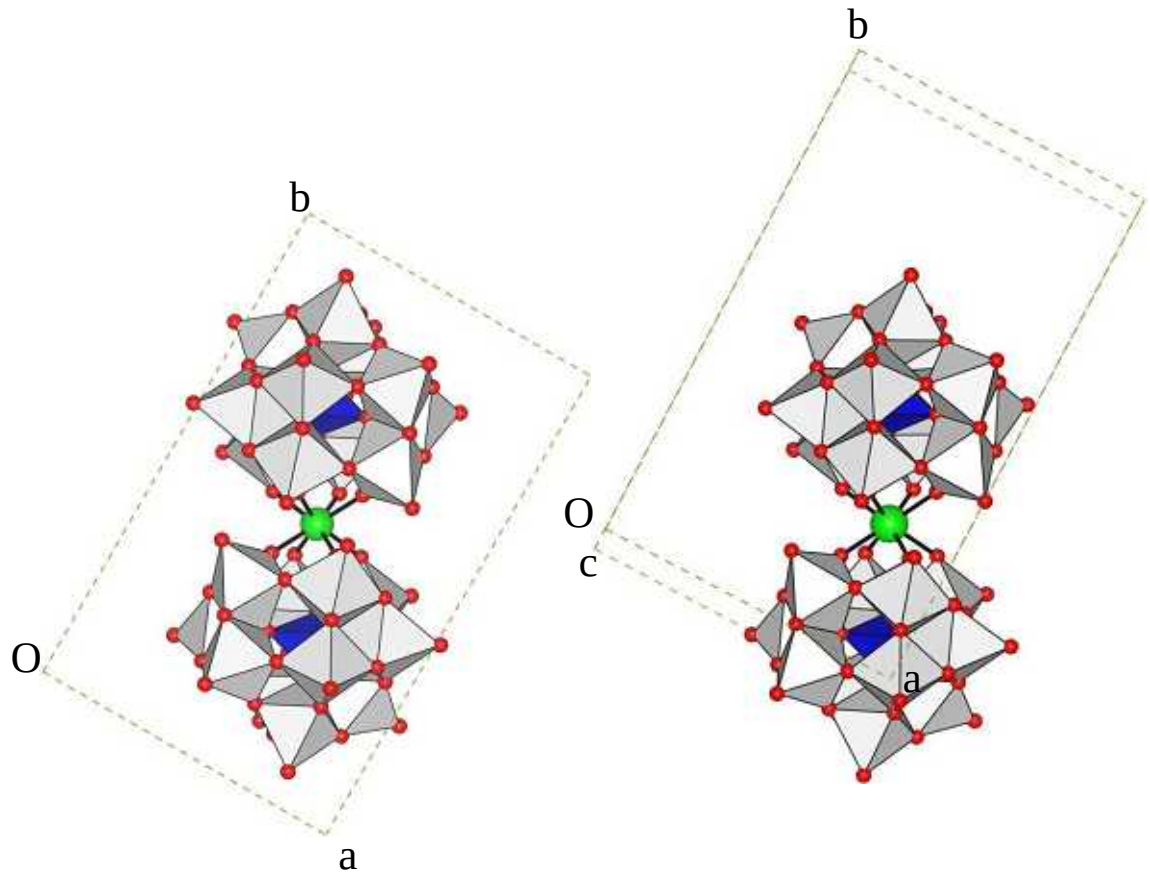

Figure 2-3. The polyanions in $[Me_2NH_2]_{10}[Hf^{IV}(\alpha\text{-}PW_{11}O_{39})_2]\cdot 8H_2O$ [7] (left) and **Ce-IV** (right) viewed along the molecular C_2 axes. Color codes are represented in the caption of **Figure 2-1**. The boxes drawn by broken lines represent the unit cells.

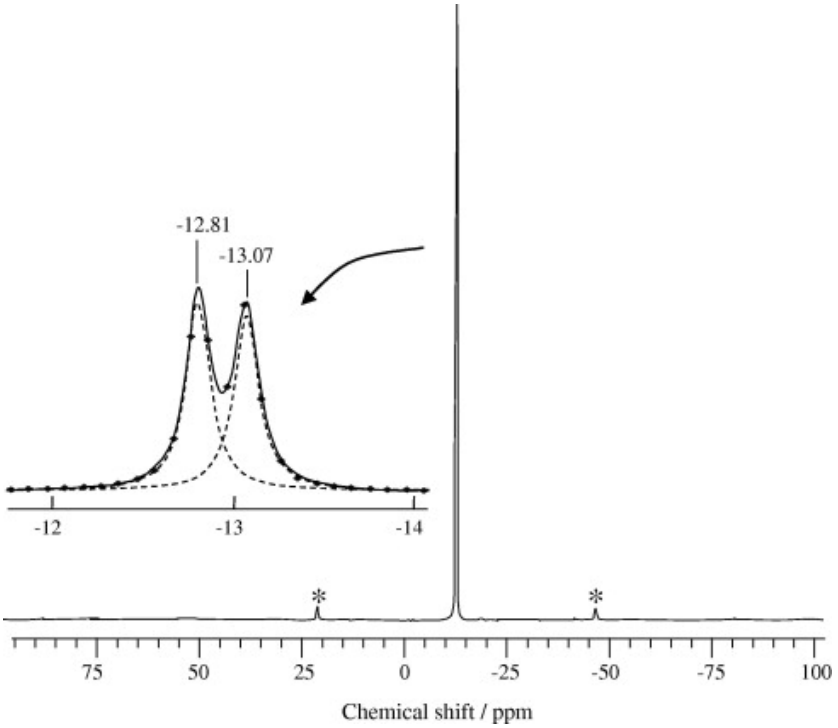

Figure 2-4. ^{31}P MAS-NMR spectrum of the **Ce-IV** solid powders. The asterisks (*) are spinning side bands. Inset: expanded spectrum in the 12-14 ppm range, where observed data (♦) were fitted with the sum (--) of two Lorentz curves (—) centered at 12.81 and 13.07 ppm with a integrated intensity ration of 1.00:0.93.

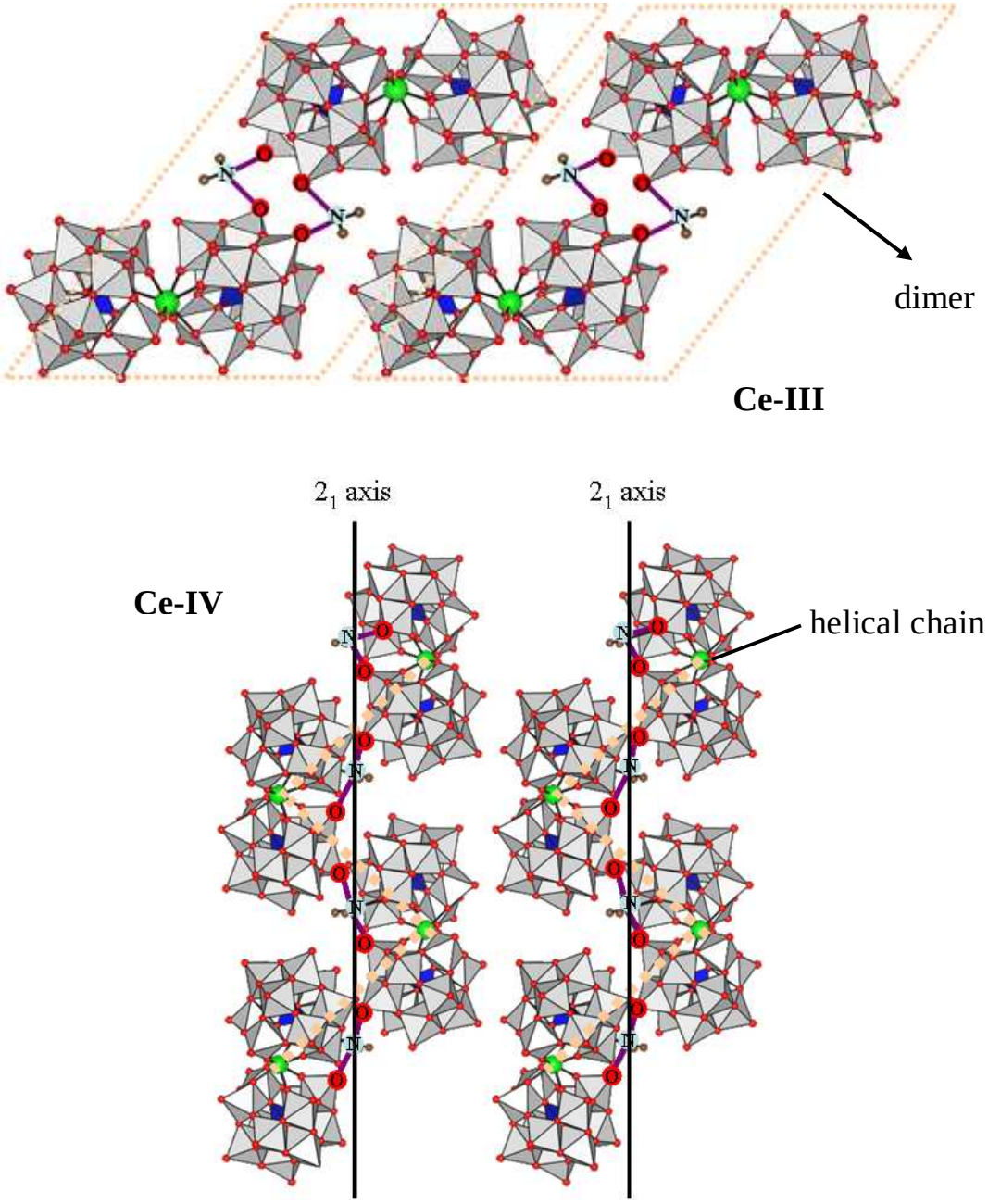

Figure 2-5. Linkage of N···O hydrogen-bonding (purple lines) between anions and DMA cations in **Ce-III** (above) and **Ce-IV** (below) viewed along the *a* axes. Lattice waters and non-linkable cations are omitted for clarity. N atom: light-blue sphere; C atom; brown sphere. Other color codes are denoted in the caption of **Figure 2-1**.

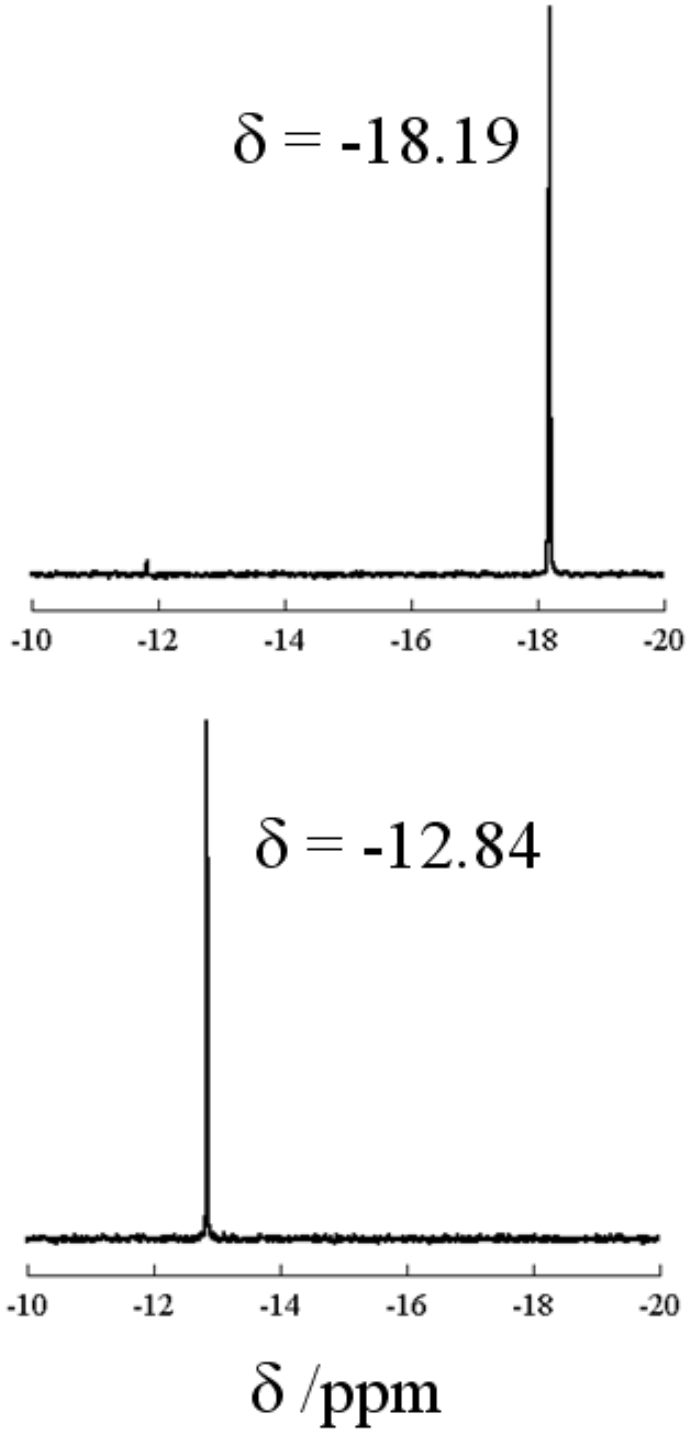

Figure 2-6. ^{31}P-NMR spectra of **Ce-III** (above) and **Ce-IV** (below) in D_2O solutions. Concentrations: 13.6 mM for **Ce-III**; saturated solution for **Ce-IV**.

Chapter 3 Controlling the coordination geometry of Ln^{3+} in $[Ln^{III}(\alpha\text{-}PW_{11}O_{39})_2]^{11-}$ (Ln = Y, La, Ce, Pr, Eu, and Er) by cationic environment

3-1 Introduction

"High coordination number" is known to be one of the characters of lanthanide (Ln) ion. By taking this original property into account in preparation, many coordination compounds containing Ln have been reported to date. For example, organometallic lanthanide complexes have received much attention in the field of nanotechnology, catalysis and biology [1-5], and inorganic metal oxides are also intensively studied due to their characteristic luminescence and magnetism [6-10]. In these materials, it is important to control and regulate their coordination chemistry and ligand field of Ln.

Polyoxometallolanthanoate (Ln-POM) is regarded as a kind of coordination compounds whose Ln is coordinated by lacunary POMs. In the case of sandwich-type $[Ln(XM_{11}O_{39})_2]^{n-}$, bearing two mono-lacunary Keggin units $[XM_{11}O_{39}]^{n-}$ as tetradentate O-donors, the central Ln ion adopts an eight-fold coordination mode (**Fig. 3-1(a)**). From the geometrical point of view, there are in theory seven types in eight-fold coordination (**Fig. 3-1(b)**), of which only cubic and square-antiprismatic (SA) coordination modes are provided for Ln in the series of $[Ln(XM_{11}O_{39})_2]^{n-}$ [11]. The coordination modes of Ln in $[Ln(\alpha\text{-}XM_{11}O_{39})_2]^{11-}$ can be expressed by relative rotation angle (ϕ) of mirror planes in $[\alpha\text{-}XW_{11}O_{39}]^{7-}$ units (**Fig. 3-2 top**), as also be described in Chapter 1. For $[Ln(\alpha\text{-}XM_{11}O_{39})_2]^{11-}$ with a cubic coordination, the rotation angle is ϕ = 0° or 180°, which corresponds to achiral polyanion with a C_{2v} or C_{2h} symmetry, respectively (**Fig. 3-2 bottom left**). On the other hand, for SA coordination, the ideal rotation angle is ϕ =

45º or 135º, which corresponds to a chiral C_2 symmetry [11] (**Fig. 3-2 bottom right**). Conformation of a series of $[Ln(\alpha\text{-}XW_{11}O_{39})_2]^{n-}$ in aqueous solutions has been particularly studied. In 1971, Fedotov et al. investigated the structures of $[Ln(\alpha\text{-}PW_{11}O_{39})_2]^{11-}$ (Ln = La^{3+} - Lu^{3+}) in aqueous solutions on the basis of ^{183}W-NMR spectroscopy, and concluded that cubic coordination species is formed for the lighter La^{3+} - Eu^{3+} ions, while SA species is formed for the heavier Gd^{3+} - Lu^{3+} ions [11]. In 1994, similar results were reported by Francesconi et al. in their ^{183}W-NMR study of aqueous $[Ln(\alpha\text{-}SiW_{11}O_{39})_2]^{13-}$ solutions; the spectrum for La^{3+} analogue allowed to expect cubic coordination type, and the spectra for Yb^{3+} and Lu^{3+} analogues allowed to expect SA coordination type [12]. However, all the isolated $[Ln(\alpha\text{-}XM_{11}O_{39})_2]^{n-}$ polyanions in crystalline solids held Ln^{3+} in a SA coordination environment (**Fig. 3-2 bottom right**) irrespective to the Ln species. Furthermore, it has not been determined that which conformation ϕ = 0º or 180º (**Fig. 3-2 bottom left**) is realized in solutions. These puzzling but basic problems should be solved, because the coordination environment (i.e. the ligand field) of Ln governs optical, luminescence, and magnetic properties of Ln-POMs arising from the characteristic $4f^n$ orbital of Ln.

In this chapter, first of all, the coordination environment of La^{3+} in $[La(\alpha\text{-}SiW_{11}O_{39})_2]^{13-}$ in potassium salt was determined by single crystal X-ray diffraction analysis, and compared with that in aqueous solutions reported by Francesconi et al. [12]. Secondly, the first example of cubic coordination type $[Ln(\alpha\text{-}PW_{11}O_{39})_2]^{11-}$ (Ln = La, Ce) was successfully synthesized by using tetramethylammonium (TMA^+) cation. Finally, the synthesis of $[Ln(\alpha\text{-}PW_{11}O_{39})_2]^{11-}$ was extended to heavier Pr, Eu, and Er lanthanides, which resulted in TMA^+ and Na^+ mixed salts of $[Ln(\alpha\text{-}PW_{11}O_{39})_2]^{11-}$ with SA conformation. These results allowed to discuss the

influence of cationic environment and ionic radius of Ln^{3+} on the molecular configuration of a series of $[Ln(\alpha\text{-}PW_{11}O_{39})_2]^{11-}$.

3-2 Experimental

3-2-1 Materials

All chemicals were commercially available and used without further purification. Starting materials for the preparation, $Na_9[A\text{-}\alpha\text{-}PW_9O_{34}]\cdot 16H_2O$ and $K_4[SiW_{12}O_{40}]\cdot 17H_2O$, were prepared according to the previous report and identified by IR spectroscopy [13].

3-2-2 Measurements

Elemental analyses of C, H, and N were performed on a Yanaco MT5 CHN CORDER. The contents of La Ce, P, and W were determined by inductively coupled plasma (ICP) atomic emission spectroscopy on an ICPS-8100 spectrometer. Raman spectra were recorded on a JASCO NRS-2100 spectrometer by using KBr disc method. These three measurements were requested to the Center for Advanced Analysis of the Tokyo Institute of Technology. IR (4000-400 cm^{-1}) spectra were recorded on a JASCO FT/IR-410 spectrometer using KBr disc method. Thermogravimetric and differential thermal analyses (TG-DTA) were conducted with a ULVAC MTS9000 + TGD9600 system. ^{31}P-NMR spectra in aqueous solutions were measured on JEOL JNM-500 spectrometer at a frequency of 202.47 MHz and Bruker Biospin AVANCE III (400MHz) at a frequency of 161.97 MHz using 85 % H_3PO_4 as an external reference.

3-2-3 Syntheses

3-2-3-1 $[Me_4N]_{10}H[La(\alpha\text{-}PW_{11}O_{39})_2]\cdot 21H_2O$ (**La-c**)

To a solution of Me_4NCl (0.28 g, 2.5 mmol) in 15 ml of H_2O was added both solid L-Proline (0.17 g, 1.5 mmol) and $LaCl_3\cdot 7H_2O$ (0.19 g, 0.5 mmol) dissolved in 3 ml of H_2O. The clear solution was heated to 60 ºC for 30 min with stirring, and the pH of the aqueous solution was adjusted to 1.5 by 1M HCl and an aqueous solution (10 ml) of $Na_9[A\text{-}\alpha\text{-}PW_9O_{34}]\cdot 16H_2O$ (2.44 g, 1.00 mmol) was added dropwise. After boiling for 1h, the solution was cooled to room temperature and the residual powders were filtered off. The resulting filtrate was left to stand at room temperature for several days. Colorless thin platelet crystals of **La-c** were obtained (yield; 0.31g, 11.5 % based on W). Found: C, 7.13; H, 1.99; N, 2.10; P, 0.95; W, 60. 39; La, 2.11; H_2O, 5.76 wt %. Calcd for $C_{40}H_{163}N_{10}O_{99}P_2LaW_{22}$: C, 7.26; H, 2.48; N, 2.12; P, 0.94; W, 61.15; La, 2.10; H_2O, 5.72 wt %. IR (KBr disk): 1485m, 1095s, 1044s, 947vs, 886m, 836s, 777s, 723m, 594w, 530w.

3-2-3-2 $[Me_4N]_{10}H[Ce(\alpha\text{-}PW_{11}O_{39})_2]\cdot 19H_2O$ (**Ce-c**)

The same procedure for **La-c** was followed, but using $CeCl_3\cdot 7H_2O$ (0.19 g, 0.5 mmol). Reddish-orange thin platelet crystals of **Ce-c** were obtained (yield; 0.31g, 11.6 % based on W). Found: C, 7.18; H, 2.03; N, 2.13; P, 0.95; W, 62.67; Ce, 2.21; H_2O, 5.27 wt %. Calcd for $C_{40}H_{163}N_{10}O_{97}P_2LaW_{22}$: C, 7.30; H, 2.44; N, 2.13; P, 0.94; W, 61.47; Ce, 2.13; H_2O, 5.20 wt %. IR (KBr disk): 1485m, 1094s, 1045s, 947vs, 888m, 830s, 781s, 732m, 594w, 543w.

3-2-3-3 $[Me_4N]_{5.5}Na_5H_{0.5}[Pr(\alpha\text{-}PW_{11}O_{39})_2]\cdot 21H_2O$ (**Pr-s**)

The same procedure for **La-c** was followed, but using $PrCl_3\cdot 7H_2O$ (0.19 g, 0.5 mmol). Light green block crystals of **Pr-s** were obtained (yield; 0.77 g, 32.8 % based on W). Found: C, 4.43; H, 1.37; N, 1.33; P, 0.95; Na, 1.90; W, 64.3; Pr, 1.97; H_2O, 6.05 wt %. Calcd for $C_{22}H_{108.5}N_{5.5}O_{99}Na_5P_2PrW_{22}$: C, 4.13; H, 1.71; N, 1.20; P, 0.97; Na, 1.80; W, 63.2; Pr, 1.97; H_2O, 5.95 wt %. IR (KBr disk): 1485m, 1094s, 1045s, 950vs, 891ms 836s, 779vs, 739s, 673w, 615w.

3-2-3-4 $[Me_4N]_{5.5}Na_5H_{0.5}[Eu(\alpha\text{-}PW_{11}O_{39})_2]\cdot 18H_2O$ (**Eu-s**)

The same procedure for **La-c** was followed, but using $EuCl_3\cdot 6H_2O$ (0.19 g, 0.5 mmol). White block crystals of **Eu-s** were obtained (yield; 1.21 g, 52.0 % based on W). Found: C, 4.39; H, 1.29; N, 1.25; P, 0.86; Na, 1.99; W, 65.4; Eu, 2.16; H_2O, 5.91 wt %. Calcd for $C_{22}H_{102.5}N_{5.5}O_{96}Na_5P_2EuW_{22}$: C, 4.16; H, 1.63; N, 1.21; P, 0.97; Na, 1.81; W, 63.7; Eu, 2.16; H_2O, 5.94 wt %. IR (KBr disk): 1486m, 1099s, 1047s, 951vs, 889s, 837s, 776vs, 734s, 595w.

3-2-3-5 $[Me_4N]_{5.5}Na_5H_{0.5}[Er(\alpha\text{-}PW_{11}O_{39})_2]\cdot 19H_2O$ (**Er-s**)

The same procedure for **La-c** was followed, but using $ErCl_3\cdot 6H_2O$ (0.19 g, 0.5 mmol). Light pink block crystals of **Er-s** were obtained (yield; 0.75 g, 32.1 % based on W). Found: C, 4.30; H, 1.31; N, 1.29; P, 0.83; Na, 1.93; W, 63.2; Er, 2.59; H_2O, 7.25 wt %. Calcd for $C_{22}H_{104.5}N_{5.5}O_{97}Na_{5.5}P_2ErW_{22}$: C, 4.14; H, 1.65; N, 1.21; P, 0.97; Na, 1.80; W, 63.3; Er, 2.62; H_2O, 6.98 wt %. IR (KBr disk): 1487m, 1105s, 1047s, 952vs, 891s, 842s, 782vs, 742s, 612w, 599w, 518w.

3-2-3-6 $[Me_4N]_{5.5}Na_3H_{2.5}[Y(\alpha\text{-}PW_{11}O_{39})_2]\cdot 22H_2O$ (**Y-s**)

The same procedure for **La-c** was followed, but using $YCl_3\cdot 6H_2O$ (0.15 g, 0.5 mmol). White block crystals of **Y-s** were obtained (yield; 0.89 g, 38.3 % based on W). Found: C, 4.38; H, 1.30; N, 1.34; H_2O, 6.17 wt %. Calcd for $C_{22}H_{112.5}N_{5.5}O_{100}Na_3P_2YW_{22}$: C, 4.18; H, 1.79; N, 1.22; H_2O, 6.27wt %. IR (KBr disk): 1484s, 1105m, 1048s, 950vs, 891m, 844m, 773m, 738w, 595w, 513w.

3-2-3-7 $K_{12}H[La(\alpha\text{-}SiW_{11}O_{39})_2]\cdot 25H_2O$ (**La-K**)

$K_4[SiW_{12}O_{40}]\cdot 17H_2O$ (6.06 g, 2.00 mmol) was dissolved in 20 ml of H_2O and the pH was adjusted to 7 with 1M KOH aqueous solution. $LaCl_3\cdot 7H_2O$ (0.33 g. 1.00 mmol) in 5 ml of H_2O was dropped into the solution, then the solution was stirred at 80 °C for 1h and allowed to cool to room temperature. KCl (0.37 g, 5.00 mmol) was added and further heated at 80 °C for 30 min with stirring. After cooling to room temperature, the residual powders were filtered off, and the filtrate was left to stand at room temperature for several days. Colorless block crystals of **La-K** were obtained (yield; 4.02 g, 63.3% based on W). Found: H, 0.79; H_2O, 7.10 wt %. Calcd for $H_{51}K_{12}O_{103}Si_2LaW_{22}$: H, 0.80; H_2O, 7.16 wt %. IR (KBr disk): 1003w, 948s, 886s, 822w, 765s, 724w, 535m.

3-2-4 X-ray Crystallography

The reflection data for the single crystal X-ray analysis of **La-c**, **Pr-s**, **Eu-s**, and **Er-s**, **Y-s,** and **La-K** were collected on a Rigaku RAXIS-RAPID imaging plate diffractometer with a graphite monochromatized MoK_α radiation (λ = 0.7107 Å) at 203-213 K. All of the structures were solved by the direct method SHELXS-97 [14] and refined by the full-matrix least squares on F^2 using the CrystalStructure [15]. All of the

atoms except for three O atoms (O107, O108 and O114) in **La-c** and the W, Si, P, Na, K, Pr, Eu, Er, Y atoms in **Pr-s**, **Eu-s**, and **Er-s Y-s**, and **La-K** were refined anisotropically and the other atoms in all of the compounds isotropically. The H atoms were not included in the refinements for all of the compounds.

The single crystal X-ray diffraction analysis of **Ce-c** was carried on a Rigaku RAXIS-RAPID II imaging plate diffractometer with graphite monochromatized filtered CuK_α radiation (λ = 1.5419 Å) at 93 K. The structure was solved by the direct method SHELXS-97 [14] and refined by the full-matrix least-squares on F^2 using the CrystalStructure [15]. The W, Ce, P and O atoms except for the water oxygen were refined anisotropically, and all of the C and N atoms in the TMA^+ cations isotropically. The nine oxygen atoms of water molecules (O101-O109) were occupied with a half-occupancy. The H atoms were not included in the refinements. The crystallographic data and the results of structure refinement are summarized in **Table 3-1**. The final atomic coordinates with thermal parameters ($B_{eq/iso}$) of the polyanion in **La-c** and **Pr-s** **La-K** are also summarized in **Table 3-2**.

3-3 Results and discussion

3-3-1 Crystal structure of **La-K**

La-K crystallizes in triclinic P-1 and consists of $[La(\alpha\text{-}SiW_{11}O_{39})_2]^{13-}$ polyanion and partially disordered K^+ cations and waters of crystallization. The polyanion is composed of two mono-lacunary Keggin $[\alpha\text{-}SiW_{11}O_{39}]^{8-}$ units sandwiching the central La^{3+} in SA coordination environment, which is disagreement with the Francesconi's result, i.e. the cubic coordination presumed by ^{183}W-NMR study in aqueous solution. The bond length of La-O are in the range of 2.458(10)-2.531(11) Å, which are

comparable to that of $[La^{III}(\alpha\text{-}PW_{11}O_{39})_2]^{11-}$ (2.467(7)-2.513(6) Å, average 2.490 Å) in $K_2H_7[\{Ln(PW_{11}O_{39})_2\}\{Cu_2(bpy)_2(\mu\text{-}ox)\}]\cdot 18H_2O$ [16]. The result possibly comes from an occurrence of cubic to SA structural conversion in crystallization process, involving a rotation of the $[\alpha\text{-}SiW_{11}O_{39}]^{8-}$ moiety. This result also demonstrates that, not only the ionic radius of Ln^{3+} but also the polyanion surrounding influences the molecular conformation. **Fig. 3-3** shows arrangement of K^+ cations around the $[La(\alpha\text{-}SiW_{11}O_{39})_2]^{13-}$ polyanion, where there are more than 30 K^+ ions that can attach to the polyanion's O atoms via K–O bonding. When **La-K** is dissolved to water, these K^+ ions would be released from the polyanion and subjected to water solvation, and the polyanion would be situated in a dynamically averaged and diminished isotropic cationic potential in aqueous solutions. Therefore, it is suggested that such isotropic cationic potential in solution induced the cubic conformation of the polyanion. In other words, a direct attachment of K^+ to the polyanion in the crystallization process may give rise to the cubic-to-SA structure conversion.

The BVS values [17] on based on the observed bond lengths are 3.3 for La, 3.9-4.0 for Si, 5.9-6.1 for W. These values are consistent with the original valences of La^{3+}, Si^{4+} and W^{6+}.

3-3-2 Molecular and crystal structures of **La-c** and **Ce-c**

Both of **La-c** and **Ce-c** were prepared by the reaction between respective Ln^{3+} ions and tri-lacunary Keggin $[A\text{-}\alpha\text{-}PW_9O_{34}]^{9-}$ in a 1:2 ratio in acidic aqueous solutions, and crystallized isostructurally in a monoclinic space group $P2_1/a$. The L-proline added in the preparation is thought to have a pH buffering effect, and is not included in the products. The polyanions in their structures are composed of two mono-lacunary

Keggin $[\alpha\text{-}PW_{11}O_{39}]^{7-}$ units sandwiching the central Ln^{3+} ion in a cubic coordination environment. The polyanion has an approximate C_{2h} symmetry with ϕ = 180º, where Ln^{3+} is imposed on the crystallographic inversion center (**Fig. 3-4(a)**, **(c)**). The bond lengths of Ln-O are in the range of 2.495(7)-2.537(7) Å for **La-c** and 2.43(1)-2.51(1) Å for **Ce-c**. They are comparable to the Ln-O distances in the same or related polyanions with SA conformation in $K_2H_7[\{La^{III}(PW_{11}O_{39})_2\}\{Cu_2(bpy)_2(\mu\text{-}ox)\}]\cdot 18H_2O$ (2.467(7)-2.513(6) Å, average 2.490 Å) [16], and in $Na_9[Ce^{III}W_{10}O_{36}]\cdot 34H_2O$ (2.43(2)-2.55(2) Å, average 2.473 Å) [18] and $K_{8.5}H_{3.5}[Ce^{III}(W_5O_{18})(\alpha\text{-}BW_{11}O_{39})]\cdot 25H_2O$ (2.39(4)-2.54(3) Å, average 2.469 Å) [19], respectively. The bond valence sums (BVS) [17] calculated from the bond lengths are 3.2 for La, 5.1 for P, 6.0–6.1 for W in **La-c**, and 3.4 for Ce, 5.1 for P, 6.0–6.4 for W in **Ce-c**, respectively. These values reasonably correspond to their formal valences of La^{3+}, Ce^{3+}, P^{5+} and W^{6+}. In a $[Ln(\alpha\text{-}PW_{11}O_{39})_2]^{11-}$ polyanion with SA conformation, there are two terminal O_A atoms, which are in close proximity to $O_{A'}$ atoms in another $[\alpha\text{-}PW_{11}O_{39}]^{7-}$ unit (**Fig. 3-3(b)**). As will be described in Chapter 6 in greater detail, the resulting $O_A\cdots O_{A'}$ interaction influences the conformation of the $[Ln(\alpha\text{-}PW_{11}O_{39})_2]^{11-}$ polyanion. The distance of $O_A\cdots O_{A'}$ in a hypothetic polyanion with ϕ = 0º will be the shortest, affording the highest steric repulsion between the two $[\alpha\text{-}PW_{11}O_{39}]^{7-}$ units. On the other hand, the cubic conformation (**Fig. 3-3(a)**) has the longest $O_A\cdots O_{A'}$ distance (8.46(1) Å; **La-c**, 8.36(2) Å; **Ce-c**) in the all conformations, and this stabilizes the polyanion (the $O_B\cdots O_{A'}$ distance is long enough (4.30(1) Å; **La-c**, 4.23(2) Å; **Ce-c**). In conclusion, the polyanion with ϕ = 180º is more stable than that with ϕ = 0º.

The crystal structure of **La-c** projected on the *ab* plane is shown in **Fig. 3-5(a) left**. The longitudinal direction of the polyanion is tilted with respect to the *b* axis, forming a

zigzag arrangement along *b*. Viewed from the *a* axis, it seems that layers of polyanion are stacked perpendicular to the *c* axis (**Fig. 3-5(a) right**). The polyanins and surrounding TMA^+ cations in **La-c** are shown in **Fig. 3-6(a)**, where N···O distances are in the range of 3.762(10)-4.226(12) Å. The N1 atom in a TMA^+ cation is located in proximity to La^{3+} with the La···N1 distance of 4.163(10) Å (**Fig. 3-6(b)**). The TMA^+ cations are symmetrically located around the polyanion; the P···N distances around a $[\alpha\text{-}PW_{11}O_{39}]^{7-}$ unit are in the 6.958(10)-7.726(8) Å range with a hexagonal arrangement (**Fig. 3-6(c)**). Taking a low hydrogen-bonding ability of the TMA^+ cation into account, the observed highly symmetrical arrangement of TMA^+ probably allows the polyanion to exist in a weak and isotropic electrostatic potential, which seems to stabilize the cubic coordination of the $[Ln(\alpha\text{-}PW_{11}O_{39})_2]^{11-}$ polyanion.

3-3-3 Molecular and crystal structures of **Pr-s**, **Eu-s**, **Er-s**, and **Y-s**

All of the isostructural **Pr-s**, **Eu-s**, **Er-s**, and **Y-s** were prepared by the same synthetic procedure of **La-c** and **Ce-c**. They all are isomorphous and crystallized in a monoclinic space group P2/n, which is different from that ($P2_1/a$) of **La-c** and **Ce-c**. The polyanions in their structures are composed of two mono-lacunary Keggin $[\alpha\text{-}PW_{11}O_{39}]^{7-}$ units sandwiching the central Ln^{3+} ion in a square-antiprismatic (SA) coordination environment. The polyanions have an approximate C_2 symmetry, indicating that this structure is optically active (**Fig. 3-4(b)**, **(d)**). The bond lengths of Ln–O are in the range of 2.444(11)-2.479(11) Å for **Pr-s**, 2.393(16)-2.439(16) Å for **Eu-s**, 2.336(13)-2.370(12) Å for **Er-s**, and 2.348(11)-2.380(13) Å for **Y-s**. These values are comparable to those in $[Pr^{III}(W_5O_{18})_2]^{9-}$ (2.43(2)-2.54(2) Å, average 2.481 Å) [20], $[Eu^{III}(W_5O_{18})_2]^{9-}$ (2.40(3)-2.46(3) Å, average 2.429 Å) [21], $[Er^{III}(W_5O_{18})_2]^{9-}$

(2.339(3)-2.387(3) Å, average 2.367 Å) [22], and $[(YOH_2)_3(CO_3)(A\text{-}\alpha\text{-}PW_9O_{34})_2]^{11-}$ (2.22(2)-2.462(12) Å, average 2.316 Å) [23]. The BVS values [19] based on the observed bond lengths are 3.3 for Pr, 5.1 for P, 5.9-6.2 for W in **Pr-s**, 3.2 for Eu, 5.3 for P, 5.8-6.2 for W in **Eu-s**, 3.2 for Er, 5.1 for P, 5.7-6.1 for W in **Er-s**, 3.2 for Y, 5.1 for P, 5.9-6.1 for W in **Y-s**, respectively. These values are consistent with the original valences of Pr^{3+}, Eu^{3+}, Er^{3+}, Y^{3+}, P^{5+} and W^{6+}.

Fig. 3-5(b) shows the crystal structure of **Pr-s** projected on the *bc* plane. The polyanion is surrounded by partially disordered Na^+ with a ring-shaped arrangement (pink dotted lines). Like the structure of $[Me_4N]_4Na_3H_4[Pr(\alpha\text{-}PW_{11}O_{39})_2]\cdot 12H_2O$ reported by Fan et at. [24], one of the Na^+ cations links the two $[\alpha\text{-}PW_{11}O_{39}]^{7-}$ units via O–Na–O bonding which seems to lock the twist angle (ϕ) of the $[\alpha\text{-}PW_{11}O_{39}]^{7-}$ units as will be discussed in Chapter 6. Due to the existence of these Na^+ cations, TMA^+ cations around a polyanion are positioned asymmetrically. It is suggested that the SA coordination mode of Ln is favored in **Pr-s**, **Eu-s**, **Er-s**, and **Y-s** rather than cubic coordination due to the anisotropic and asymmetric cationic potential by surrounding Na^+ with strong coordination ability to the polyanion (**Fig. 3-7**).

3-3-4 Structural and spectrochemical properties of the $[Ln(\alpha\text{-}PW_{11}O_{39})_2]^{11-}$ anions with cubic and SA conformations

<Effect on the Structures>

To examine the effect of ionic radius (R_{Ln}) [25] of the central Ln^{3+} ion on the overall geometry of the polyanion, intramolecular P···P (d(P···P)) distances in **La-c**, **Ce-c**, **Pr-s**, **Eu-s**, **Er-s**, and **Y-s** were plotted against R_{Ln} (**Fig. 3-8**). In the case of **Pr-s**, **Eu-s**, **Er-s**, and **Y-s** with SA coordination, a linear correlation was observed. This

tendency results from a decrease of Ln-O bond distance with decreasing of R_{Ln}. However, a drastic jump of 0.252 Å occurred between **Pr-s** and **Ce-c**. In order to understand the gap of *d*(P···P) through the conformational change from SA to cubic, a hypothetical $[Ce(\alpha\text{-}PW_{11}O_{39})_2]^{11-}$ polyanion with SA coordination is considered. The geometrical arrangements of P and Ln in the polyanion for **Ce-c** and **Pr-s** are schematically described in **Fig. 3-9**. The ∠(P-Ln-P) angle in **Pr-s** is approximately 161º, which is almost invariable through **Pr-s** to **Er-s** (**Fig. 3-9 right**). The hypothetical $[Ce(\alpha\text{-}PW_{11}O_{39})_2]^{11-}$ with SA coordination was modeled by rotating the $[\alpha\text{-}PW_{11}O_{39}]^{7-}$ unit so that the angle ∠(P-Ce-P') was adjusted to 161º under the constant *d*(Ce···P). The resulting hypothetical model has *d*(P···P') = 9.124 Å, which is still longer by 0.139 Å than that in **Pr-s**. It is understood that the remaining difference (0.139 Å) between *d*(P···P) (8.985(4) Å) in **Pr-s** and the hypothetical model (9.124 Å) corresponds to the expansion of the LnO_8 polyhedron through the exchange of Ln from Pr and Ce and conformational change from SA to cubic. In summary, the 0.252 Å jump of *d*(P···P) from **Pr-s** to **Ce-c** is a sum of contributions of purely rotation effect (0.114 Å) of the $[\alpha\text{-}PW_{11}O_{39}]^{7-}$ units and increase of spacing between $\{O_4\}$-squares (0.139 Å) in the LnO_8 polyhedron along with the change from SA to cubic. The latter would include the small contribution of R_{Ln} (because of similar R_{Ln} between Pr^{3+} and Ce^{3+}) and major influence of $O_4\cdots O_4$ repulsion.

<Effect on vibrational spectra>

The effect of geometrical change around Ln^{3+} derived from the coordination modes of $[\alpha\text{-}PW_{11}O_{39}]^{7-}$ units were investigated by IR and Raman spectroscopy. In the case of IR spectra, similar spectral patterns were observed for all the compounds (**Fig. 3-10**).

Full assignments in the region of 1200-600 cm^{-1} are listed in **Table 3-3**. Compared with the starting material $Na_9[A\text{-}\alpha\text{-}PW_9O_{34}]\cdot 16H_2O$, the peaks attributed to asymmetric stretching mode of ν(P-O) and ν(W-O) in the region of 1100-950 cm^{-1} shifted to higher frequency region. While, the red shift and split of the peaks belong to ν(W-O-W) asymmetric stretching mode were also observed in the region of 900-750 cm^{-1}. Thus, these observations are probably due to the structure change to $[\alpha\text{-}PW_{11}O_{39}]^{7-}$ and its coordination to Ln^{3+}. For the Raman spectroscopy, a small difference of two $\nu(W\text{-}O_t)$ stretching modes in the region of 1000-950 cm^{-1} was observed [26]; two peaks for cubic coordination species shifted to lower frequency region (**Fig. 3-11**). Generally, it was reported that $\nu(W\text{-}O_t)$ stretching modes in Keggin units are sensitive to certain interactions such as hydrogen bonding or electrostatic polyanion···polyanion interaction [27]. The former causes a red shift, while the latter a blue shift. The observed red shift for cubic coordination species may be responsible for the larger spacing of $[\alpha\text{-}PW_{11}O_{39}]^{7-}$ units than SA coordination species (**Fig. 3-8**). In summary, it is suggested that the difference in the gap of intramolecular d(P···P) between SA and cubic coordination modes could be perceptibly detected by Raman spectroscopy.

<Solution NMR spectroscopy>

The ^{31}P-NMR spectra of fresh saturated aqueous solutions of **La-c** (35 mM) and **Ce-c** (47 mM) show three resonance peaks (**Fig. 3-12**), suggesting that partial dissociations of polyanions occurred. Referring to the study on solution chemistry of $[Ce(PW_{11}O_{39})_2]^{11-}$ [**28**], the shifts -11.2, -16.7, and -21.0 ppm with a 1:5:1 ratio for **Ce-c** are assignable to $[PW_{11}O_{39}]^{7-}$, $[Ce(PW_{11}O_{39})_2]^{11-}$, and $[Ce(H_2O)_n(PW_{11}O_{39})]^{4-}$, respectively. Similarly, the spectrum of **La-c** can also be assigned to $[PW_{11}O_{39}]^{7-}$ (-11.2

ppm), $[La(PW_{11}O_{39})_2]^{11-}$ (-11.5 ppm), and $[La(H_2O)_n(PW_{11}O_{39})]^{4-}$ (-11.7 ppm) species with a 1:2:1 ratio. The dissociation is describable as follows,

$$[Ln(PW_{11}O_{39})_2]^{11-} + nH_2O \rightarrow [Ln(H_2O)_n(PW_{11}O_{39})]^{4-} + [PW_{11}O_{39}]^{7-}$$

The lower concentration for **Ce-c** would cause the higher dissociation. No such partial dissociation was reported for the Na salt solutions of $[Ln(PW_{11}O_{39})_2]^{11-}$ (Ln = La, Ce). In contrast, the spectra of **Pr-s** (27 mM), **Eu-s** (20 mM), and **Er-s** (20 mM) showed main single peaks at -12.6, -1.2, and 68.6 ppm, respectively (**Fig. 3-13**), which is assignable to the corresponding $[Ln(\alpha\text{-}PW_{11}O_{39})_2]^{11-}$ species [11]. Also, the other peaks with very small integration at *c.a.* -11.7 ppm were observed for three compounds, which can be assigned to $[\alpha\text{-}PW_{11}O_{39}]^{7-}$. Therefore, despite lower concentrations than **La-c** and **Ce-c**, the partial dissociation of the polyanion hardly occurs through dissolution in aqueous solutions, probably due to the presence of Na^+ cations. Thus, the behavior of the $[Ln(\alpha\text{-}PW_{11}O_{39})_2]^{11-}$ in aqueous solutions are dependent on the cationic environment. Since the ^{31}P-NMR spectroscopy provides no information on the coordination geometry of the LnO_8 center, we attempted to observe ^{183}W-NMR spectra of **La-c** and **Ce-c**. Unfortunately, the measurement was unsuccessful because of their low solubility to water.

3-4 Conclusion

The successful isolation and structural characterization of **La-K** revealed that cubic and SA conformation are adopted in an aqueous solution and in the solid state, respectively. This observation suggests that attachment of many K^+ cations on

crystallization breaks an isotropic cationic environment around the polyanion, which induces the SA conformation. **La-c** and **Ce-c** with a cubic coordination were successfully isolated by the balanced isotropic arrangement of TMA^+. Structural analysis of **La-c** and **Ce-c** determined the twist angle ϕ = 180º of cubic conformation. Structural investigation of a series of $[Ln(\alpha\text{-}PW_{11}O_{39})_2]^{11-}$ (Ln = La, Ce, Pr, Eu, Er, and Y) shows the R_{Ln} as well as the cationic environment around the polyanion is a key factor of directing the molecular conformation.

3-5 References

[1] K. Gholivand, H. R. Mahzouni, M. Pourayoubi, S. Amiri, *Inorg. Chim. Acta.*, **363(10)**, 2318 (2010).

[2] M. A. Katkova, T. V. Balashova, V. A. Ilichev, A. N. Konev, N. A. Isachenkov, G. K. Fukin, S. Y. Ketkov, M. N. Bochkarev, *Inorg. Chem.*, **49(11)**, 5094 (2010).

[3] J. A. Nathanson, R. Freedman, B. J. Hoffer, *Nature*, **261**, 330 (1976).

[4] Z. Y. Hao, Q. W. Liu, J. Xu, L. Jia, S. B. Li, *Chem. Pharm. Bull.*, **58(10)**, 1306 (2010).

[5] T. Nitabaru, N. Kumagai, M. Shibasaki, *Molecules*, **15(3)**, 1280 (2010).

[6] S. Wang, R. Deng, H. Guo, S. Song, F. Cao, X. Li, S. Su, H. Zhang, *Dalton Trans.*, **39**, 9153 (2010).

[7] C. H. Hervoches, C. Greaves, *J. Mater. Chem.*, **20(32)**, 6759 (2010).

[8] V. Venkatramu, M. Giarola, G. Mariotto, S. Enzo, S. Polizzi, C. K. Jayasankar, F. Piccinelli, M. Bettinelli, A. Speghini, *Nanotechnology*, **21(17)**, 175703 (2010).

[9] R. T. Wegh, H. Donker, K. D. Oskam, A. Meijerink, *Science*, **29**, 663 (1999).

[10] Y. Ma, X. Wang, S. Li, M.S. Toprak, B. Zhu, M. Muhammed, *Adv. Mater.*, **22(14)**, 1640 (2010).

[11] M. A. Fedotov, B. Z. Pertsikov, D. K. Danovich, *Polyhedron* **9**, 1249 (1990).

[12] J. Bartis, S. Sukal, M. Dankova, E. Kraft, R. Kronzon, M. Blumenstein, L. C. Francesconi, *J. Chem. Soc., Dalton Trans.*, 1937 (**1997**).

[13] A. P. Ginsburg, *Inorg. Synth.*, **27**, 96 (1990).

[14] G. M. Sheldrick, SHELXS-97, Program for Crystal Structure Solution, University of Gettingen, Germany, 1997.

[15] G. M. Sheldrick, SHELXL-97, Program for Crystal Structure Refinement, University of Gettingen, Germany, 1997.

[16] J. Cao, S. Liu, R. Cao, L. Xie, Y. Ren, C. Gao, L. Xu, *Dalton Trans.*, 115 (2008).

[17] I. D. Brown, "Structure and Bonding in Crystals," ed by M. O'keeffe, A. Navrotsky, Academic Press, New York **Vol. II**, 1 (1980).

[18] G. Xue, B. Liu, W. Wang, Q. Li, H. Li, *Acta Chim. Sin.*, **60**, 2022 (2002).

[19] H. Naruke, T. Yamase, *Bull. Chem. Soc. Jpn.*, **73**, 375 (2000).

[20] T. Ozeki, T. Yamase, *Acta. Crystalllogr.*, **B50**, 128 (1994).

[21] M. Sugeta, T. Yamase, *Bull. Chem. Soc. Jpn.*, **66**, 444 (1993).

[22] M. A. AlDamen, S. Cardona-Serra, M. Clemente-Juan, E. Coronado, A. Gaita-Ariño, C. Marti-Gastaldo, F. Luis, O. Montero, *Inorg. Chem.*, **2009**, *48*, 3467-3479.

[23] X. Fang, T. M. Anderson, W. A. Neiwert, C. L. Hill, *Inorg. Chem.*, **42**, 8600 (2003).

[24] L. Fan, L. Xu, C. Zhang, F. Li, Z. Li, X. Liu, *Struct. Chem.*, **18**, 917 (2007).

[25] R. D. Shannon, *Acta Crystallogr.*, **A32**, 751 (1976).

[26] T. Okuhara, N. Mizuno, M. Misono, *Advances in Catalysis*, Academic Press, Inc. **46**, 113 (1996).

[27] (a) M. Fournier, R. Thouvenot, C. R. Deltcheff, *J. Chem. Soc. Faraday Trans.*, **87**, 349 (1991). (b) C. R. Deltcheff, M. Fournier, R. Franck, R. Thouvenot, *Inorg. Chem.*, **22**, 207 (1983).

[28] N. Belai, M. Sadakane, M. T. Pope, *J. Am. Chem. Soc.*, **123**, 2087 (2001).

Table 3-1. Crystallographic data and refinement results of **La-c** and **Ce-c**.

	La-c	**Ce-c**
Empirical formula	$C_{40}H_{163}N_{10}O_{99}P_2W_{22}La$	$C_{40}H_{159}N_{10}O_{97}P_2W_{22}Ce$
Formula weight	6614.29	6579.47
Crystal system	Monoclinic	Monoclinic
Space group	$P2_1/a$	$P2_1/a$
a (Å)	13.2348(2)	13.1835(4)
b (Å)	39.0392(7)	38.3734(9)
c (Å)	13.2435(2)	13.0234(5)
β (°)	90.6854(7)	90.688(3)
V (Å^3)	6842.1(2)	6588.0(4)
Z	2	2
θ range (°)	3.0-27.5	4.8-68.2
Limiting indices reflections	$-17 \leqq h \leqq 17$	$-15 \leqq h \leqq 15$
	$-50 \leqq k \leqq 50$	$-46 \leqq k \leqq 46$
	$-17 \leqq l \leqq 17$	$-15 \leqq l \leqq 15$
Crystal size (mm^3)	0.28 × 0.21 × 0.05	0.13 × 0.10 × 0.10
D_c (g cm^{-3})	3.210	3.317
F(000)	5960.00	5922.00
μ (mm^{-1})	18.857	38.152
Todal data collected	109753	77304
Unique data	15682	12051
[$R_{(int)}$]	0.078	0.106
Goodness-of-fit (GOF)	1.073	1.067
R_1 [$I > 2\sigma(I)$][a]	0.0405	0.0777
wR_2[b]	0.0959	0.1828

[a] $R_1 = (\Sigma||F_0|-|F_c||)/(\Sigma|F_c|)$.

[b] $wR_2 = \Sigma[w(F_0^2-F_c^2)^2]/\Sigma[w(F_0^2)^2]^{1/2}$.

w (for **La-c**) = $1/[\sigma^2(F_0^2) + (0.0227 \cdot P)^2 + 128.3373 \cdot P]$, where $P = (Max(F_0^2,0) + 2F_c^2)/$

w (for **Ce-c**) = $1/[\sigma^2(F_0^2) + (0.0490 \cdot P)^2 + 393.8222 \cdot P]$, where $P = (Max(F_0^2,0) + 2F_c^2)/$

Table 3-1. (Continued) Crystallographic data and refinement results of **Pr-s**, **Eu-s**, **Er-s**, and **Y-s**.

	Pr-s	**Eu-s**	**Er-s**	**Y-s**
Empirical formula	$C_{22}H_{108.5}N_{5.5}O_{99}Na_5P_2W_{22}Pr$	$C_{22}H_{102.5}N_{5.5}O_{96}Na_5P_2W_{22}Eu$	$C_{22}H_{104.5}N_{5.5}O_{97}Na_5P_2W_{22}Er$	$C_{22}H_{112.5}N_{5.5}O_{97}Na_3P_2W_{22}Y$
Formula weight	6397.08	6354.09	6387.40	6319.13
Crystal system	Monoclinic	Monoclinic	Monoclinic	Monoclinic
Space group	P2/n	P2/n	P2/n	P2/n
a (Å)	13.2007(3)	13.2390(9)	13.3015(3)	13.2437(6)
b (Å)	12.6355(3)	12.6686(9)	12.6718(3)	12.6727(6)
c (Å)	35.4266(7)	35.208(3)	34.9283(8)	35.023(2)
β (°)	98.1765(7)	97.970(2)	98.1050(8)	97.751(2)
V (Å^3)	5849.0(2)	5848.0(7)	5828.5(3)	5824.4(5)
Z	2	2	2	2
θ range (°)	3.1-27.5	3.1-27.4	3.0-27.7	3.0-27.5
Limiting indices reflections	-17≦h≦17 -16≦k≦15 -45≦l≦45	-17≦h≦17 -16≦k≦16 -45≦l≦45	-17≦h≦17 -14≦k≦16 -45≦l≦45	-17≦h≦16 -16≦k≦16 -45≦l≦45
Crystal size (mm^3)	0.28 × 0.28 × 0.13	0.18 × 0.14 × 0.09	0.38 × 0.24 × 0.20	0.25 × 0.19 × 0.08
D_c (g cm^{-3})	3.632	3.608	3.639	3.603
F(000)	5686.00	5634.00	5664.00	5626.00
μ (mm^{-1})	22.1183	22.2385	22.4956	22.2893
Todal data collected	89139	90367	79892	87054
Unique data	13372	13364	12670	13332
[$R_{(int)}$]	0.1292	0.1215	0.0984	0.112
Goodness-of-fit (GOF)	1.150	1.128	1.138	1.091
R_1 [$I > 2\sigma(I)$][a]	0.0601	0.0878	0.0591	0.0651
wR_2[b]	0.1486	0.2425	0.1382	0.1438

[a] $R_1 = (\Sigma||F_0|-|F_c||)/(\Sigma|F_c|)$.

[b] $wR_2 = \Sigma[w(F_0^2-F_c^2)^2]/\Sigma[w(F_0^2)^2]^{1/2}$.

w (for **Pr-s**) = $1/[\sigma^2(F_0^2) + (0.0000\cdot P)^2 + 216.5132\cdot P]$, where $P = (\mathrm{Max}(F_0^2,0) + 2F_c^2)/$

w (for **Eu-s**) = $1/[\sigma^2(F_0^2) + (0.1192\cdot P)^2 + 144.7737\cdot P]$, where $P = (\mathrm{Max}(F_0^2,0) + 2F_c^2)/$

w (for **Er-s**) = $1/[\sigma^2(F_0^2) + (0.0000\cdot P)^2 + 226.4720\cdot P]$, where $P = (\mathrm{Max}(F_0^2,0) + 2F_c^2)/$

w (for **Y-s**) = $1/[\sigma^2(F_0^2) + (0.0189\cdot P)^2 + 306.8065\cdot P]$, where $P = (\mathrm{Max}(F_0^2,0) + 2F_c^2)/3$

Table 3-1. (Continued) Crystallographic data and refinement results of **La-K**.

	La-K
Empirical formula	$H_{51}K_{12}O_{103}W_{22}SiLa$
Formula weight	6408.30
Crystal system	Triclinic
Space group	P-1
a (Å)	13.7106(4)
b (Å)	19.6276(6)
c (Å)	20.5955(6)
α (°)	110.2554(8)
β (°)	105.2506(8)
γ (°)	98.4287(8)
V (Å^3)	4840.5(3)
Z	2
θ range (°)	3.0-27.4
Limiting indices reflections	-15≦h≦17
	-25≦k≦25
	-26≦l≦26
Crystal size (mm^3)	0.25 × 0.16 × 0.09
D_c (g cm^{-3})	4.396
F(000)	5632.00
μ (mm^{-1})	27.1422
Todal data collected	78718
Unique data	21992
[$R_{(int)}$]	0.1099
Goodness-of-fit (GOF)	1.055
R_1 [$I > 2\sigma(I)$][a]	0.0446
wR_2[b]	0.1184

[a] $R_1 = (\Sigma||F_0|-|F_c||)/(\Sigma|F_c|)$.

[b] $wR_2 = \Sigma[w(F_0^2-F_c^2)^2]/\Sigma[w(F_0^2)^2]^{1/2}$.

w (for **La-K**) = $1/[\sigma^2(F_0^2) + (0.0142\cdot P)^2 + 134.0813\cdot P]$, where $P = (Max(F_0^2,0) + 2F_c^2$

Table 3-2 Atomic coordinates and B_{eq} ($Å^2$) of **La-c**.

atom	x	y	z	Beq	occ
W(1)	0.23761(2)	0.044054(9)	0.88130(3)	2.036(6)	
W(2)	0.46877(3)	0.071460(10)	0.76501(3)	2.107(6)	
W(3)	0.61363(2)	0.091155(9)	1.10195(3)	1.897(6)	
W(4)	0.39799(3)	0.065477(10)	1.21403(3)	2.121(6)	
W(5)	0.15063(2)	0.085763(10)	1.09444(3)	2.026(6)	
W(6)	0.60228(2)	0.140345(9)	0.86308(3)	1.992(6)	
W(7)	0.13874(3)	0.127720(10)	0.86739(3)	2.273(7)	
W(8)	0.37392(3)	0.155557(9)	0.74502(3)	2.083(6)	
W(9)	0.51787(3)	0.182032(9)	1.09432(3)	2.358(7)	
W(10)	0.29759(3)	0.155719(10)	1.20576(3)	2.330(7)	
W(11)	0.28882(3)	0.198849(10)	0.97872(3)	2.614(7)	
La(1)	0.5000	0.0000	1.0000	1.783(11)	1/2
P(1)	0.38135(15)	0.11244(5)	0.98780(17)	1.72(3)	
O(1)	0.1798(5)	0.0111(2)	0.8171(6)	3.40(13)	
O(2)	0.4977(5)	0.0492(2)	0.6574(5)	3.19(13)	
O(3)	0.7317(4)	0.0945(2)	1.1570(5)	3.07(13)	
O(4)	0.3836(5)	0.0537(2)	1.3384(5)	3.30(13)	
O(5)	0.0509(5)	0.0743(2)	1.1692(6)	3.69(15)	
O(6)	0.7176(5)	0.15473(19)	0.8245(6)	3.28(13)	
O(7)	0.0325(4)	0.1419(2)	0.8055(5)	3.29(14)	
O(8)	0.3517(5)	0.1799(2)	0.6405(6)	3.57(14)	
O(9)	0.5991(5)	0.21209(19)	1.1414(6)	3.54(14)	
O(10)	0.2503(5)	0.1696(2)	1.3199(6)	3.82(15)	
O(11)	0.2369(5)	0.23802(19)	0.9536(6)	3.38(13)	
O(12)	0.4414(4)	0.08802(17)	1.0566(4)	2.30(10)	
O(13)	0.4347(4)	0.11786(17)	0.8874(4)	2.30(10)	
O(14)	0.3723(4)	0.14744(16)	1.0414(4)	2.27(10)	
O(15)	0.2742(4)	0.09858(17)	0.9684(5)	2.43(11)	
O(16)	0.3306(4)	0.0244(2)	0.9560(5)	2.99(12)	
O(17)	0.5088(4)	0.04565(18)	0.8641(5)	2.70(11)	
O(18)	0.6132(4)	0.04813(17)	1.0604(5)	2.63(11)	
O(19)	0.4285(4)	0.02563(19)	1.1562(5)	2.79(12)	
O(20)	0.3291(4)	0.06172(19)	0.7872(5)	2.76(12)	
O(21)	0.5854(4)	0.10173(18)	0.7774(5)	2.63(11)	
O(22)	0.6351(4)	0.11108(17)	0.9700(5)	2.47(11)	
O(23)	0.5370(4)	0.08071(19)	1.2218(5)	2.92(12)	
O(24)	0.2610(4)	0.06565(18)	1.1647(5)	2.66(11)	
O(25)	0.1484(4)	0.04894(18)	0.9997(5)	2.61(11)	
O(26)	0.1434(4)	0.08229(16)	0.8280(5)	2.47(11)	
O(27)	0.4092(5)	0.11405(18)	0.6927(5)	2.86(12)	
O(28)	0.5710(5)	0.14115(18)	1.1315(5)	2.95(12)	

O(29)	0.3640(5)	0.11627(19)	1.2385(5)	2.95(12)
O(30)	0.2427(4)	0.13871(19)	0.7754(5)	2.74(11)
O(31)	0.5153(4)	0.16476(17)	0.7705(5)	2.50(11)
O(32)	0.5669(5)	0.17339(18)	0.9618(5)	2.90(12)
O(33)	0.4235(5)	0.18119(19)	1.2061(5)	3.19(13)
O(34)	0.1900(5)	0.12799(19)	1.1544(5)	2.92(12)
O(35)	0.0818(4)	0.11301(19)	0.9941(5)	2.74(11)
O(36)	0.1846(4)	0.16749(18)	0.9401(6)	3.02(12)
O(37)	0.3491(4)	0.18712(18)	0.8545(5)	2.81(12)
O(38)	0.4183(5)	0.21254(18)	1.0290(6)	3.07(13)
O(39)	0.2489(5)	0.1920(2)	1.1173(5)	3.26(13)

$B_{eq} = 8/3\ \pi^2(U_{11}(aa^*)^2 + U_{22}(bb^*)^2 + U_{33}(cc^*)^2 + 2U_{12}(aa^*bb^*)\cos\gamma + 2U_{13}(aa^*cc^*)\cos\beta + 2U_23(bb^*cc^*)\cos\alpha)$

Table 3-2. (Continued) Atomic coordinates and B_{eq} ($Å^2$) of **Pr-s**.

atom	x	y	z	Beq	occ
W(1)	0.35083(5)	0.44935(5)	0.19613(2)	2.55(2)	
W(2)	0.08915(5)	0.36607(5)	0.16397(2)	2.43(2)	
W(3)	0.21596(5)	-0.00136(4)	0.15839(2)	2.04(1)	
W(4)	0.45758(5)	0.07610(5)	0.18860(2)	2.17(1)	
W(5)	0.55008(5)	0.33680(5)	0.15701(2)	2.54(2)	
W(6)	0.04206(5)	0.17604(5)	0.09412(2)	2.22(1)	
W(7)	0.38819(5)	0.50483(5)	0.10171(2)	2.42(2)	
W(8)	0.12123(5)	0.41890(5)	0.06984(2)	2.30(2)	
W(9)	0.25463(5)	0.04464(4)	0.05591(2)	2.07(1)	
W(10)	0.50005(5)	0.12297(5)	0.08639(2)	2.18(1)	
W(11)	0.33667(5)	0.28960(4)	0.03034(2)	2.15(1)	
Pr(1)	0.2500	0.18750(9)	0.2500	2.29(2)	1/2
P(1)	0.2987(3)	0.2440(3)	0.12705(9)	1.67(6)	
O(1)	0.358(1)	0.550(1)	0.2295(4)	3.5(3)	
O(2)	-0.002(1)	0.433(1)	0.1863(4)	3.7(3)	
O(3)	0.1661(9)	-0.1273(8)	0.1569(3)	2.8(2)	
O(4)	0.5618(9)	-0.000(1)	0.2068(3)	3.1(2)	
O(5)	0.6791(9)	0.355(1)	0.1713(4)	3.5(3)	
O(6)	-0.0722(9)	0.1134(9)	0.0789(4)	3.1(2)	
O(7)	0.421(1)	0.6192(8)	0.0802(4)	3.2(3)	
O(8)	0.0575(9)	0.5056(9)	0.0381(4)	3.1(2)	
O(9)	0.2124(9)	-0.0592(9)	0.0265(3)	2.8(2)	
O(10)	0.6129(9)	0.0689(9)	0.0754(3)	2.8(2)	
O(11)	0.347(1)	0.3328(9)	-0.0146(3)	3.1(2)	

O(12)	0.3093(8)	0.1589(8)	0.1572(3)	2.0(2)
O(13)	0.1887(8)	0.2826(7)	0.1179(3)	1.7(2)
O(14)	0.3334(7)	0.1994(7)	0.0901(3)	1.7(2)
O(15)	0.3684(8)	0.3391(8)	0.1399(3)	2.1(2)
O(16)	0.3347(9)	0.3348(9)	0.2222(3)	2.9(2)
O(17)	0.1388(9)	0.2694(9)	0.1969(3)	2.7(2)
O(18)	0.1980(8)	0.0421(8)	0.2046(3)	2.2(2)
O(19)	0.4068(8)	0.1111(8)	0.2298(3)	2.4(2)
O(20)	0.2084(9)	0.4531(8)	0.1744(3)	2.5(2)
O(21)	0.0020(8)	0.2654(9)	0.1333(3)	2.7(2)
O(22)	0.1050(8)	0.0804(8)	0.1319(3)	2.3(2)
O(23)	0.3578(8)	-0.0340(8)	0.1735(3)	2.3(2)
O(24)	0.5218(8)	0.2130(9)	0.1836(3)	2.6(2)
O(25)	0.4968(9)	0.4227(8)	0.1938(3)	2.6(2)
O(26)	0.3705(9)	0.5468(8)	0.1505(3)	2.7(2)
O(27)	0.0679(9)	0.4508(8)	0.1138(3)	2.9(2)
O(28)	0.2551(8)	-0.0079(8)	0.1036(3)	2.3(2)
O(29)	0.4846(9)	0.0648(8)	0.1326(3)	2.3(2)
O(30)	0.2458(8)	0.4967(8)	0.0871(3)	2.4(2)
O(31)	0.0294(9)	0.2986(8)	0.0619(3)	2.6(2)
O(32)	0.1306(9)	0.1158(9)	0.0612(3)	2.7(2)
O(33)	0.4019(8)	0.0273(8)	0.0598(3)	2.2(2)
O(34)	0.5500(9)	0.2501(9)	0.1136(3)	2.9(2)
O(35)	0.5209(9)	0.4547(8)	0.1226(3)	2.7(2)
O(36)	0.3943(8)	0.4016(8)	0.0618(3)	2.2(2)
O(37)	0.2090(9)	0.3424(8)	0.0390(3)	2.6(2)
O(38)	0.2744(9)	0.1554(8)	0.0188(3)	2.5(2)
O(39)	0.4629(8)	0.2147(8)	0.0423(3)	2.3(2)

$B_{eq} = 8/3\ \pi^2(U_{11}(aa^*)^2 + U_{22}(bb^*)^2 + U_{33}(cc^*)^2 + 2U_{12}(aa^*bb^*)\cos\gamma + 2U_{13}(aa^*cc^*)\cos\beta + 2U_{23}(bb^*cc^*)\cos\alpha)$

Table 3-2. (Continued) Atomic coordinates and B_{eq} ($Å^2$) of **La-K**.

atom	x	y	z	Beq	occ
W(1)	0.57490(4)	0.05468(3)	0.39906(3)	1.235(8)	
W(2)	0.82399(4)	0.46406(3)	0.71782(3)	1.082(8)	
W(3)	0.77729(4)	0.30185(3)	0.73337(3)	1.160(8)	
W(4)	1.00719(4)	0.37362(3)	0.54443(3)	1.055(8)	
W(5)	0.52726(4)	0.34709(3)	0.38124(3)	1.049(8)	
W(6)	1.07678(4)	0.53440(3)	0.69591(3)	1.143(8)	

W(7)	0.39546(4)	0.25252(3)	0.44846(3)	1.110(8)
W(8)	0.60564(4)	0.24272(3)	0.22033(3)	1.236(8)
W(9)	0.31679(4)	0.04216(3)	0.36186(3)	1.360(9)
W(10)	1.03690(4)	0.36408(3)	0.88830(3)	1.480(9)
W(11)	0.72557(4)	0.15992(3)	0.32612(3)	1.205(8)
W(12)	1.25929(4)	0.42490(3)	0.85929(3)	1.474(9)
W(13)	0.19067(4)	0.14296(3)	0.25830(3)	1.403(9)
W(14)	1.08396(4)	0.52912(3)	0.87395(3)	1.356(8)
W(15)	0.97436(4)	0.18771(3)	0.72571(3)	1.417(9)
W(16)	0.32684(4)	0.23796(3)	0.18933(3)	1.363(9)
W(17)	1.24810(4)	0.42963(3)	0.67775(3)	1.242(8)
W(18)	0.95123(4)	0.19246(3)	0.55972(3)	1.228(8)
W(19)	0.39767(4)	-0.05250(3)	0.22611(3)	1.514(9)
W(20)	0.55130(4)	0.05369(3)	0.15109(3)	1.450(9)
W(21)	1.19202(4)	0.24635(3)	0.69341(3)	1.479(9)
W(22)	0.26906(4)	0.04774(3)	0.11811(3)	1.513(9)
La(1)	0.70200(5)	0.28604(4)	0.52797(4)	1.05(1)
Si(1)	0.4578(3)	0.1510(2)	0.2966(2)	1.19(6)
Si(2)	1.0145(3)	0.3639(2)	0.7141(2)	1.11(5)
O(1)	0.6392(7)	0.3619(5)	0.4557(5)	1.3(2)
O(2)	0.6058(7)	0.1482(5)	0.4646(5)	1.3(2)
O(3)	0.6509(7)	0.0130(5)	0.4483(6)	1.7(2)
O(4)	0.5160(6)	0.2774(5)	0.5214(5)	1.2(2)
O(5)	0.4431(7)	0.0267(5)	0.4153(5)	1.4(2)
O(6)	0.4970(7)	-0.0147(5)	0.1879(5)	1.5(2)
O(7)	0.4436(7)	0.0771(5)	0.3167(5)	1.1(2)
O(8)	0.2347(7)	0.0090(5)	0.4006(6)	1.8(2)
O(9)	0.2221(7)	0.0681(5)	0.2939(6)	1.8(2)
O(10)	0.3486(7)	0.1440(5)	0.2343(5)	1.3(2)
O(11)	0.2010(7)	0.2121(5)	0.2108(6)	1.8(2)
O(12)	0.4592(7)	0.2324(5)	0.1762(5)	1.6(2)
O(13)	0.4266(7)	0.3424(5)	0.4313(5)	1.3(2)
O(14)	0.3626(6)	0.1467(5)	0.4262(5)	1.3(2)
O(15)	0.3134(7)	0.2810(5)	0.4988(5)	1.4(2)
O(16)	0.0647(7)	0.1386(6)	0.2573(6)	1.8(2)
O(17)	0.3964(7)	0.3052(5)	0.2848(5)	1.4(2)
O(18)	0.5350(7)	0.4380(5)	0.3859(5)	1.3(2)
O(19)	0.5944(7)	0.3101(5)	0.3078(5)	1.4(2)
O(20)	0.4846(6)	0.2276(5)	0.3695(5)	1.1(2)
O(21)	0.6822(7)	0.0785(5)	0.2199(5)	1.4(2)
O(22)	0.8539(7)	0.1573(5)	0.3454(5)	1.7(2)
O(23)	0.3039(7)	-0.0502(5)	0.2809(5)	1.5(2)
O(24)	0.5061(7)	-0.0445(5)	0.3055(5)	1.4(2)

O(25)	0.1584(7)	0.0635(5)	0.1581(6)	1.7(2)
O(26)	0.1956(8)	-0.0171(6)	0.0296(6)	2.3(2)
O(27)	0.2923(8)	0.2960(6)	0.1465(6)	2.3(2)
O(28)	0.4068(7)	0.0583(5)	0.1140(6)	1.8(2)
O(29)	0.2699(7)	0.2150(5)	0.3479(5)	1.4(2)
O(30)	0.2993(7)	-0.0174(5)	0.1662(5)	1.7(2)
O(31)	0.6612(8)	0.3029(5)	0.1879(6)	1.8(2)
O(32)	0.7303(7)	0.2283(5)	0.2758(5)	1.3(2)
O(33)	0.5892(8)	0.1488(5)	0.1416(6)	1.8(2)
O(34)	0.5521(7)	0.1523(5)	0.2618(5)	1.2(2)
O(35)	0.6619(7)	0.0791(5)	0.3468(6)	1.6(2)
O(36)	0.7357(7)	0.4138(5)	0.6259(5)	1.4(2)
O(37)	0.8759(7)	0.3613(5)	0.5411(5)	1.4(2)
O(38)	0.8334(7)	0.2182(5)	0.5561(5)	1.5(2)
O(39)	0.6929(6)	0.2639(5)	0.6394(5)	1.2(2)
O(40)	0.9193(8)	0.1161(5)	0.4761(6)	2.0(2)
O(41)	0.6961(7)	0.2711(6)	0.7746(6)	1.8(2)
O(42)	0.8522(7)	0.2243(5)	0.7176(5)	1.5(2)
O(43)	0.9288(7)	0.1376(5)	0.6204(5)	1.4(2)
O(44)	1.0346(7)	0.2661(5)	0.8212(5)	1.5(2)
O(45)	1.1146(7)	0.1842(6)	0.7284(6)	1.9(2)
O(46)	1.1032(7)	0.1872(5)	0.5978(5)	1.5(2)
O(47)	1.0271(6)	0.2788(5)	0.6838(5)	1.2(2)
O(48)	0.9024(7)	0.3489(5)	0.8327(5)	1.5(2)
O(49)	0.8929(6)	0.3646(5)	0.7003(5)	1.0(2)
O(50)	0.7588(7)	0.4027(5)	0.7592(5)	1.4(2)
O(51)	1.0126(7)	0.2748(5)	0.5394(5)	1.1(2)
O(52)	0.9974(7)	0.3640(5)	0.4556(5)	1.4(2)
O(53)	1.0355(7)	0.4833(5)	0.5909(5)	1.3(2)
O(54)	0.9364(7)	0.5065(5)	0.6913(5)	1.5(2)
O(55)	1.1699(6)	0.3981(5)	0.5801(5)	1.0(2)
O(56)	1.0661(6)	0.4092(5)	0.6724(5)	1.0(2)
O(57)	0.9463(7)	0.5044(5)	0.8186(5)	1.5(2)
O(58)	1.1163(7)	0.5516(5)	0.7969(5)	1.3(2)
O(59)	1.2164(7)	0.5257(5)	0.6987(5)	1.4(2)
O(60)	1.0918(7)	0.6264(5)	0.7029(5)	1.6(2)
O(61)	1.3719(7)	0.4520(5)	0.6740(6)	1.8(2)
O(62)	1.2765(7)	0.4519(5)	0.7824(5)	1.5(2)
O(63)	1.2285(7)	0.5197(5)	0.9037(5)	1.8(2)
O(64)	1.2319(7)	0.3274(5)	0.6676(5)	1.5(2)
O(65)	1.0809(6)	0.4059(5)	0.8024(5)	1.4(2)
O(66)	1.0572(7)	0.4725(6)	0.9298(5)	1.7(2)
O(67)	1.2977(7)	0.2084(5)	0.6948(6)	2.0(2)

O(68)	1.1903(7)	0.3873(6)	0.9148(6)	1.7(2)
O(69)	1.3875(7)	0.4461(6)	0.9151(6)	2.2(2)
O(70)	1.0233(8)	0.3463(6)	0.9618(6)	2.4(2)
O(71)	0.9411(7)	0.1122(6)	0.7468(6)	2.0(2)
O(72)	0.7727(7)	0.5395(5)	0.7495(5)	1.6(2)
O(73)	1.1044(7)	0.6196(5)	0.9351(5)	1.7(2)
O(74)	1.2378(7)	0.3235(5)	0.7919(5)	1.6(2)
O(75)	0.7237(8)	0.2316(5)	0.4065(6)	1.9(2)
O(76)	0.5667(8)	-0.0057(6)	0.0732(6)	2.2(2)
O(77)	0.2697(7)	0.1391(5)	0.1041(6)	1.8(2)
O(78)	0.3668(8)	-0.1464(5)	0.1730(6)	1.9(2)

$B_{eq} = 8/3\ \pi^2(U_{11}(aa^*)^2 + U_{22}(bb^*)^2 + U_{33}(cc^*)^2 + 2U_{12}(aa^*bb^*)\cos\gamma + 2U_{13}(aa^*cc^*)\cos\beta + 2U_{23}(bb^*cc^*)\cos\alpha)$

Table 3-3. Full assignments of IR spectra in the region of 1200-600 cm^{-1}.

	ν_{as}(P-O)	ν (W-O_t)	ν (W-O_b-W)	ν (W-O_c-W)
Y-s	1105 1048	950	891 844	773 773
Er-s	1105 1047	952	891 842	782 742
Eu-s	1099 1047	951	889 837	776 734
Pr-s	1094 1045	950	891 836	779 739
Ce-c	1094 1045	948	888 830	781 733
La-c	1095 1044	947	886 837	777 723
[A-α-PW_9O_{34}]$^{9-}$	1052 1017	935	826	757

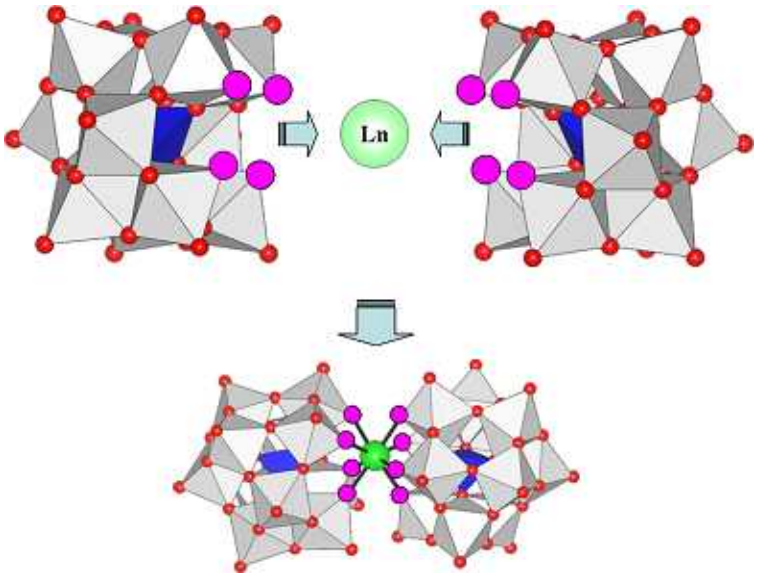

(a)

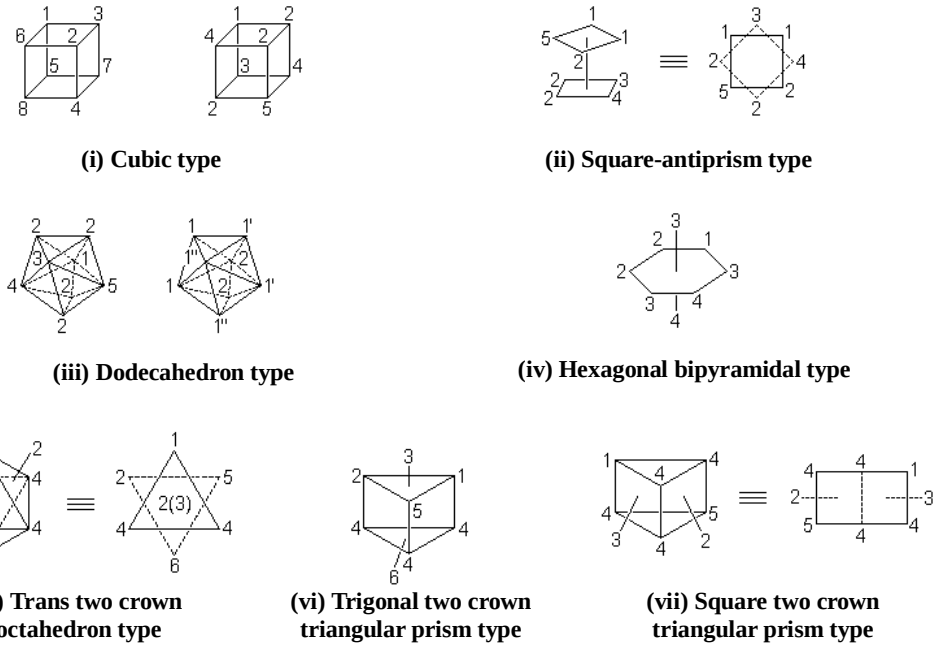

(i) Cubic type

(ii) Square-antiprism type

(iii) Dodecahedron type

(iv) Hexagonal bipyramidal type

(v) Trans two crown octahedron type

(vi) Trigonal two crown triangular prism type

(vii) Square two crown triangular prism type

(b)

Figure 3-1. (a) Formation of an eight-fold coordination mode of Ln^{3+} by two tetradentate $[XM_{11}O_{39}]^{n-}$ units. (b) Theoretical seven types in eight-fold coordination.

The pink spheres in (a) denote the coordination O-sites.

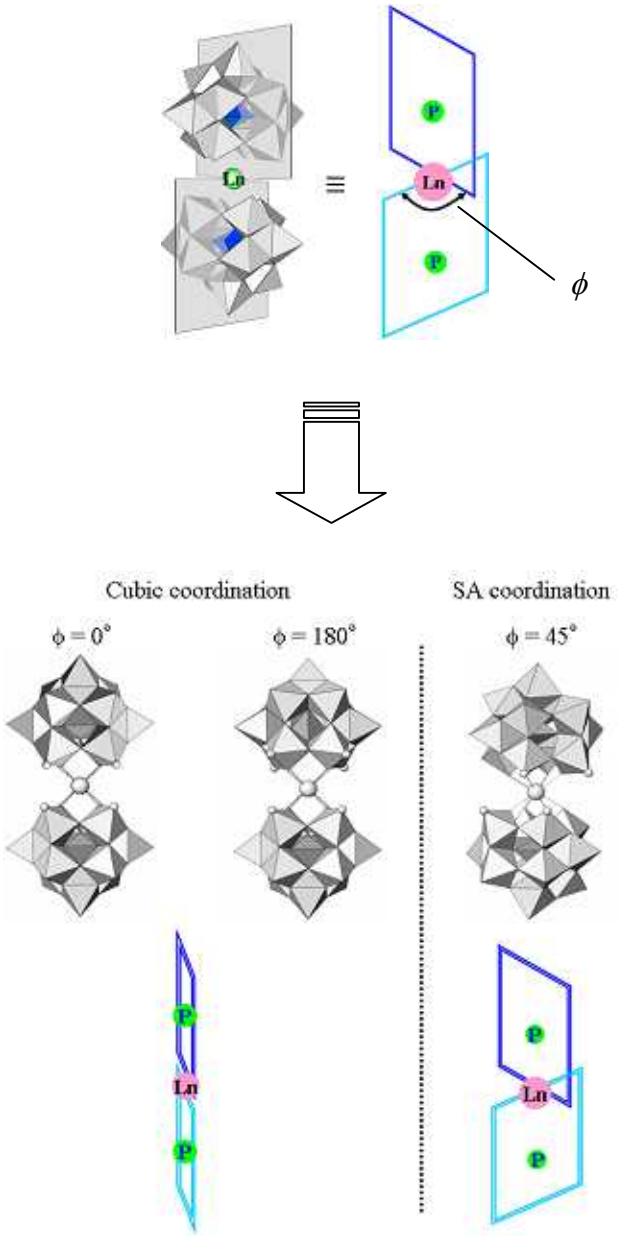

Figure 3-2. Top: Definition of rotation angle (ϕ) of $[\alpha\text{-}XM_{11}O_{39}]^{n-}$ units in $[Ln(\alpha\text{-}XM_{11}O_{39})_2]^{n-}$. Bottom left: Two cubic coordination modes (ϕ = 0° and 180°). Bottom right: Square-antiprismatic (SA) coordination mode (ϕ = 45°). The mirror plane in each $[\alpha\text{-}XM_{11}O_{39}]^{n-}$ unit is schematically represented by rectangle.

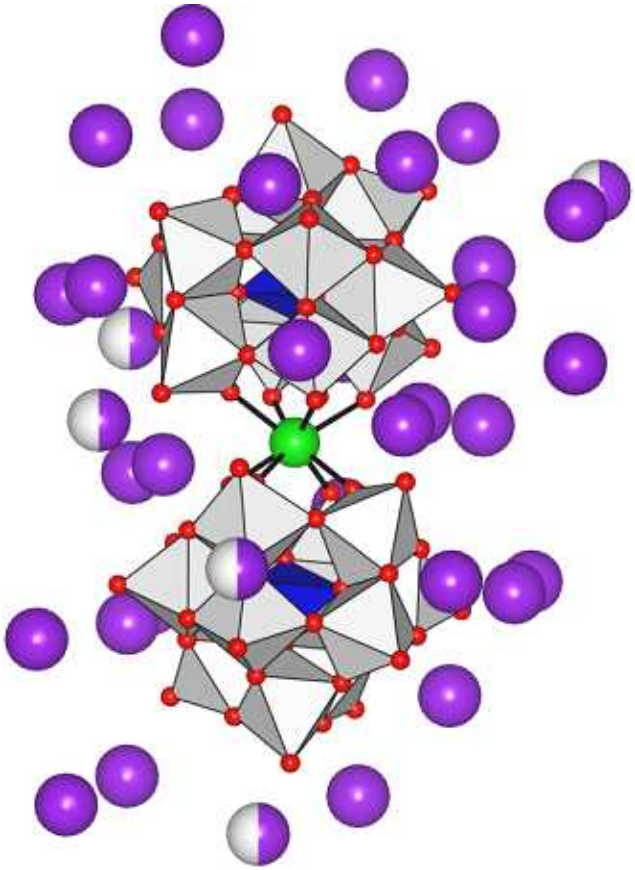

Figure 3-3. The $[La(\alpha\text{-}SiW_{11}O_{39})_2]^{13-}$ polyanion and surrounding K^+ cations in **La-K**. The K^+ cations with a half occupancy are denoted as half-filled spheres. White octahedra = WO_6, blue tetrahedra = SiO_4, green sphere = La^{3+}, red spheres = O, purple spheres = K.

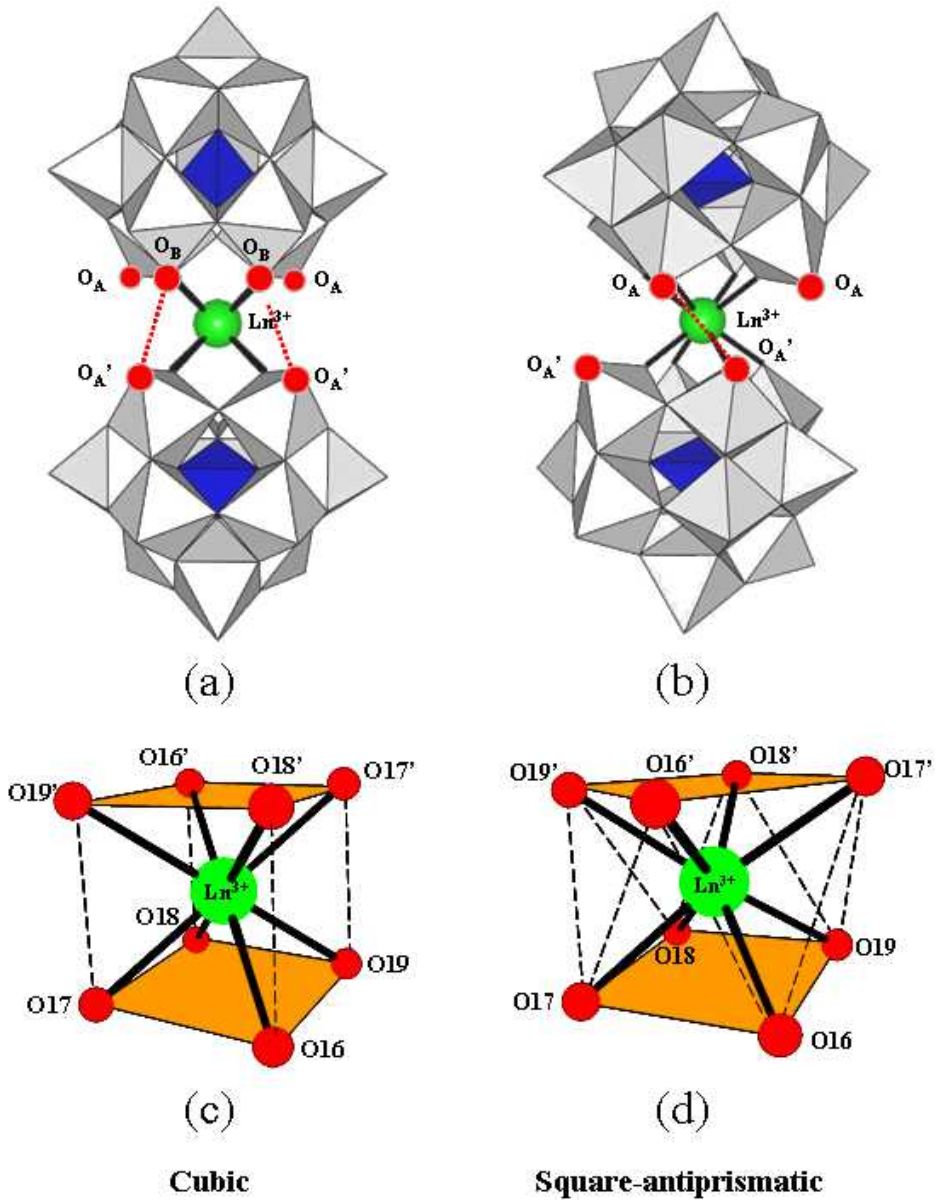

Figure 3-4. Structures of the $[Ln(\alpha\text{-}PW_{11}O_{39})_2]^{11-}$ polyanions with cubic (a) and square-antiprismatic (b) coordination; white octahedra = WO_6, blue tetrahedra = PO_4, green spheres = Ln^{3+}, red spheres = O. Views of the LnO_8 centers with cubic (c) and square-antiprismatic (d) coordination. The orange O_4-tetragons are least-square planes defined by the four O atoms coordinated with Ln^{3+}.

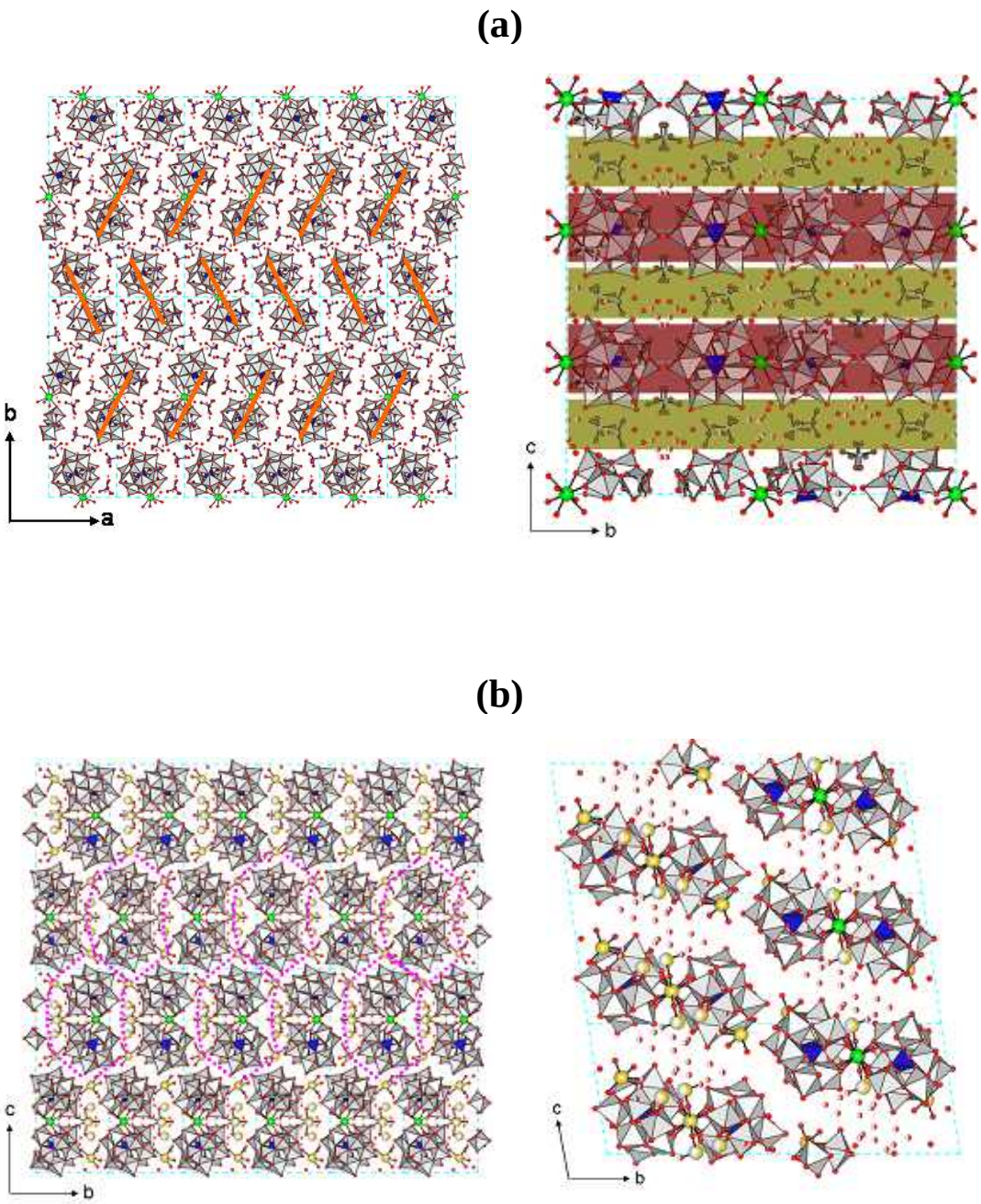

Figure 3-5. Crystal packing of **La-c** (a) and **Pr-s** (b) viewed on the ab and bc plane, respectively (white octahedra = WO_6, blue tetrahedra = PO_4, green spheres = Ln^{3+}, red spheres = O, light blue spheres = C, brown spheres = N, yellow spheres = Na).

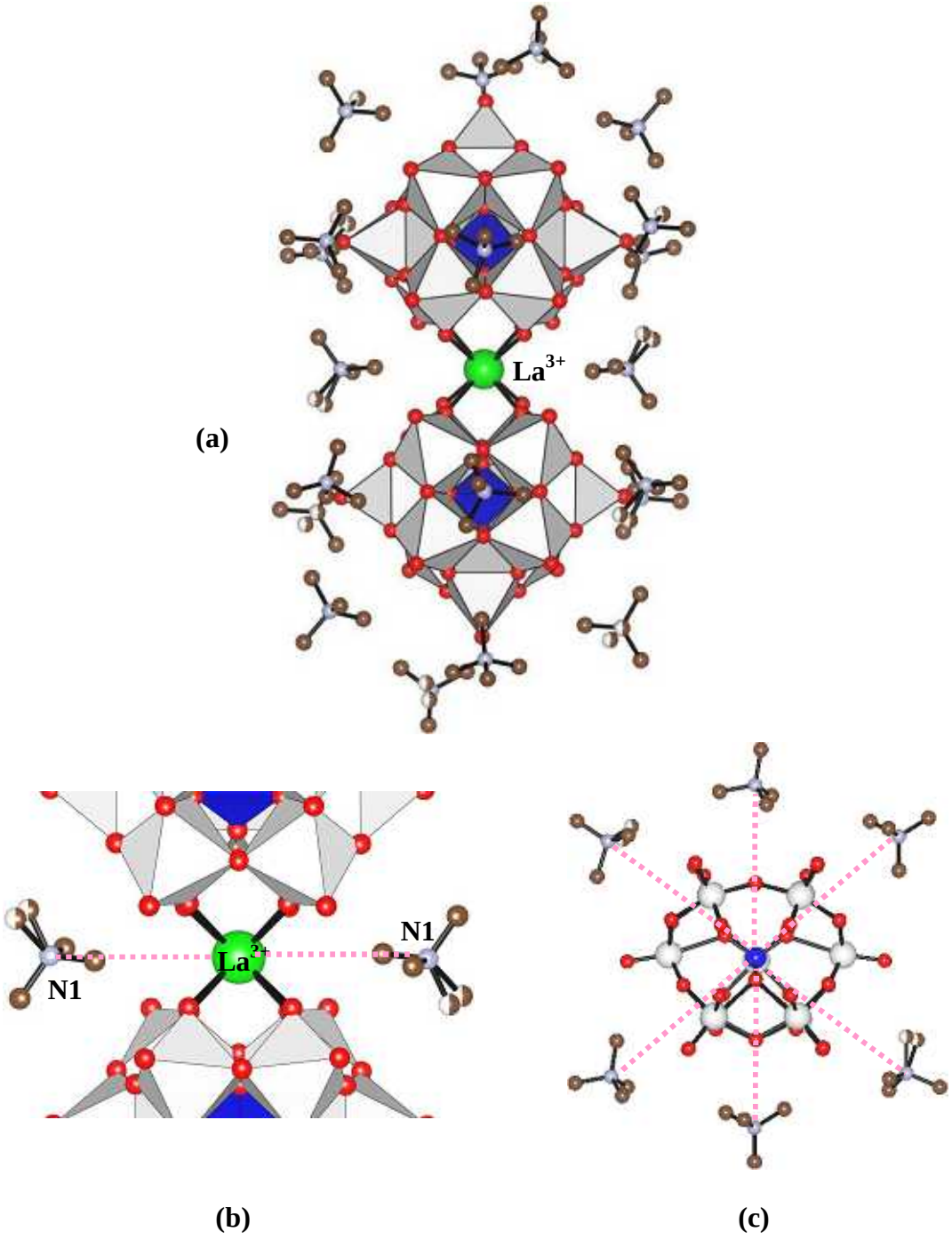

Figure 3-6. The $[La(\alpha\text{-}PW_{11}O_{39})_2]^{11-}$ polyanion and surrounding TMA^+ cations in **La-c** with $N\cdots O_{anion}$ distances less than 4.3 Å. White octahedra = WO_6, blue tetrahedra = PO_4, green sphere = Ln^{3+}, red spheres = O, light blue spheres = N, brown spheres = C. **Ce-c** shows the similar structure.

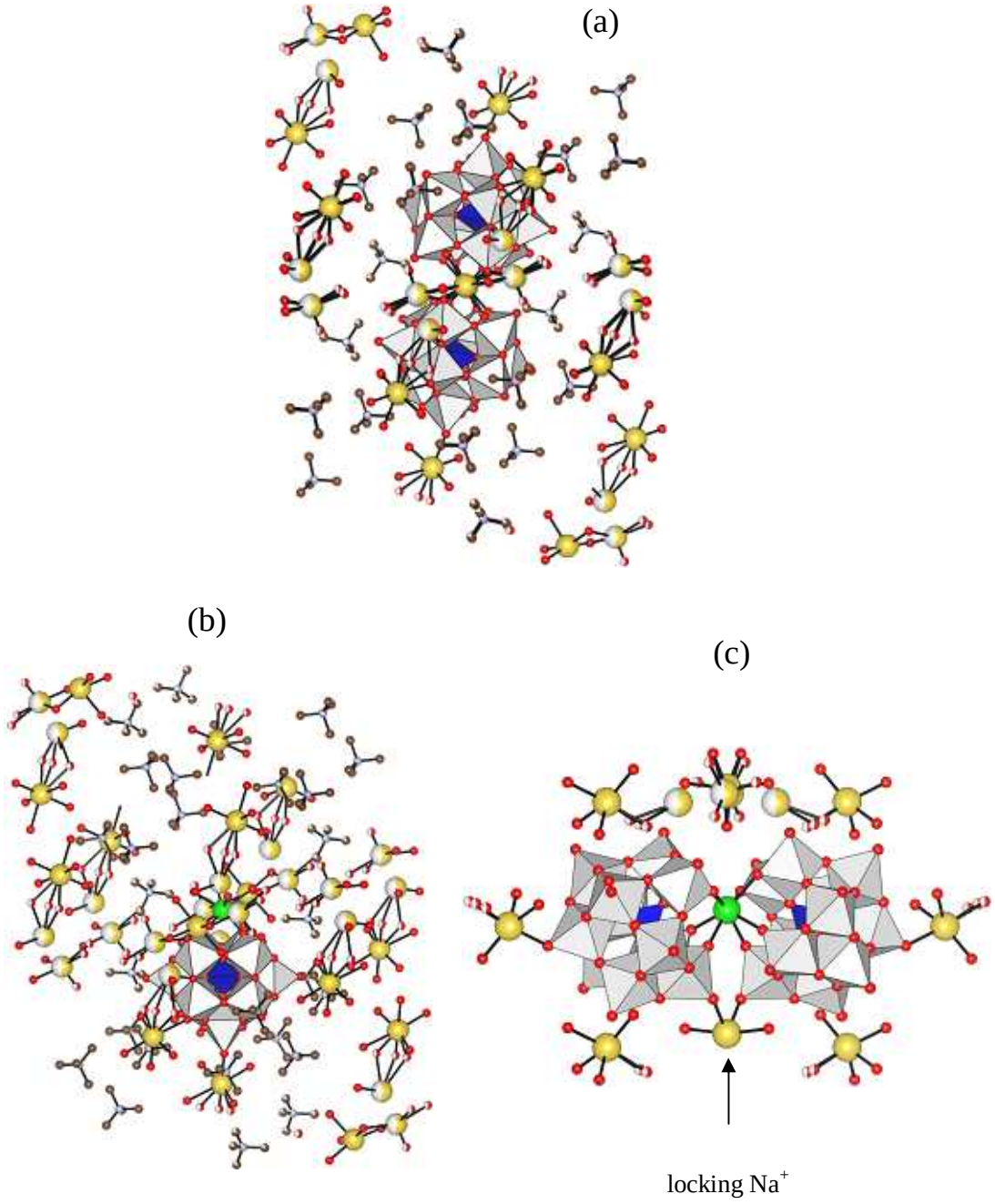

Figure 3-7. The $[Pr(\alpha\text{-}PW_{11}O_{39})_2]^{11-}$ polyanion and surrounding Na^+ and TMA^+ cations in **Pr-s** with $N\cdots O_{anion}$ distances less than 4.3 Å. White octahedra = WO_6, blue tetrahedra = PO_4, green sphere = Ln^{3+}, red spheres = O, light blue spheres = N, brown spheres = C, yellow spheres = Na. Both **Eu-s** and **Er-s** show the similar structure. (a) Viewed along the molecular C_2 axis, (b) Viewed perpendicular to the mirror plane in $[\alpha\text{-}PW_{11}O_{39}]^{7-}$ unit. (c) The Na^+ attachment of the polyanion.

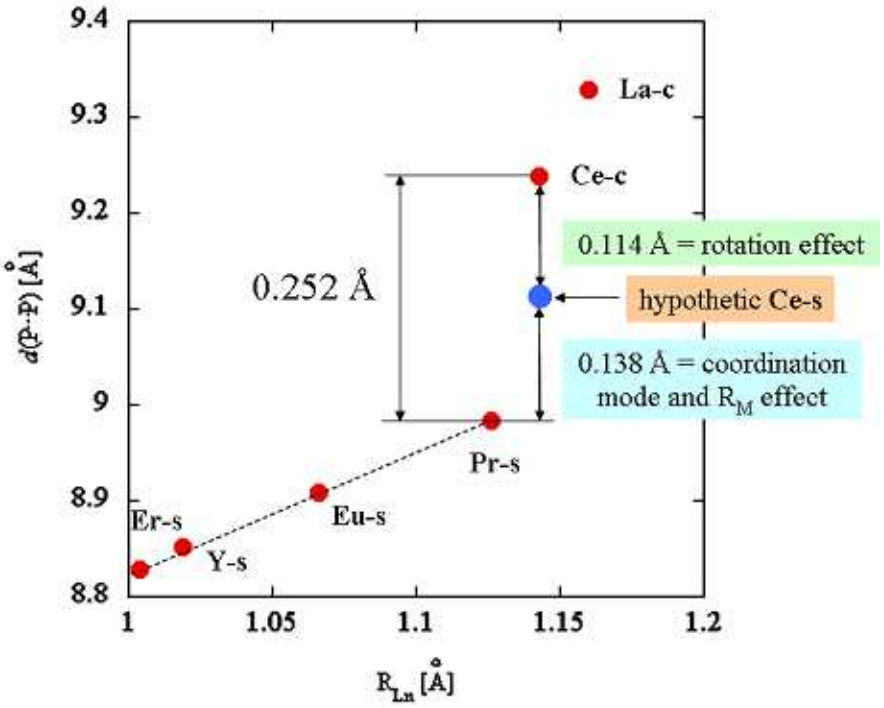

Figure 3-8. Plots of ionic radius of Ln^{3+} (R_{Ln}) vs. intramoleculer P···P distance (d(P···P)).

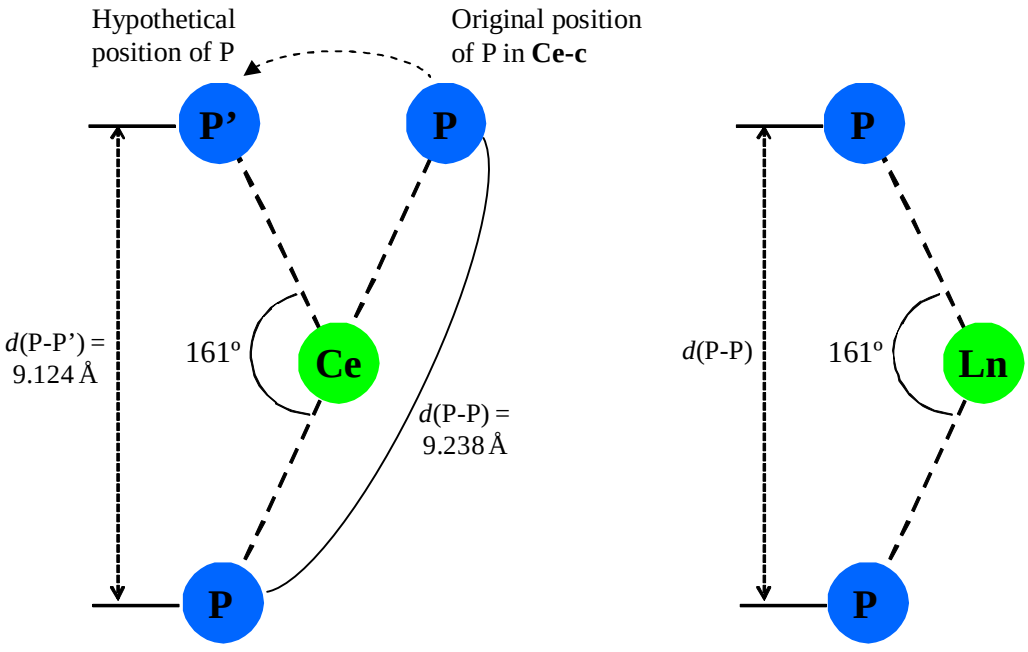

Figure 3-9. The schematic geometrical arrangements of P and Ln atoms in **Ce-c** (left) and **Ln-s** (Ln = Pr, Eu, Er) (right). P' in left denotes the position of P in the hypothetical $[Ce(\alpha\text{-}PW_{11}O_{39})_2]^{11-}$ with SA coordination (see text).

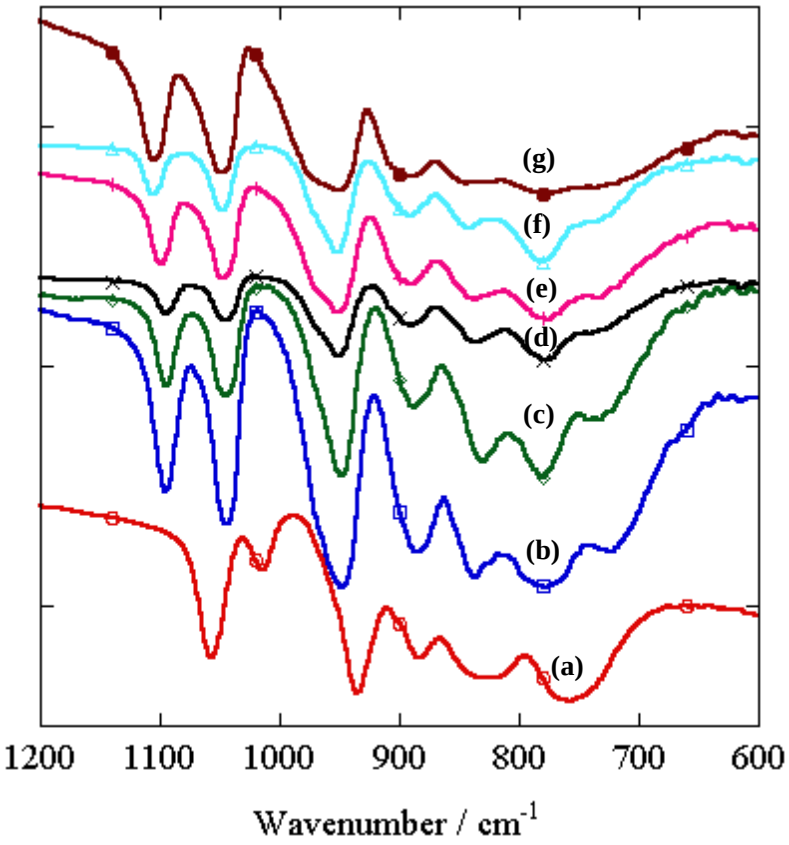

Figure 3-10. IR spectra of $[A\text{-}\alpha\text{-}PW_9O_{34}]^{9-}$ (a), **La-c** (b), **Ce-c** (c), **Pr-s** (d), **Eu-s** (e), **Er-s** (f), and **Y-s** (g).

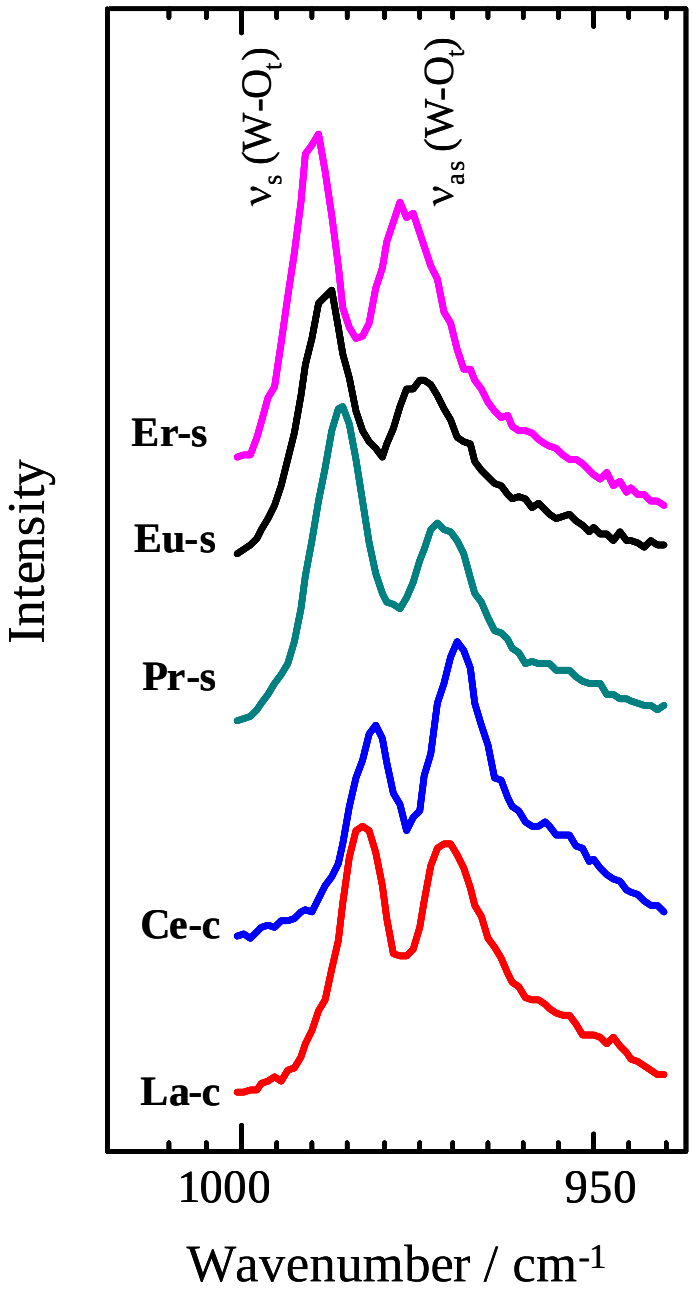

Figure 3-11. Raman spectra of **La-c** (red), **Ce-c** (blue), **Pr-s** (green), **Eu-s** (black), and **Er-s** (pink).

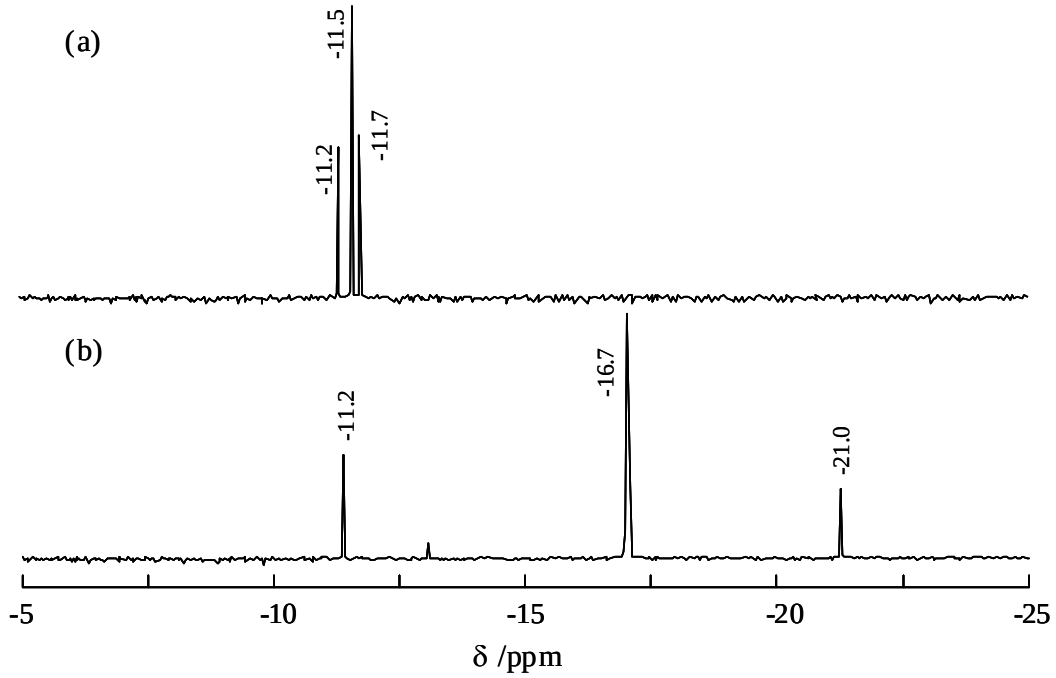

Figure 3-12. ^{31}P-NMR spectra of **La-c** (a) (35 mM), **Ce-c** (b) (47 mM) in D_2O solutions.

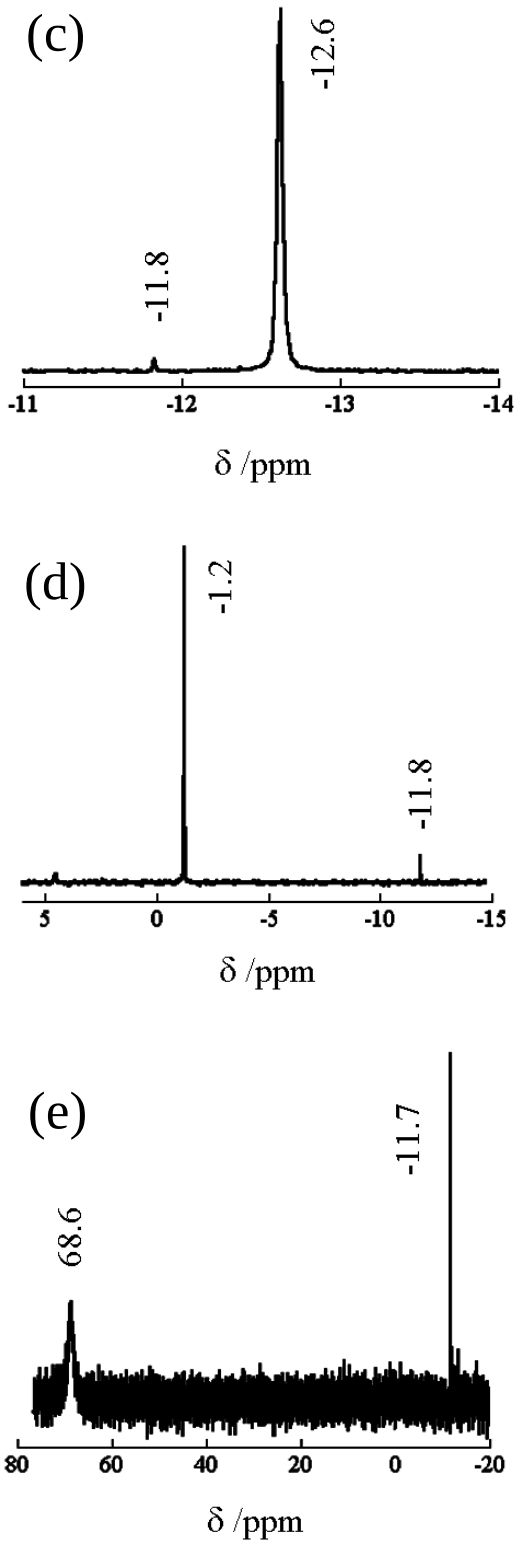

Figure 3-13. ^{31}P-NMR spectra of **Pr-s** (c) (27 mM), **Eu-s** (d) (20 mM), and **Er-s** (e) (20 mM) in D_2O solutions.

Chapter 4 Enantioselective synthesis of sandwich-type $[Ln(\alpha\text{-}PW_{11}O_{39})_2]^{11-}$ (Ln = La, Pr, Nd, Sm, Eu, Gd, Tb, Dy, Er, Tm, Yb, and Y) with D- and L-proline

4-1 Introduction

Chiral polyoxometalates (POMs) has become the focus of attention for a long time owing to their numerous potential applications in medicine, enantioselective catalysis, chiral sensing, and non-linear optics. Standout works have been intensively developed by Yamase, Pope, Hill, Kortz, Cronin, Hasenknopf and Wang [1-12]. But, most of the reported chiral POMs are racemic in solutions as well as in the solid states because of their rapid racemization and partial hydrolysis.

In a great number of reports about chiral POMs, there are a few examples of the enantiomerically isolated chiral POMs. These examples are categorized to two synthetic strategies; spontaneous resolution and optical resolution. The spontaneous resolution is a phenomenon that each of enantiomers selectively crystallizes without any external chiral reagent, although the mother liquor is racemic, forming a mixture of crystals of enantiomers. Since the first report about the spontaneous resolution of NH_4^+ salt of $[MnMo_9O_{32}]^{6-}$ by Pauling in 1954 [13], two kinds of DMA salts of $[Hf(\alpha\text{-}PW_{11}O_{39})_2]^{10-}$ and $[Zr(\alpha\text{-}PW_{11}O_{39})_2]^{10-}$ have been continuously delivered to be rare examples of this phenomenon [14, 15]. In Chapter 2 of this thesis, the spontaneous resolution of the similar DMA salt of $[Ce(\alpha\text{-}PW_{11}O_{39})_2]^{10-}$ is described as the first example of the sandwich-type polyoxometallolanthanoates [16]. However, as the spontaneous resolution occurs accidentally and produces enantiomixture, this phenomenon is not

appropriate for one of the synthetic strategies for chiral resolution of POMs and its applications. The optical resolution requires a chiral auxiliary. In 1970, Ama et al. succeeded in optical resolution of $[H_4Co_2Mo_{10}O_{36}]^{6-}$ by using chiral $[Co(en)_3]^{3+}$ and confirmed by circular dichroism spectroscopy [17]. Recent studies about separation of $[P_2Mo_{18}O_{62}]^{6-}$, whose chirality is expressed by Mo-O bond alternation, provided useful information that amino acids such as lysine and histidine can be the chiral auxiliaries for optical resolution of POMs [18, 19].

In this chapter, based on the latter synthetic strategy, an enantioselective synthesis of sandwich-type $[Ln(\alpha\text{-}PW_{11}O_{39})_2]^{11-}$ using chiral L and D-proline molecules as chiral auxiliaries was attempted. The proline has been reported to play a key role in chiral sensing of POMs [20, 21] and asymmetric catalysis in organic chemistry [22, 23], but detailed stereoselective interaction with POM anions is still undetermined. This chapter aims to distinguish the chirality in solutions and in the solid states by means of circular dichroism (CD), NMR spectroscopy, and single crystal X-ray diffraction analysis.

4-2 Experimental

4-2-1 Materials

All chemicals were commercially available and used without further purification. $Na_9[A\text{-}\alpha\text{-}PW_9O_{34}]\cdot 16H_2O$ was prepared according to the previous report and identified by IR spectroscopy [24].

4-2-2 Measurements

Elemental analysis of C, H, and N were performed on a Yanaco MT5 CHN CORDER. The contents of all lanthanide elements, P, Na, K, and W were determined by

inductively coupled plasma (ICP) atomic emission spectroscopy on an ICPS-8100 spectrometer. These two measurements were requested to the Center for Advanced Analysis of the Tokyo Institute of Technology. IR (4000-400 cm^{-1}) spectra were recorded on a JASCO FT/IR-410 spectrometer using KBr disc method. Thermogravimetric and differential thermal analyses (TG-DTA) were conducted with a ULVAC MTS9000 + TGD9600 system. UV-Vis absorption spectra were recorded on a JASCO V-570 UV/VIS/NIR spectrophotometer. Circular dichroism (CD) spectra were recorded on a JASCO J-800 spectropolarimeter. Luminescence and excitation spectra in the solid state and aqueous solution were recorded on HITACHI F-4500 spectrofluorometer. Solution ^{13}C-NMR spectra were measured on Bruker Biospin AVANCE III at a frequency of 100.62 MHz, and ^{31}P-NMR spectra were also recorded at a frequency of 161.97 MHz using and 85 % H_3PO_4 as an external reference. Magic angle spinning nuclear magnetic resonance (MAS-NMR) spectroscopy for ^{13}C was carried out on a JEOL JNM-ECA 600 at a frequency of 150.92 MHz. The adamantane $C_{10}H_{16}$ was used as a reference.

4-2-3 Syntheses

All of the compounds were synthesized by the same following procedure. The Ln ions were introduced as corresponding chloride or nitrate. Especially for **Pr-D** and **Er-D**, D-form of proline was used as a chiral resource. The synthetic procedure of **Pr-L** is exemplified here. For **Tm-L**, Tm_2O_3 dissolved in concHNO_3 was used as a Tm^{3+} source instead of using chloride or nitrate.

4-2-3-1 $K_{1.3}Na_{3.2}H_{6.5}[Pr(\alpha\text{-}PW_{11}O_{39})_2]\cdot 8.3(L\text{-}C_5H_9NO_2)\cdot 21.5H_2O$ (**Pr-L**)

To a solution of KCl (0.0751 g, 1.0 mmol) in 15 ml of H_2O was added both solid L-Proline (0.520 g, 4.5 mmol) and $PrCl_3\cdot 7H_2O$ (0.1856 g, 0.5 mmol) dissolved in 3 ml of H_2O. The light green solution was heated to 60 ℃ for 30 min with stirring, and the pH of the aqueous solution was adjusted to 1.5 by 1M HCl and an aqueous solution (10 ml) of $Na_9[A\text{-}\alpha\text{-}PW_9O_{34}]\cdot 16H_2O$ (2.4353 g, 1.00 mmol) was added dropwise. After boiling for 1 h, the solution was cooled to room temperature and the residual powders were filtered off. The resulting filtrate was concentrated to less than half of initial volume and stood at room temperature for several days. Light green platelet crystals of **Pr-L** were obtained (yield; 0.37 g, 14.7% based on W). Found: C, 7.04; H, 1.34; N, 1.67; K, 0.81; Na, 1.18; P, 0.95; W, 56.5; Pr, 2.29; H_2O, 5.54 wt %. Calcd for $O_{116.1}PrP_2W_{22}K_{1.3}Na_{3.2}C_{41.5}N_{8.3}H_{124.2}$: C, 7.15; H, 1.80; N, 1.67; K, 0.73; Na, 1.06; P, 0.89; W, 58.0; Pr, 2.02; H_2O, 5.56 wt %. IR (KBr disk): 1733s, 1624s, 1457m, 1417w, 1368m, 1338w, 1251m, 1187w, 1092vs, 1043vs, 952vs, 888m, 829m, 774m, 727m.

4-2-3-2 $K_{1.3}Na_{3.2}H_{6.5}[Nd(\alpha\text{-}PW_{11}O_{39})_2]\cdot 8.3(L\text{-}C_5H_9NO_2)\cdot 17H_2O$ (**Nd-L**)

Light bluenish purple platelet crystals of **Nd-L** were obtained (yield; 0.65 g, 25.9% based on W). Found: C, 7.05; H, 1.53; N, 1.70; H_2O, 4.18 wt %. Calcd for $O_{111.6}NdP_2W_{22}K_{1.3}Na_{3.2}C_{41.5}N_{8.3}H_{115.2}$: C, 7.23; H, 1.68; N, 1.69; H_2O, 4.44 wt %. IR (KBr disk): 1733s, 1624m, 1473w, 1457s, 1418w, 1368m, 1339w, 1247m, 1186w, 1092vs, 1043vs, 953s, 888m, 833w, 781w, 720w.

4-2-3-3 $K_{1.3}Na_{3.2}H_{6.5}[Sm(\alpha\text{-}PW_{11}O_{39})_2]\cdot 8.3(L\text{-}C_5H_9NO_2)\cdot 20.5H_2O$ (**Sm-L**)

Light yellow platelet crystals of **Sm-L** were obtained (yield; 0.19 g, 7.35% based

on W). Found: C, 7.04; H, 1.36; N, 1.72; K, 0.85; Na, 1.24; P, 0.92 W, 56.4; Pr, 2.37; H_2O, 5.29 wt %. Calcd for $O_{115.1}SmP_2W_{22}K_{1.3}Na_{3.2}C_{41.5}N_{8.3}H_{122.2}$: C, 7.16; H, 1.77; N, 1.67; K, 0.73; Na, 1.06; P, 0.89; W, 58.1; Sm, 2.16; H_2O, 5.31 wt %. IR (KBr disk): 1735s, 1627s, 1457m, 1370m, 1340w, 1255m, 1187w, 1096vs, 1047vs, 956vs, 894m, 838m, 784m, 724m.

4-2-3-4 $K_{1.3}Na_{3.2}H_{6.5}[Gd(\alpha\text{-}PW_{11}O_{39})_2]\cdot 8.3(L\text{-}C_5H_9NO_2)\cdot 26H_2O$ (**Gd-L**)

Colorless block crystals of **Gd-L** were obtained (yield; 0.14 g, 5.5% based on W). Found: C, 7.14; H, 1.31; N, 1.74; H_2O, 6.70 wt %. Calcd for $O_{120.6}GdP_2W_{22}K_{1.3}Na_{3.2}C_{41.5}N_{8.3}H_{133.2}$: C, 7.05; H, 1.90; N, 1.66; H_2O, 6.63 wt %. IR (KBr disk): 1733s, 1624m, 1559m, 1542s, 1457s, 1418w, 1397w, 1368m, 1338w, 1251m, 1097vs, 1045vs, 953vs, 889s, 834m, 773m, 734w.

4-2-3-5 $K_{1.3}Na_{3.2}H_{6.5}[Tb(\alpha\text{-}PW_{11}O_{39})_2]\cdot 8.3(L\text{-}C_5H_9NO_2)\cdot 18.5H_2O$ (**Tb-L**)

Colorless block crystals of **Tb-L** were obtained (yield; 0.42 g, 16.7% based on W). Found: C, 7.11; H, 1.27; N, 1.74; K, 0.94; Na, 1.21; P, 0.87; W, 59.2; Pr, 2.39; H_2O, 4.63 wt %. Calcd for $O_{113.1}TbP_2W_{22}K_{1.3}Na_{3.2}C_{41.5}N_{8.3}H_{118.2}$: C, 7.19; H, 1.72; N, 1.68; K, 0.73; Na, 1.06; P, 0.89; W, 58.3; Tb, 2.29; H_2O, 4.81 wt %. IR (KBr disk): 1734s, 1625s, 1457m, 1419w, 1374m, 1340w, 1254m, 1100vs, 1048vs, 955vs, 895m, 838m, 776m, 728m.

4-2-3-6 $K_{1.3}Na_{3.2}H_{6.5}[Dy(\alpha\text{-}PW_{11}O_{39})_2]\cdot 8.3(L\text{-}C_5H_9NO_2)\cdot 18H_2O$ (**Dy-L**)

Colorless block crystals of **Dy-L** were obtained (yield; 0.39 g, 15.3% based on W). Found: C, 7.20; H, 1.30; N, 1.74; K, 0.89; Na, 1.15; P, 0.88; W, 57.3; Pr, 2.49; H_2O,

4.80 wt %. Calcd for $O_{112.6}DyP_2W_{22}K_{1.3}Na_{3.2}C_{41.5}N_{8.3}H_{117.2}$: C, 7.20; H, 1.71; N, 1.68; K, 0.73; Na, 1.06; P, 0.89; W, 58.4; Dy, 2.35; H_2O, 4.68 wt %. IR (KBr disk): 1734s, 1627s, 1457m, 1418w, 1418w, 1371m, 1340w, 1255m, 1197w, 1101vs, 1046vs, 957vs, 895m, 838m, 781m, 726m.

4-2-3-7 $K_{1.3}Na_{3.2}H_{6.5}[Er(\alpha\text{-}PW_{11}O_{39})_2]\cdot 8.3(L\text{-}C_5H_9NO_2)\cdot 22.5H_2O$ (**Er-L**)

Light pink block crystals of **Er-L** were obtained (yield; 1.88 g, 36.6% based on W). Found: C, 7.26; H, 1.36; N, 1.75; K, 0.77; Na, 1.14; P, 0.91; W, 57.0; Er, 2.55; H_2O, 5.77 wt %. Calcd for $O_{117.1}ErP_2W_{22}K_{1.3}Na_{3.2}C_{41.5}N_{8.3}H_{126.2}$: C, 7.11; H, 1.81; N, 1.66; K, 0.72; Na, 1.05; P, 0.88; W, 57.7; Er, 2.38; H_2O, 5.78 wt %. IR (KBr disk): 1735s, 1627s, 1458m, 1418w, 1370m, 1335w, 1254m, 1191w, 1103vs, 1048vs, 956vs, 893m, 841m, 776m, 725m.

4-2-3-8 $K_{1.3}Na_{3.2}H_{6.5}[Tm(\alpha\text{-}PW_{11}O_{39})_2]\cdot 8.3(L\text{-}C_5H_9NO_2)\cdot 19H_2O$ (**Tm-L**)

White platelet crystals of **Tm-L** were obtained (yield; 0.32 g, 6.26% based on W). Found: C, 7.29; H, 1.51; N, 1.82; H_2O, 5.07 wt %. Calcd for $O_{113.6}TmP_2W_{22}K_{1.3}Na_{3.2}C_{41.5}N_{8.3}H_{119.2}$: C, 7.17; H, 1.73; N, 1.67; H_2O, 4.92 wt %. IR (KBr disk): 1734s, 1627s, 1458m, 1372m, 1340w, 1257m, 1188w, 1105vs, 1049vs, 956vs, 895m, 841m, 775m, 725m.

4-2-3-9 $K_{1.3}Na_{3.2}H_{6.5}[Yb(\alpha\text{-}PW_{11}O_{39})_2]\cdot 8.3(L\text{-}C_5H_9NO_2)\cdot 17H_2O$ (**Yb-L**)

White block crystals of **Yb-L** were obtained (yield; 0.48 g, 19.1% based on W). Found: C, 7.11; H, 1.22; N, 1.72; H_2O, 4.43 wt %. Calcd for $O_{111.6}YbP_2W_{22}K_{1.3}Na_{3.2}C_{41.5}N_{8.3}H_{115.2}$: C, 7.20; H, 1.68; N, 1.68; H_2O, 4.43 wt %. IR

(KBr disk): 1734s, 1635s, 1457m, 1418w, 1375m, 1340w, 1254m, 1192w, 1105vs, 1049vs, 956vs, 893m, 841m, 782m, 741m.

4-2-3-10 $K_{1.3}Na_{3.2}H_{6.5}[Y(\alpha\text{-}PW_{11}O_{39})_2]\cdot 8.3(L\text{-}C_5H_9NO_2)\cdot 22H_2O$ (**Y-L**)

White block crystals of **Y-L** were obtained (yield; 0.30 g, 12.0 % based on W). Found: C, 7.26; H, 1.51; N, 1.79; H_2O, 5.73 wt %. Calcd for $O_{106.6}YP_2W_{22}K_{1.3}Na_{3.2}C_{41.5}N_{8.3}H_{105.2}$: C, 7.20; H, 1.82; N, 1.68; H_2O, 5.72 wt %. IR (KBr disk): 1733s, 1624m, 1559s, 1542s, 1509s, 1457s, 1418w, 1370m, 1338w, 1251m, 1187w, 1102vs, 1047vs, 955vs, 893m, 838w, 781w, 738w.

4-2-3-11 $K_{1.2}Na_2H_{7.8}[La(\alpha\text{-}PW_{11}O_{39})_2]\cdot 8.5(L\text{-}C_5H_9NO_2)\cdot 15H_2O$ (**La-L**)

Colorless block crystals of **La-L** were obtained (yield; 0.48 g, 19.1% based on W). Found: C, 7.51; H, 1.51; N, 1.79; H_2O, 4.06 wt %. Calcd for $O_{110}LaP_2W_{22}K_{1.2}Na_2C_{42.5}N_{8.5}H_{114.3}$: C, 7.46; H, 1.68; N, 1.74; H_2O, 3.95 wt %. IR (KBr disk): 1734s, 1625s, 1458m, 1421w, 1369m, 1341w, 1248m, 1187w, 1089vs, 1045vs, 952vs, 893m, 832m, 781m, 730m.

4-2-3-12 $K_{1.2}Na_2H_{7.8}[Eu(\alpha\text{-}PW_{11}O_{39})_2]\cdot 8.5(L\text{-}C_5H_9NO_2)\cdot 18H_2O$ (**Eu-L**)

Colorless block crystals of **Eu-L** were obtained (yield; 0.28 g, 11.1% based on W). Found: C, 7.41; H, 1.52; N, 1.83; K, 0.71; Na, 0.72; P, 0.84; W, 55.7; Eu, 2.10; H_2O, 4.63 wt %. Calcd for $O_{113}EuP_2W_{22}K_{1.2}Na_2C_{42.5}N_{8.5}H_{120.3}$: C, 7.39; H, 1.75; N, 1.72; K, 0.68; Na, 0.67; P, 0.90; W, 58.5; Eu, 2.20; H_2O, 4.69 wt %. IR (KBr disk): 1735s, 1626s, 1457m, 1419w, 1371m, 1341w, 1250m, 1189w, 1097vs, 1047vs, 956vs, 892m, 836m, 783m, 729m.

4-2-3-13 $K_{1.3}Na_{3.2}H_{6.5}[Pr(\alpha\text{-}PW_{11}O_{39})_2]\cdot 8.3(D\text{-}C_5H_9NO_2)\cdot 17H_2O$ (**Pr-D**)

Light green platelet crystals of **Pr-D** were obtained (yield; 0.75 g, 14.8% based on W). Found: C, 7.24; H, 1.44; N, 1.73; H_2O, 4.42 wt %. Calcd for $O_{111.6}PrP_2W_{22}K_{1.3}Na_{3.2}C_{41.5}N_{8.3}H_{115.2}$: C, 7.24; H, 1.69; N, 1.69; H_2O, 4.45 wt %. IR (KBr disk): 1731m, 1625m, 1473w, 1457s, 1416w, 1368m, 1331w, 1252m, 1184w, 1092vs, 1043vs, 952vs, 890s, 828m, 771m, 732m.

4-2-3-14 $K_{1.3}Na_{3.2}H_{6.5}[Er(\alpha\text{-}PW_{11}O_{39})_2]\cdot 8.3(D\text{-}C_5H_9NO_2)\cdot 14H_2O$ (**Er-D**)

Light pink platelet crystals of **Er-D** were obtained (yield; 2.38 g, 47.4% based on W). Found: C, 7.35; H, 1.39; N, 1.74; H_2O, 3.53 wt %. Calcd for $O_{108.6}ErP_2W_{22}K_{1.3}Na_{3.2}C_{41.5}N_{8.3}H_{109.2}$: C, 7.27; H, 1.60; N, 1.69; H_2O, 3.68 wt %. IR (KBr disk): 1733s, 1624m, 1473w, 1457s, 1418w, 1368m, 1339w, 1247m, 1186w, 1092vs, 1043vs, 953s, 888m, 853w, 781w, 720w.

4-2-4 X-ray crystallography

The reflection data for the single crystal X-ray analysis of all the compounds were collected on a Rigaku RAXIS-RAPID imaging plate diffractometer with a graphite monochromatized MoK_α radiation (λ = 0.7107 Å) at 193-213 K. All of the structures were solved by the direct method SHELXS-97 [25] and refined by the full-matrix least squares on F^2 using the CrystalStructure [26]. The absolute structures in all the compounds were determined by the Flack parameter refinement [27]. All of the lanthanides, W, P, Na, and K atoms were refined anisotropically, and the other atoms and the disordered atoms in all of the compounds isotropically. The H atoms were not included in the refinements for all of the compounds. The crystallographic data and the

results of structure refinement are summarized in **Table 4-1**.

4-3 Results and discussion

4-3-1 Determination of the chemical formula

All the compounds were prepared using the same synthetic method — the reaction between the respective Ln^{3+} and the tri-lacunary Keggin precursor $[PW_9O_{34}]^{9-}$ in the presence of K^+ and D- or L-proline with a molar ratio K^+: proline: Ln^{3+}: $[PW_9O_{34}]^{9-}$ = 2:9:1:2. As will be described in 4-3-3, the products crystallize in two different forms; Forms A and B, which have different unit cell volumes and Z but similar packing ways of the $[Ln(\alpha\text{-}PW_{11}O_{39})_2]^{11-}$ anions. The Forms A and B have slightly different compositions $K_{1.2}Na_2H_{7.8}[Ln(\alpha\text{-}PW_{11}O_{39})_2]\cdot 8.5(C_5H_9NO_2)\cdot xH_2O$ (**La-L**, **Eu-L**), and $K_{1.3}Na_{3.2}H_{6.5}[Ln(\alpha\text{-}PW_{11}O_{39})_2]\cdot 8.3(C_5H_9NO_2)\cdot xH_2O$ (**Pr-L**, **Nd-L**, **Sm-L**, **Gd-L**, **Tm-L**, **Dy-L**, **Er-L**, **Pr-D**, and **Er-D**), respectively. Of the 8.5 and 8.3 equivalences of proline estimated from the CHN and ICP elemental analyses and TG-DTA in Forms A and B, respectively, only 6 and 4 molecules have been found by the crystallographic analysis. This result allows to presume that a part of proline molecules is highly disordered. By close investigation of the single crystal X-ray diffraction analysis, the crystal structures of all the compounds have abnormal large voids in their lattices as exemplified by **Pr-L** and **Pr-D** (**Fig. 4-1**), suggesting that the other proline molecules are contained in these voids. **Fig. 4-2(above)** shows difference Fourier maps after the final refinements, where one can see residual electron density distributions in the voids. Some of them form shapes of proline or its ring fragment. **Fig. 4-2(below)** represents relatively well-defined electron density assemblies possessing the proline structure. All attempts to refine these peaks as proline molecules using rigid models or partially restrained models failed in

divergences of proline molecules. Therefore, we concluded that the remaining proline molecules are in positional, orientational, and/or occupational disordering state(s) in the voids. Similarly, crystallographically undefined Na^+ and K^+ might be distributed in these voids.

4-3-2 Outline of the crystal structures

All of the compounds are mixed salts of Na^+ and K^+ cations, of which Na^+ originates from the precursor $Na_9[A\text{-}\alpha\text{-}PW_9O_{34}]\cdot 16H_2O$. They are composed of Na, K, proline and the polyanion. The pKa (1.95 and 10.47) of proline [28] and the pH condition (2.6-2.9) in the synthetic procedure suggest that one or two proline molecules are protonated and the others are zwitterionic.

The $[Ln(\alpha\text{-}PW_{11}O_{39})_2]^{11-}$ polyanion in all compounds is composed of two O-donor mono-lacunary Keggin units $[\alpha\text{-}PW_{11}O_{39}]^{7-}$ coordinating to Ln^{3+}, forming a LnO_8 square-antiprism polyhedron (**Fig. 4-3**). The Ln-O and W-O lengths, and bond valence sums (BVS) [29] for Ln, W, and P centers in the polyanions are summarized in **Table 4-2**. The bond lengths of Ln-O are comparable to those in the reported $[Ln(W_5O_{18})_2]^{9-}$. The BVS values calculated from the bond lengths are reasonably corresponded to their formal valences of Ln^{3+}, P^{5+} and W^{6+}.

Fig. 4-1 shows the crystal structures of **Pr-L** and **Pr-D**, indicating that only the L-form polyanion L-$[Ln(\alpha\text{-}PW_{11}O_{39})_2]^{11-}$ and D-form polyanion D-$[Ln(\alpha\text{-}PW_{11}O_{39})_2]^{11-}$ are contained in **Pr-L** and **Pr-D**, respectively. Therefore, the L-$[Ln(\alpha\text{-}PW_{11}O_{39})_2]^{11-}$ and D-$[Ln(\alpha\text{-}PW_{11}O_{39})_2]^{11-}$ polyanions are enantioselectively isolated together with the Na^+, K^+, and proline molecules as the chiral inducer. Details will be described later.

4-3-3 Crystal forms

The compounds crystallized in two kinds, Forms-A and B, which have the same space group (P1) but different unit cell volumes (**Table 4-1**); **La-L** and **Eu-L** belong to Form-A, **Pr-L**, **Nd-L**, **Sm-L**, **Gd-L**, **Tm-L**, **Dy-L**, **Er-L**, **Pr-D**, and **Er-D** belong to Form-B. The unit cell volume (V) of Form A with Z = 3 is about three times larger than that of Form B with Z = 1. As there is no observable tendency between the crystal forms and ionic radius of Ln^{3+}, small differences in synthetic and/or crystallizing conditions may influence the resulting forms.

The crystal structures of **Eu-L** (Form-A) is described in **Fig. 4-4**. One can see that the Form-A has a similar cell packing to that in **Pr-L** (Form-B) (**Fig. 4-1 top**), but has less void region. In fact, 6 of 8.5 equivalences of proline could be determined in the single crystal X-ray diffraction analysis of **Eu-L**. This observation indicates that proline molecules in Form-A are less disordering. **Fig. 4-5** compares three adjacent polyanions and their neighboring proline molecules and K^+ cations in **Eu-L** (Form-A) and **Pr-L** (Form-B). The three polyanions in **Pr-L** (**Fig. 4-5(a)**) are crystallographically equivalent, while those in **Eu-L** (**Fig. 4-5(b)**) are independent (denoted by polyanions-1, -2, and -3) and these have approximately the same molecular orientation. It is noticeable that two proline molecules exist in the vicinity of each of polyanions-1 and -3, whereas only one molecule is located around the polyanion-2. Positions and numbers of the K^+ ions also differ in the three polyanions in **Eu-L**; in the polyanion-1, one K^+ ion is coordinated by carboxylate O atoms in the two proline molecules; in the polyanion-2, K^+ is coordinated by the proline; in the polyanion-3, two K^+ ions are coordinated by the two proline. These slight differences in distribution of proline molecules and K^+ ions in the crystal lower the disordering in Form-A and triplicate its cell volume.

4-3-4 Emergence of chirality in aqueous solutions and crystals

By addition of proline molecule as chiral auxiliaries, how the chirality was expressed in aqueous solution and in the solid state was investigated using single crystal X-ray diffraction, circular dichroism (CD) spectroscopy, and NMR spectroscopy in further detail. The structural chemistry around the Ln^{3+} was interpreted with a help of single crystal X-ray diffraction analysis. The CD spectroscopy provides us chiral preservation of the polyanion in aqueous solution. The ^{31}P-NMR spectroscopy gives us some useful information about stability of the polyanion in aqueous solution. Also, the ^{13}C-NMR spectroscopy can allow to explain the interaction between the polyanion and proline both in aqueous solution and in the solid state.

4-3-4-1 Crystallographic study

A chirality in the solid state can be discussed with a help of single crystal X-ray diffraction analysis from structural point of view. **Fig. 4-6** displays the intermolecular interaction between the L-/D-$[Ln(\alpha\text{-}PW_{11}O_{39})_2]^{11-}$ and L-/D-proline near the polyanion in **Pr-L** and **Pr-D**, respectively. The distances between amino-N atoms in proline and Pr^{3+} in the polyanion are 4.03(2) and 4.11(2) Å for **Pr-L** and 4.01(2) and 4.09(1) Å for **Pr-D**. Also, the distances from these N atoms to the oxygen atoms coordinating to Pr^{3+} ion are 2.88(2)-3.18(2) Å and 2.83(2)-3.14(2) Å for **Pr-L** and **Pr-D**, respectively, suggesting that there are hydrogen-bondings between L-/D-$[Ln(\alpha\text{-}PW_{11}O_{39})_2]^{11-}$ and L-/D-proline. Viewed along the molecular C_2 axis, it is understood that four hydrogen-bondings in two directions fix two $[\alpha\text{-}PW_{11}O_{39}]^{7-}$ units and stabilize a SA coordination of Pr^{3+} to exhibit the molecular chirality.

Fig. 4-7 shows the molecular association between L-$[Ln(\alpha\text{-}PW_{11}O_{39})_2]^{11-}$ and

L-proline in **Pr-L** represented by the space-filling model. The two proline molecules giving a hydrogen-bonding interaction have slightly different conformations (**Fig. 4-7** inset). The C^{α}, C^{β}, C^{δ}, and N atoms are nearly planar for both molecules. The C^{γ} atom is in a *cis* position with respect to the carboxyl group in L-proline1, whereas that in L-proline2 is in a *trans* position. The two L-proline molecules are captured by two grooves formed by O atoms (red spheres in **Fig. 4-7**). It is of significance that this molecular association is stereoselective; i.e., the molecular surface of L-proline specifically fits to the internal surface of the groove in L-$[Ln(\alpha\text{-}PW_{11}O_{39})_2]^{11-}$, making the L-proline molecules accessible to the PrO_8 center to allow the hydrogen-bonding (**Fig. 4-7**). In fact, hypothetical model composed of proline molecules with opposite chirality demonstrates a steric hindrance. Particularly, the estimated shortest distances d(N···O) ~ 3.4-4.1 Å between L-$[Ln(\alpha\text{-}PW_{11}O_{39})_2]^{11-}$ and *cis*-D-pro1 within a rigid model approximation (**Fig. 4-7**) exceed the typical hydrogen-bonding distance. In other words, the groove in L-$[Ln(\alpha\text{-}PW_{11}O_{39})_2]^{11-}$ inhibits the hydrogen-bonding with D-proline and *vice versa*. Other L-proline molecules in **Pr-L** do not participate in a specific association with L-$[Ln(\alpha\text{-}PW_{11}O_{39})_2]^{11-}$, but serve as chiral fillers positioned among the polyanion in the crystal. **Pr-D** has the inverse structure of **Pr-L**; the two D-proline1 and D-proline2 molecules attached to the D-$[Ln(\alpha\text{-}PW_{11}O_{39})_2]^{11-}$ have *cis* and *trans* conformations (**Fig. 4-7**). Therefore, it is suggested that the proline has suitable molecular size and structure to express and sustain the chirality of $[Ln(\alpha\text{-}PW_{11}O_{39})_2]^{11-}$ from structural chemistry point of view.

4-3-4-2 CD spectroscopy

To examine the chirality expression and preservation in solution, the CD spectra of

Er-L, **-D** and **Pr-L**, **-D** in aqueous solutions were measured. First of all, the CD spectra of mother liquors from the synthetic processes for these compounds are shown in **Fig. 4-8**, in which couples of mirror-imaged spectra due to f-f transitions in Pr^{3+} and Er^{3+} are observed. This indicates that Pr^{3+} and Er^{3+} are positioned in chiral centers before crystallization.

Secondly, a chirality expression by proline was confirmed for both Pr and Er derivatives. The initial racemic solutions of $[Ln(\alpha\text{-}PW_{11}O_{39})_2]^{11-}$ were prepared according to the scheme in **Fig 4-9(a)**. Then, CD spectra were measured successively as shown in **Fig. 4-9(b)**. The results are shown in **Fig. 4-9(c)**. In the absence of proline, the racemic mixture of the polyanion had no CD activity. However, it was not until the proline was added that chirality was induced. This fact demonstrates that a racemization equilibrium is present between the enantiomers of $[Ln(\alpha\text{-}PW_{11}O_{39})_2]^{11-}$, and the equilibrium is shifted to either one by interaction with proline.

Thirdly, an effect of the amounts of L- and D-proline and their mixtures on the ellipticity was examined for Er derivative. When equivalent amounts of L-proline (4.5 mmol) and D-proline (4.5 mmol) were added to the racemic solution of $[Er(\alpha\text{-}PW_{11}O_{39})_2]^{11-}$ (1mmol Er^{3+} is contained), no CD activity was induced (**Fig. 4-10(a)**, dark brown line), because the chiral environment of the polyanion is cancelled by the opposite chirality of proline. A gradual increase of L-proline (4.5→6.0→7.5 mmol) and decrease of D-proline (4.5→3.0→1.5 mmol) added to the racemic solution resulted in an induction and enhancement of chirality (**Fig. 4-10(a)**, dark green and gray lines). This strongly suggests that the equilibrium between the enantiomers described above is shifted to L-$[Er(\alpha\text{-}PW_{11}O_{39})_2]^{11-}$ by the domination of L-proline. An increase of L-proline (9.0→80.0 mmol) in the absence of D-proline produced a great enhancement

of ellipticity as shown in **Fig. 4-10(b)**. As an ellipticity is proportional to a concentration of a surplus enantiomer, the enhanced intensity means that racemization equilibrium is remarkably shifted to L-$[Er(\alpha\text{-}PW_{11}O_{39})_2]^{11-}$. Ellipticity of the 524 nm-band is plotted as a function of the amount of L-proline in **Fig. 4-10(c)**. The result demonstrates that the ellipticity is proportional to the L-proline at lower concentration, but tends to saturate at higher concentration.

Lastly, the CD spectra of aqueous solutions of the isolated **Pr-L**, **Pr-D**, **Er-L**, and **Er-D** crystals were measured. As will be discussed in the next subsection, ^{31}P-NMR spectroscopy proved the existence of $[Ln(\alpha\text{-}PW_{11}O_{39})_2]^{11-}$ (Ln = Pr and Er) polyanions in aqueous solutions. For the both Pr and Er derivatives, couples of mirror-imaged spectra similar to those for the mother liquors were observed (**Fig. 4-11**).

These results allow to conclude that enantioselective synthesis of sandwich-type $[Ln(\alpha\text{-}PW_{11}O_{39})_2]^{11-}$ was achieved with the aid of proline, and the chirality of polyanions is retained in solutions. Additionally, it is of significant that the chirality of the $[Pr(\alpha\text{-}PW_{11}O_{39})_2]^{11-}$ polyanion in solutions was proved, because solution ^{183}W-NMR study for the corresponding sodium salts by Fedotov et al. [30] revealed that the $[Pr(\alpha\text{-}PW_{11}O_{39})_2]^{11-}$ has C_{2h} or C_{2v} symmetry and should not exhibit chirality. This fact supports the chiral induction by the co-existence of proline.

4-3-4-3 ^{31}P-NMR study

In order to examine the stability of the $[Ln(\alpha\text{-}PW_{11}O_{39})_2]^{11-}$ polyanion in aqueous solution, the ^{31}P-NMR spectra of **Pr-L**, **Nd-L**, **Tb-L**, **Er-L**, **Yb-L**, **Y-L**, **Pr-D**, and **Er-D** were measured at room temperature (298K). The major single peaks at -13.3, -23.0, and -13.3 ppm for **Pr-L**, **Nd-L**, and **Pr-D** (**Figs. 4-13(i)**, **(ii)**, and **(viii))** can be attributed to

$[Pr(\alpha\text{-}PW_{11}O_{39})_2]^{11-}$, $[Nd(\alpha\text{-}PW_{11}O_{39})_2]^{11-}$, and $[Pr(\alpha\text{-}PW_{11}O_{39})_2]^{11-}$, respectively. The minor peaks (-18.9, -25.0, and -18.9 ppm) with much smaller integrated ratios (~ 1 %) than the major peaks are due to mono-substituted $[Ln(H_2O)_n(\alpha\text{-}PW_{11}O_{39})]^{4-}$ (Ln = Pr, Nd, and Pr) species. These observations suggest that species of $[Pr(\alpha\text{-}PW_{11}O_{39})_2]^{11-}$ and $[Nd(\alpha\text{-}PW_{11}O_{39})_2]^{11-}$ stably exist in aqueous solutions. **Figs. 4-13(iii)-(vii)**, and **(ix)** show the ^{31}P-NMR spectra of **Tb-L**, **Dy-L**, **Er-L**, **Yb-L**, **Y-L**, and **Er-D**. With the aid of the Fedotov's study [30], the major doubly split bands at -192.8 and -196.1 ppm for **Tb-L**, -95.1 and -96.4 ppm for **Dy-L**, 71.5 and 69.5 ppm for **Er-L**, 33.7 and 33.0 ppm for **Yb-L**, -12.9 and -13.1 ppm for **Y-L**, and 71.4 and 69.4 ppm for **Er-D** are attributable to the parent $[Ln(\alpha\text{-}PW_{11}O_{39})_2]^{11-}$ (Ln = Tb, Dy, Er, Yb, and Y) polyanions. The second major peaks at -227.3 ppm for **Tb-L**, -126.9 ppm for **Dy-L**, 85.2 ppm for **Er-L**, 28.3 ppm for **Yb-L**, and 85.0 ppm for **Er-D** with relatively large chemical shifts and large line widths are probably due to the $[Ln(H_2O)_n(\alpha\text{-}PW_{11}O_{39})]^{4-}$ (Ln = Tb, Dy, Er, and Yb) species. A single peak at -11.7 ppm commonly observed for **Tb-L**, **Dy-L**, **Er-L**, **Yb-L**, **Y-L**, and **Er-D** is the resonance of $[\alpha\text{-}PW_{11}O_{39}]^{7-}$. The integrated intensities for $[Ln(H_2O)_n(\alpha\text{-}PW_{11}O_{39})]^{4-}$ and $[\alpha\text{-}PW_{11}O_{39}]^{7-}$ are in the range of 20~30 % of that for $[Ln(\alpha\text{-}PW_{11}O_{39})_2]^{11-}$. Thus, it is suggested that in the solutions of **Tb-L**, **Dy-L**, **Er-L**, **Yb-L**, and **Er-D**, the $[Ln(\alpha\text{-}PW_{11}O_{39})_2]^{11-}$ polyanion partially dissociates into mono-substituted $[Ln(H_2O)_n(\alpha\text{-}PW_{11}O_{39})]^{4-}$ and $[\alpha\text{-}PW_{11}O_{39}]^{7-}$ polyanions following the scheme.

$$[Ln(\alpha\text{-}PW_{11}O_{39})_2]^{11-} + nH_2O \rightarrow [Ln(H_2O)_n(\alpha\text{-}PW_{11}O_{39})]^{4-} + [\alpha\text{-}PW_{11}O_{39}]^{7-} \quad \textbf{Eq. 4-1}$$

Next, let us consider the mechanism of the double split and non-split ^{31}P-NMR

resonance peaks for the $[Ln(\alpha\text{-}PW_{11}O_{39})_2]^{11-}$ (Ln = Tb, Dy, Er, Yb, Y, and Er) polyanions. Herein, taking **Er-L** as an example, discussion will be delivered (**Fig. 4-14 Scheme A**). From the fact that the CD activity was induced by addition of proline into the racemic aqueous solution of $[Er(\alpha\text{-}PW_{11}O_{39})_2]^{11-}$ (**Fig. 4-9(c)**), it seems that dissolution of **Er-L** crystals to water results in a partial transformation from L-$[Er(\alpha\text{-}PW_{11}O_{39})_2]^{11-}$ into D-$[Er(\alpha\text{-}PW_{11}O_{39})_2]^{11-}$ to accomplish a racemization equilibrium between the L-form and D-form. Since this solution is CD active (**Fig. 4-11** right), the equilibrium is possibly inclined toward the L-form by interaction with co-existent L-proline,

$$\text{L-}[Er(\alpha\text{-}PW_{11}O_{39})_2]^{11-} \underset{\text{L-proline}}{\rightleftharpoons} \text{D-}[Er(\alpha\text{-}PW_{11}O_{39})_2]^{11-}. \qquad \textbf{Eq. 4-2}$$

The doubly split bands in the ^{31}P-NMR spectrum for **Er-L** suggest that the difference in interactions between the L/D-form of polyanions and L-proline (L-form↔L-proline and D-form↔L-proline) is recognized by ^{31}P-NMR. Also, based on this hypothesis, the strong and weak peaks are assignable to L-form and D-form, respectively.

The observed split resonance bands suggest that structural conversion between the enantiomers is slower than the NMR timescale. Generally, the rate of structural conversion in equilibrium increases with temperature. So, when the ^{31}P-NMR spectrum of **Er-L** aqueous solution is measured at higher temperature, it is expected that the two shifts would approach to each other, and fuse into a single peak when the conversion is more rapid than the NMR timescale. In fact, at 323 K, we observed nearly single resonance peak at 55.6 ppm (**Fig. 4-13(x)**). This observation can be explained in terms of an accelerated exchange between the L-form and D-form induced by the temperature

elevation.

Moreover, to confirm the assignment of the doubly split peaks in the ^{31}P-NMR spectra of **Er-L**, we measured for racemic solutions of $[Er(\alpha\text{-}PW_{11}O_{39})_2]^{11-}$ in the absence and presence of L-proline (**Figs. 4-13(xi)** and **(xii)**) at room temperature. In the absence of L-proline, the ^{31}P-NMR spectrum shows a single peak at 71.0 ppm due to D/L-$[Er(\alpha\text{-}PW_{11}O_{39})_2]^{11-}$ species. Addition of L-proline to this solution ($[Er(\alpha\text{-}PW_{11}O_{39})_2]^{11-}$: proline = 1:9) resulted in a slight split of the peak into 70.1 and 69.5 ppm. Note that these shifts are approximately consistent with those (71.5 and 69.5 ppm) for the aqueous solution of **Er-L** (**Fig. 4-13(v)**), suggesting that similar equilibrium (**Eq. 4-2**) is established in these solutions. As already described, the same procedure gave rise to the CD activity (**Fig. 4-9**; light blue). These demonstrate that the racemic equilibrium between equimolar L-form and D-form was shifted to L-form by addition of L-proline, and that the interaction of L-proline with L-form and D-form was differentiated by ^{31}P-NMR.

Furthermore, temperature dependence of CD spectroscopy was measured for aqueous solution of **Er-L**. A gradual decrease of ellipticity was observed by temperature elevation from 298K to 324K (**Fig. 4-12**). It is expected that, at high temperature, an interaction between polyanion and proline is reduced by thermal perturbation of molecules, resulting in a low CD activity. Such a decline of polyanion-proline interaction would lower the differentiation in ^{31}P-NMR, and this effect may contribute to the singlet ^{31}P-NMR peak of the **Er-L** solution observed at 323K (**Fig. 4-13(x)**).

On the other hand, the assumed equilibrium in **Pr-L** aqueous solution is demonstrated in **Scheme B** in **Fig. 4-14**. As is the case in **Er-L**, the racemization equilibrium,

$$\text{L-}[Pr(\alpha\text{-}PW_{11}O_{39})_2]^{11-} \underset{\text{L-proline}}{\rightleftharpoons} \text{D-}[Pr(\alpha\text{-}PW_{11}O_{39})_2]^{11-} \qquad \textbf{Eq. 4-3}$$

is established, in which L-$[Pr(\alpha\text{-}PW_{11}O_{39})_2]^{11-}$ is dominant as demonstrated in the CD spectra (**Fig. 4-11(left)**). However, since enantiomeric exchange and/or formation equilibrium for polyanion-L-proline association (i.e. L-form + L-proline and D-form + L-proline) are faster than NMR timescale, no split of resonance band for the **Pr-L** solution was observed. So, even the exchange rate is lowered by cooling in order to detect the difference in enantiomeric interaction, it is probably impossible to measure the ^{31}P-NMR of **Pr-L** in aqueous solution due to its crystallization.

Comparison of the ^{31}P-NMR spectra for all Ln derivatives revealed that single (non-split) resonance peak of $[Ln(\alpha\text{-}PW_{11}O_{39})_2]^{11-}$ was observed for lighter Ln = Pr and Nd with little dissociation, while doubly split peaks were observed for heavier Ln = Tb, Dy, Yb, and Y involving a considerable dissociation following **Eq. 4-1**. These facts strongly suggest that enantiomeric conversion between L-form and D-form occurs through an 'on-site' rotation of the $[\alpha\text{-}PW_{11}O_{39}]^{7-}$ unit within the $[Ln(\alpha\text{-}PW_{11}O_{39})_2]^{11-}$ molecule for lighter Ln, and a 'dissociation-association' route for heavier Ln as follows,

$$\text{L-}[Ln(\alpha\text{-}PW_{11}O_{39})_2]^{11-} + nH_2O \rightleftharpoons [Ln(H_2O)_n(\alpha\text{-}PW_{11}O_{39})]^{4-} + [\alpha\text{-}PW_{11}O_{39}]^{7-}$$
$$\rightleftharpoons \text{D-}[Ln(\alpha\text{-}PW_{11}O_{39})_2]^{11-} + nH_2O. \qquad \textbf{Eq. 4-4}$$

The rapid enantiomeric conversion which is undetectable by ^{31}P-NMR may be due to the 'on-site' rotation mechanism. On the other hand, it is reasonable to consider that the latter 'dissociation-association' occurs slower than the ^{31}P-NMR timescale because the $[Ln(H_2O)_n(\alpha\text{-}PW_{11}O_{39})]^{4-}$ and $[\alpha\text{-}PW_{11}O_{39}]^{7-}$ species were detected in the spectra (**Figs.**

4-13(v) and **(ix)**). It seems that ionic radius of Ln^{3+} causes the different mechanisms as suggested by Müller et al [2] — the polyanions with the larger Ln^{3+} may have a smaller barrier to the $[\alpha\text{-}PW_{11}O_{39}]^{7-}$ rotation.

4-3-4-4 ^{13}C-NMR study

In order to investigate the interaction between the polyanion and proline molecules in aqueous solution, the ^{13}C-NMR spectra of **Pr-L** with paramagnetic Pr^{3+}, **Y-L** with non-paramagnetic Y^{3+}, and free L-proline were measured in both aqueous solutions and in the solid states.

All of the spectra (**Fig. 4-15**) in solutions have similar patterns with the same chemical shifts, and no peak splitting or broadening was observed. In conjunction with the fact that the CD signal was observed for the aqueous solution of **Pr-L** (**Fig. 4-11**), molecular interaction between the polyanion and proline is not reflected in the ^{13}C-NMR spectra. This suggests that the influence on electronic states of C atoms is negligible and/or all of the proline molecules are dynamically averaged within the NMR timescale.

Solid state ^{13}C-MAS-NMR spectra of **Pr-L**, **Y-L**, and crystalline L-proline are shown in **Fig. 4-15**. In the spectrum for **Pr-L** (**Fig. 4-16(i)**), the resonance peaks are broadened compared with that of L-proline, while the finely split peaks were observed for **Y-L** (**Fig. 4-16(ii)**). The broadening of bands for **Pr-L** is due to (i) the presence of crystallographically independent eight prolines, part of which is highly disordered, and/or (ii) paramagnetic effect of Pr^{3+}. The sharper spectral bands for **Y-L** including non-paramagnetic Y^{3+} demonstrate that the latter (ii) is significant for **Er-L**. However, the former (i) effect is still ineligible; the bands of C4 and C5 were not clearly resolved

even for **Y-L**.

4-3-5 Photoluminescent spectra

Photoluminescent spectra of the mother liquor and the crystals for **Sm-L**, **Eu-L**, **Tb-L**, and **Dy-L** were measured at room temperature and 77 K.

4-3-5-1 In aqueous solutions

For all compounds, no emission could be observed by photoexcitation of the O→W LMCT bands (~ 250 nm) of $[\alpha\text{-}PW_{11}O_{39}]^{7-}$ at room temperature. It is suggested that excitation energy absorbed by mono-lacunary Keggin units is high enough to cause photoluminescence, but was not efficiently transferred to the Ln^{3+} ion. On the other hand, for all of the compounds except for **Tb-L**, photoluminescence characteristic of Ln^{3+} f-f transitions was observed by direct excitation into the f-f absorption bands. The three characteristic peaks in **Sm-L** for excitation with $^6H_{5/2}\rightarrow{}^6P_{5/2}$ absorption are shown in **Fig. 4-17(a)**, and they are attributed to $^4G_{5/2}\rightarrow{}^6H_J$ (J = 5/2, 7/2, 9/2); $^4G_{5/2}\rightarrow{}^6H_{5/2}$ (561.8 nm), $^4G_{5/2}\rightarrow{}^6H_{7/2}$ (596.6, 603.8 nm), $^4G_{5/2}\rightarrow{}^6H_{9/2}$ (643.6 nm) for **Sm-L**. The five f-f characteristic peaks in **Eu-L** for excitation with $^7F_0\rightarrow{}^5D_3$ absorption shown in **Fig. 4-17(b)** are attributed to $^5D_0\rightarrow{}^7F_J$ (J = 0, 1, 2, 3, 4); $^5D_0\rightarrow{}^7F_0$ (578.8 nm), $^5D_0\rightarrow{}^7F_1$ (589.8, 593 nm), $^5D_0\rightarrow{}^7F_2$ (612.6, 616.8 nm), $^5D_0\rightarrow{}^7F_3$ (648.6 nm), $^5D_0\rightarrow{}^7F_4$ (698.4 nm). The two characteristic emission peaks by photoexcitation of $^6H_{15/2}\rightarrow{}^6P_{19/2}$ absorption can be seen for **Dy-L** (**Fig. 4-17(c)**), which are attributed to $^4F_{9/2}\rightarrow{}^6H_J$ (J = 15/2, 13/2); $^4F_{9/2}\rightarrow{}^6H_{15/2}$ (480.2, 487.6 nm), $^4F_{9/2}\rightarrow{}^6H_{13/2}$ (573, 581 nm) [31].

4-3-5-2 In the solid state

The luminescence spectra of **Tb-L** at 77 K (**Fig. 4-18**) are assignable to $^5D_4 \rightarrow ^7F_4$ (581.4, 587 nm), $^5D_4 \rightarrow ^7F_5$ (544.4 nm), $^5D_4 \rightarrow ^7F_6$ (491.4 nm) for O→W LMCT excitation and $^5D_4 \rightarrow ^7F_3$ (620.2 nm), $^5D_4 \rightarrow ^7F_4$ (580.6, 587 nm), $^5D_4 \rightarrow ^7F_5$ (544.4 nm), $^5D_4 \rightarrow ^7F_6$ (491 nm) for Tb^{3+}: $^7F_6 \rightarrow ^5L_7$ excitation (330 nm). For **Sm-L** and **Dy-L**, no emission was observed under photoexcitation into O→W LMCT bands at 298 K. Emission spectra of **Sm-L** by O→W LMCT excitation and direct excitation of Sm^{3+} at 77 K are shown in **Fig. 4-19**. These are attributable to $^4G_{5/2} \rightarrow ^6H_{5/2}$ (562.6, 565.8 nm), $^4G_{5/2} \rightarrow ^6H_{7/2}$ (598.2, 605.4 nm), $^4G_{5/2} \rightarrow ^6H_{9/2}$ (648.8 nm) for O→W LMCT excitation, and $^4G_{5/2} \rightarrow ^6H_{5/2}$ (562.8, 565.6 nm), $^4G_{5/2} \rightarrow ^6H_{7/2}$ (598.2, 605.4 nm), $^4G_{5/2} \rightarrow ^6H_{9/2}$ (648.6 nm) for Sm^{3+}: $^6H_{5/2} \rightarrow ^6P_{5/2}$ excitation. Emission spectra of **Dy-L** at 77 K are shown in **Fig. 4-20**, which consists of $^4F_{9/2} \rightarrow ^6H_{15/2}$ (480.2, 483.8, 489.4 nm), $^4F_{9/2} \rightarrow ^6H_{13/2}$ (574, 581.2 nm) for O→W LMCT excitation, and $^4F_{9/2} \rightarrow ^6H_{15/2}$ (480.2, 483.8, 489.4 nm), $^4F_{9/2} \rightarrow ^6H_{13/2}$ (574.4, 581.2 nm) for Dy^{3+}: $^6H_{15/2} \rightarrow ^6P_{19/2}$ excitation. Also, at 298 K, the luminescence spectra of **Sm-L** and **Dy-L** are similar to those observed at 77 K; **Sm-L**: $^4G_{5/2} \rightarrow ^6H_{5/2}$ (558.6, 562.8 nm), $^4G_{5/2} \rightarrow ^6H_{7/2}$ (598.2, 605 nm), $^4G_{5/2} \rightarrow ^6H_{9/2}$ (644 nm); **Dy-L**: $^4F_{9/2} \rightarrow ^6H_{15/2}$ (480, 488.2 nm), $^4F_{9/2} \rightarrow ^6H_{13/2}$ (574, 580.6 nm) (**Fig. 4-21**). Photoluminescence of **Eu-L** (**Figs. 4-22**, **4-23**) exhibits similar spectra irrespective to the excitation band and temperature; the transition peaks are attributed to $^5D_0 \rightarrow ^7F_1$ (590.2, 592.4 nm), $^5D_0 \rightarrow ^7F_2$ (612.8 nm), $^5D_0 \rightarrow ^7F_4$ (696.4 nm) for O→W LMCT excitation and $^5D_0 \rightarrow ^7F_0$ (579 nm), $^5D_0 \rightarrow ^7F_1$ (589.4, 593.4 nm), $^5D_0 \rightarrow ^7F_2$ (612.4 nm), $^5D_0 \rightarrow ^7F_3$ (648.8 nm), $^5D_0 \rightarrow ^7F_4$ (697.8 nm) for Eu^{3+}: $^7F_0 \rightarrow ^5D_3$ excitation at 298 K (Fig. 4-19), and $^5D_0 \rightarrow ^7F_0$ (579.8 nm), $^5D_0 \rightarrow ^7F_1$ (590.4, 593.2 nm), $^5D_0 \rightarrow ^7F_2$ (613.2, 621.6 nm), $^5D_0 \rightarrow ^7F_3$ (648.6 nm), $^5D_0 \rightarrow ^7F_4$ (698.6 nm) for O→W LMCT excitation and $^5D_0 \rightarrow$

$^7F_0$ (579.8 nm), $^5D_0 \rightarrow {}^7F_1$ (590.4, 593.2 nm), $^5D_0 \rightarrow {}^7F_2$ (613.2, 621 nm), $^5D_0 \rightarrow {}^7F_3$ (648.2 nm), $^5D_0 \rightarrow {}^7F_4$ (697.4 nm) for Eu^{3+}: $^7F_0 \rightarrow {}^5D_3$ excitation (**Fig. 4-23**) at 77 K. The studies about relationship between ligand field of Eu^{3+} and emission intensity of $^5D_0 \rightarrow {}^7F_1$ and $^5D_0 \rightarrow {}^7F_2$ transitions have been intensively developed to date [32]. The emission spectral pattern of Sm, Eu, Dy, and Tb derivatives is similar both in aqueous solution and in the solid state, suggesting that the structures of $[Ln(\alpha\text{-}PW_{11}O_{39})_2]^{11-}$ anion are maintained in aqueous solutions. Moreover, if **Ln-D** (Ln = Sm, Eu, Dy, and Tb) could be synthesized, it would show the same luminescence property as that of the corresponding Ln-L because of the equivalent Ln^{3+} environment between two enantiomers.

4-4 Conclusion

The enantioselective synthesis of C_2-symmetric L- and D-$[Ln(\alpha\text{-}PW_{11}O_{39})_2]^{11-}$ polyanions was achieved by using L- and D-proline as chiral auxiliary agents. The emergence of chirality for the $[Ln(\alpha\text{-}PW_{11}O_{39})_2]^{11-}$ polyanion was confirmed by the aqueous solution CD spectroscopy. It is suggested that the association of the polyanion and two proline molecules by an exquisite enantio- and stereo-selective hydrogen-bonding interaciton involves an exhibition of chirality in the solid state. The solution CD and ^{31}P-NMR studies revealed that, in aqueous solutions, the enantiopure L- and D-compounds are partially racemized to L- and D-forms, where the equilibrium is shifted to L-form by interaction with L-proline, and *vice versa*. This racemization is rapid for lighter Ln and enantiomers could not be differentiated by ^{31}P-NMR, while it is slow for heavier Ln and L- and D-$[Ln(\alpha\text{-}PW_{11}O_{39})_2]^{11-}$ could be detected as doubly split peaks in ^{31}P-NMR.

The result of this study may open new ways for exploring interactions between

$[Ln(\alpha\text{-}PW_{11}O_{39})_2]^{11-}$ polyanion and organic molecules by modification of proline to other derivatives such as oligopeptides and proteins.

4-5 References

[1] D. A. J. Judd, H. Nettles, N. Nevins, J. P. Snyder, D. C. Liotta, J. Tang, J. Ermolieff, R. F. Schinazi, C. L. Hill, *J. Am. Chem. Soc.*, **123**, 886 (2001).

[2] A. Müller, F. Perters, M. T. Pope, D. Gatteschi, *Chem. Rev.*, 239 (1998).

[3] F. B. Xin, M. T. Pope, *J. Am. Chem. Soc.*, **118**, 7731 (1996).

[4] M Inoue, T. Yamase, *Bull. Chem. Soc. Jpn.*, **68**, 3055 (1995).

[5] M Inoue, T. Yamase, *Bull. Chem. Soc. Jpn.*, **69**, 2863 (1996).

[6] D. L. Long, P. Kőgerler, L. J. Farrugia, L Cronin, *Chem. Asian J.* **1**, 352 (2006).

[7] D. L. Long, E. Burkholder, L. Cronin, *Chem. Soc. Rev.*, **36**, 105 (2007).

[8] C. Streb, D. L. Long, L. Cronin, *Chem. Commun.*, 471 (2007).

[9] U. Kortz, M. G. Savelieff, F. Y. Ghali, L. M. Khalil, S. A. Maalouf, D. I. Sinno, *Angew. Chem., Int. Ed.* **41**, 4070 (2002).

[10] X. K. Fang, T. M. Anderson, C. L. Hill, *Angew. Chem., Int. Ed*. **44**, 3540 (2005).

[11] X. K. Fang, T. M. Anderson, Y. Hou, C. L. Hill, *Chem. Commun.*, **40**, 5044 (2005).

[12] B. Hasenknopf, K. Micoine, E. Lacôte, S. Thorimbert, M. Malacria, R. Thoubenot, *Eur. J. Inorg. Chem.*, 5001 (2008).

[13] J. L. T. Waugh, D. P. Shoemaker, L. Pauling, *Acta Crystallogr.*, **7**, 438 (1954).

[14] Y. Hou, X. Fang, C.L. Hill, *Chem. Eur. J.*, **13**, 9442 (2007).

[15] L. Cai, Y. Li, C. Yu, H. Ji, Y. Liu, S. Liu, *Inorg. Chim. Acta*, **362**, 2895 (2009).

[16] J. Iijima, E. Ishikawa, Y. Nakamura, H. Naruke, *Inorg. Chim. Acta*, **363**, 1500 (2010).

[17] T. Ama, J. Hidaka, Y. Shimura, *Bull. Chem. Soc. Jpn.*, **43**, 2654 (1970).

[18] D. Liu, H. Q. Tan, W. L. Chen, Y. G. Li, E. B. Wang, *Cryst. Eng. Commun.*, **12**, 2044 (2010).

[19] J. Liu, J. Peng, E. Wang, L. Bi, S. Guo, *J. Mol. Struct.*, **525**, 71 (2000).

[20] M. Sadakane, M. H. Dickman, M. T. Pope, *Inorg. Chem.*, **40**, 2715 (2001).

[21] C. Boglio, B. Hasenknopf, G. Lenoble, P. Rémy, P. Gouzerh, S. Thorimbert, E. Lacôte, M. Malacria, R. Thouvenot, *Chem. Eur. J.*, **14**, 1532 (2008).

[22] Z. G. Hajos, D. R. Parrish, *J. Org. Chem.*, **39**, 1615 (1974).

[23] U. Eder, G. Sauer, R. Wiechert, *Angew. Chem. Int. Ed*, **10**, 496 (1971).

[24] A. P. Ginsburg, *Inorg. Synth.*, **27**, 96 (1990).

[25] G. M. Sheldrick, SHELXS-97, Program for Crystal Structure Solution, University of Gettingen, Germany, 1997.

[26] G. M. Sheldrick, SHELXL-97, Program for Crystal Structure Refinement, University of Gettingen, Germany, 1997.

[27] H. D. Flack, *Acta Crystallogr.*, **A39**, 876 (1983).

[28] Ed.: Lide; D. E. *Handbook of Chemistry and Physics, 88th*, 7 (2007).

[29] I. D. Brown, "Structure and Bonding in Crystals," ed by M. O'keeffe, A. Navrotsky, Academic Press, New York **Vol. II**, 1 (1980).

[30] M.A. Fedotov, B.Z. Pertsikov, D.K. Danovich, *Polyhedron*, **9**, 1249 (1990).

[31] J. Xia, B. Zhao, H. S. Wang, W. Shi, Y. Ma, H. B. Song, P. Cheng, D. Z. liao, S. P. Yan, *Inorg. Chem.*, **46**, 3450 (2007).

[32] G. Blasse, G. J. Dirksen, *J. Inorg. Nucl. Chem.*, **43**, 2847 (1981)

Table 4-1. Crystallographic data and refinement results.

	Pr-L	**Nd-L**	**Sm-L**	**Gd-L**	**Tb-L**
Empirical formula	$O_{116.1}PrP_2W_{22}K_{1.3}Na_{3.2}C_{41.5}N_{8.3}H_{124.2}$	$O_{111.6}NdP_2W_{22}K_{1.3}Na_{3.2}C_{41.5}N_{8.3}H_{115.2}$	$O_{115.1}SmP_2W_{22}K_{1.3}Na_{3.2}C_{41.5}N_{8.3}H_{122.2}$	$O_{120.6}GdP_2W_{22}K_{1.3}Na_{3.2}C_{41.5}N_{8.3}H_{133.2}$	$O_{113.1}TbP_2W_{22}K_{1.3}Na_{3.2}C_{41.5}N_{8.3}$
Formula weight	6969.37	6891.64	6960.85	7066.78	6933.35
Crystal system	Triclinic	Triclinic	Triclinic	Triclinic	Triclinic
Space group	P1	P1	P1	P1	P1
a (Å)	12.8544(3)	12.8260(5)	12.8341(3)	12.8744(6)	12.8558(5)
b (Å)	13.2986(3)	13.3186(5)	13.2819(3)	13.3048(7)	13.2973(5)
c (Å)	19.7777(5)	19.8495(8)	19.7712(4)	19.7946(9)	19.7631(7)
α (°)	103.6597(7)	103.7577(9)	103.7138(8)	103.687(2)	103.7061(9)
β (°)	92.6904(7)	93.004(1)	93.0424(7)	93.159(1)	92.930(1)
γ (°)	97.6256(7)	97.6501(9)	97.6039(7)	97.526(2)	97.5649(9)
V (Å^3)	3245.4(2)	3251.7(2)	3232.8(2)	3252.9(3)	3241.8(2)
Z	1	1	1	1	1
θ range (°)	3.1-27.5	3.1-27.4	3.1-27.5	3.1-27.5	3.1-27.4
Limiting indices reflections	-15≦h≦16 -17≦k≦17 -25≦l≦25	-16≦h≦15 -17≦k≦17 -25≦l≦25	-15≦h≦16 -17≦k≦17 -25≦l≦25	-15≦h≦16 -17≦k≦17 -25≦l≦25	-16≦h≦16 -17≦k≦17 -25≦l≦25
Crystal size (mm^3)	0.40 × 0.17 × 0.15	0.30 × 0.13 × 0.09	0.55 × 0.28 × 0.10	0.13 × 0.06 × 0.78	0.36 × 0.09× 0.09
D_c (g cm^{-3})	3.566	3.519	3.575	3.607	3.551
F(000)	3137.00	3093.00	3130.00	3187.00	3113.00
μ (mm^{-1})	19.9926	19.9748	20.1491	20.0892	20.1817
Todal data collected	52693	52740	52639	52620	52269
Unique data	25622	25642	25581	25663	26625
[$R_{(int)}$]	0.0582	0.0612	0.0597	0.0824	0.0483
Goodness-of-fit (GOF)	1.038	1.038	1.050	1.053	1.043
R_1 [$I > 2\sigma(I)$][a]	0.0509	0.0461	0.0516	0.0702	0.0576
wR_2[b]	0.1529	0.1428	0.1535	0.2023	0.1561
Flack parameter	0.004(11)	-0.012(11)	0.033(12)	0.030(16)	0.023(14)

[a] $R_1 = (\Sigma||F_0|-|F_c||)/(\Sigma|F_c|)$.

[b] $wR_2 = \Sigma[w(F_0^2-F_c^2)^2]/\Sigma[w(F_0^2)^2]^{1/2}$.

w (for **Pr-L**) = $1/[\sigma^2(F_0^2) + (0.0920\cdot P)^2 + 24.1757\cdot P]$, where P = (Max($F_0^2$,0) + 2$F_c^2$)/3

w (for **Nd-L**) = $1/[\sigma^2(F_0^2) + (0.0772\cdot P)^2 + 26.5536\cdot P]$, where P = (Max($F_0^2$,0) + 2$F_c^2$)/3

w (for **Sm-L**) = $1/[\sigma^2(F_0^2) + (0.0917\cdot P)^2 + 32.9900\cdot P]$, where P = (Max($F_0^2$,0) + 2$F_c^2$)/

w (for **Gd-L**) = $1/[\sigma^2(F_0^2) + (0.1054\cdot P)^2 + 13.4388\cdot P]$, where P = (Max($F_0^2$,0) + 2$F_c^2$)/

w (for **Tb-L**) = $1/[\sigma^2(F_0^2) + (0.0798\cdot P)^2 + 72.2398\cdot P]$, where P = (Max($F_0^2$,0) + 2$F_c^2$)/3

Table 4-1 (Continued). Crystallographic data and refinement results.

	Dy-L	**Er-L**	**Tm-L**	**Yb-L**	**Y-L**
Empirical formula	$O_{112.6}DyP_2W_{22}K_{1.3}Na_{3.2}C_{41.5}N_{8.3}H_{117.2}$	$O_{117.1}ErP_2W_{22}K_{1.3}Na_{3.2}C_{41.5}N_{8.3}H_{126.2}$	$O_{113.6}TmP_2W_{22}K_{1.3}Na_{3.2}C_{41.5}N_{8.3}H_{119.2}$	$O_{111.6}YbP_2W_{22}K_{1.3}Na_{3.2}C_{41.5}N_{8.3}H_{115.2}$	$O_{106.6}YP_2W_{22}K_{1.3}Na_{3.2}C_{41.5}N_{8.3}H_{105}$
Formula weight	6927.91	7013.74	6952.36	6920.44	6746.23
Crystal system	Triclinic	Triclinic	Triclinic	Triclinic	Triclinic
Space group	P1	P1	P1	P1	P1
a (Å)	12.8751(6)	12.8505(5)	12.8257(4)	12.8441(3)	12.8442(6)
b (Å)	13.3000(7)	13.2454(6)	13.2693(4)	13.2571(3)	13.2756(7)
c (Å)	19.730(1)	19.6811(8)	19.8320(6)	19.6876(4)	19.7854(9)
α (°)	103.880(2)	103.768(1)	103.6051(9)	103.7946(7)	103.646(2)
β (°)	92.7303(2)	92.871(1)	93.8931(9)	93.0243(7)	93.522(2)
γ (°)	97.642(2)	97.549(1)	97.666(1)	97.5524(7)	97.618(2)
V (Å^3)	3239.6(3)	3214.0(3)	3233.8(2)	3215.0(2)	3234.4(3)
Z	1	1	1	1	1
θ range (°)	3.1-27.5	3.1-27.5	3.1-27.4	3.1-27.5	3.1-27.5
Limiting indices reflections	-16≦h≦16	-16≦h≦14	-16≦h≦16	-16≦h≦16	-15≦h≦16
	-17≦k≦17	-17≦k≦17	-17≦k≦17	-17≦k≦17	-17≦k≦17
	-25≦l≦25	-25≦l≦25	-25≦l≦25	-25≦l≦25	-25≦l≦25
Crystal size (mm^3)	0.38 × 0.10× 0.08	0.53 × 0.10× 0.09	0.24 × 0.12 × 0.08	0.37 × 0.20 × 0.18	0.36 × 0.10 × 0.09
D_c (g cm^{-3})	3.551	3.623	3.570	3.574	3.463
F(000)	3109.00	3156.00	3122.00	3103.00	3022.00
μ (mm^{-1})	20.2279	20.4633	20.3706	20.5265	20.1267
Todal data collected	51878	51805	52574	52167	52025
Unique data	26588	25345	25552	25402	25515
[$R_{(int)}$]	0.0734	0.0722	0.0541	0.0481	0.0604
Goodness-of-fit (GOF)	1.060	1.073	1.041	1.032	1.072
R_1 [$I > 2\sigma(I)$][a]	0.0812	0.0583	0.0449	0.0468	0.0584
wR_2[b]	0.2426	0.1681	0.1451	0.1368	0.1672
Flack parameter	0.05(2)	0.028(14)	0.031(12)	0.014(12)	0.020(13)

[a] $R_1 = (\Sigma||F_0|-|F_c||)/(\Sigma|F_c|)$.

[b] $wR_2 = \Sigma[w(F_0^2-F_c^2)^2]/\Sigma[w(F_0^2)^2]^{1/2}$.

w (for **Dy-L**) = $1/[\sigma^2(F_0^2) + (0.1381\cdot P)^2 + 77.8849\cdot P]$, where P = $(Max(F_0^2,0) + 2F_c^2)/$

w (for **Er-L**) = $1/[\sigma^2(F_0^2) + (0.0809\cdot P)^2 + 19.8623\cdot P]$, where P = $(Max(F_0^2,0) + 2F_c^2)/$

w (for **Tm-L**) = $1/[\sigma^2(F_0^2) + (0.0922\cdot P)^2 + 20.0245\cdot P]$, where P = $(Max(F_0^2,0) + 2F_c^2)/$

w (for **Yb-L**) = $1/[\sigma^2(F_0^2) + (0.0809\cdot P)^2 + 43.5842\cdot P]$, where P = $(Max(F_0^2,0) + 2F_c^2)/$

w (for **Y-L**) = $1/[\sigma^2(F_0^2) + (0.1034\cdot P)^2 + 0.0000\cdot P]$, where P = $(Max(F_0^2,0) + 2F_c^2)/3$

Table 4-1 (Continued). Crystallographic data and refinement results.

	La-L	Eu-L	Pr-D	Er-D
Empirical formula	$O_{110}LaP_2W_{22}K_{1.2}Na_2C_{42.5}N_{8.5}H_{114.3}$	$O_{113}EuP_2W_{22}K_{1.2}Na_2C_{42.5}N_{8.5}H_{120.3}$	$O_{111.6}PrP_2W_{22}K_{1.3}Na_{3.2}C_{41.5}N_{8.3}H_{115.2}$	$O_{108.6}ErP_2W_{22}K_{1.3}Na_{3.2}C_{41.5}N_{8.3}H_{109.2}$
Formula weight	6843.11	6910.21	6888.31	6860.61
Crystal system	Triclinic	Triclinic	Triclinic	Triclinic
Space group	P1	P1	P1	P1
a (Å)	17.5783(4)	17.4826(4)	12.8016(4)	12.8410(4)
b (Å)	22.7463(4)	22.6885(4)	13.2173(5)	13.2876(5)
c (Å)	25.9258(5)	25.8377(5)	19.7108(7)	19.8313(6)
α (°)	102.2551(7)	102.2596(7)	103.714(2)	103.5786(9)
β (°)	96.1105(7)	96.3784(7)	92.569(2)	93.9442(8)
γ (°)	101.0296(7)	100.6991(7)	97.660(2)	97.6353(9)
V (Å^3)	9825.3(4)	9719.2(3)	3201.0(2)	3242.4(2)
Z	3	3	1	1
θ range (°)	3.0-27.5	3.0-27.5	3.1-27.5	3.1-27.4
Limiting indices reflections	-22≦h≦22	-22≦h≦21	-15≦h≦16	-16≦h≦16
	-29≦k≦29	-29≦k≦29	-17≦k≦17	-17≦k≦17
	-33≦l≦33	-33≦l≦33	-25≦l≦25	-25≦l≦25
Crystal size (mm^3)	0.25 × 0.23 × 0.10	0.53 × 0.11 × 0.04	0.37 × 0.13 × 0.15	0.35 × 0.10 × 0.08
D_c (g cm^{-3})	3.469	3.542	3.573	3.513
F(000)	9205.80	9313.80	3092.00	3071.00
μ (mm^{-1})	19.7523	20.1258	20.2654	20.2751
Todal data collected	159648	157200	52075	52617
Unique data	77593	76787	25513	25604
[$R_{(int)}$]	0.0752	0.0792	0.0465	0.0578
Goodness-of-fit (GOF)	1.022	1.043	1.047	1.051
R_1 [$I > 2\sigma(I)$][a]	0.0636	0.0625	0.0430	0.0478
wR_2[b]	0.1782	0.1790	0.1425	0.1429
Flack parameter	0.034(9)	0.011(10)	0.032(10)	0.043(11)

[a] $R_1 = (\Sigma||F_0|-|F_c||)/(\Sigma|F_c|)$.

[b] $wR_2 = \Sigma[w(F_0^2-F_c^2)^2]/\Sigma[w(F_0^2)^2]^{1/2}$.

w (for **La-L**) = $1/[\sigma^2(F_0^2) + (0.0918\cdot P)^2 + 130.2807\cdot P]$, where $P = (Max(F_0^2,0) + 2F_c^2)$

w (for **Eu-L**) = $1/[\sigma^2(F_0^2) + (0.0778\cdot P)^2 + 112.8139\cdot P]$, where $P = (Max(F_0^2,0) + 2F_c^2)$

w (for **Pr-D**) = $1/[\sigma^2(F_0^2) + (0.0955\cdot P)^2 + 14.6824\cdot P]$, where $P = (Max(F_0^2,0) + 2F_c^2)/3$

w (for **Er-D**) = $1/[\sigma^2(F_0^2) + (0.0932\cdot P)^2 + 6.2134\cdot P]$, where $P = (Max(F_0^2,0) + 2F_c^2)/3$

Table 4-2 The bond lengths of Ln-O, W-O and BVS values for all the compounds.

	d (Ln-O) / [Å]		*d* (W-O) / [Å]	BVS		
	Range	Average		Ln	P	W
Pr-L	2.41(1)-2.46(2)	2.45	1.67(2)-2.53(2)	3.4	4.6	5.6-6.3
Nd-L	2.39(1)-2.49(2)	2.44	1.68(2)-2.51(1)	3.4	4.6	5.7-6.2
Sm-L	2.36(1)-2.45(2)	2.41	1.67(3)-2.49(2)	3.4	5.0	5.8-6.4
Gd-L	2.34(2)-2.44(2)	2.39	1.67(2)-2.50(2)	3.4	5.4	5.3-6.3
Tb-L	2.33(2)-2.41(2)	2.38	1.65(2)-2.50(2)	3.3	5.1	5.7-6.4
Dy-L	2.27(3)-2.47(3)	2.38	1.64(3)-2.53(3)	3.2	5.3	5.5-6.8
Er-L	2.28(2)-2.40(2)	2.34	1.67(2)-2.48(2)	3.3	4.6	5.5-6.5
Tm-L	2.30(2)-2.39(1)	2.34	1.66(2)-2.47(1)	3.1	5.1	5.7-6.4
Yb-L	2.28(1)-2.37(1)	2.33	1.66(2)-2.46(1)	3.1	5.2	5.5-6.2
Y-L	2.30(2)-2.42(1)	2.36	1.67(2)-2.48(1)	3.2	5.0	5.6-6.4
La-L	2.43(2)-2.56(2)	2.50	1.65(2)-2.52(2)	3.3	5.1	5.6-6.4
Eu-L	2.34(2)-2.46(1)	2.4	1.65(1)-2.51(1)	3.3	5.2	5.6-6.4
Pr-D	2.40(1)-2.48(1)	2.44	1.68(2)-2.53(1)	3.5	4.5	5.8-6.4
Er-D	2.32(1)-2.39(1)	2.35	1.68(2)-2.49(1)	3.2	4.6	5.6-6.4

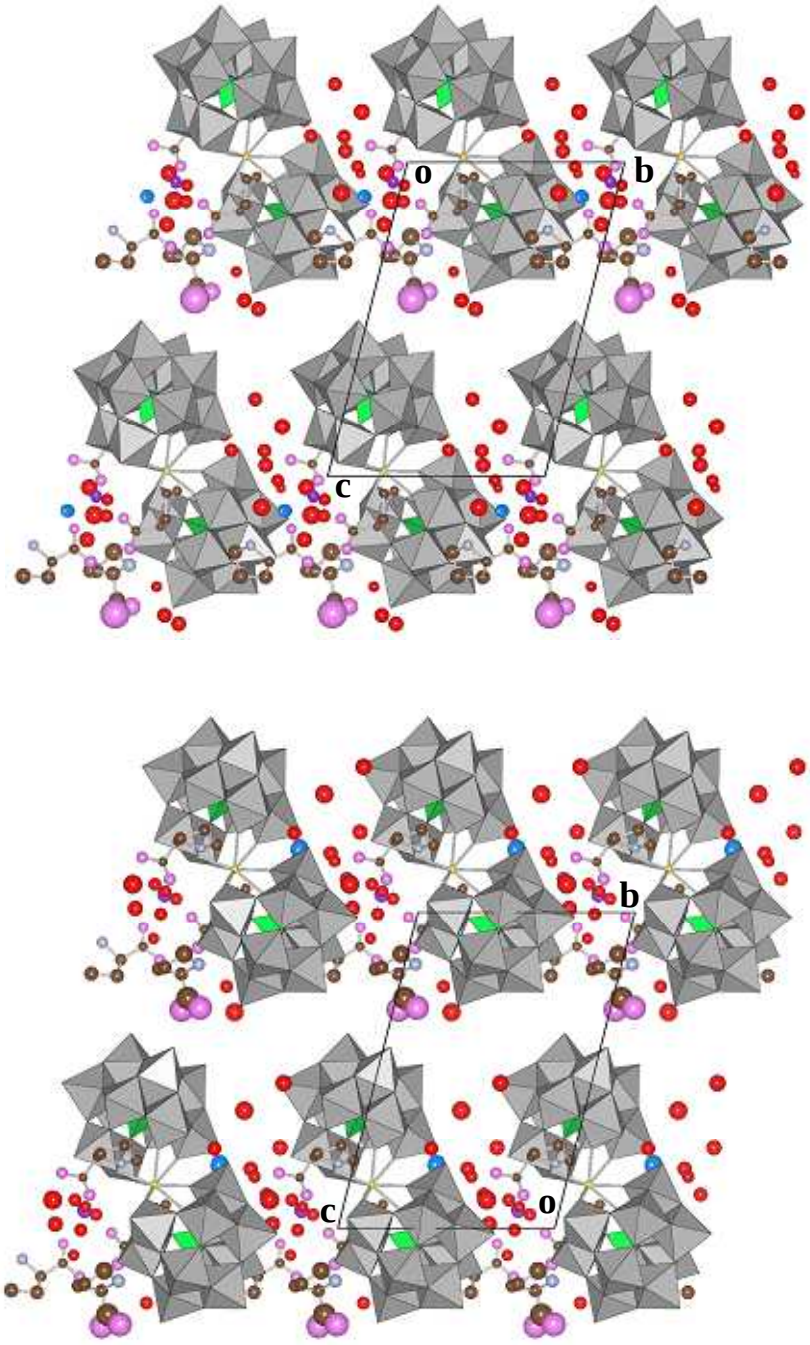

Figure 4-1. The large crystal voids in **Pr-L** (top) and **Pr-D** (bottom) viewed along the a axis. Dark gray: WO_6 octahedra; Green: PO_4 tetrahedra; Yellow: Pr; Blue: Na; Violet: K; Red: O of water of crystallization; Brown: C; Light gray: Amino N in proline; Pink: Carboxyl O in proline.

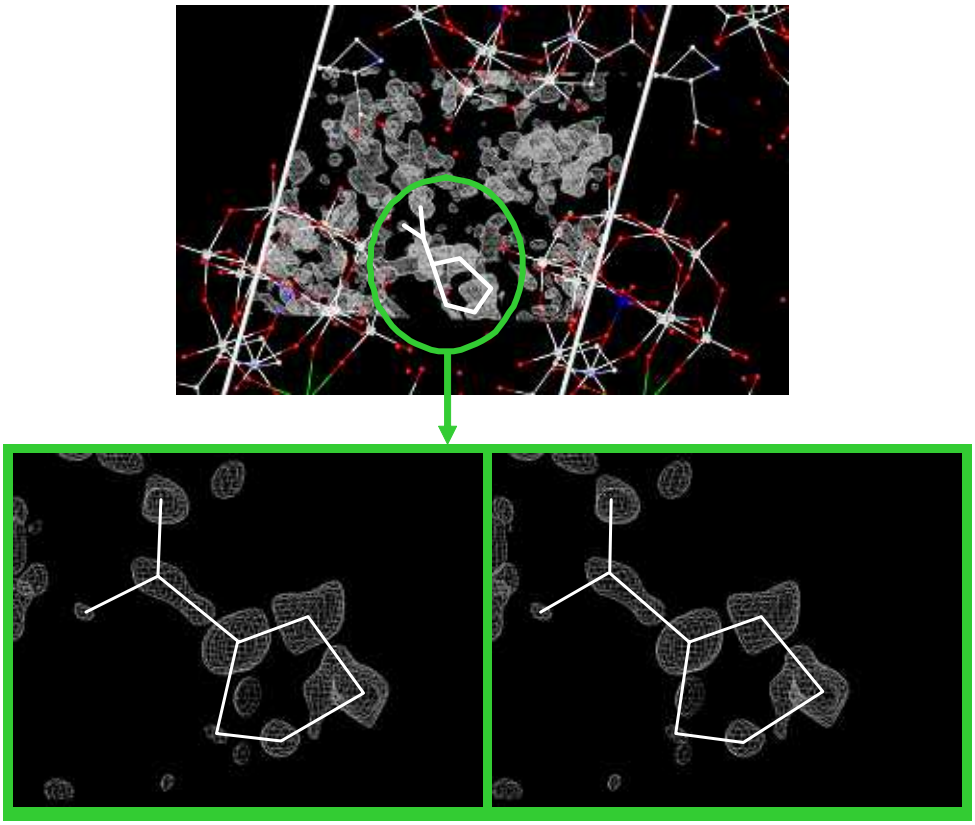

Figure 4-2. Partial difference Fourier maps in the **Pr-L**. (Top): The map around the voids in the crystal structures. (Bottom): Stereographic views of the map in selected areas, in which proline-shaped electron density distributions are observed.

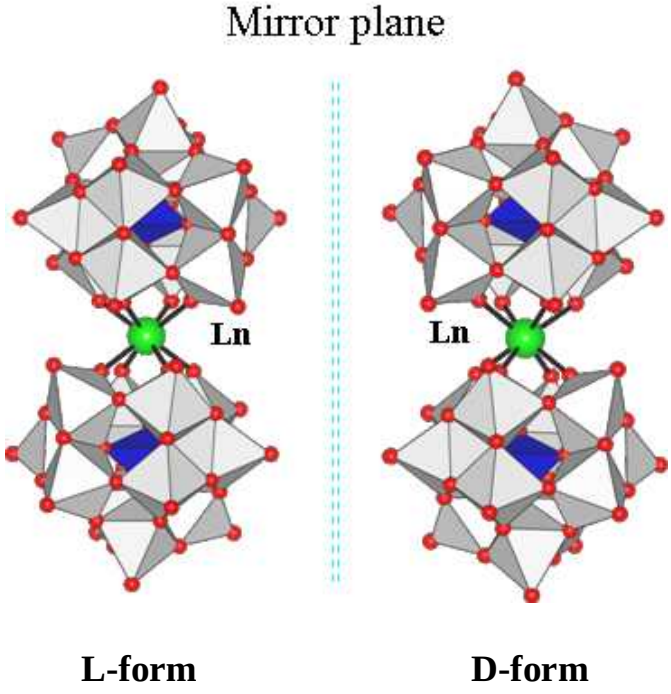

Figure 4-3. Combined polyhedral and ball-and-stick representation of two enantiomers of the $[Ln^{III/IV}(\alpha\text{-}PW_{11}O_{39})_2]^{11-/10-}$ anion viewed along the molecular C_2 axis. Left: L-form, Right: D-form. (WO_6: white octahedra, PO_4: blue tetrahedra, O atom: red spheres, Ln: green spheres).

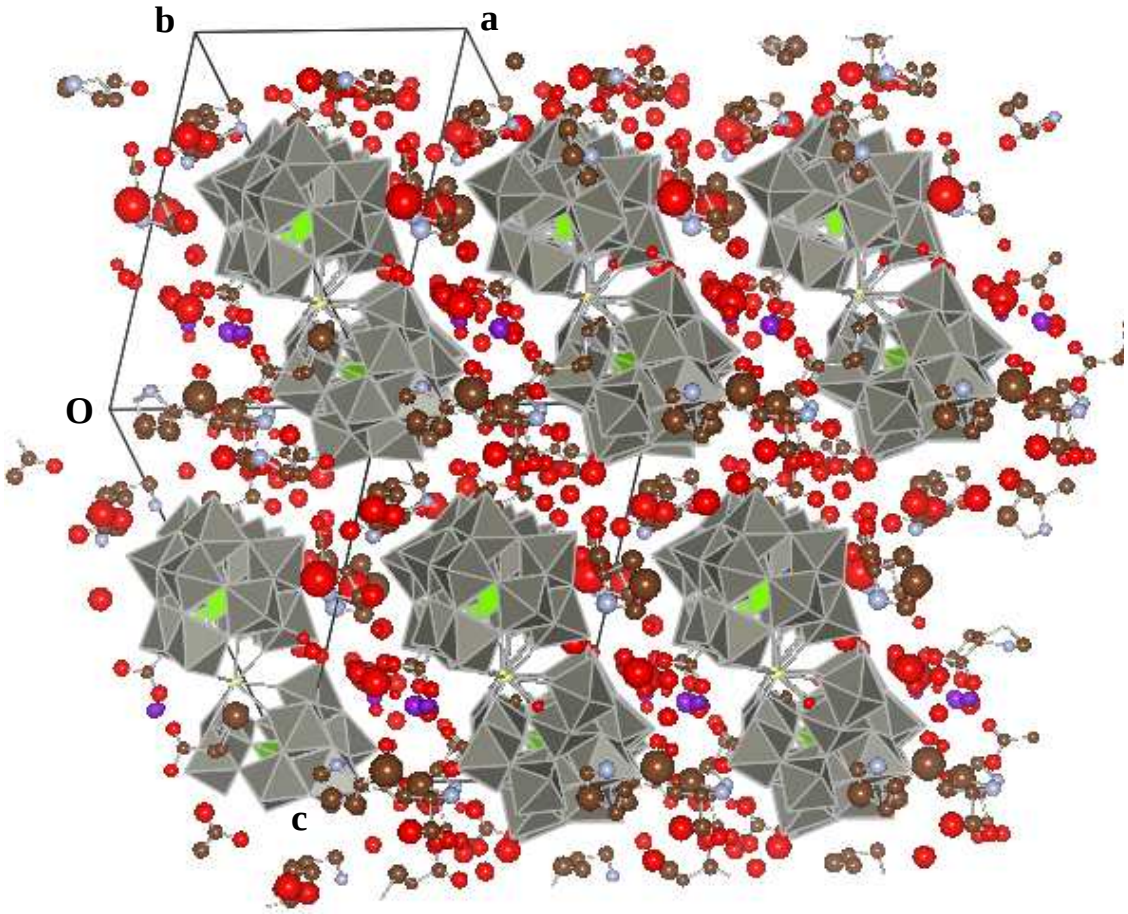

Figure 4-4. The crystal packing of **Eu-L**. Dark gray: WO_6 octahedra; Green: PO_4 tetrahedra; Yellow: Eu; Violet: K; Red: O (water of crystallization, and carboxyl O in proline); Brown: C; Light gray: Amino N in proline.

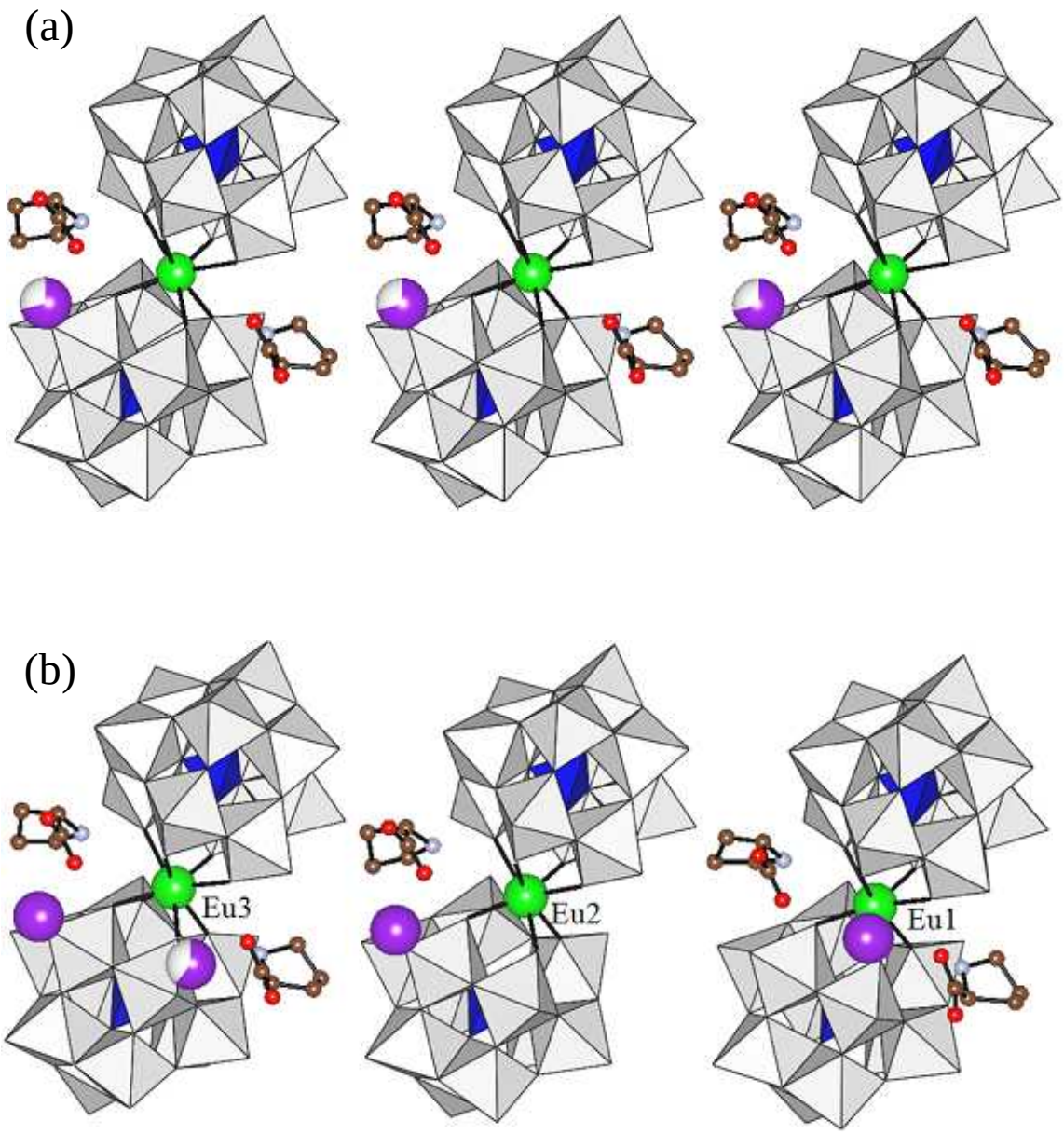

Figure 4-5. The comparison of the partial crystal structures of **Pr-L** (Form-B) (a) and **Eu-L** (Form-A) (b). White: WO_6 octahedra; Blue: PO_4 tetrahedra; Green: Pr and Eu; Violet: K; Red: O (carboxylate O in proline); Brown: C; Light gray: Amino N in proline.

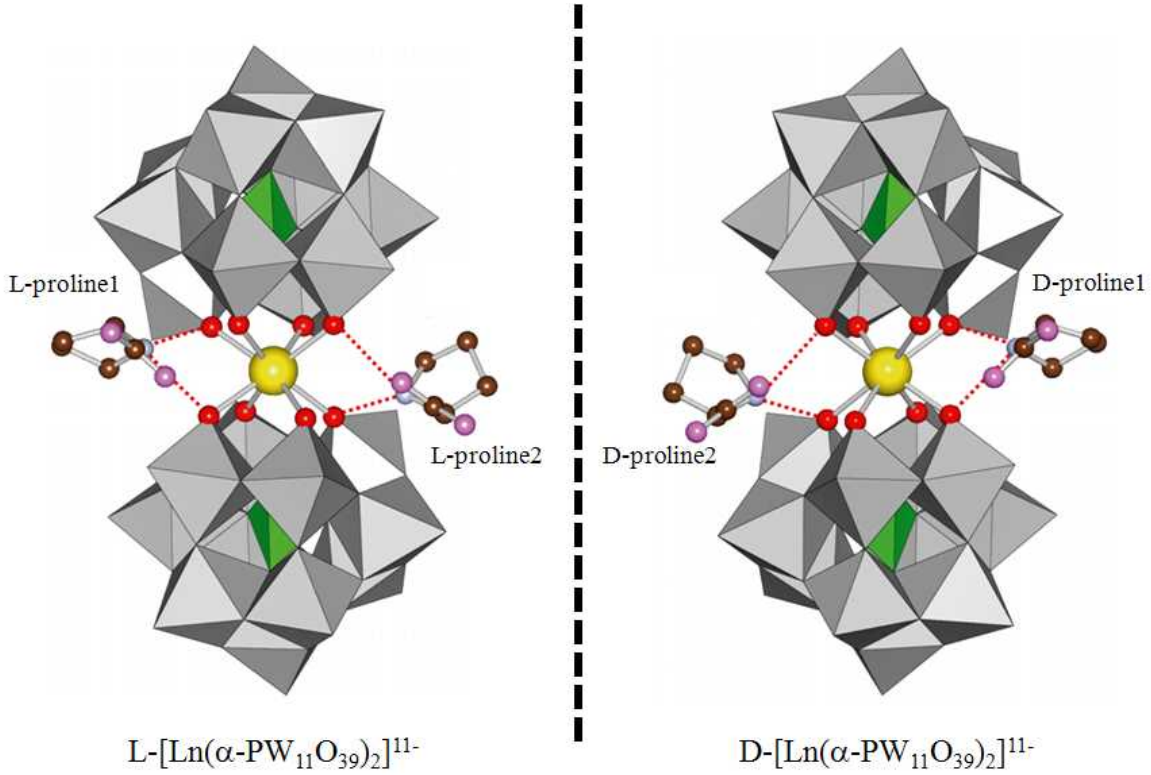

Figure 4-6. The interaction between the L-form polyanion and L-proline, D-form polyanion and D-proline through hydrogen bonding. Dark gray: WO_6 octahedra; Green: PO_4 tetrahedra; Yellow: Pr; Red: O coordinating to Pr; Pink: carboxyl O; Brown: C; Light gray: amino-N; Red dotted lines: N···O hydrogen-bonds.

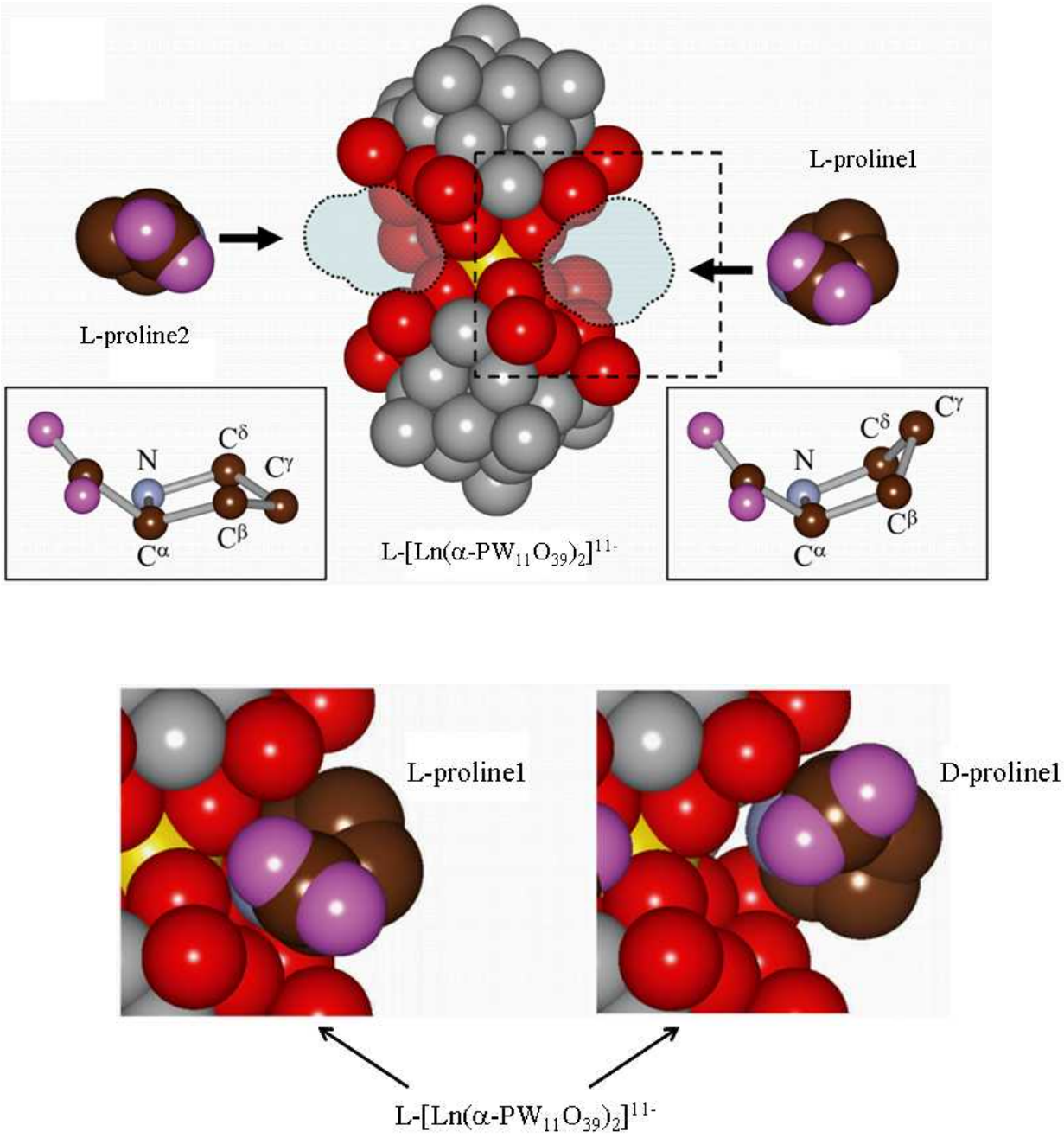

Figure 4-7. (a) Space-filling model of L-$[Pr(\alpha\text{-}PW_{11}O_{39})_2]^{11-}$ attached by two L-proline molecules in **Pr-L**. Inset: Conformations of the L-proline molecules. (b)-left: Close-up view of the boxed area in (a). (b)-right: Hypothetical association model between L-$[Pr(\alpha\text{-}PW_{11}O_{39})_2]^{11-}$ and D-proline1. The groove-forming O atoms capturing the proline molecules are shown by the red spheres.

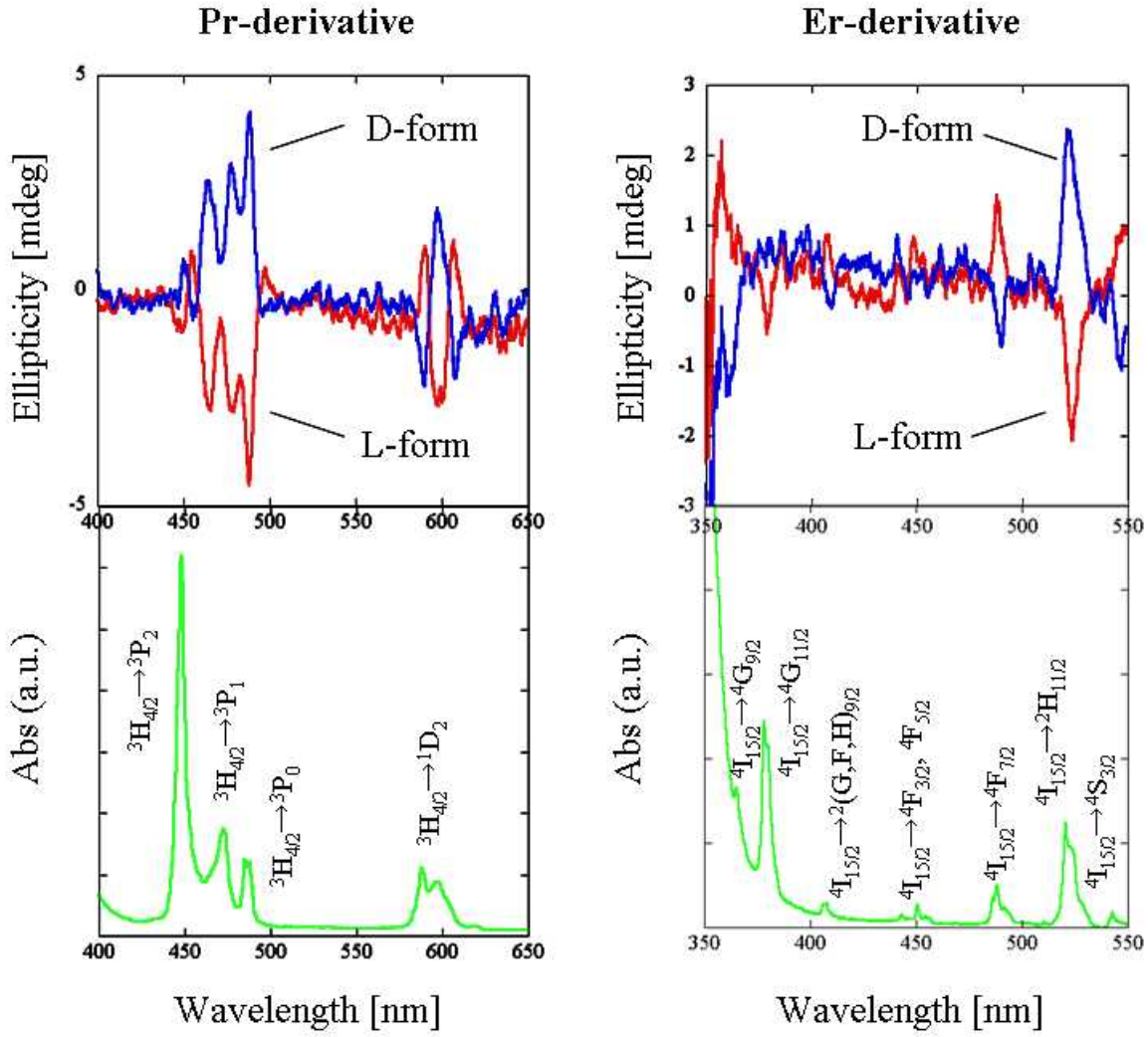

Figure 4-8. The CD spectra of the mother liquors of Pr (left) and Er (right) derivatives (above). Each spectrum is corresponded to the respective UV-Vis absorption spectrum (below).

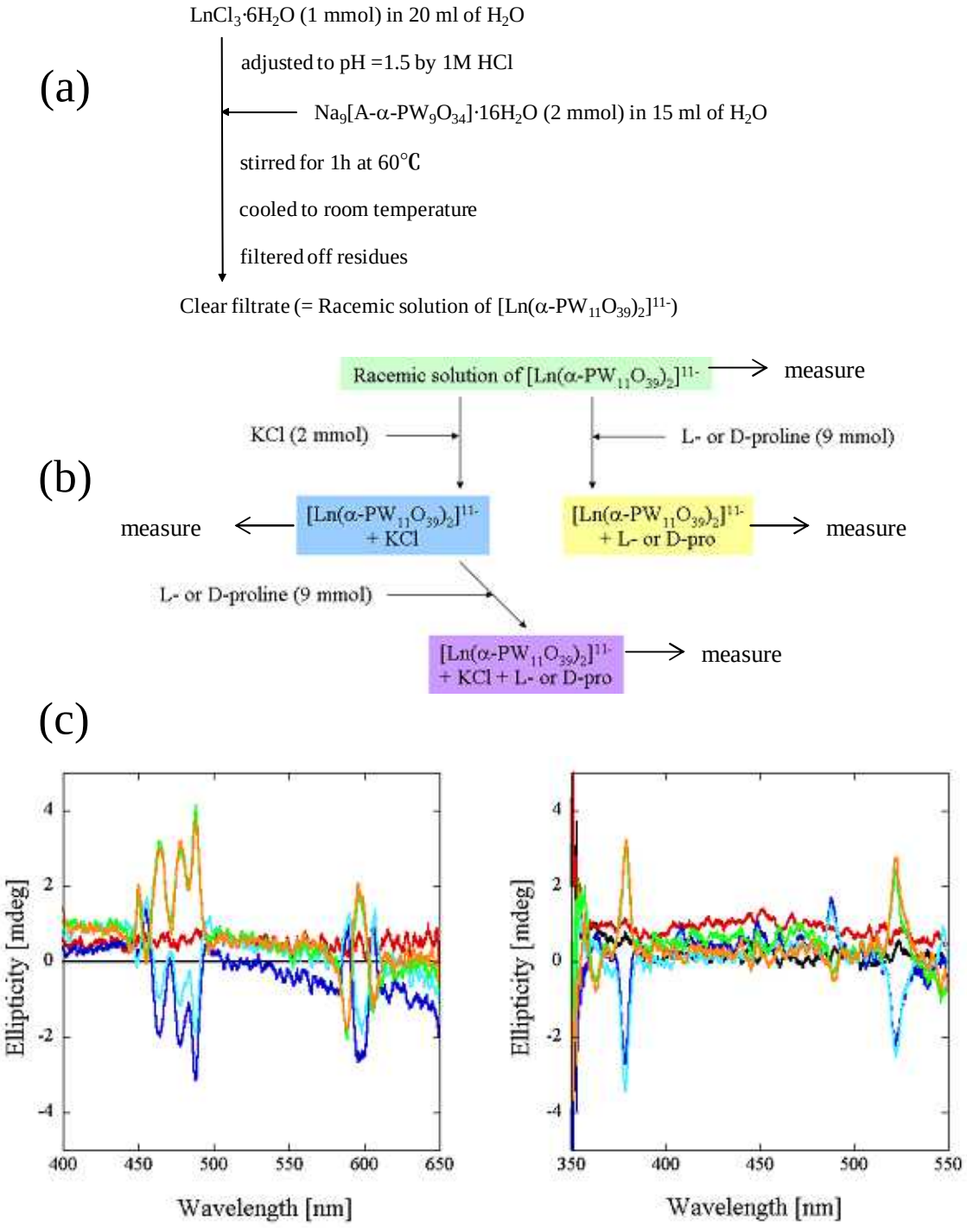

Figure 4-9. The procedure and results of CD spectroscopy for $[Ln(\alpha\text{-}PW_{11}O_{39})_2]^{11-}$ (Ln = Pr, Er) by proline; (a) Preparation procedure of racemic solution (b) The scheme of sample preparation. The CD spectra of the colored-background (green, blue, yellow, purple) sample were measured. (c) The CD spectra of Pr (left) and Er (right) derivatives. Black line; racemic solution, Red line; + KCl (2 mmol), Blue line; + L-proline (9 mmol), Green line; + D-proline (9 mmol), Light blue line; + KCl (2 mmol) + L-proline (9 mmol), Orange line; +KCl (2 mmol) + D-proline (9 mmol).

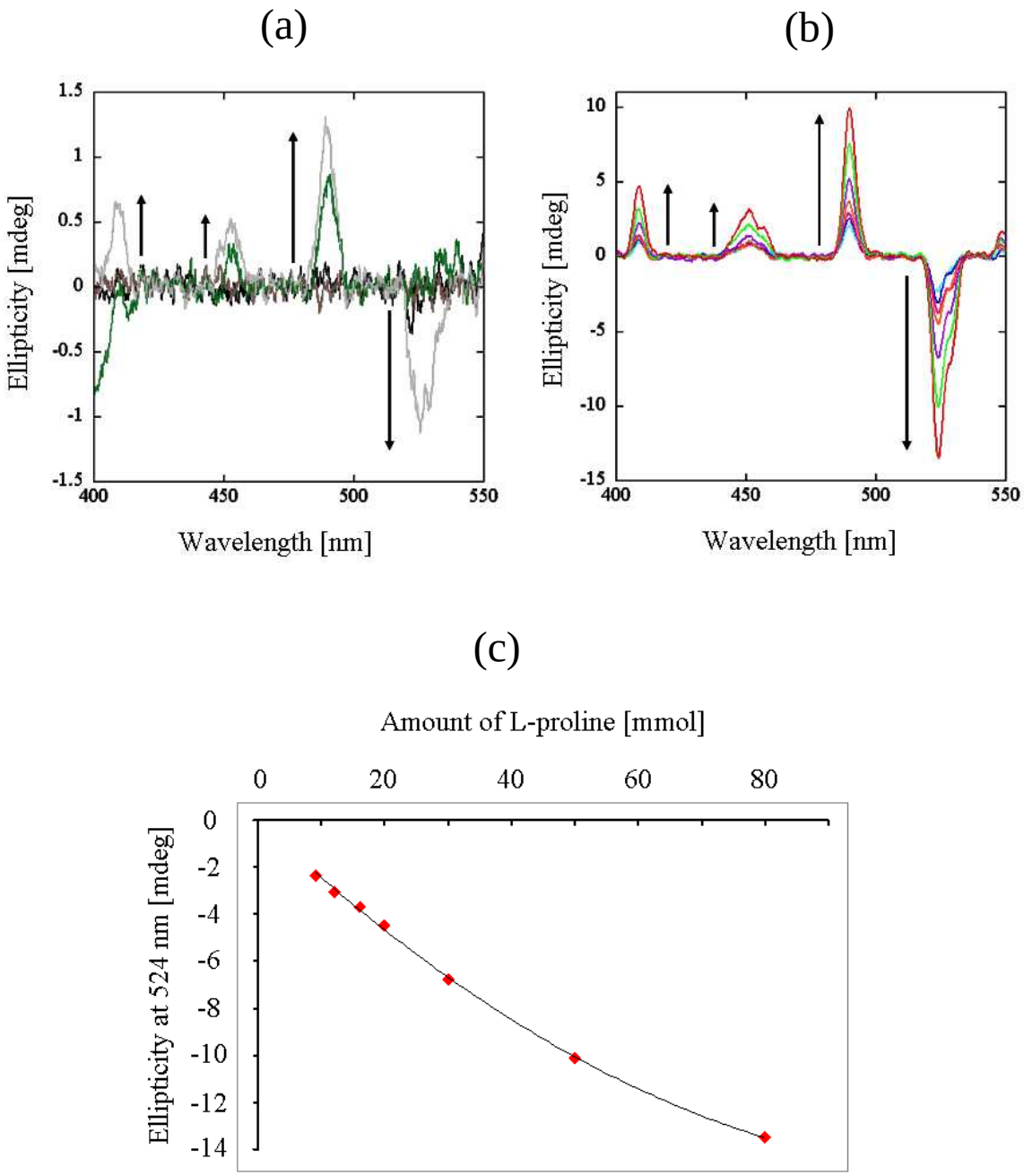

Figure 4-10. The changes in ellipticity by stepwise addition of L- and D-proline. (a) Black line; racemic solution, Dark brown line; + (L-proline:D-proline) = (4.5 mmol:4.5 mmol), Dark green line; + (L-proline:D-proline) = (6.0 mmol:3.0 mmol), Gray line; + (L-proline:D-proline) = (7.5 mmol:1.5 mmol), (b) Light blue line; +9 mmol, Blue line; +12 mmol, Pink line; +16 mmol, Orange line; +20 mmol, Purple line; +30 mmol, Green line; +50 mmol, Red line; +80 mmol, (c) The plots of ellipticity at 524 nm in **Fig. 4-10(b)** vs. the added amount of L-proline. The solid line is drawn to guide the correlation.

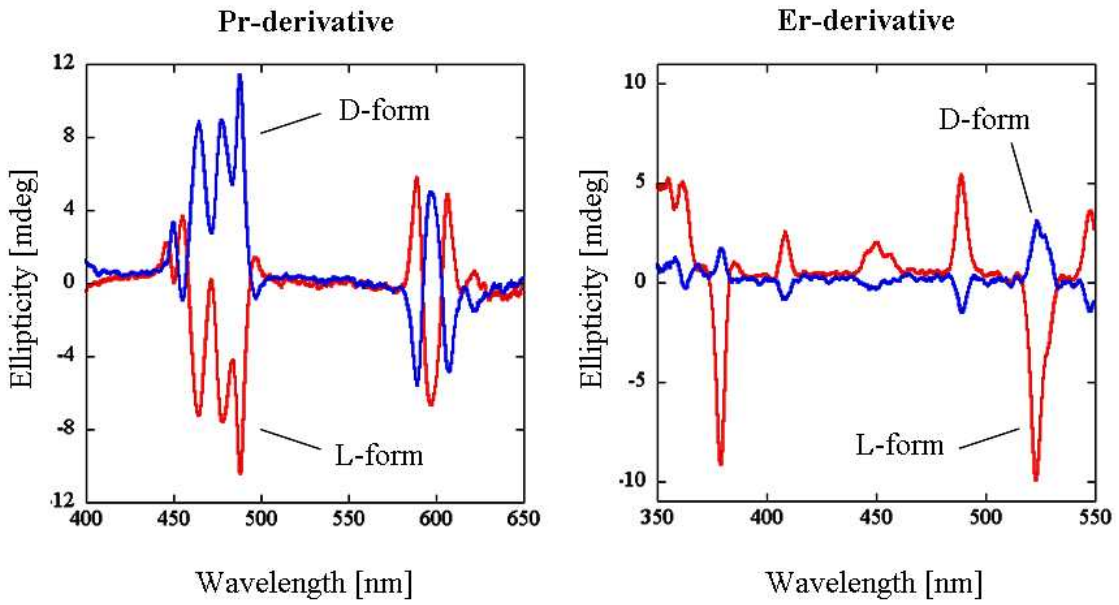

Figure 4-11. The CD spectra of aqueous solutions of **Pr-L** and **Pr-D** (left), and **Er-L** and **Er-D** (right).

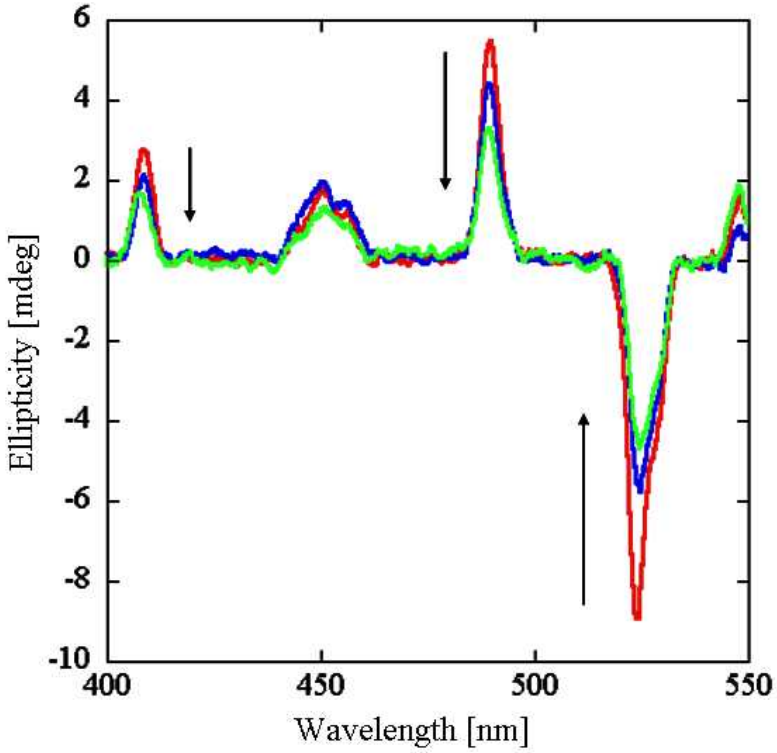

Figure 4-12. The change of CD activity of **Er-L** aqueous solution by temperature elevation. Red line; 297K, Blue line; 313K, Green line; 324K.

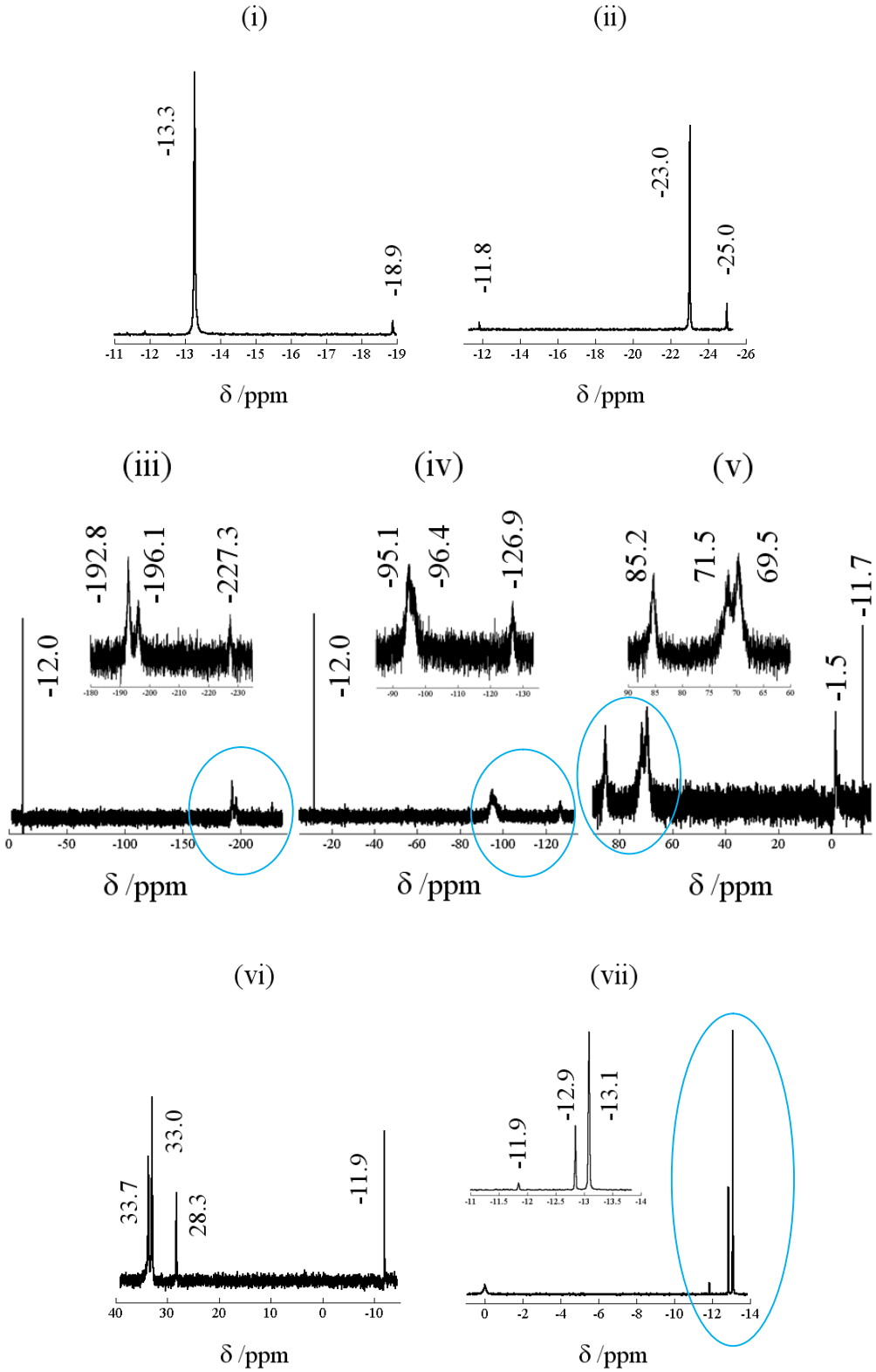

Figure 4-13. The ^{31}P-NMR spectra of **Pr-L** (i), **Nd-L** (ii), **Tb-L** (iii), **Dy-L** (iv), **Er-L** (v), **Yb-L** (vi), and **Y-L** (vii) in D_2O solutions at room temperature (298K). The insets are demonstrated by expanding the blue circled region.

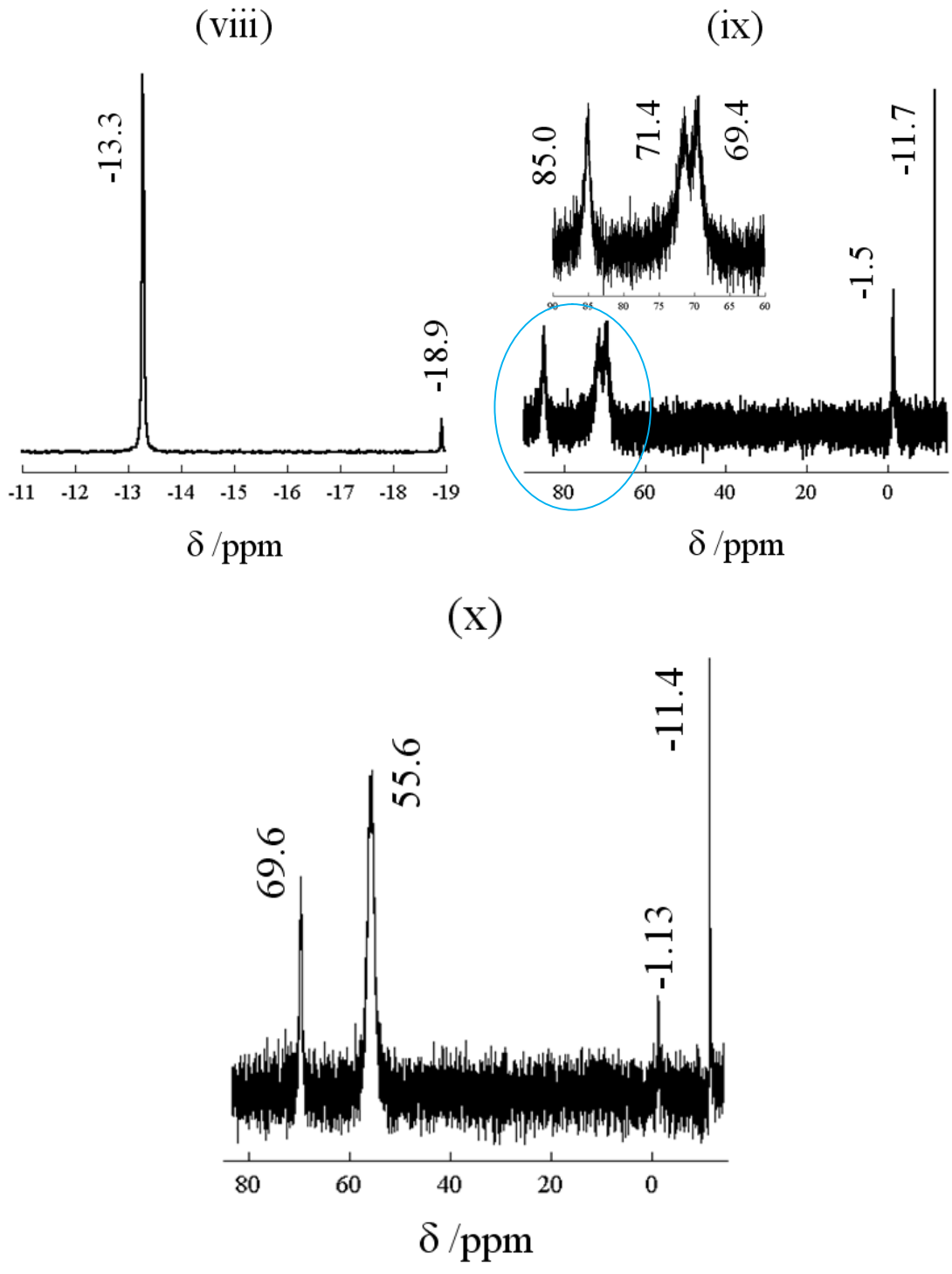

Figure 4-13(Continued). The ^{31}P-NMR spectra of **Pr-D** (viii), and **Er-D** (ix) at room temperature (298K) and **Er-L** (x) at 323K in D_2O solutions. The inset is demonstrated by expanding the blue circled region.

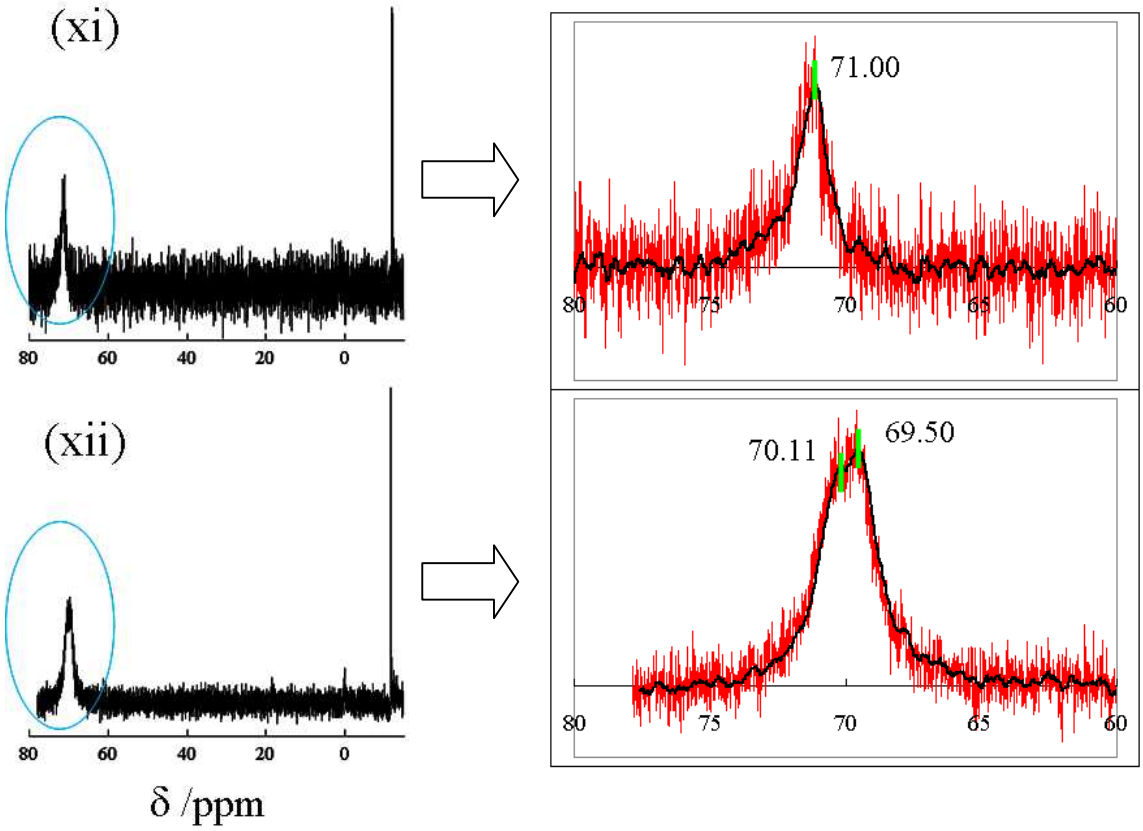

Figure 4-13(Continued). The ^{31}P-NMR spectra of two aqueous solutions; (xi) racemic solution of $[Er(\alpha\text{-}PW_{11}O_{39})_2]^{11-}$ (green shaded sample in **Fig 4-9(b)**), (xii) $[Er(\alpha\text{-}PW_{11}O_{39})_2]^{11-}$ + KCl + L-pro (purple shaded sample in **Fig. 4-9(b)**) (left). The expanded views of the blue circled region in left spectra are demonstrated by red line spectra next to each (right). The black lines in expanded spectra are the smoothed spectrogram by simple moving average method.

Scheme A

Heavier lanthanide Er

$K_{1.3}Na_{3.2}H_{6.5}[L\text{-}Er(\alpha\text{-}PW_{11}O_{39})_2]\cdot 8.3(L\text{-proline})\cdot 22.5H_2O$ (**Er-L**)

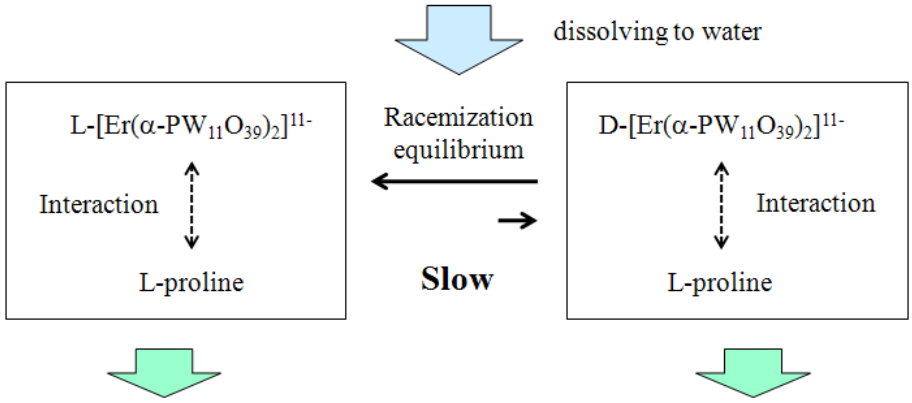

^{31}P-NMR	69.5 ppm 71.5 ppm
CD	Active (Fig. 4-11 right)

Scheme B

Lighter lanthanide Pr

$K_{1.3}Na_{3.2}H_{6.5}[L\text{-}Pr(\alpha\text{-}PW_{11}O_{39})_2]\cdot 8.3(L\text{-proline})\cdot 21.5H_2O$ (**Pr**-L)

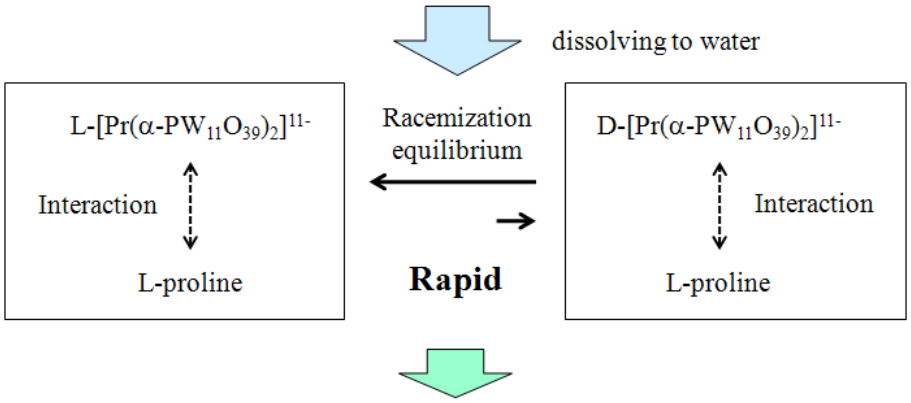

^{31}P-NMR	-13.3 ppm
CD	Active (Fig. 4-11 left)

Figure 4-14. The relationship between racemization equilibrium of the polyanion and ^{31}P-NMR, CD activity. Some compounds with heavier lanthanide (Tb, Dy, Yb, and Y) are following the Scheme A, and the other compound with lighter lanthanide (Nd) are the Scheme B, respectively.

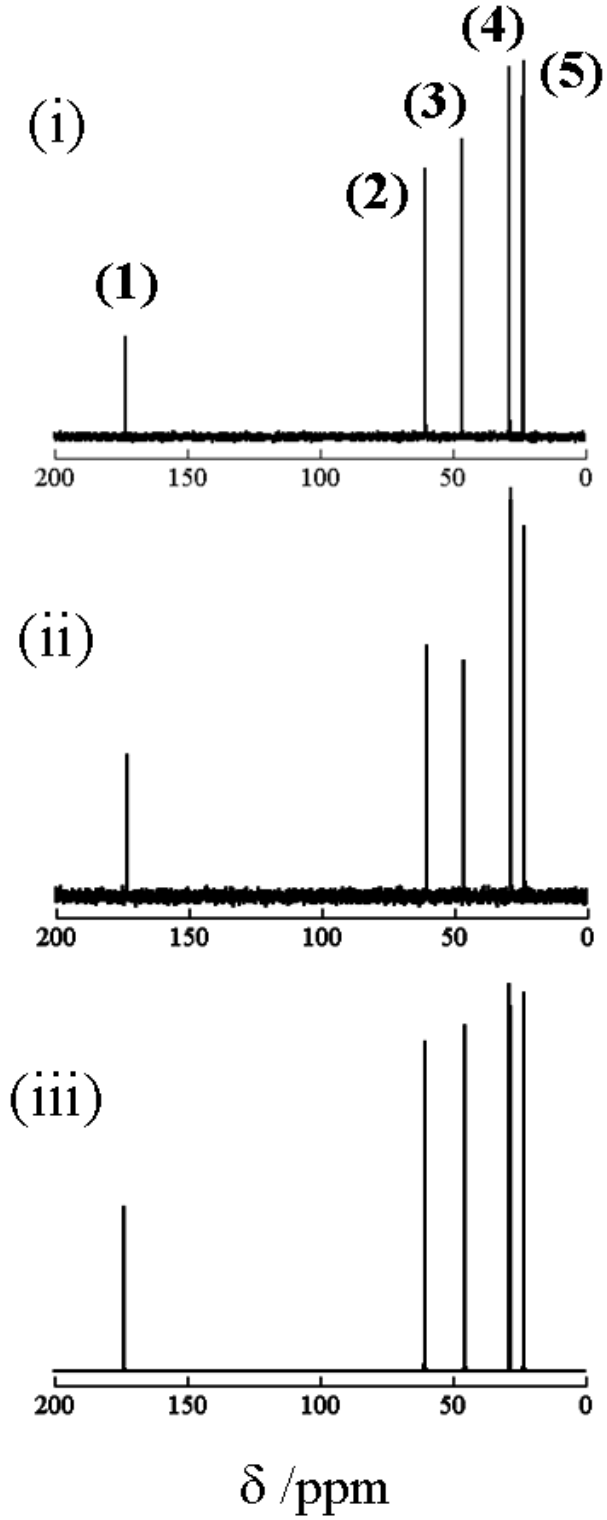

L-proline

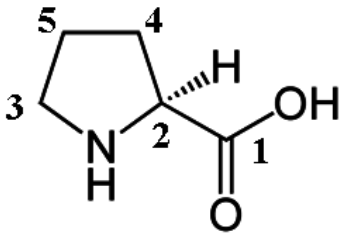

	Chemical shit [ppm]		
	Pr-L	Y-L	L-proline
C1	173.3	173.4	173.8
C2	60.4	60.6	60.7
C3	46.5	46.6	45.5
C4	28.7	28.8	28.8
C5	23.6	23.7	23.4

Figure 4-15. The ^{13}C-NMR spectra of **Pr-L** (i), **Y-L** (ii), and L-proline (iii) in D_2O solutions.

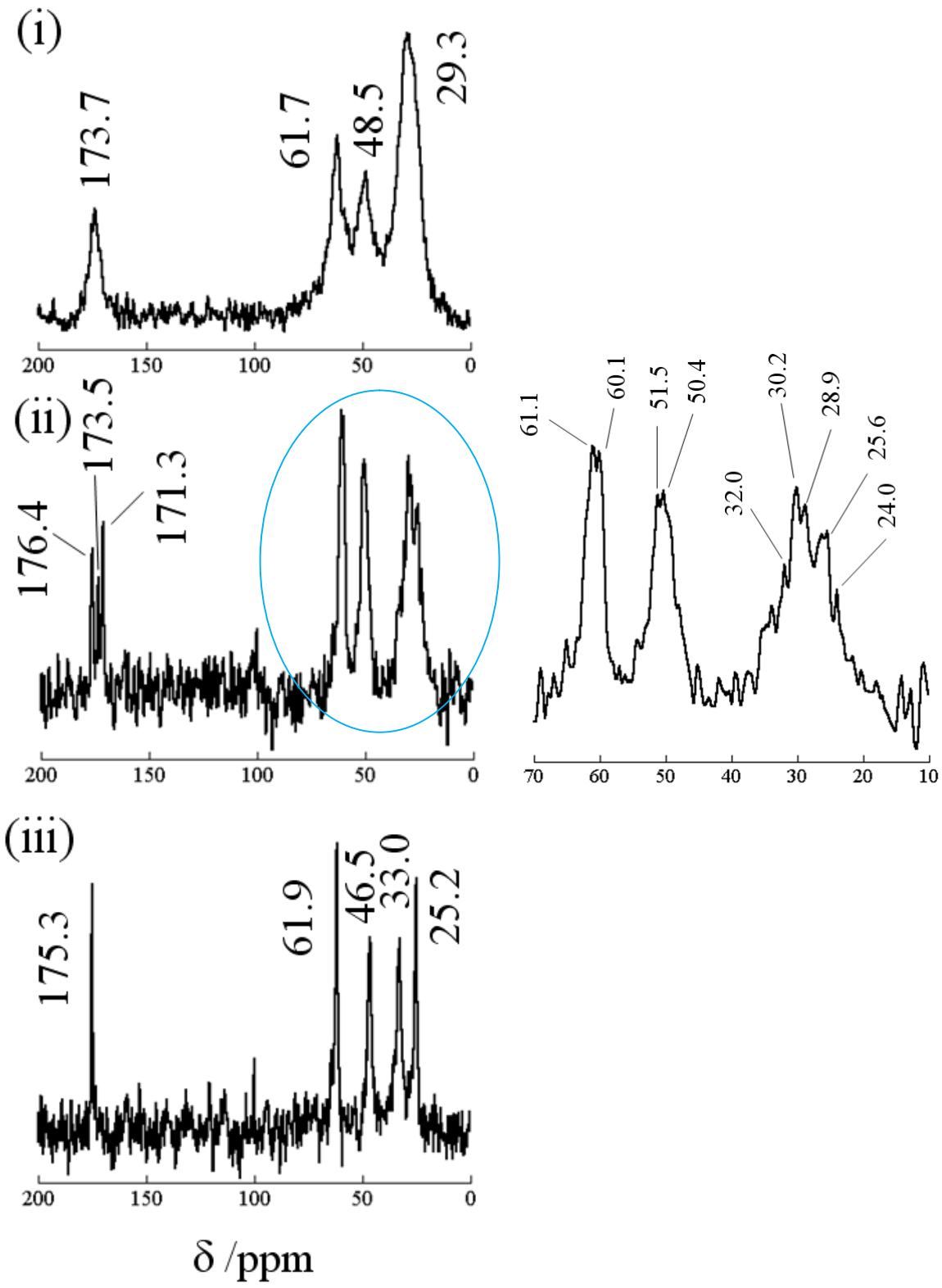

Figure 4-16. The ^{13}C-NMR spectra of **Pr-L** (i), **Y-L** (ii), and L-proline (iii) in the solid state.

The spectrum beside **Y-L** (ii) is the expanded view in the blue circled region.

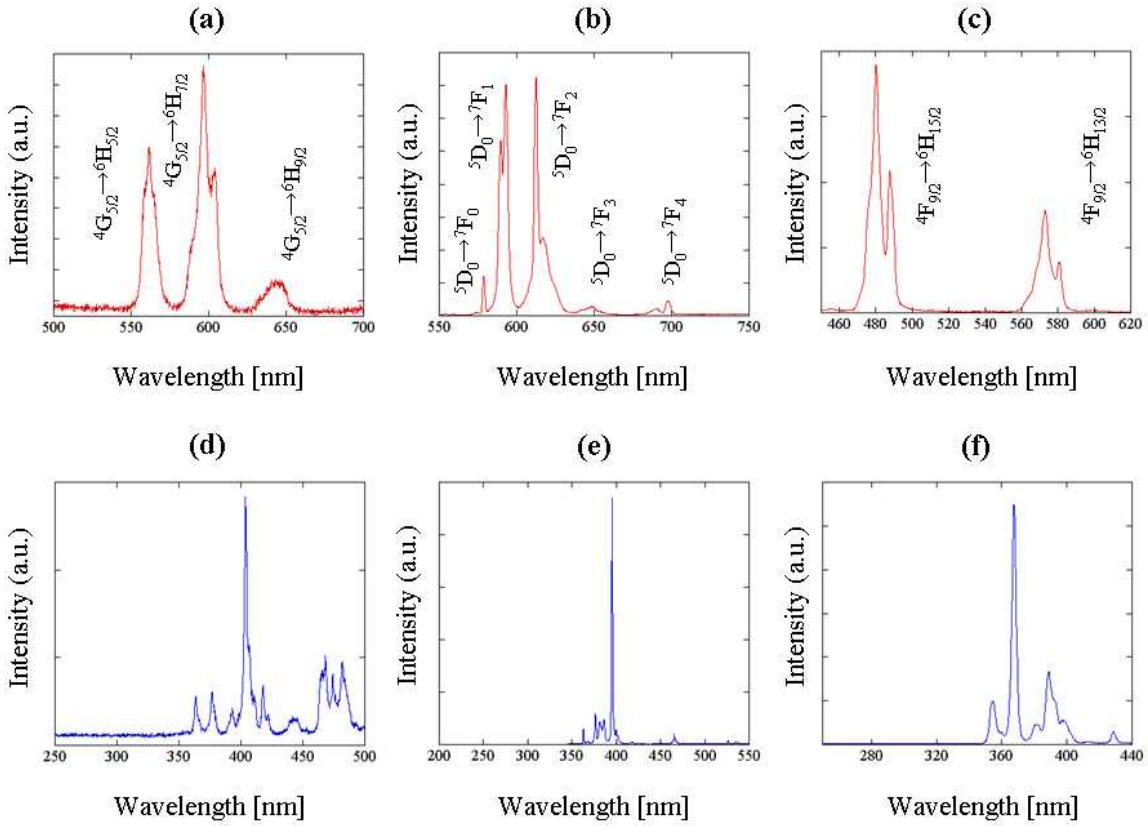

Figure 4-17. Emission (a, b, c) and excitation (d, e, f) spectra of the mother liquor of Sm, Eu, and Dy derivatives. (a) Sm^{3+} excitation (404 nm), (b) Eu^{3+} excitation (395 nm), (c) Dy^{3+} excitation (367 nm), (d) monitored at 597 nm ($^4G_{5/2}\rightarrow{}^6H_{7/2}$), (e) monitored at 612 nm ($^5D_0\rightarrow{}^7F_2$), (f) monitored at 480 nm ($^4F_{9/2}\rightarrow{}^6H_{15/2}$).

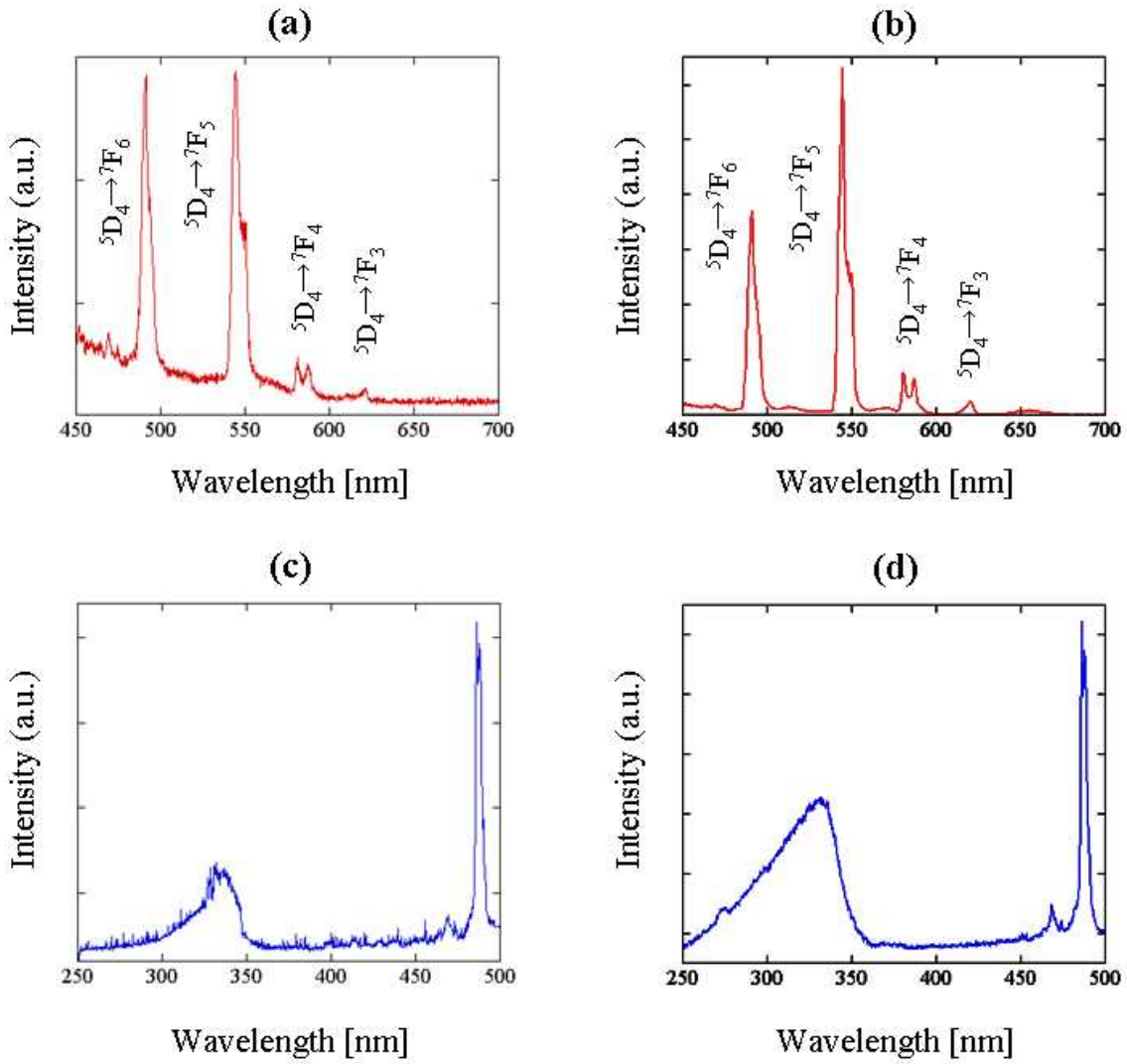

Figure 4-18. Emission (a, b) and (c, d) excitation spectra of the crystal of **Tb-L** at 77K. (a) O→W LMCT excitaion (280 nm), (b) Tb^{3+} excitation (330 nm), (c) monitored at 544 nm ($^5D_4 \rightarrow ^7F_5$), (d) monitored at 544 nm ($^5D_4 \rightarrow ^7F_5$).

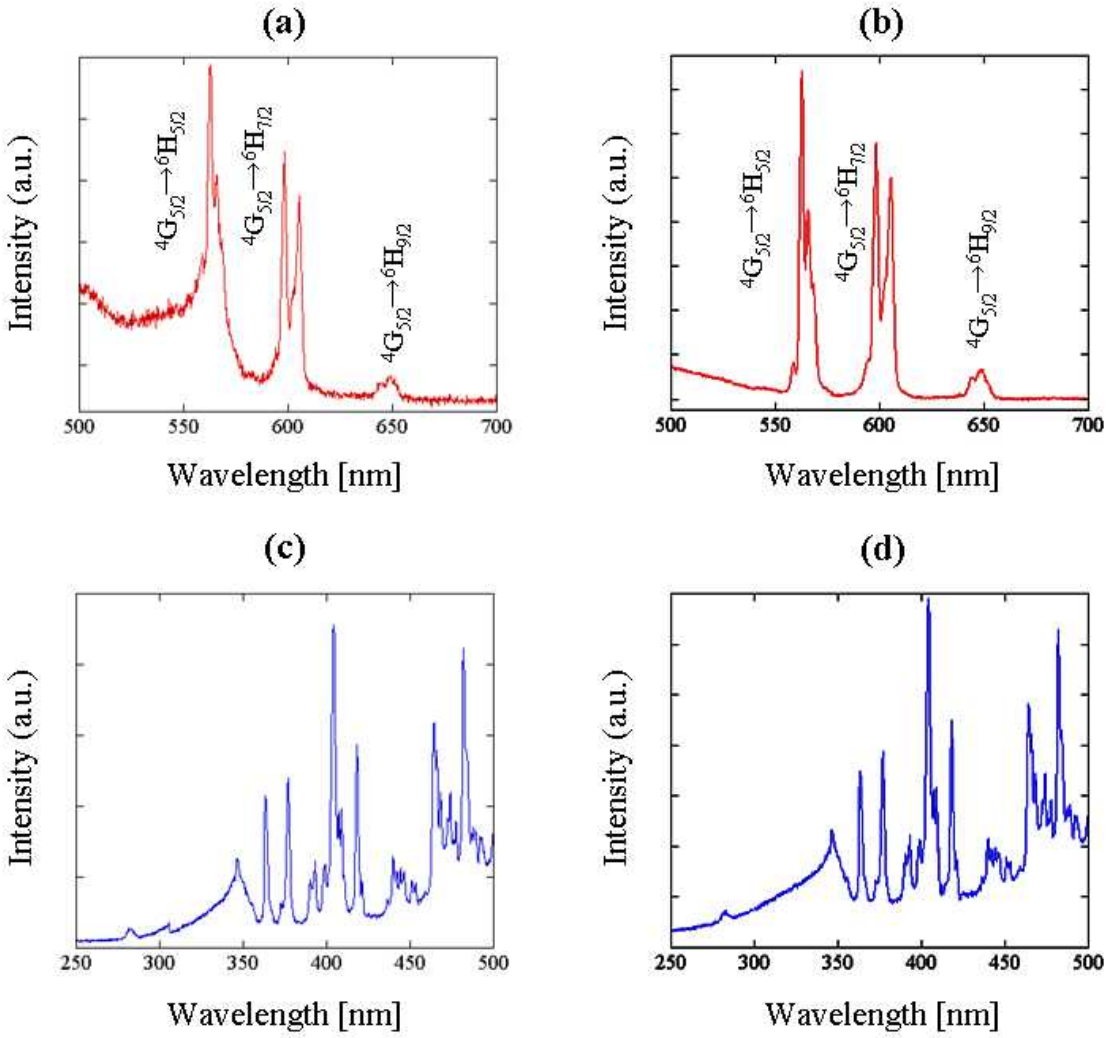

Figure 4-19. Emission (a, b) and excitation (c, d) spectra of the crystal of **Sm-L** at 77K. (a) O→W LMCT excitaion (280 nm), (b) Sm^{3+} excitation (404 nm), (c) monitored at 563 nm ($^4G_{5/2}\rightarrow{}^6H_{5/2}$), (d) monitored at 563 nm ($^4G_{5/2}\rightarrow{}^6H_{5/2}$).

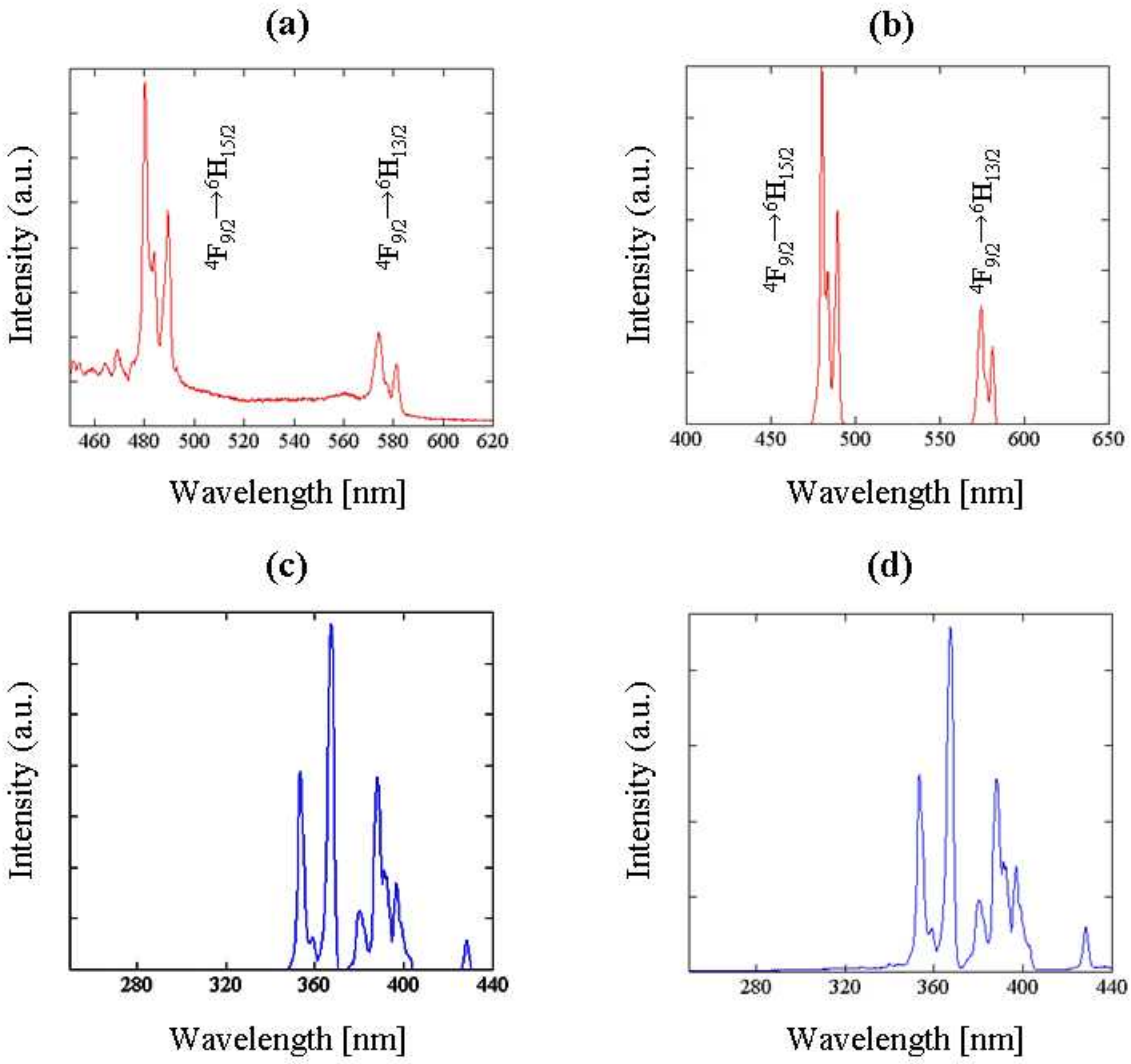

Figure 4-20. Emission (a, b) and (c, d) excitation spectra of the crystal of **Dy-L** at 77K. (a) O→W LMCT excitaion (280 nm), (b) Dy^{3+} excitation (367 nm), (c) monitored at 480 nm ($^4F_{9/2}\rightarrow{}^6H_{15/2}$), (d) monitored at 480 nm ($^4F_{9/2}\rightarrow{}^6H_{15/2}$).

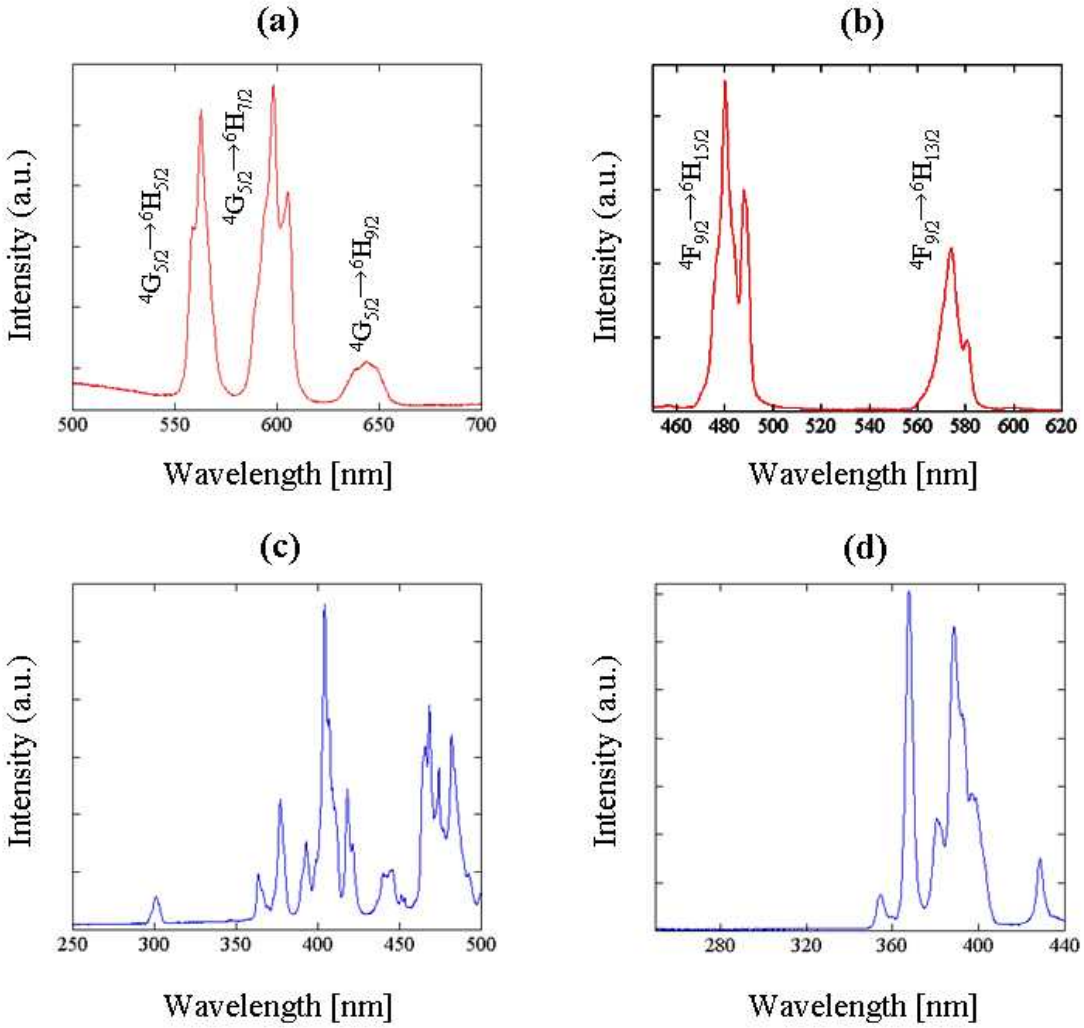

Figure 4-21. Emission (a, b) and excitation (c, d) spectra of the crystal of **Sm-L** (left) and **Dy-L** (right) at 298K. (a) Sm^{3+} excitation (404 nm), (b) Dy^{3+} excitation (367 nm), (c) monitored at 598 nm ($^4G_{5/2}\rightarrow{}^6H_{7/2}$), (d) monitored at 480 nm ($^4F_{9/2}\rightarrow{}^6H1_{5/2}$).

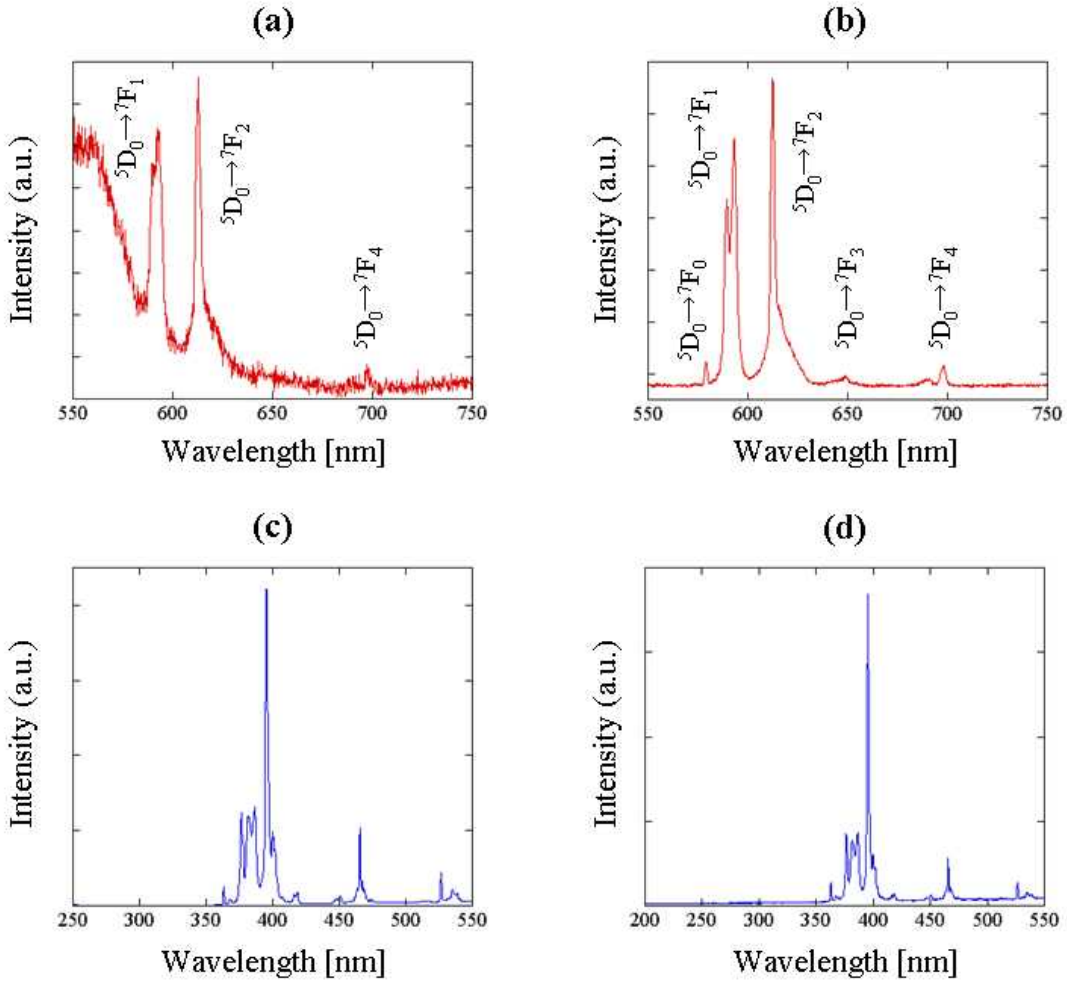

Figure 4-22. Emission (a, b) and excitation (c, d) spectra of the crystal of **Eu-L** at 298K. (a) O→W LMCT excitation (280 nm), (b) Eu^{3+} excitation (395 nm), (c) monitored at 612 nm ($^5D_0 \rightarrow ^7F_2$), (d) monitored at 612 nm ($^5D_0 \rightarrow ^7F_2$).

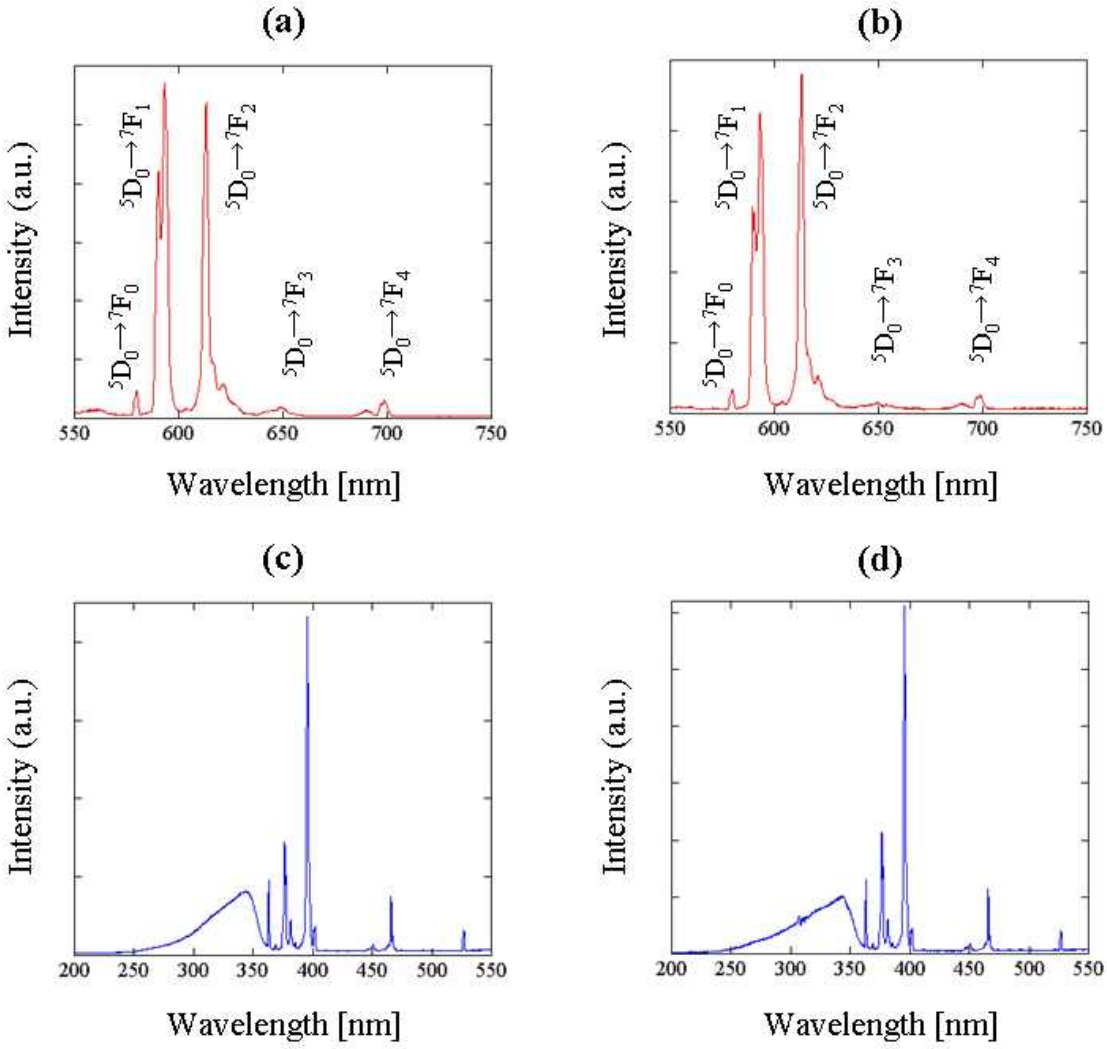

Figure 4-23. Emission (a, b) and excitation (c, d) spectra of the crystal of **Eu-L** at 77K. (a) O→W LMCT excitation (280 nm), (b) Eu^{3+} excitation (395 nm), (c) monitored at 612 nm ($^5D_0 \rightarrow {}^7F_2$), (d) monitored at 613 nm ($^5D_0 \rightarrow {}^7F_2$).

Chapter 5 Enantioselective synthesis of sandwich-type $[Ln(\alpha_2\text{-}P_2W_{17}O_{61})_2]^{17-}$ (Ln = La, Sm, Eu, Gd, Tb, Dy, Er, and Yb) with D- and L-proline

5-1 Introduction

Chiral polyoxometalates have received much anticipation to various kinds of application such as nonlinear optics, asymmetric catalysis, and inorganic medicine [1-12]. Wells-Dawson structure $[X_2M_{18}O_{62}]^{6-}$ (X = P, As; M = W, Mo) is one of the typical species in polyoxometalate chemistry as well as Keggin structure. The structure of $[X_2M_{18}O_{62}]^{6-}$ is considered as a dimer of tri-lacunary Keggin-type $[XM_9O_{34}]^{9-}$ polyanion sharing ring-shaped six O atoms (**Fig. 5-1**). There are two types (α_1 and α_2) of mono-lacunary Wells-Dawson species (**Fig. 5-2**), which are derived from parent $[X_2M_{18}O_{62}]^{6-}$ by removal of a {M=O} unit from 'belt' and 'cap' positions, respectively. Like the mono-lacunary Keggin $[XW_{11}O_{39}]^{n-}$ polyanion, $[\alpha_1\text{-}X_2M_{17}O_{61}]^{10-}$ and $[\alpha_2\text{-}X_2M_{17}O_{61}]^{10-}$ polyanions have ability to coordinate to $Ln^{3+/4+}$ cation as tetradentate ligands to form sandwich-type $[Ln(\alpha_1\text{-}X_2M_{17}O_{61})_2]^{n-}$ and $[Ln(\alpha_2\text{-}X_2M_{17}O_{61})_2]^{n-}$ complexes [13-15]. As shown in Chapter 1, a mixed-ligand type $[Ac(\alpha_1\text{-}X_2M_{17}O_{61})(\alpha_2\text{-}X_2M_{17}O_{61})]^{n-}$ (Ac = U^{4+} and Th^{4+}) has recently been prepared [16]. These mono-lacunary Wells-Dawson sandwich-type polyanions are of interest, as they exhibit chirality resulting from their C_2 (for $[Ln(\alpha_1\text{-}X_2M_{17}O_{61})_2]^{n-}$ and $[Ln(\alpha_2\text{-}X_2M_{17}O_{61})_2]^{n-}$) or C_1 (for $[Ac(\alpha_1\text{-}X_2M_{17}O_{61})(\alpha_2\text{-}X_2M_{17}O_{61})]^{n-}$) symmetry. However, in contrast to the relatively well-defined and characterized $[Ln(XM_{11}O_{39})_2]^{n-}$ polyanions both in solutions and in solids, there have been rather a few studies on $[M(X_2M_{17}O_{61})_2]^{n-}$. Wells-Dawson type polyoxometalates are known to have higher

electron reduction potential than Keggin species, and are easily multi-electron reduced by UV light or chemical reductants. Successful synthesis of the Wells-Dawson based chiral polyoxometalate will make a new application such as electrochemical chiral sensing [17] and asymmetric catalysis and inorganic medicine. Since the local structure around the Ln center in $[Ln(\alpha_2\text{-}P_2M_{17}O_{61})_2]^{n-}$ is identical to that in the $[Ln(\alpha\text{-}PM_{11}O_{39})_2]^{n-}$, the stereoselective polyanion-proline interaction observed in Chapter 4 is expected to occur in a $[Ln(\alpha_2\text{-}P_2M_{17}O_{61})_2]^{n-}$-proline system. In this chapter, enantioselective synthesis of sandwich-type $[Ln(\alpha_2\text{-}P_2W_{17}O_{61})_2]^{17-}$ (Ln = La, Sm, Eu, Gd, Tb, Dy, Er, and Yb) (**Fig. 5-3**) was attempted by the same method in Chapter 4 using L- and D-proline as chiral inductive agents.

5-2 Experimental

5-2-1 Materials

All chemicals were commercially available and used without further purification. $K_6[P_2W_{18}O_{62}]\cdot 6H_2O$ was prepared according to the previous report and identified by IR spectroscopy [18].

5-2-2 Measurements

Elemental analysis of C, H, and N were performed on a Yanaco MT5 CHN CORDER. This measurement was requested to the Center for Advanced Analysis of the Tokyo Institute of Technology. IR (4000-400 cm^{-1}) spectra were recorded on a JASCO FT/IR-410 spectrometer using KBr disc method. Thermogravimetric and differential thermal analyses (TG-DTA) were conducted with a ULVAC MTS9000 + TGD9600 system. UV-Vis absorption spectra were recorded on a JASCO V-570 UV/VIS/NIR

spectrophotometer. Circular dichrorism (CD) spectra were recorded on a JASCO J-800 spectrometer. Luminescence and excitation spectra in the solid state and aqueous solutions were recorded on HITACHI F-4500 spectrofluorometer. Solution ^{31}P-NMR spectra were measured on Bruker Biospin AVANCE III at a frequency of 161.94 MHz using 85 % H_3PO_4 as an external reference.

5-2-3 Syntheses

All of the compounds were synthesized by the same procedures. The Ln ions were introduced as corresponding chloride or nitrate. Especially for **Er-D**, D-form of proline was used as a chiral resource. The synthetic procedure of **Yb-L** is exemplified here.

5-2-3-1 $K_{12}H_5[Yb(\alpha_2\text{-}P_2W_{17}O_{61})_2]\cdot 2(L\text{-}C_5H_9NO_2)\cdot 42H_2O$ (**Yb-L**)

To a solution of KCl (0.15 g, 2.0 mmol) in 20 ml of H_2O was added both L-proline solid (0.58 g, 5 mmol) and $Yb(NO_3)\cdot 4H_2O$ (0.44 g, 1 mmol) dissolved in 5 ml of H_2O. The clear solution was heated to 60 °C for 30 min with stirring. Afterwards, the solution was acidified with 1M HCl to pH = 1.5 and an aqueous solution (20 ml) of $K_6[P_2W_{18}O_{62}]\cdot 6H_2O$ (9.22 g, 2 mmol) was added dropwise. After adjusting the pH to c.a. 5 by addition of Li_2CO_3 solid, the solution was boiled for 1 h and cooled to room temperature. The residual powders were filtered off and the resulting filtrate was concentrated to less than half of initial volume and stood at room temperature for several days. White block crystals of **Yb-L** were obtained (yield; 1.09 g, 11.0 % based on W). Found: C, 1.19; H, 0.51; N, 0.27; H_2O, 7.64 wt %. Calcd for $O_{168}YbP_4W_{34}K_2C_{10}N_2H_{107}$: C, 1.19; H, 0.51; N, 0.27; H_2O, 7.60 wt %. IR (KBr disk): 1620m, 1458w, 1407w, 1384w, 1332w, 1162w, 1085vs, 1057w, 1026w, 1016w, 939s,

914w, 820w, 776m, 731w.

5-2-3-2 $K_{12}H_5[La(\alpha_2\text{-}P_2W_{17}O_{61})_2]\cdot 2(L\text{-}C_5H_9NO_2)\cdot 43H_2O$ (**La-L**)

Colorless block crystals of **La-L** were obtained (yield; 2.08 g, 20.8 % based on W). Found: C, 1.68; H, 0.60; N, 0.46; H_2O, 7.76 wt %. Calcd for $O_{169}LaP_4W_{34}K_2C_{10}N_2H_{109}$: C, 1.21; H, 1.02; N, 0.28; H_2O, 7.79 wt %. IR (KBr disk): 1625m, 1473w, 1457w, 1418w, 1388w, 1363w, 1331w, 1243w, 1083vs, 1055w, 1017w, 939s, 922w, 887w, 819w, 785m, 731w.

5-2-3-3 $K_{12}H_5[Sm(\alpha_2\text{-}P_2W_{17}O_{61})_2]\cdot 2(L\text{-}C_5H_9NO_2)\cdot 39H_2O$ (**Sm-L**)

White block crystals of **Sm-L** were obtained (yield; 1.13 g, 11.5 % based on W). Found: C, 0.99; H, 0.62; N, 0.27; H_2O, 6.92 wt %. Calcd for $O_{165}SmP_4W_{34}K_2C_{10}N_2H_{101}$: C, 1.22; H, 0.95; N, 0.28; H_2O, 7.11 wt %. IR (KBr disk): 1624m, 1473w, 1457w, 1418w, 1376w, 1273w, 1255w, 1085vs, 1056w, 1018w, 940s, 918w, 886w, 822w, 772m, 735w.

5-2-3-4 $K_{12}H_5[Eu(\alpha_2\text{-}P_2W_{17}O_{61})_2]\cdot 2(L\text{-}C_5H_9NO_2)\cdot 37H_2O$ (**Eu-L**)

White block crystals of **Eu-L** were obtained (yield; 1.70 g, 17.0 % based on W). Found: C, 1.56; H, 0.89; N, 0.34; H_2O, 6.64 wt %. Calcd for $O_{163}EuP_4W_{34}K_2C_{10}N_2H_{97}$: C, 1.22; H, 0.91; N, 0.28; H_2O, 6.77 wt %. IR (KBr disk): 1624m, 1473w, 1457w, 1418w, 1375w, 1270w, 1254w, 1084vs, 1056w, 1023w, 940s, 920w, 891w, 822w, 770m, 735w.

5-2-3-5 $K_{12}H_5[Gd(\alpha_2\text{-}P_2W_{17}O_{61})_2]\cdot 2(L\text{-}C_5H_9NO_2)\cdot 41H_2O$ (**Gd-L**)

White block crystals of **Gd-L** were obtained (yield; 0.30 g, 5.61 % based on W). Found: C, 1.14; H, 0.47; N, 0.36; H_2O, 6.49 wt %. Calcd for $O_{167}GdP_4W_{34}K_2C_{10}N_2H_{105}$: C, 1.21; H, 1.07; N, 0.28; H_2O, 7.44 wt %. IR (KBr disk): 1624m, 1473w, 1457w, 1418w, 1376w, 1362w, 1273w, 1256w, 1085vs, 1056w, 1024w, 940s, 917w, 889w, 824w, 774m, 734w.

5-2-3-6 $K_{12}H_5[Tb(\alpha_2\text{-}P_2W_{17}O_{61})_2]\cdot 2(L\text{-}C_5H_9NO_2)\cdot 40H_2O$ (**Tb-L**)

Light greenish yellow block crystals of **Tb-L** were obtained (yield; 2.111 g, 21.3 % based on W). Found: C, 1.03; H, 0.74; N, 0.31; H_2O, 7.21 wt %. Calcd for $O_{166}TbP_4W_{34}K_2C_{10}N_2H_{103}$: C, 1.21; H, 0.97; N, 0.28; H_2O, 7.27 wt %. IR (KBr disk): 1624m, 1458w, 1411w, 1361w, 1331w, 1274w, 1255w, 1084vs, 1056w, 1025w, 1016w, 939s, 917w, 891w, 828w, 770m, 732w.

5-2-3-7 $K_{12}H_5[Dy(\alpha_2\text{-}P_2W_{17}O_{61})_2]\cdot 2(L\text{-}C_5H_9NO_2)\cdot 42H_2O$ (**Dy-L**)

Colorless block crystals of **Dy-L** were obtained (yield; 0.99 g, 9.88 % based on W). Found: C, 1.05; H, 0.70; N, 0.27; H_2O, 7.32 wt %. Calcd for $O_{168}DyP_4W_{34}K_2C_{10}N_2H_{107}$: C, 1.21; H, 1.08; N, 0.28; H_2O, 7.60 wt %. IR (KBr disk): 1618m, 1457w, 1417w, 1377w, 1362w, 1331w, 1273w, 1255w, 1084vs, 1058w, 1025w, 1016w, 940s, 917w, 890w, 826w, 773m, 737w.

5-2-3-8 $K_{12}H_5[Er(\alpha_2\text{-}P_2W_{17}O_{61})_2]\cdot 2(L\text{-}C_5H_9NO_2)\cdot 44H_2O$ (**Er-L**)

Light pink block crystals of **Er-L** were obtained (yield; 3.43 g, 34.4 % based on W). Found: C, 1.18; H, 0.52; N, 0.28; H_2O, 7.86 wt %. Calcd for $O_{170}ErP_4W_{34}K_2C_{10}N_2H_{111}$:

C, 1.20; H, 1.04; N, 0.28; H_2O, 7.93 wt %. IR (KBr disk): 1623m, 1457w, 1412w, 1385w, 1362w, 1331w, 1274w, 1256w, 1084vs, 1056w, 1027w, 1015w, 940s, 916w, 888w, 826w, 777m, 729w.

5-2-3-9 $K_{12}H_5[Er(\alpha_2\text{-}P_2W_{17}O_{61})_2]\cdot 2(D\text{-}C_5H_9NO_2)\cdot 42H_2O$ **(Er-D)**

Light pink block crystals of **Er-D** were obtained (yield; 1.14 g, 11.4 % based on W). Found: C, 0.99; H, 0.69; N, 0.28; H_2O, 7.57 wt %. Calcd for $O_{168}ErP_4W_{34}K_2C_{10}N_2H_{107}$: C, 1.21; H, 1.00; N, 0.28; H_2O, 7.60 wt %. IR (KBr disk): 1624m, 1508w, 1473w, 1457w, 1418w, 1375w, 1362w, 1338w, 1084vs, 1057w, 1026w, 1015w, 940s, 918w, 883w, 825w, 773m, 736w.

5-2-4 X-ray crystallography

The reflection data for the single crystal X-ray analysis of all the compounds were collected on a Rigaku RAXIS-RAPID imaging plate diffractometer with a graphite monochromatized MoK_α radiation (λ = 0.7107 Å) at 213 K. All of the structures were solved by the direct method SHELXS-97 [19] and refined by the full-matrix least squares on F^2 using the CrystalStructure [20]. All of the lanthanide, W, P, K, C, and N atoms were refined anisotropically. The O atoms in proline were refined anisotropically, while the other O atoms were isotropically. The H atoms were not included in the refinements for all of the compounds. The crystallographic data and the results of structure refinement are summarized in **Table 5-1**. The final atomic coordinates with thermal parameters ($B_{eq/iso}$) for **Er-L** and **Er-D** are also summarized in **Table 5-2**.

5-3 Results and discussion

5-3-1 Determination of the chemical formula

All compounds were prepared by the reaction between Ln^{3+} and plenary $[P_2W_{18}O_{62}]^{6-}$ in a 1:2 molar ratio in the presence of K^+ and D- or L-proline, and crystallized isostructurally in $P2_12_12$ with similar crystallographic parameters (**Table 5-1**). Unlike highly disordering alkaline cations and proline molecules in the mono-lacunary Keggin-sandwich compounds in Chapter 4, all of the K^+ and proline in all of the derivatives were completely determined by single crystal X-ray diffraction analysis, and formulated to be $K_{12}H_5[Ln(\alpha_2\text{-}P_2W_{17}O_{61})_2]\cdot 2(L/D\text{-}C_5H_9NO_2)\cdot xH_2O$. This chemical formula of the compounds is consistent with the result of CHN elemental analysis and TG-DTA.

5-3-2 Crystal structures

Asymmetric unit consists of the half of the polyanion, six K^+ ions, a L- or D-proline molecule, and some waters of crystallization. It is of significance that only one enantiomer was selectively crystallized, i.e. enantiopure crystals containing L-form were obtained in the presence of L-proline, and *vice versa*. Chirality of the crystals is supported by the reasonably small Flack parameters in the final refinements. The pKa (1.95 and 10.47) of proline [21] and the neutral solution condition at pH = 5 in the synthetic procedure suggest that all the proline molecules are zwitterionic. For all of the compounds, the proline molecule coordinates to K^+ ion. The two carboxylate C-O bondings in the proline molecules have similar lengths (mean 1.2 ´), additionally suggesting a resonance structure in zwitterionic state. The polyanion is composed of two mono-lacunary Wells-Dawson $[\alpha_2\text{-}P_2W_{17}O_{61}]^{10-}$ units coordinating to Ln^{3+} (**Fig.**

5-3) with a square-antiprism. The Ln^{3+} center is positioned on the crystallographic C_2 axis parallel to the *c* axis. Therefore, the polyanion has an ideal C_2 point symmetry in the crystal. The bond distances of Ln-O and W-O, and the bond valence sum (BVS) values of Ln, W, P, [22] are summarized in **Table 5-3**. The bond lengths of Ln-O are comparable to those in $[Ln(W_5O_{18})_2]^{9-}$ (Ln = La, Eu, Gd, Tb, Dy, Er) and $[Yb(\alpha_2\text{-}P_2W_{17}O_{61})_2]^{17-}$ [23-27]. The BVS values calculated from the bond length are reasonably corresponded to their formal valences of Ln^{3+}, P^{5+}, and W^{6+}.

The K3 and symmetry-related K3' atoms coordinate to two $[\alpha_2\text{-}P_2W_{17}O_{61}]^{10-}$ units in a polyanion and are linked through three water oxygens (O_w) forming a scheme W=O–K3–$(O_w)_3$–K3'–O=W (**Fig. 5-4**). There are several direct O–K–O linkages between adjacent polyanions (**Figs. 5-5** and **5-6**). Both 7-coordinate K6 and 5-coodinate K5 link the polyanions in the *a*-axis direction (**Fig. 5-5(a)** and **(b)**). The K4 in 6-fold coordination doubly links the polyanions in the *b*-axis direction (**Fig. 5-5(c)**). Moreover, the K1 in 7-fold coordination links the polyanions to form a 2D network parallel to the *ab* plane (**Fig. 5-6(a)**). On the other hand, the only K2 in 7-fold coordination links the polyanions along the *c* axis (**Fig. 5-6 below**). As a result, the polyanions are three-dimensionally connected via these O–K–O linkages (**Fig. 5-7 above**). As shown in **Fig. 5-7 below,** three O_w atoms link the polyanions along the *a* axis through hydrogen-bonding.

5-3-3 Emergence of chirality in aqueous solutions and crystals

Here, the emergence of the chirality in $[Ln(\alpha_2\text{-}P_2W_{17}O_{61})_2]^{17-}$ by proline is studied by means of the same methods used in Chapter 4. First of all, the structural analyses of the isolated crystals were made with the aid of single crystal X-ray crystallography.

Secondly, the CD spectroscopy in aqueous solutions was carried out to confirm the preservation of chirality in the polyanion. Finally, the ^{31}P-NMR spectroscopy in aqueous solutions was performed to assign polyanion species in solution and, if possible, to discriminate the enantiomers. The ^{13}C-NMR spectroscopy was also attempted for detecting interaction between the polyanion and proline both in aqueous solution.

5-3-3-1 Crystallographic study

Fig. 5-8 shows the D-[Er(α_2-$P_2W_{17}O_{61}$)$_2$]$^{17-}$ polyanion and two D-proline molecules located near the Ln center in **Er-D**. The distance between amino-N atom in proline and Er in the polyanion is 4.114(11) ´. This value is similar to the corresponding Er···N distances (4.09(2) and 4.193(13) ´) in $K_{1.3}Na_{3.2}H_{6.5}$[D-Er(α-$PW_{11}O_{39}$)$_2$]·8.3(D-$C_5H_9NO_2$)·14H_2O shown in Chapter 4. Also, the distances from the amino-N atoms in proline to oxygen atoms coordinating to Er^{3+} ion are 2.806(15) and 3.008(14) ´, which are within hydrogen-bonding distances (**Fig. 5-8 right**). The enantiomeric crystal of **Er-L** has an identical structure (instead of chirality) including L-[Er(α_2-$P_2W_{17}O_{61}$)$_2$]$^{17-}$ and L-proline. All the other Ln-L and Ln-D samples are isostructural with **Er-L** and **Er-D**, respectively. **Fig. 5-9** shows the space-filling model of D-proline and D-[Ln(α_2-$P_2W_{17}O_{61}$)$_2$]$^{17-}$. The two proline molecules fit to 'minor grooves' formed by O atoms in the polyanion (**Fig. 5-9**). Since the structure of the groove and hydrogen-bonding interaction of the two proline molecules are similar to those in the Keggin-based compounds shown in Chapter 4, the same discussion is possible here, i.e. the L-proline cannot fit to the grooves in the D-form of polyanion and cannot approach the Ln center to make hydrogen bondings due to a steric repulsion. In other words, the hydrogen-bonding interaction between polyanion and proline has an

enantioselectivity. This interaction might be the mechanism in the enantioselective isolation of $K_{12}H_5[Ln(\alpha_2\text{-}P_2W_{17}O_{61})_2]\cdot 2(L/D\text{-proline})\cdot xH_2O$.

5-3-3-2 CD spectroscopy

To investigate the chirality in solution, the solution CD spectra of **Er-L** and **Er-D** were measured. For the both enantiomers, weak mirror-imaged spectra due to f-f transitions in Er^{3+} were observed (**Fig. 5-10 above**), which are barely consistent with visible-region absorption bands of aqueous **Er-L** solution (**Fig. 5-10 below**). However, the signals are weak and ill-defined compared with those of $K_{1.3}Na_{3.2}H_{6.5}[L\text{-}Er(\alpha\text{-}PW_{11}O_{39})_2]\cdot 8.3(L\text{-}C_5H_9NO_2)\cdot 22.5H_2O$ and $K_{1.3}Na_{3.2}H_{6.5}[D\text{-}Er(\alpha\text{-}PW_{11}O_{39})_2]\cdot 8.3(D\text{-}C_5H_9NO_2)\cdot 14H_2O$ observed in Chapter 4 (**Fig. 4-10 right**). As will be shown later, the ^{31}P-NMR spectra of **Er-L** and **Er-D** in aqueous solutions indicate that the structure of polyanion is retained in aqueous solutions. The weak CD activity comes from a partial racemization of the polyanion in solution, because the amount of the co-existing proline (two equivalents per polyanion) is insufficient for maintaining the chirality.

5-3-3-3 ^{31}P-NMR study

In order to examine the stability and chirality of the $[Ln(\alpha_2\text{-}P_2W_{17}O_{61})_2]^{17-}$ polyanion in aqueous solutions, ^{31}P-NMR spectra of all the compounds except for **Gd-L** were measured. A pair of major peaks was observed for every compound (**Fig. 5-11**), which are assignable to the two phosphorus sites in the $[\alpha_2\text{-}P_2W_{17}O_{61}]^{10-}$ unit. Here, P1 denotes the atom closest to Ln^{3+}, and P2 does the atom away from Ln^{3+}. These assignments are referred to the previous study on ^{31}P-NMR of $[Ln(\alpha\text{-}PW_{11}O_{39})_2]^{11-}$ by

Fedotov et al., because the local structures around the central Ln^{3+} and P1 atoms are identical in the $[Ln(\alpha\text{-}PW_{11}O_{39})_2]^{11-}$ and $[Ln(\alpha_2\text{-}P_2W_{17}O_{61})_2]^{17-}$ polyanions [28]. Especially for **Tb-L**, **Dy-L**, **Er-L**, **Er-D**, the observed resonance peaks of P1 close to the Ln^{3+} centers are broadened due to the paramagnetic effect of the corresponding Ln^{3+}. In some of the spectra, a couple of minor peaks (< 5 % of the parent $[Ln(\alpha_2\text{-}P_2W_{17}O_{61})_2]^{17-}$ species) at 7.4-7.9 and 14.2-14.5 ppm has been observed, and these are attributable to free $[\alpha_2\text{-}P_2W_{17}O_{61}]^{10-}$ species dissociated from $[Ln(\alpha_2\text{-}P_2W_{17}O_{61})_2]^{17-}$. As expected, the spectrum of **Er-D** is identical to that of **Er-L**.

In 2001, Sadakane et al. reported that addition of excess of L-proline to the aqueous solution of a chiral $[\{Ce(\alpha_1\text{-}P_2W_{17}O_{61})(H_2O)_4\}_2]^{14-}$ polyanion resulted in splitting of ^{31}P-NMR signal for the P atom close to Ln^{3+} because of the formation of diastereomeric pairs of POM-proline complexes [29], and the split width was dependent on the concentration of L-proline. In agreement with this result, in Chapter 4, similar peak splitting was observed for $K_{1.3}Na_{3.2}H_{6.5}[Ln(\alpha\text{-}PW_{11}O_{39})_2]\cdot 8.3(L\text{-}C_5H_9NO_2)\cdot xH_2O$ (Ln = Tb, Dy, Er, and Yb), which was explained by recognition of the $[Ln(\alpha\text{-}PW_{11}O_{39})_2]^{11-}$ enantiomers in the presence of L-proline. However, in **Fig. 5-11**, no splitting of ^{31}P-NMR signals in the major $[Ln(\alpha_2\text{-}P_2W_{17}O_{61})_2]^{17-}$ polyanion was observed for all samples. One possible reason for the non-split peaks is that the ratio of proline to the polyanion (proline:$[Ln(\alpha_2\text{-}P_2W_{17}O_{61})_2]^{17-}$ = 2:1) is smaller than that (~ 8:1) for $K_{1.3}Na_{3.2}H_{6.5}[Ln(\alpha\text{-}PW_{11}O_{39})_2]\cdot 8.3(L\text{-}C_5H_9NO_2)\cdot xH_2O$. So, we attempted to enrich L-proline in the **Er-L** solution up to proline:$[Er(\alpha_2\text{-}P_2W_{17}O_{61})_2]^{17-}$ = 80:1, and measured ^{31}P-NMR. However, no spectral change was observed (**Fig. 5-11(ix)**). This observation allows to presume that the dissolving of **Er-L** to water results in partial racemization to achieve an equilibrium between L-$[Er(\alpha_2\text{-}P_2W_{17}O_{61})_2]^{17-}$ and D-$[Er(\alpha_2\text{-}P_2W_{17}O_{61})_2]^{17-}$, in

which the inter-exchange is more rapid than the NMR timescale (**Fig. 5-12**). Such exchange between the enantiomers would occur through a relative rotation of the two $[\alpha_2\text{-}P_2W_{17}O_{61}]^{10-}$ units.

5-3-3-4 ^{13}C-NMR study

In order to investigate the interaction between the polyanion and proline molecules in aqueous solution, the ^{13}C-NMR spectra of **Er-L** with paramagnetic Er^{3+}, **La-L** with non-paramagnetic La^{3+}, and free L-proline were compared (**Fig. 5-13**). There was no observable difference in the spectra, indicating that little interaction is present between proline and polyanion in solutions.

5-3-4 Photoluminescent spectra

Photoluminescent spectra of **Sm-L**, **Eu-L**, **Dy-L** and **Tb-L** were measured in the solid state. In the case of Tb derivative, No emission was observed at both 298K (room temperature) and 77 K (liquid N_2) by photoexcitaion of the O→W LMCT bands of $[\alpha_2\text{-}P_2W_{17}O_{61}]^{10-}$ and f-f transition band of Tb^{3+} ion. Similar low luminescence has been observed for $Na_9[Tb(W_5O_{18})_2]\cdot 18H_2O$ [30]. It has been suggested that excitation energy of the LMCT state is quenched non-radioactively via a charge transfer state Tb^{4+}–W^{5+} [31]. In the case of **Sm-L**, **Eu-L** and **Dy-L**, characteristic emission by photoexcitation of f-f transition band of respective Ln^{3+} ion was observed at both 298 K and 77 K. For the **Sm-L**, three characteristic peaks are shown in **Fig. 5-14**, and they are attributed to $^4G_{5/2}\rightarrow{}^6H_{5/2}$ (559.2, 561.6, 564.8 nm), $^4G_{5/2}\rightarrow{}^6H_{7/2}$ (596.6, 603.8 nm), and $^4G_{5/2}\rightarrow{}^6H_{9/2}$ (644.8 nm) at 298 K, and $^4G_{5/2}\rightarrow{}^6H_{5/2}$ (559.2, 562.2 nm), $^4G_{5/2}\rightarrow{}^6H_{7/2}$ (598, 604.2 nm), and $^4G_{5/2}\rightarrow{}^6H_{9/2}$ (645.2 nm) at 77 K [32]. For **Eu-L**, four f-f characteristic bands shown

in **Fig. 5-15** are attributed to $^5D_0 \rightarrow {}^7F_0$ (579.6 nm), $^5D_0 \rightarrow {}^7F_1$ (590.2, 593.6 nm), $^5D_0 \rightarrow {}^7F_2$ (613.2 nm), $^5D_0 \rightarrow {}^7F_3$ (649.4 nm), $^5D_0 \rightarrow {}^7F_4$ (698.4 nm) at 298K, and $^5D_0 \rightarrow {}^7F_0$ (580 nm), $^5D_0 \rightarrow {}^7F_1$ (590.6, 593.6 nm), $^5D_0 \rightarrow {}^7F_2$ (613.4 nm), $^5D_0 \rightarrow {}^7F_3$ (649 nm), and $^5D_0 \rightarrow {}^7F_4$ (698.4 nm) at 77 K. The spectral shapes and intensity ratio of $^5D_0 \rightarrow {}^7F_1$ to $^5D_0 \rightarrow {}^7F_2$ transitions in **Eu-L** is very similar to those for $[Ln(\alpha_2\text{-}P_2W_{17}O_{61})_2]^{17-}$ and $[Eu(SiW_{11}O_{39})_2]^{13-}$ in K^+ salts which both have a Eu^{3+} ion in a SA environment [33]. For **Dy-L**, two characteristic emission peaks are observed (**Fig. 5-16)**, which are attributed to $^4F_{9/2} \rightarrow {}^6H_{15/2}$ (480.4, 487.8 nm) and $^4F_{9/2} \rightarrow {}^6H_{13/2}$ (573.2, 581 nm) at 298 K, and $^4F_{9/2} \rightarrow {}^6H_{15/2}$ (480.6, 489.4 nm) and $^4F_{9/2} \rightarrow {}^6H_{13/2}$ (573.6, 581 nm) at 77 K [30]. If **Ln-D** (Ln = Sm, Eu, and Dy) could be synthesized, these would have the same luminescent spectra to Ln-L because of identical local environment of Ln^{3+} instead of chirality.

5-4 Conclusion

The enantioselective synthesis of C_2-symmetric L- and D-$[Ln(\alpha_2\text{-}P_2W_{17}O_{61})_2]^{17-}$ polyanions was accomplished by utilizing L- and D- proline as chiral inducers. It is suggested that a hydrogen bonding interaction between $[Ln(\alpha_2\text{-}P_2W_{17}O_{61})_2]^{17-}$ polyanion and two proline molecules, which are similar to that of $[Ln(\alpha\text{-}PW_{11}O_{39})_2]^{11-}$ in Chapter 4, are related to an expression of chirality in the solid state. However, in aqueous solutions, CD activity is smaller than the $[Ln(\alpha\text{-}PW_{11}O_{39})_2]^{11-}$ series. In addition to the occurrence of racemization in solutions, low content of proline with respect to polyanion (proline:$[Ln(\alpha_2\text{-}P_2W_{17}O_{61})_2]^{17-}$ = 2:1) may result in the small CD signal. The stability of polyanion in solutions was demonstrated by ^{31}P-NMR, but enantiomers could not be recognized probably by rapid racemization equilibrium. However, the knowledge obtained in this Chapter would build a bridge between resolution of a chiral

polyoxometalate by organic molecules and the following new application.

5-5 References

[1] D. A. J. Judd, H. Nettles, N. Nevins, J. P. Snyder, D. C. Liotta, J. Tang, J. Ermolieff, R. F. Schinazi, C. L. Hill, *J. Am. Chem. Soc.*, **123**, 886 (2001).

[2] A. Müller, F. Perters, M. T. Pope, D. Gatteschi, *Chem. Rev.*, 239 (1998).

[3] F. B. Xin, M. T. Pope, *J. Am. Chem. Soc.*, **118**, 7731 (1996).

[4] M Inoue, T. Yamase, *Bull. Chem. Soc. Jpn.*, **68**, 3055 (1995).

[5] M Inoue, T. Yamase, *Bull. Chem. Soc. Jpn.*, **69**, 2863 (1996).

[6] D. L. Long, P. Kőgerler, L. J. Farrugia, L Cronin, *Chem. Asian J.* **1**, 352 (2006).

[7] D. L. Long, E. Burkholder, L. Cronin, *Chem. Soc. Rev.*, **36**, 105 (2007).

[8] C. Streb, D. L. Long, L. Cronin, *Chem. Commun.*, 471 (2007).

[9] U. Kortz, M. G. Savelieff, F. Y. Ghali, L. M. Khalil, S. A. Maalouf, D. I. Sinno, *Angew. Chem., Int. Ed.* **41**, 4070 (2002).

[10] X. K. Fang, T. M. Anderson, C. L. Hill, *Angew. Chem., Int. Ed*. **44**, 3540 (2005).

[11] X. K. Fang, T. M. Anderson, Y. Hou, C. L. Hill, *Chem. Commun.*, **40**, 5044 (2005).

[12] B. Hasenknopf, K. Micoine, E. Lacôte, S. Thorimbert, M. Malacria, R. Thoubenot, *Eur. J. Inorg. Chem.*, 5001 (2008).

[13] R.-Q. Sun, H.-H Zhang, S.-L. Zhao, C.-C. Huang, X.-L. Zheng, *Jiegon Huaxue*, **20**, 413 (2001).

[14] C. Zhang, R. C. Howell, Q.-H. luo, H. L. Fieselmann, J. Todaro, L. C. Francesconi, *Inorg. Chem.*, **44**, 3569 (2005).

[15] J.-Y. Niu, J. Zhao, D. Guo, J.-P. Wang, *J. Mol. Struct.*, **692**, 223 (2004).

[16] A. Ostuni, R. E. Bachman, M. T. Pope, *J. Cluster Sci.*, **43**, 431 (2003).

[17] M. Matsunaga, T. Nakanishi, T. Asahi, T. Osaka, *Electrochem. Commun.*, **9**, 725 (2007).

[18] D. K. Lyon, W. K. Miller, T. Novet, P. J. Domaille, E. Evitt, D. C. Johnson, R. G. Finke, *J. Am. Chem. Soc.*, **113**, 7209 (1991).

[19] G. M. Sheldrick, SHELXS-97, Program for Crystal Structure Solution, University of Gettingen, Germany, 1997.

[20] G. M. Sheldrick, SHELXL-97, Program for Crystal Structure Refinement, University of Gettingen, Germany, 1997.

[21] Ed.: Lide; D. E. *Handbook of Chemistry and Physics, 88th*, 7 (2007).

[22] I. D. Brown, "Structure and Bonding in Crystals," ed by M. O'keeffe, A. Navrotsky, Academic Press, New York **Vol. II**, 1 (1980).

[23] F. A. A. Paz, M. S. S. Balula, A. M. V. Cavaleiro, J. Klinowski, H. I. S. Nogueira, *Acta Crystallogr.*, **E61**, i28 (2005).

[24] M. Sugeta, T. Yamase, *Bull. Chem. Soc. Jpn.*, **66**, 444 (1993).

[25] T. Ozeki, T. Yamase, *Acta Crystallogr.*, **B50**, 128, (1994).

[26] M. A. AlDamen, S. Cardona-Serra, J. M. Clemente-Juan, E. Coronado, A. Gaita-Ariño, C. Martí-Gastaldo, F. Luis, O. Montero, *Inorg. Chem.*, **48**, 3467 (2009).

[27] J.-Y. Niu, J. Zhao, D. Guo, J.-P. Wang, *J. Mol. Struct.*, **692**, 223 (2004).

[28] M. A. Fedotov, B. Z. Pertsikov, D. K. Danovich, *Polyhedron* **9**, 1249 (1990).

[29] M. Sadakane, M. H. Dickman, M. T. Pope, *Inorg. Chem.*, **40**, 2715 (2001).

[30] G. Balsse, G. J. Dirksen, F. Zonnevijlle, *Chem. Phys. Lett.*, **83**, 449 (1981).

[31] G. Blasse, Handbook on the Physics and Chemistry of Rare Earths, K. A. Geschneider Jr. and L. Eyling ed. North-Holland, Amsterdam, (1979).

[32] J. Xia, B. Zhao, H. S. Wang, W. Shi, Y. Ma, H. B. Song, P. Cheng, D. Z. liao, S. P. Yan, *Inorg. Chem.*, **46**, 3450 (2007).

[33] G. Blasse, G. J. Dirksen, *J. Inorg. Nucl. Chem.*, **43**, 2847 (1981).

Table 5-1. Crystallographic data and refinement results.

	La-L	Eu-L	Gd-L	Tb-L	Dy-L
Empirical formula	$O_{169}ErP_4W_{34}K_{12}C_{10}N_2H_{109}$	$O_{163}EuP_4W_{34}K_{12}C_{10}N_2H_{97}$	$O_{161}GdP_4W_{34}K_{12}C_{10}N_2H_{105}$	$O_{166}TbP_4W_{34}K_{12}C_{10}N_2H_{103}$	$O_{168}DyP_4W_{34}K_{12}C_{10}N_2H_{107}$
Formula weight	9944.76	9849.73	9831.08	9910.74	9950.34
Crystal system	orthorhombic	orthorhombic	orthorhombic	orthorhombic	orthorhombic
Space group	$P2_12_12$ (#18)	$P2_12_12$ (#18)	$P2_12_12$ (#18)	$P2_12_12$ (#18)	$P2_12_12$ (#18)
a (Å)	12.4853(3)	12.4597(3)	12.4638(2)	12.4786(3)	12.4882(3)
b (Å)	43.550(1)	43.2888(8)	43.2722(7)	43.275(1)	43.2505(8)
c (Å)	14.8113(3)	14.7705(3)	14.7638(2)	14.7787(3)	14.7649(3)
V (Å^3)	8053.3(4)	7966.6(3)	7962.7(2)	7980.7(4)	7974.8(3)
Z	2	2	2	2	2
θ range (°)	3.1-27.6	3.1-27.6	3.1-27.6	3.1-27.7	3.1-27.6
Limiting indices reflections	-16≦h≦16	-16≦h≦14	-16≦h≦16	-16≦h≦14	-15≦h≦16
	-56≦k≦56	-56≦k≦56	-56≦k≦56	-56≦k≦56	-56≦k≦56
	-19≦l≦19	-19≦l≦19	-19≦l≦19	-19≦l≦19	-19≦l≦19
Crystal size (mm^3)	0.23×0.19×0.14	0.25×010×0.09	0.77×0.12×0.03	0.46×0.20×0.16	0.48×0.15×0.14
D_c (g cm^{-3})	4.101	4.106	4.100	4.124	4.143
F(000)	8792.00	8684.00	8670.00	8748.00	8790.00
μ (mm^{-1})	24.9307	25.3226	25.3583	25.3307	25.3776
Todal data collected	130656	127601	128973	116107	128877
Unique data	18442	18242	18243	17339	18233
[$R_{(int)}$]	0.0939	0.0538	0.1217	0.0847	0.0929
Goodness-of-fit (GOF)	1.106	1.075	1.035	1.035	1.096
R_1 [$I > 2\sigma(I)$][a]	0.0327	0.0294	0.0342	0.0477	0.0335
wR_2[b]	0.0828	0.0757	0.0880	0.1176	0.0877
Flack parameter	0.020(9)	0.014(9)	0.009(9)	0.025(14)	0.019(9)

[a] $R_1 = (\Sigma||F_0|-|F_c||)/(\Sigma|F_c|)$.

[b] $wR_2 = \Sigma[w(F_0^2-F_c^2)^2]/\Sigma[w(F_0^2)^2]^{1/2}$.

w (for **La-L**) = $1/[\sigma^2(F_0^2) + (0.0122\cdot P)^2 + 134.1826\cdot P]$, where $P = (Max(F_0^2,0) + 2F_c^2)$

w (for **Eu-L**) = $1/[\sigma^2(F_0^2) + (0.0270\cdot P)^2 + 170.0315\cdot P]$, where $P = (Max(F_0^2,0) + 2F_c^2)$

w (for **Gd-L**) = $1/[\sigma^2(F_0^2) + (0.0242\cdot P)^2 + 57.4918\cdot P]$, where $P = (Max(F_0^2,0) + 2F_c^2)/$

w (for **Tb-L**) = $1/[\sigma^2(F_0^2) + (0.0410\cdot P)^2 + 392.8142\cdot P]$, where $P = (Max(F_0^2,0) + 2F_c^2)$

w (for **Dy-L**) = $1/[\sigma^2(F_0^2) + (0.0297\cdot P)^2 + 122.3826\cdot P]$, where $P = (Max(F_0^2,0) + 2F_c^2)$

Table 5-1 (Continued). Crystallographic data and refinement results.

	Er-L	Er-D	Yb-L
Empirical formula	$O_{170}ErP_4W_{34}K_{12}C_{10}N_2H_{111}$	$O_{168}ErP_4W_{34}K_{12}C_{10}N_2H_{107}$	$O_{168}YbP_4W_{34}K_{12}C_{10}N_2H_{107}$
Formula weight	9991.13	9955.10	9960.88
Crystal system	orthorhombic	orthorhombic	orthorhombic
Space group	$P2_12_12$ (#18)	$P2_12_12$ (#18)	$P2_12_12$ (#18)
a (Å)	12.4842(3)	12.4609(3)	12.4520(3)
b (Å)	43.1675(8)	43.1877(8)	43.1081(8)
c (Å)	14.7853(3)	14.7655(3)	14.7479(3)
V (Å^3)	7967.9(3)	7946.1(3)	7916.4(3)
Z	2	2	2
θ range (°)	3.1-27.5	3.1-27.6	3.1-27.6
Limiting indices reflections	-16≦h≦15	-16≦h≦15	-16≦h≦15
	-56≦k≦56	-56≦k≦55	-55≦k≦55
	-19≦l≦19	-19≦l≦19	-19≦l≦19
Crystal size (mm^3)	0.49×0.09×0.08	0.26×0.12×0.10	0.61×0.17×0.17
D_c (g cm^{-3})	4.164	4.160	4.178
F(000)	8834.00	8794.00	8798.00
μ (mm^{-1})	25.4574	25.5255	25.6829
Todal data collected	129264	128366	128514
Unique data	18256	18206	18128
[$R_{(int)}$]	0.0566	0.0845	0.0943
Goodness-of-fit (GOF)	1.078	1.044	1.081
R_1 [$I > 2\sigma(I)$][a]	0.0265	0.0345	0.0346
wR_2[b]	0.0664	0.0878	0.0918
Flack parameter	0.010(8)	0.014(9)	0.025(10)

[a] $R_1 = (\Sigma||F_0|-|F_c||)/(\Sigma|F_c|)$.

[b] $wR_2 = \Sigma[w(F_0^2-F_c^2)^2]/\Sigma[w(F_0^2)^2]^{1/2}$.

w (for **Er-L**) = $1/[\sigma^2(F_0^2) + (0.0178\cdot P)^2 + 139.9908\cdot P]$, where $P = (\mathrm{Max}(F_0^2,0) + 2F_c^2)$

w (for **Er-D**) = $1/[\sigma^2(F_0^2) + (0.0398\cdot P)^2 + 101.6486\cdot P]$, where $P = (\mathrm{Max}(F_0^2,0) + 2F_c^2)$

w (for **Yb-L**) = $1/[\sigma^2(F_0^2) + (0.0372\cdot P)^2 + 117.4386\cdot P]$, where $P = (\mathrm{Max}(F_0^2,0) + 2F_c^2)$

Table 5-2. Atomic coordinates and B_{eq} ($Å^2$) of **Er-L**.

Atom	x	y	z	Beq	occ
W(1)	0.10673(3)	0.154368(8)	0.60001(3)	1.080(6)	
W(2)	0.11745(3)	0.040467(8)	0.26336(3)	0.976(6)	
W(3)	0.11108(3)	0.219222(8)	0.42552(3)	1.315(7)	
W(4)	0.34538(3)	0.192396(9)	0.34711(3)	1.393(7)	
W(5)	-0.13587(3)	0.068562(8)	0.34512(3)	0.934(6)	
W(6)	0.12257(3)	0.104720(9)	0.08167(3)	1.145(7)	
W(7)	-0.14176(3)	0.125970(8)	0.50019(3)	0.980(6)	
W(8)	0.34131(3)	0.127903(9)	0.52194(3)	1.164(7)	
W(9)	0.26859(3)	0.21375(1)	0.11145(3)	1.568(7)	
W(10)	0.03508(3)	0.185262(9)	0.02600(3)	1.312(7)	
W(11)	0.03236(4)	0.241017(9)	0.18940(3)	1.456(7)	
W(12)	-0.14228(3)	0.190034(9)	0.32707(3)	1.209(7)	
W(13)	-0.13757(3)	0.134332(9)	0.16880(3)	1.085(6)	
W(14)	0.34846(3)	0.070306(9)	0.34244(3)	1.168(7)	
W(15)	0.25116(3)	0.045607(8)	0.56987(3)	1.001(6)	
W(16)	0.01952(3)	0.071674(8)	0.64468(3)	0.904(6)	
W(17)	0.35181(3)	0.133304(9)	0.16600(3)	1.411(7)	
Er(1)	0.0000	0.0000	0.48808(4)	0.880(9)	1/2
K(1)	0.6113(3)	0.18217(6)	0.4890(2)	2.78(5)	
K(2)	0.0322(3)	0.12997(6)	0.8365(2)	3.29(6)	
K(3)	-0.0594(3)	0.04215(7)	0.9125(2)	3.35(6)	
K(4)	0.1008(5)	0.24128(9)	0.6754(4)	5.8(1)	
K(5)	0.6116(4)	0.0815(2)	0.1814(5)	9.8(3)	
K(6)	0.5703(5)	0.2158(2)	0.0118(5)	9.0(2)	
P(1)	0.1073(2)	0.09679(5)	0.4345(2)	0.79(4)	
P(2)	0.1088(2)	0.16481(5)	0.2458(2)	0.95(4)	
O(1)	0.0866(7)	0.2520(2)	0.4880(6)	1.9(2)	
O(2)	0.4710(7)	0.2075(2)	0.3618(6)	2.0(2)	
O(3)	0.3393(6)	0.1667(2)	0.4443(5)	1.3(1)	
O(4)	0.1283(6)	0.1905(2)	0.5161(5)	1.3(1)	
O(5)	0.4676(6)	0.1350(2)	0.5641(5)	1.7(2)	
O(6)	0.2595(6)	0.1529(2)	0.6057(5)	1.3(1)	
O(7)	0.0835(6)	0.1766(2)	0.6937(6)	1.8(2)	
O(8)	0.0925(6)	0.2391(2)	0.3076(5)	1.6(2)	
O(9)	0.3093(6)	0.0914(2)	0.5763(5)	1.2(1)	
O(10)	0.0874(6)	0.1163(2)	0.6483(5)	1.3(1)	
O(11)	0.0949(6)	0.0204(2)	0.3653(5)	1.1(1)	
O(12)	0.1726(6)	0.0127(2)	0.5430(5)	1.1(1)	
O(13)	-0.0969(6)	0.0421(2)	0.4305(5)	1.1(1)	
O(14)	-0.0250(6)	0.0344(2)	0.6094(5)	1.2(1)	
O(15)	0.3572(6)	0.0296(2)	0.6291(5)	1.6(2)	
O(16)	0.1058(6)	0.0116(2)	0.1829(5)	1.5(2)	
O(17)	-0.0290(6)	0.0747(2)	0.7539(5)	1.5(2)	
O(18)	-0.2442(6)	0.0501(2)	0.2963(5)	1.6(2)	
O(19)	-0.0887(6)	0.0946(2)	0.5798(5)	1.1(1)	

O(20)	0.3157(6)	0.0498(2)	0.4516(5)	1.2(1)	
O(21)	0.1645(6)	0.0585(2)	0.6717(5)	1.2(1)	
O(22)	0.4773(7)	0.0575(2)	0.3270(6)	2.0(2)	
O(23)	0.2730(6)	0.0415(2)	0.2716(5)	1.2(1)	
O(24)	0.1075(6)	0.0721(2)	0.5108(5)	1.0(1)	
O(25)	-0.0211(6)	0.0597(2)	0.2651(5)	1.1(1)	
O(26)	0.1680(5)	0.0836(2)	0.3519(5)	0.9(1)	
O(27)	0.1639(5)	0.1260(2)	0.4718(5)	0.9(1)	
O(28)	-0.2481(6)	0.1381(2)	0.5661(5)	1.5(2)	
O(29)	-0.0100(5)	0.1040(2)	0.4083(5)	0.8(1)	
O(30)	0.3728(6)	0.1073(2)	0.4109(5)	1.4(2)	
O(31)	-0.0301(6)	0.1520(2)	0.5439(5)	1.4(2)	
O(32)	-0.1624(6)	0.1556(2)	0.4061(5)	1.3(1)	
O(33)	-0.2483(6)	0.2121(2)	0.3634(5)	1.6(2)	
O(34)	0.1648(6)	0.1777(2)	0.3306(5)	1.4(2)	
O(35)	-0.0320(6)	0.2042(2)	0.4049(5)	1.4(1)	
O(36)	-0.2089(6)	0.1677(2)	0.2311(5)	1.3(2)	
O(37)	-0.0083(6)	0.1571(2)	0.2640(5)	1.1(1)	
O(38)	0.3458(6)	0.0979(2)	0.2381(5)	1.5(2)	
O(39)	0.1415(6)	0.0736(2)	0.1622(5)	1.2(1)	
O(40)	-0.1561(6)	0.1073(2)	0.2591(5)	1.3(1)	
O(41)	0.4799(7)	0.1294(2)	0.1244(6)	2.2(2)	
O(42)	0.1106(6)	0.1911(2)	0.1730(5)	1.2(1)	
O(43)	-0.0212(6)	0.1119(2)	0.1213(5)	1.3(1)	
O(44)	-0.2390(6)	0.1235(2)	0.0971(5)	1.6(2)	
O(45)	-0.0806(6)	0.1687(2)	0.0860(5)	1.3(1)	
O(46)	-0.0068(6)	0.2263(2)	0.0728(5)	1.5(2)	
O(47)	0.3693(7)	0.2347(2)	0.0595(6)	2.3(2)	
O(48)	0.1046(6)	0.1475(2)	0.0241(5)	1.5(2)	
O(49)	0.1017(6)	0.0852(2)	-0.0190(5)	1.7(2)	
O(50)	0.3190(6)	0.1727(2)	0.1053(6)	1.7(2)	
O(51)	0.3751(6)	0.1587(2)	0.2689(5)	1.5(2)	
O(52)	-0.0849(6)	0.2189(2)	0.2403(5)	1.4(2)	
O(53)	-0.0095(7)	0.1886(2)	-0.0841(6)	2.1(2)	
O(54)	0.1753(6)	0.2060(2)	0.0111(5)	1.6(2)	
O(55)	-0.2122(6)	0.0957(2)	0.4293(5)	1.1(1)	
O(56)	-0.0176(7)	0.2780(2)	0.1833(6)	2.1(2)	
O(57)	0.1736(6)	0.2480(2)	0.1417(6)	1.8(2)	
O(58)	0.3124(6)	0.2142(2)	0.2327(5)	1.6(2)	
O(59)	0.2624(6)	0.2239(2)	0.4097(5)	1.4(2)	
O(60)	0.2747(6)	0.1135(2)	0.0711(5)	1.3(1)	
O(61)	0.1692(6)	0.1374(2)	0.2066(5)	1.0(1)	
O(62)	-0.300(2)	0.0645(4)	0.8278(9)	6.6(4)	
O(63)	-0.233(1)	0.0235(3)	0.7578(9)	4.2(3)	
O(64)	-0.1221(8)	0.0470(2)	1.0910(7)	3.0(2)	
O(65)	0.0000	0.0000	0.784(2)	4.7(4)	1/2
O(66)	-0.144(1)	0.1040(3)	0.9226(9)	4.6(3)	
O(67)	-0.107(1)	0.2182(3)	0.7752(8)	4.0(2)	

O(68)	0.515(4)	0.160(1)	-0.042(3)	9(1)	1/2
O(69)	-0.162(2)	0.1519(4)	0.750(1)	5.6(3)	
O(70)	0.590(1)	0.0077(3)	0.230(1)	5.0(3)	
O(71)	0.5941(9)	0.1313(3)	0.3522(8)	3.8(2)	
O(72)	0.5000	0.0000	0.756(2)	4.5(4)	1/2
O(73)	0.346(2)	0.2169(5)	0.615(2)	8.4(5)	
O(74)	0.853(2)	0.2138(4)	0.581(2)	7.5(4)	
O(75)	0.3369(7)	0.1804(2)	0.7590(6)	1.9(2)	
O(76)	0.662(2)	0.1983(4)	0.668(2)	7.2(4)	
O(77)	0.130(1)	0.0146(3)	0.9868(9)	4.7(3)	
O(78)	0.249(2)	0.0358(4)	0.839(1)	6.3(4)	
O(79)	0.236(2)	0.2126(4)	0.810(2)	2.0(3)	1/2
O(80)	0.766(2)	0.2236(4)	0.074(1)	6.6(4)	
O(81)	0.087(2)	0.3058(4)	0.817(1)	5.3(3)	
O(82)	0.254(2)	0.1162(5)	0.793(2)	4.0(5)	1/2
O(83)	0.408(2)	0.0497(6)	0.092(2)	4.5(5)	1/2
O(84)	0.379(2)	0.0818(6)	0.926(2)	4.4(5)	1/2
O(85)	0.734(3)	0.1779(7)	-0.084(2)	6.2(7)	1/2
O(86)	0.451(2)	0.1648(5)	0.732(2)	8.3(5)	
O(87)	0.615(3)	0.0073(7)	0.167(3)	6.2(7)	1/2
O(88)	0.594(4)	0.154(1)	-0.023(3)	9(1)	1/2
O(89)	0.679(3)	0.0463(9)	0.021(3)	8.2(9)	1/2
O(90)	0.570(3)	0.1118(8)	0.868(3)	7.3(8)	1/2
O(91)	0.592(3)	0.1767(8)	0.188(3)	6.6(8)	1/2
O(92)	0.215(2)	0.2287(6)	0.828(2)	3.6(4)	1/2
N(1)	-0.2628(8)	0.0456(3)	0.5904(7)	1.9(2)	
C(1)	-0.276(1)	0.0494(4)	0.759(1)	3.1(3)	
C(2)	-0.2982(9)	0.0652(3)	0.6684(9)	2.2(2)	
C(3)	-0.415(1)	0.0727(4)	0.648(1)	3.4(3)	
C(4)	-0.426(1)	0.0684(3)	0.547(1)	2.7(3)	
C(5)	-0.358(1)	0.0399(3)	0.5280(9)	2.4(2)	

$B_{eq} = 8/3\ \pi^2(U_{11}(aa^*)^2 + U_{22}(bb^*)^2 + U_{33}(cc^*)^2 + 2U_{12}(aa^*bb^*)\cos\gamma + 2U_{13}(aa^*cc^*)\cos\beta + 2U_23(bb^*cc^*)\cos\alpha)$

Table 5-2 (Continued). Atomic coordinates and B_{eq} ($Å^2$) of **Er-D**.

atom	x	y	z	Beq	occ
W(1)	0.10570(4)	0.84572(1)	1.10143(3)	1.405(7)	
W(2)	-0.14278(4)	0.87428(1)	1.00155(3)	1.265(7)	
W(3)	0.11711(4)	0.95943(1)	0.76408(3)	1.238(7)	
W(4)	-0.13648(4)	0.93153(1)	0.84590(3)	1.211(7)	
W(5)	0.12227(4)	0.89511(1)	0.58233(3)	1.410(7)	
W(6)	0.11000(4)	0.78084(1)	0.92710(3)	1.601(8)	
W(7)	0.34468(4)	0.80748(1)	0.84843(3)	1.674(8)	
W(8)	0.34073(4)	0.87202(1)	1.02315(3)	1.490(7)	
W(9)	0.34818(4)	0.92929(1)	0.84255(3)	1.498(7)	
W(10)	0.25120(4)	0.95442(1)	1.07011(3)	1.345(7)	
W(11)	0.01921(4)	0.92850(1)	1.14570(3)	1.229(7)	
W(12)	0.35146(4)	0.86623(1)	0.66624(3)	1.712(8)	
W(13)	0.03459(4)	0.81456(1)	0.52696(3)	1.679(8)	
W(14)	0.26795(4)	0.78587(2)	0.61283(4)	1.930(9)	
W(15)	0.03098(4)	0.75898(1)	0.69092(3)	1.807(8)	
W(16)	-0.14332(4)	0.81015(1)	0.82867(3)	1.487(7)	
W(17)	-0.13844(4)	0.86564(1)	0.66968(3)	1.379(7)	
Er(1)	0.0000	1.0000	0.98853(5)	1.19(1)	1/2
K(1)	0.1101(3)	0.68198(8)	1.0111(3)	3.26(6)	
K(2)	0.0302(4)	0.87029(7)	0.3380(2)	3.60(7)	
K(3)	-0.0595(4)	0.95785(8)	0.4138(3)	3.49(7)	
K(4)	0.6108(5)	0.9175(2)	0.6820(5)	8.9(3)	
K(5)	0.1048(7)	0.7593(2)	1.1743(5)	8.6(2)	
K(6)	0.5717(5)	0.7836(2)	0.5115(5)	8.5(2)	
P(1)	0.1086(3)	0.83505(6)	0.7467(2)	1.30(5)	
P(2)	0.1070(3)	0.90317(6)	0.9352(2)	1.20(4)	
O(1)	0.1056(7)	0.9883(2)	0.6839(6)	1.9(2)	
O(2)	-0.2455(7)	0.9498(2)	0.7961(6)	1.9(2)	
O(3)	-0.2397(8)	0.8761(2)	0.5981(6)	2.1(2)	
O(4)	0.1012(8)	0.9143(2)	0.4813(6)	2.0(2)	
O(5)	-0.0100(8)	0.8115(2)	0.4165(6)	2.3(2)	
O(6)	-0.0203(8)	0.7217(2)	0.6844(6)	2.3(2)	
O(7)	0.3686(9)	0.7648(3)	0.5616(7)	2.8(2)	
O(8)	0.4698(8)	0.7920(2)	0.8627(6)	2.2(2)	
O(9)	0.0838(8)	0.7486(2)	0.9904(6)	2.1(2)	
O(10)	0.4661(7)	0.8654(2)	1.0657(6)	2.0(2)	
O(11)	0.0812(8)	0.8234(3)	1.1948(6)	2.3(2)	
O(12)	0.3570(7)	0.9704(2)	1.1290(6)	2.0(2)	
O(13)	-0.0307(7)	0.9257(2)	1.2548(5)	1.5(2)	
O(14)	0.4767(8)	0.9425(2)	0.8281(6)	2.3(2)	
O(15)	0.4791(8)	0.8697(3)	0.6255(7)	2.7(2)	

O(16)	-0.2511(8)	0.7884(2)	0.8652(6)	2.1(2)
O(17)	-0.1633(7)	0.8446(2)	0.9077(6)	1.6(2)
O(18)	-0.0862(7)	0.7813(2)	0.7417(6)	1.8(2)
O(19)	0.1297(7)	0.8098(2)	1.0177(6)	1.6(2)
O(20)	0.0849(7)	0.8838(2)	1.1503(6)	1.7(2)
O(21)	-0.0905(6)	0.9056(2)	1.0798(5)	1.3(2)
O(22)	-0.0318(7)	0.8478(2)	1.0455(5)	1.4(2)
O(23)	-0.0334(7)	0.7961(2)	0.9071(6)	1.8(2)
O(24)	-0.1578(7)	0.8927(2)	0.7590(6)	1.7(2)
O(25)	-0.0811(7)	0.8315(2)	0.5874(6)	1.8(2)
O(26)	0.1030(7)	0.8523(2)	0.5254(6)	1.9(2)
O(27)	-0.0091(7)	0.7735(2)	0.5741(6)	1.8(2)
O(28)	0.1755(8)	0.7939(2)	0.5136(6)	2.1(2)
O(29)	0.3457(7)	0.9016(2)	0.7386(6)	1.8(2)
O(30)	0.1421(7)	0.9264(2)	0.6619(5)	1.5(2)
O(31)	-0.2131(7)	0.9046(2)	0.9312(5)	1.4(2)
O(32)	0.2748(7)	0.8863(2)	0.5710(6)	1.6(2)
O(33)	-0.2103(7)	0.8323(2)	0.7320(6)	1.5(2)
O(34)	0.2736(7)	0.9585(2)	0.7717(6)	1.6(2)
O(35)	-0.2484(7)	0.8627(2)	1.0660(6)	2.0(2)
O(36)	0.0915(7)	0.7606(2)	0.8096(6)	1.8(2)
O(37)	0.1652(7)	0.9419(2)	1.1725(6)	1.7(2)
O(38)	0.2595(7)	0.8475(2)	1.1066(6)	1.8(2)
O(39)	0.3156(7)	0.9504(2)	0.9529(6)	1.5(2)
O(40)	-0.0216(7)	0.9400(2)	0.7652(5)	1.4(2)
O(41)	0.3727(7)	0.8926(2)	0.9128(6)	1.8(2)
O(42)	0.3748(7)	0.8415(2)	0.7701(6)	1.8(2)
O(43)	0.3163(7)	0.8273(2)	0.6054(6)	2.0(2)
O(44)	0.1727(8)	0.7523(3)	0.6445(7)	2.4(2)
O(45)	0.2608(7)	0.7761(2)	0.9110(6)	1.9(2)
O(46)	0.3117(7)	0.7855(2)	0.7342(6)	1.8(2)
O(47)	0.3084(7)	0.9088(2)	1.0776(6)	1.7(2)
O(48)	0.1079(6)	0.9279(2)	1.0110(5)	1.2(2)
O(49)	-0.0109(6)	0.8961(2)	0.9099(5)	1.3(2)
O(50)	0.1670(6)	0.9162(2)	0.8522(5)	1.1(2)
O(51)	0.1635(6)	0.8740(2)	0.9735(5)	1.2(2)
O(52)	-0.0242(7)	0.9652(2)	1.1101(5)	1.3(2)
O(53)	0.1734(7)	0.9873(2)	1.0427(5)	1.4(2)
O(54)	-0.0088(7)	0.8426(2)	0.7658(5)	1.4(2)
O(55)	0.1632(7)	0.8222(2)	0.8311(5)	1.5(2)
O(56)	0.1694(7)	0.8627(2)	0.7064(5)	1.3(2)
O(57)	0.1108(7)	0.8088(2)	0.6731(5)	1.5(2)
O(58)	0.0955(7)	0.9795(2)	0.8652(5)	1.4(2)

O(59)	-0.0970(7)	0.9579(2)	0.9303(5)	1.3(2)	
O(60)	0.3393(7)	0.8333(2)	0.9453(6)	1.7(2)	
O(61)	-0.0223(7)	0.8882(2)	0.6211(6)	1.6(2)	
O(62)	-0.234(2)	0.9764(4)	0.261(2)	6.4(4)	
O(63)	-0.308(2)	0.9364(5)	0.331(2)	8.8(6)	
O(64)	-0.132(1)	1.0148(3)	0.4874(8)	4.1(3)	
O(65)	-0.1230(9)	0.9525(3)	0.5908(7)	3.1(2)	
O(66)	0.0000	1.0000	0.284(2)	5.9(5)	1/2
O(67)	-0.147(1)	0.8969(3)	0.4253(9)	4.3(3)	
O(68)	-0.164(2)	0.8493(5)	0.252(2)	7.1(4)	
O(69)	0.252(2)	0.8837(6)	0.296(2)	4.2(5)	1/2
O(70)	0.234(2)	0.7890(4)	1.310(1)	0.9(3)	1/2
O(71)	-0.1102(9)	0.7833(3)	1.2773(7)	3.2(2)	
O(72)	0.092(1)	0.6312(3)	1.1453(9)	4.5(3)	
O(73)	0.342(2)	0.7829(5)	1.116(2)	9.2(6)	
O(74)	0.587(1)	0.8093(3)	0.6840(9)	4.4(3)	
O(75)	0.6619(9)	0.1793(3)	0.2578(8)	3.5(2)	
O(76)	0.411(2)	0.0067(4)	0.732(1)	5.6(3)	
O(77)	0.5000	0.0000	0.254(2)	6.0(5)	1/2
O(78)	0.747(2)	0.0364(4)	0.341(2)	6.9(4)	
O(79)	0.156(2)	0.6972(5)	0.836(2)	3.3(4)	1/2
O(80)	0.675(4)	0.956(1)	0.521(3)	9(1)	1/2
O(81)	0.765(2)	0.7735(5)	0.581(2)	7.9(5)	
O(82)	0.737(3)	0.8227(8)	0.421(2)	5.9(7)	1/2
O(83)	0.406(3)	0.9497(6)	0.589(2)	11.2(7)	
O(84)	0.619(3)	0.9942(9)	0.664(3)	7.3(9)	1/2
O(85)	0.616(3)	0.0811(7)	0.426(2)	5.3(6)	1/2
O(86)	-0.157(2)	0.7885(5)	1.085(2)	8.3(5)	
O(87)	0.587(6)	0.880(2)	0.363(5)	15(2)	1/2
O(88)	0.553(2)	0.1658(4)	0.232(1)	5.5(3)	
O(89)	0.524(4)	0.839(1)	0.458(3)	8(1)	1/2
O(90)	0.221(3)	0.7760(7)	1.322(2)	4.1(5)	1/2
N(1)	-0.2618(9)	0.9551(3)	0.0897(8)	2.1(2)	
C(1)	-0.277(2)	0.9506(5)	0.259(2)	4.3(4)	
C(2)	-0.299(2)	0.9342(4)	0.170(1)	3.0(3)	
C(3)	-0.417(2)	0.9265(6)	0.151(2)	5.1(5)	
C(4)	-0.427(2)	0.9311(5)	0.045(2)	4.3(4)	
C(5)	-0.358(2)	0.9609(4)	0.030(2)	3.5(3)	

$B_{eq} = 8/3\ \pi^2(U_{11}(aa^*)^2 + U_{22}(bb^*)^2 + U_{33}(cc^*)^2 + 2U_{12}(aa^*bb^*)\cos\gamma + 2U_{13}(aa^*cc^*)\cos\beta + 2U_23(bb^*cc^*)\cos\alpha)$

Table 5-3 The bond lengths of Ln-O, W-O and BVS values for all the compounds.

	d (Ln-O) / [Å]		*d* (W-O) / [Å]	BVS		
	Range	Average		Ln	P	W
La-L	2.473(8)-2.509(8)	2.493	1.694(9)-2.403(8)	3.4	5.0	5.9-6.3
Eu-L	2.387(7)-2.407(6)	2.401	1.706(7)-2.386(6)	3.3	4.9	6.0-6.1
Gd-L	2.384(7)-2.409(7)	2.393	1.691(8)-2.389(7)	3.3	4.9	5.9-6.2
Tb-L	2.359(13)-2.407(13)	2.383	1.694(13)-2.399(12)	3.2	4.9	5.9-6.2
Dy-L	2.358(7)-2.375(7)	2.366	1.706(8)-2.393(7)	3.3	5.0	5.8-6.1
Er-L	2.338(6)-2.366(6)	2.349	1.712(7)-2.392(6)	3.2	5.0	5.9-6.2
Er-D	2.343(7)-2.370(7)	2.355	1.701(8)-2.386(7)	3.1	5.0	5.8-6.2
Yb-L	2.312(7)-2.335(8)	2.323	1.695(9)2.387(7)	3.2	5.0	5.7-6.2

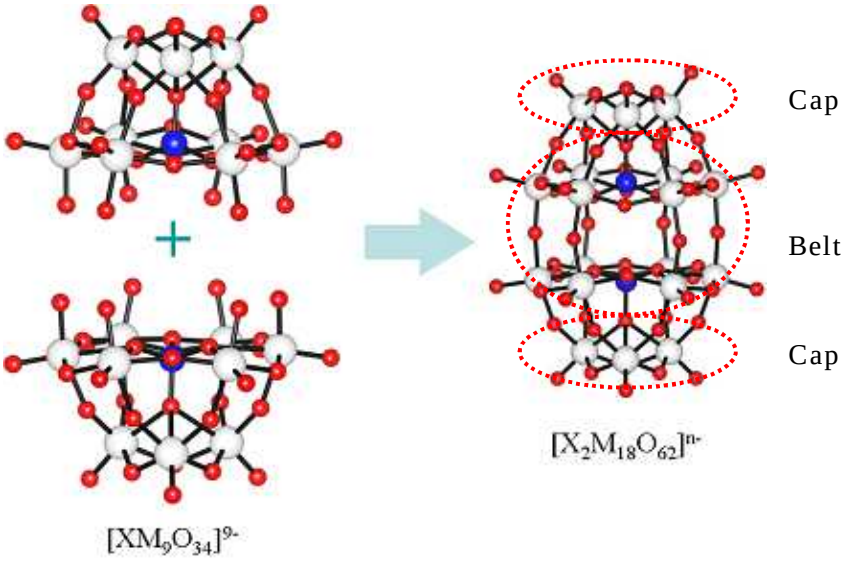

Figure 5-1. The structural relationship between tri-lacunary Keggin type $[XM_9O_{34}]^{n-}$ and Wells-Dawson $[X_2M_{18}O_{62}]^{n-}$ (M atom: white sphere, P atom: blue sphere, O atom: red sphere).

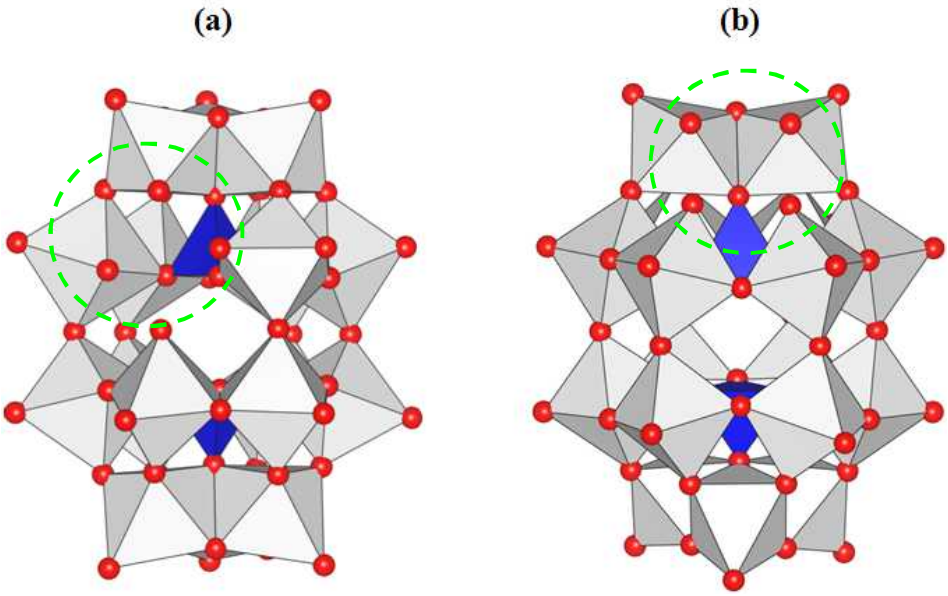

Figure 5-2. The two types of mono-lacunary Wells-Dawson species; (a) α_1 type, (b) α_2 type (WO_6: white octahedron, PO_4: blue tetrahedron, O atom: red sphere). The circles denote the vacant positions.

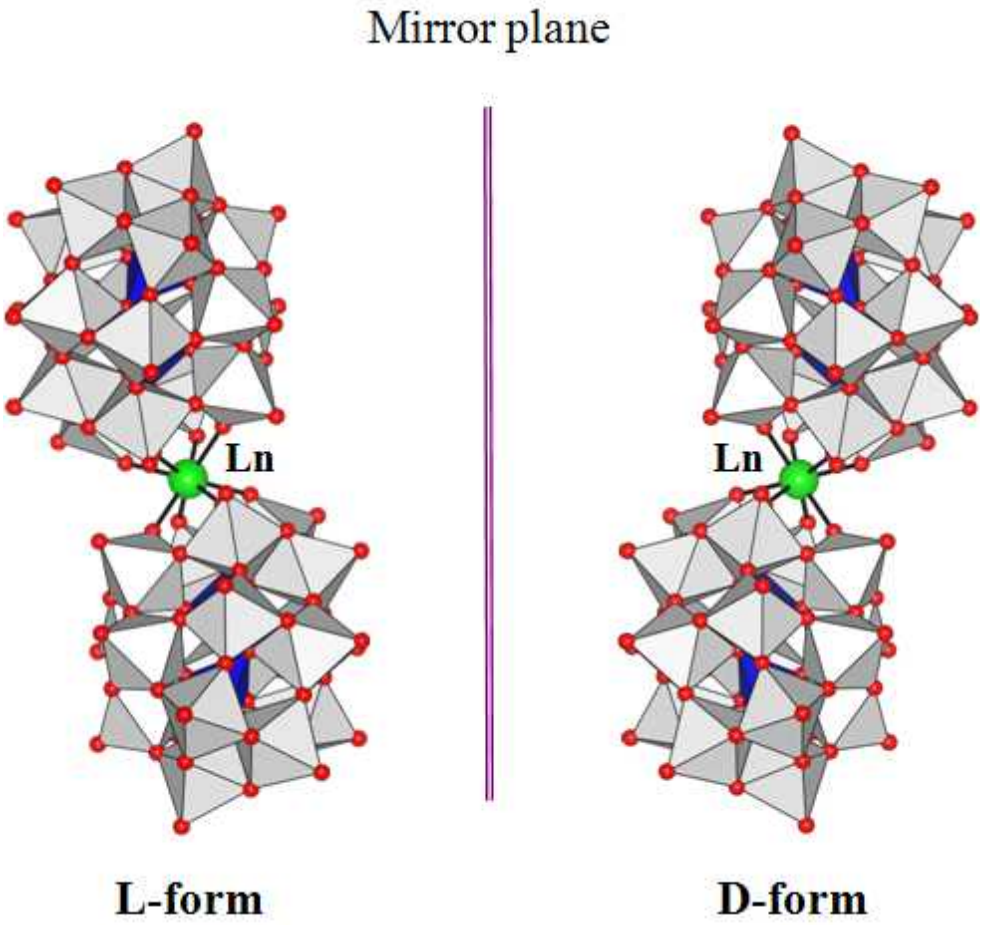

Figure 5-3. Combined polyhedral and ball-and-stick representation of two enantiomers of the $[Ln(\alpha_2\text{-}P_2W_{17}O_{61})_2]^{17-}$ polyanion viewed along the molecular C_2 axis. Left: L-form, Right: D-form (WO_6: white octahedron, PO_4: blue tetrahedron, O atom: red sphere, Ln: green sphere).

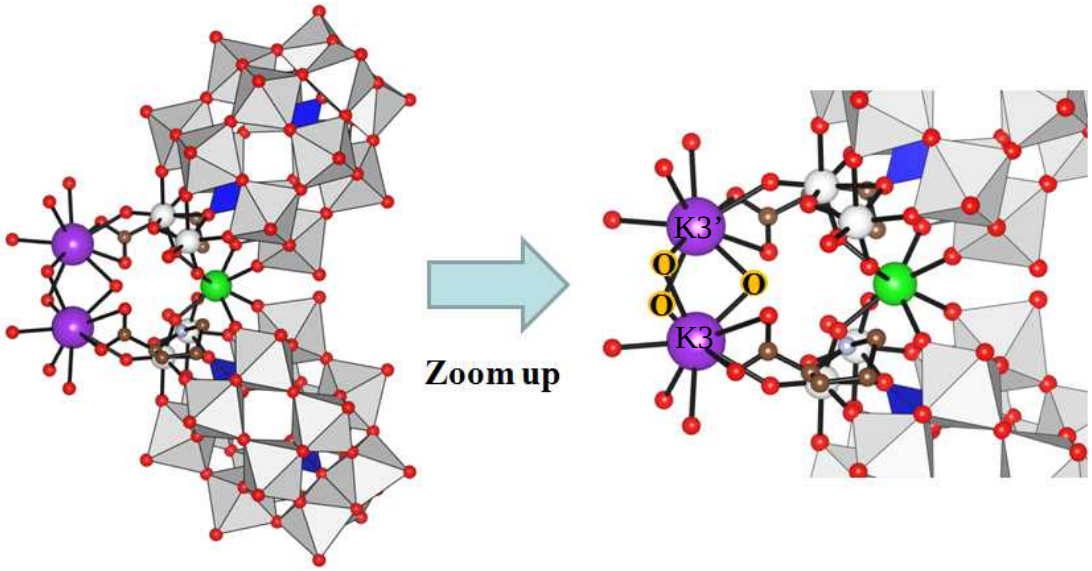

Figure 5-4. Attachment of K3 and symmetry related K3' atoms to the polyanion.. These K atoms (purple) are linked by crystal water O atoms (orange).

(a)

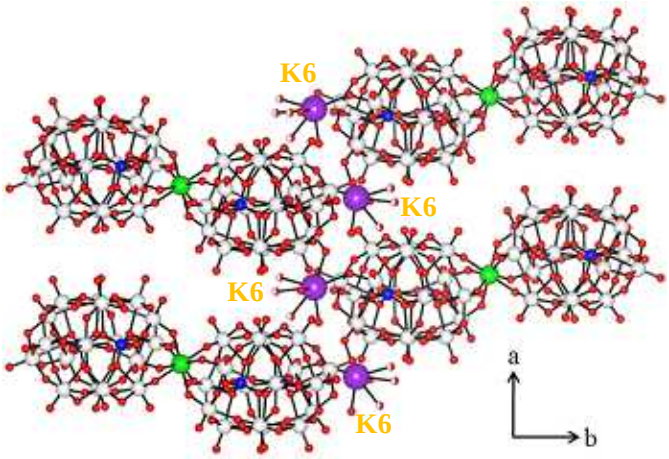

(b)

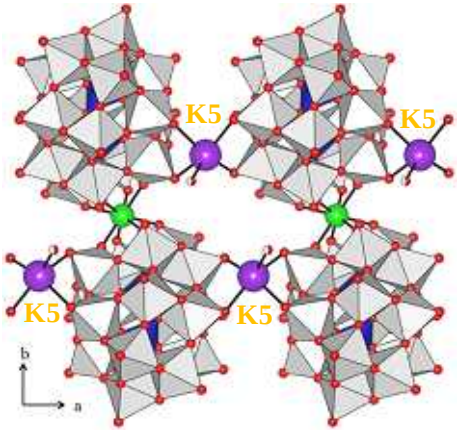

(c)

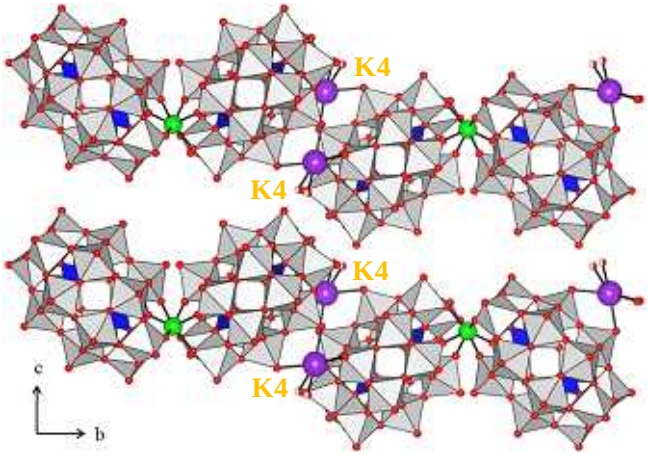

Figure 5-5. The linkages of polyanions via K6–O (a), K5–O (b) and K4–O (c) bondings. Color codes are denoted in the captions of **Figs. 5-3** and **5-4**.

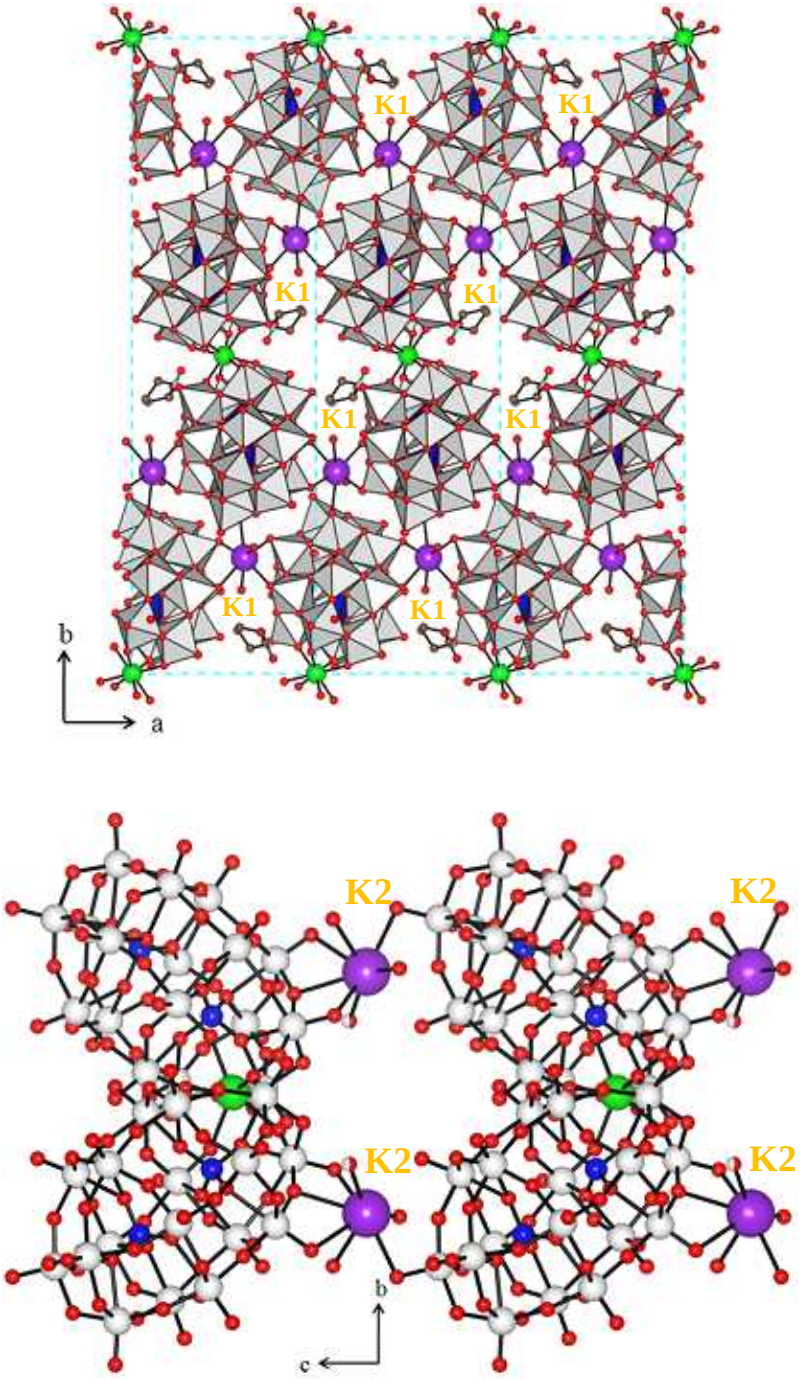

Figure 5-6. The linkage of polyanions via K1–O (above) and K2–O (below) bondings.

Color codes are denoted in the captions of **Figs. 5-3** and **5-4**.

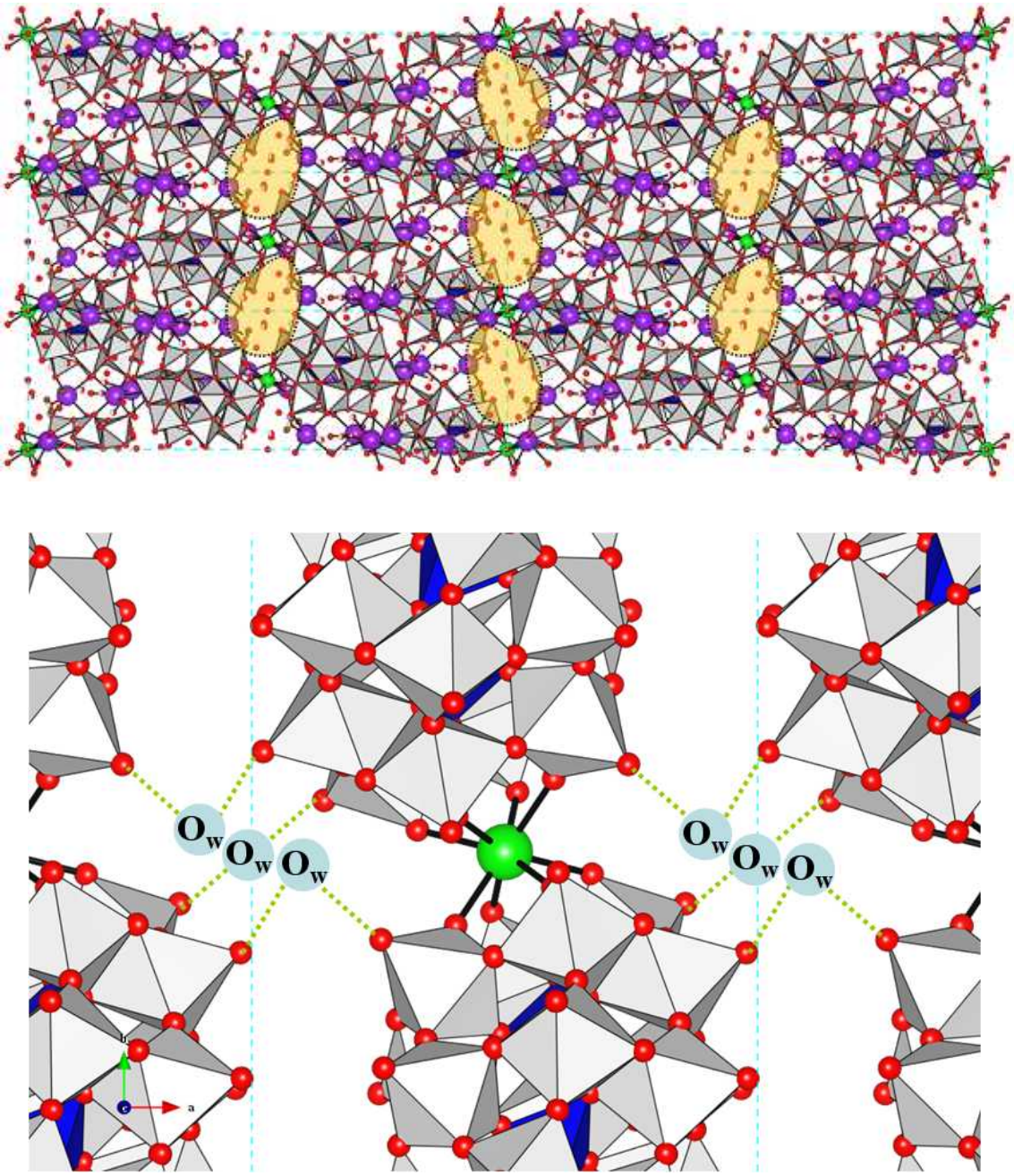

Figure 5-7. Crystal structure (above) and hydrogen-bondings via waters of crystallization (below). The orange-colored region in the above includes the water oxygen (O_w) atoms in the below. Color codes are denoted in the caption of **Figs. 5-3** and **5-4**.

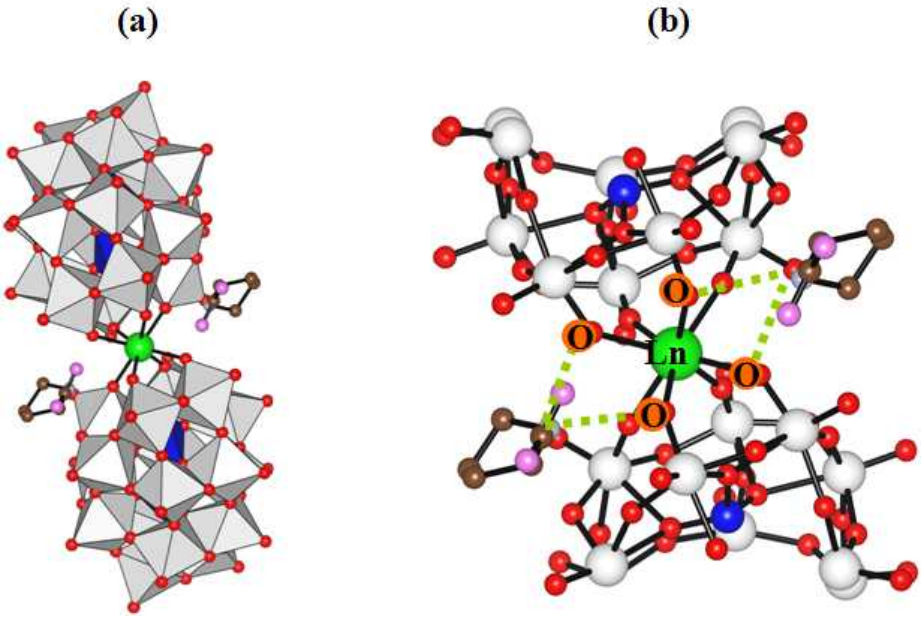

Figure 5-8. The hydrogen-bonding interaction between the D-[Er(α_2-$P_2W_{17}O_{61}$)$_2$]$^{17-}$ polyanion and two D-proline molecules. (a) overall view. (b) enlarged view. N atom: light blue sphere, C atom: brown sphere, O atom in proline: pink sphere. The other color codes are denoted in the captions of **Figs. 5-3** and **5-4**.

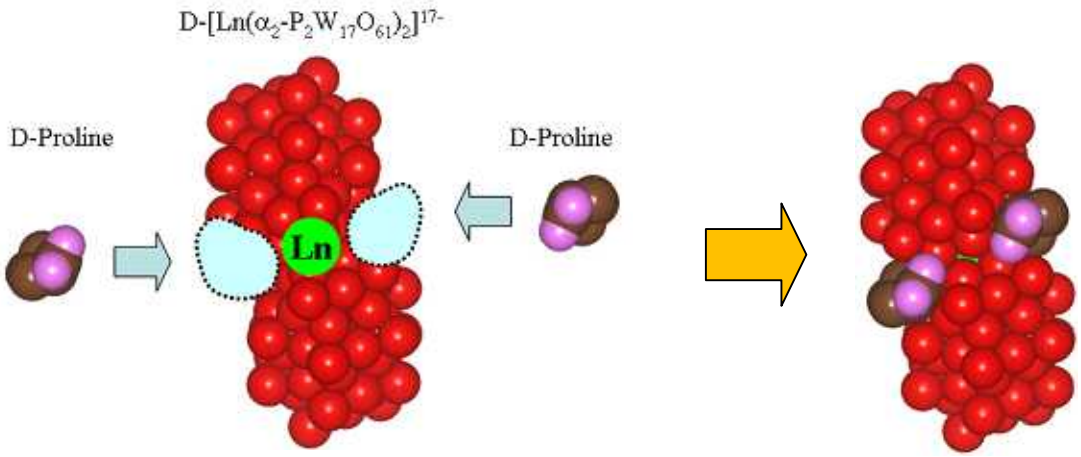

Figure 5-9. Space-filling model of D-[Ln(α_2-$P_2W_{17}O_{61}$)$_2$]$^{17-}$ polyanion and two D-proline molecules.

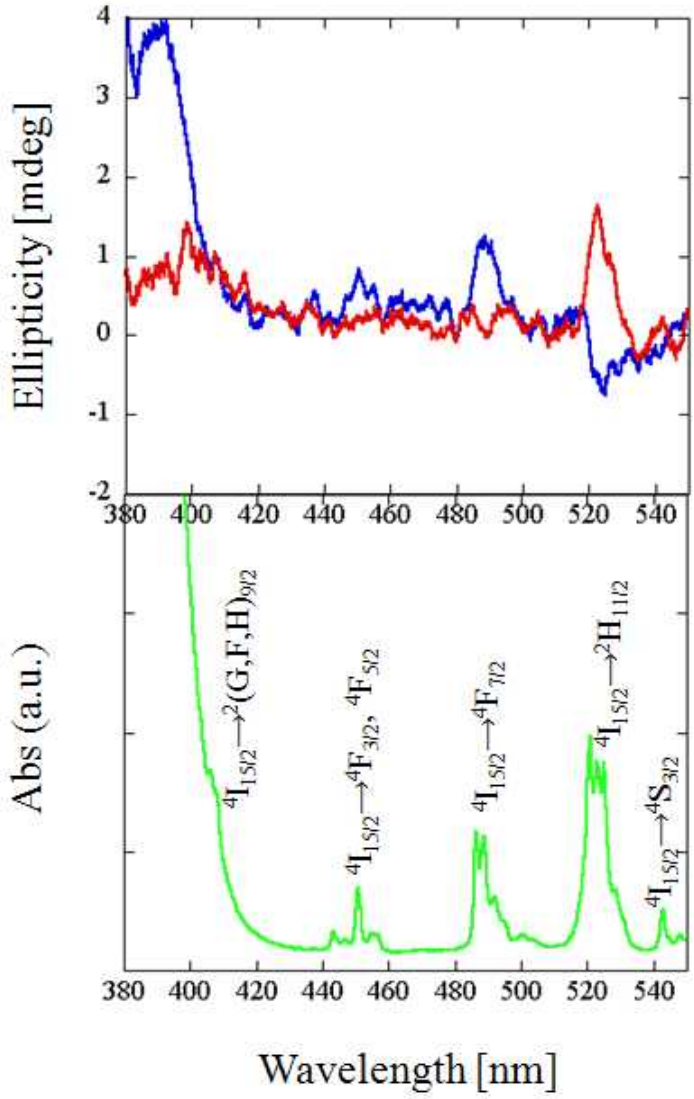

Figure 5-10. Above: The CD spectra of the aqueous solutions (25 mM) of **Er-D** (red) and **Er-L** (blue). Below: UV-Vis absorption spectrum of **Er-L** in aqueous solution.

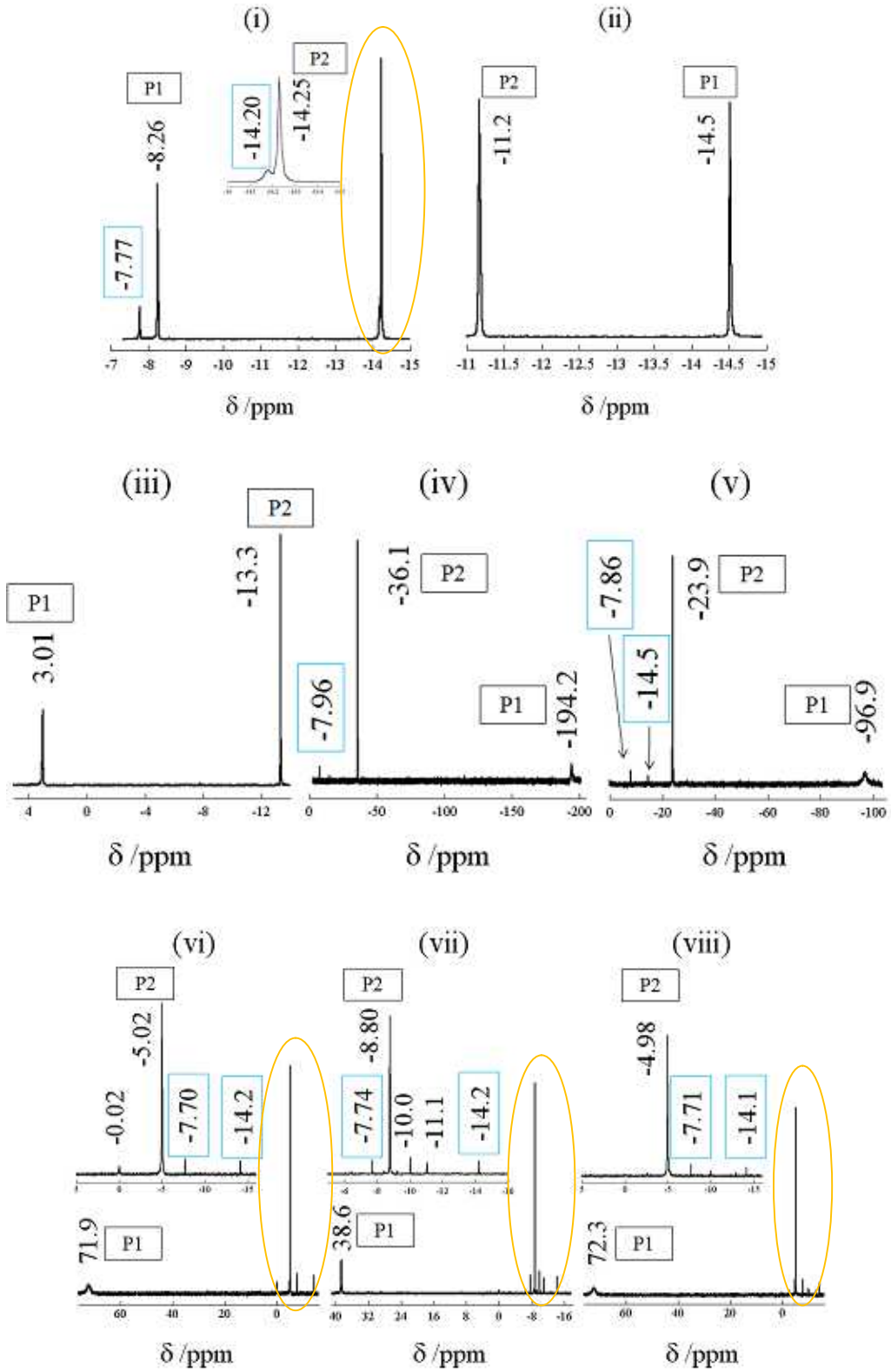

Figure 5-11. The ^{31}P-NMR spectra of **La-L** (i), **Sm-L** (ii), **Eu-L** (iii), **Tb-L** (iv), **Dy-L** (v), **Er-L** (vi), **Yb-L** (vii), and **Er-D** (viii) in D_2O solutions. The insets are demonstrated by expanding the orange circled region. A pair of resonance peaks attributable to $[\alpha_2\text{-}P_2W_{17}O_{61}]^{10-}$ is indicated as blue circled values.

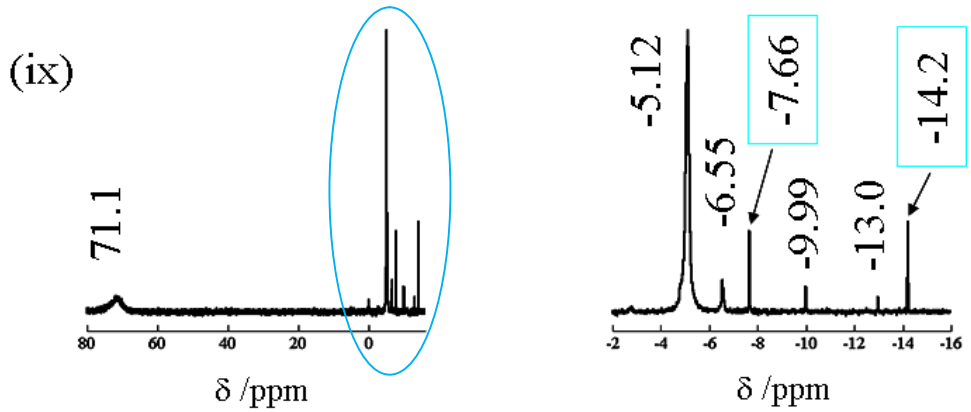

Figure 5-11 (Continued). The ^{31}P-NMR of **Er-L** (ix) in D_2O solution in which 78-fold stoichiometric L-proline was further added. The left spectrum is overall view and the right one is demonstrated by expanding the blue circled region in left one.

Assignment summary for the chemical shift in **Fig. 5-11**.

Ln in $[Ln(\alpha_2\text{-}P_2W_{17}O_{61})_2]^{17-}$	Compound name	P1 (ppm)	P2 (ppm)	P (ppm) in $[Ln(\alpha\text{-}PW_{11}O_{39})_2]^{11-}$
La	La-L	-8.26	-14.25	-11.9
Sm	Sm-L	-14.5	-11.2	-15.4
Eu	Eu-L	3.01	-13.3	-1.2
Tb	Tb-L	-194.2	-36.1	-223
Dy	Dy-L	-96.9	-23.9	-108
Er	Er-L	71.9	-5.02	61.4
Er	Er-D	72.3	-4.98	61.4
Yb	Yb-L	38.6	-8.80	32

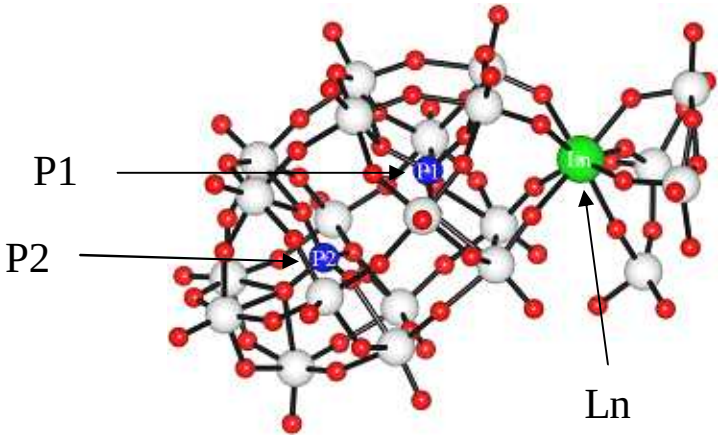

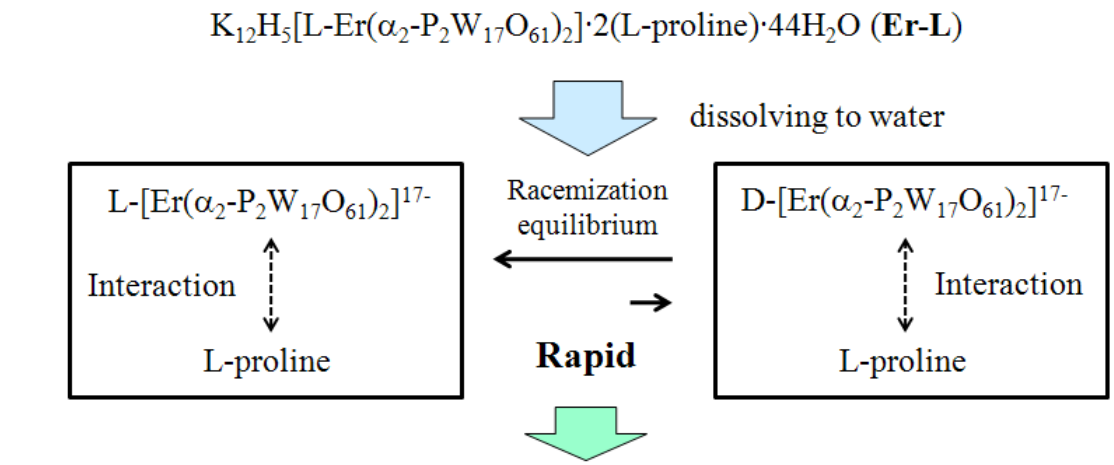

^{31}P-NMR	71.9 ppm (P1) -5.02 ppm (P2)
CD	Active but weak (**Fig. 5-10**)

Figure 5-12. Presumed equilibrium scheme of **Er-L** in aqueous solution and relation to ^{31}P-NMR and CD spectroscopy.

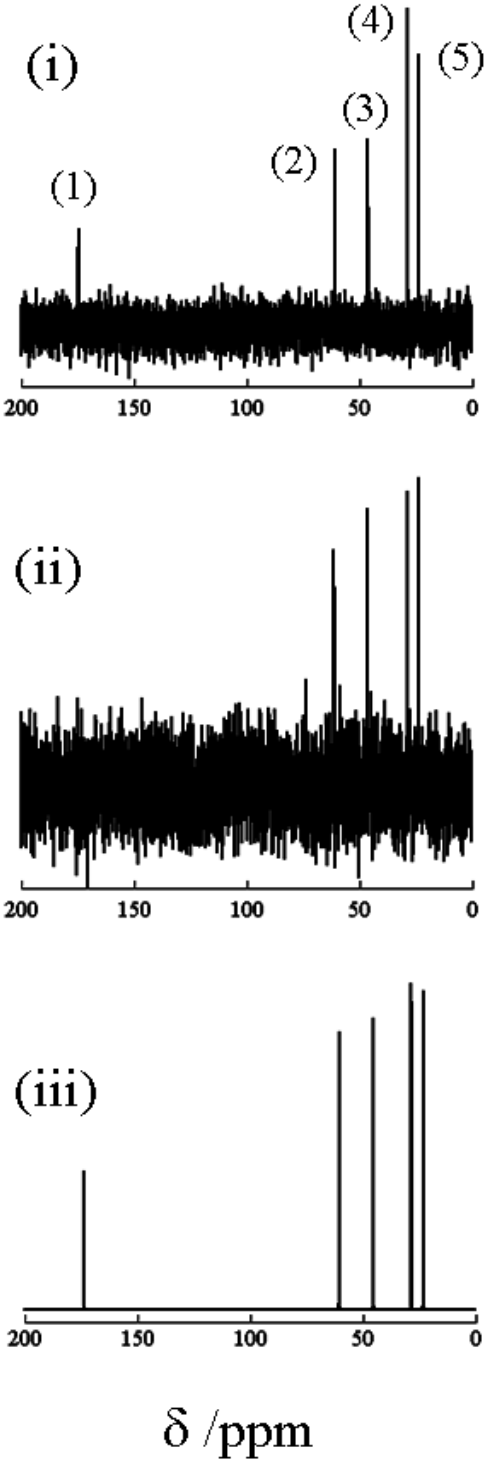

L-proline

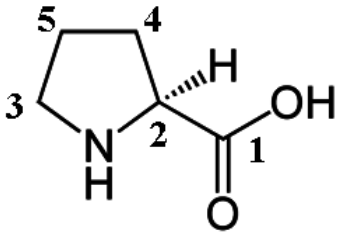

	Chemical shit [ppm]		
	Er-L	La-L	L-proline
C1	174.7	------	173.8
C2	61.3	61.4	60.7
C3	46.4	46.5	45.5
C4	29.1	29.1	28.8
C5	23.9	23.9	23.4

Figure 5-13. The ^{13}C-NMR spectra of **Er-L** (i), **La-L** (ii) and L-proline (iii) in D_2O solutions.

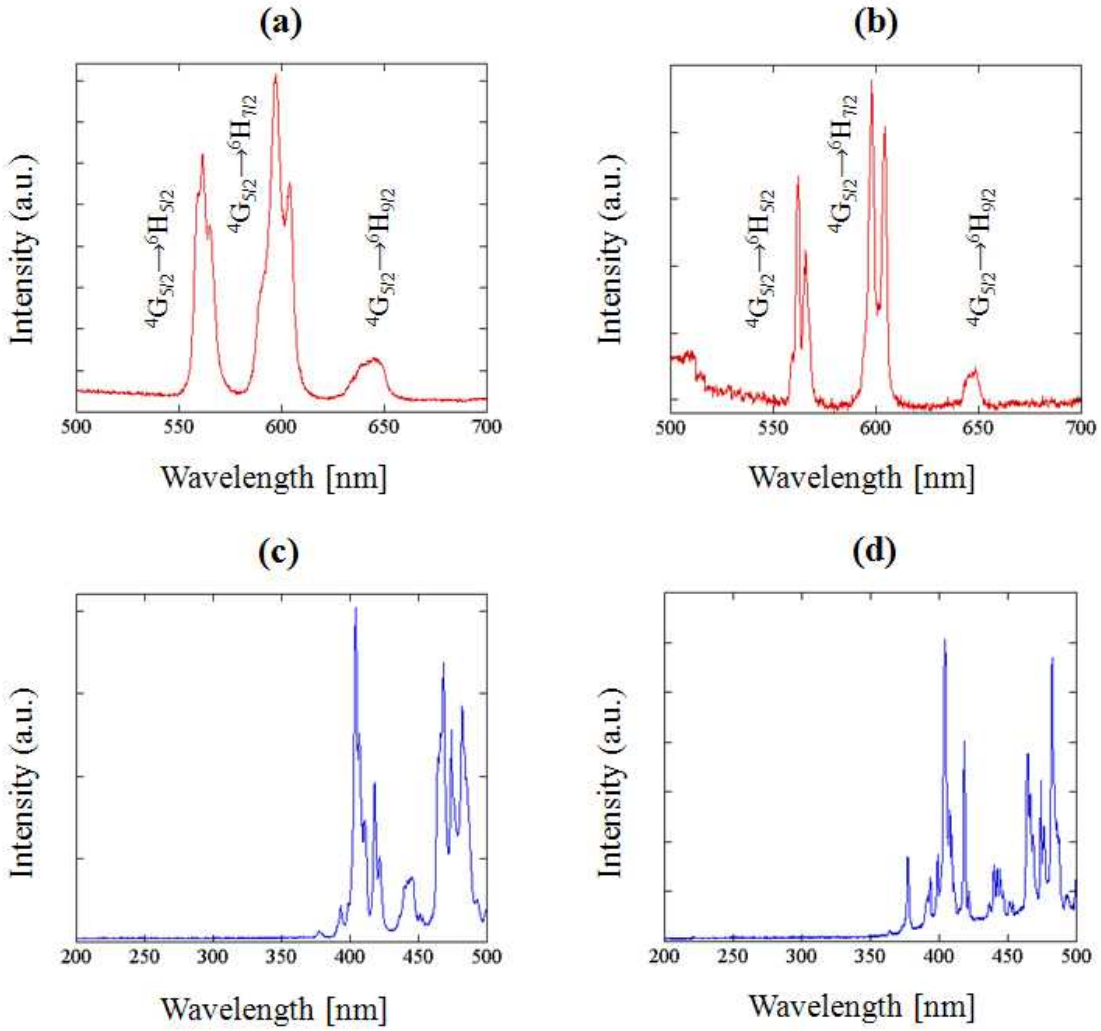

Figure 5-14. Emission (a, b) and excitation (c, d) spectra of the crystal of **Sm-L** at 298 K (a, c) and 77 K (b, d). The emission spectra were observed by Sm^{3+} excitation at 404 nm, while the excitation spectra were monitored at 598 nm ($^4G_{5/2}\rightarrow{}^6H_{7/2}$).

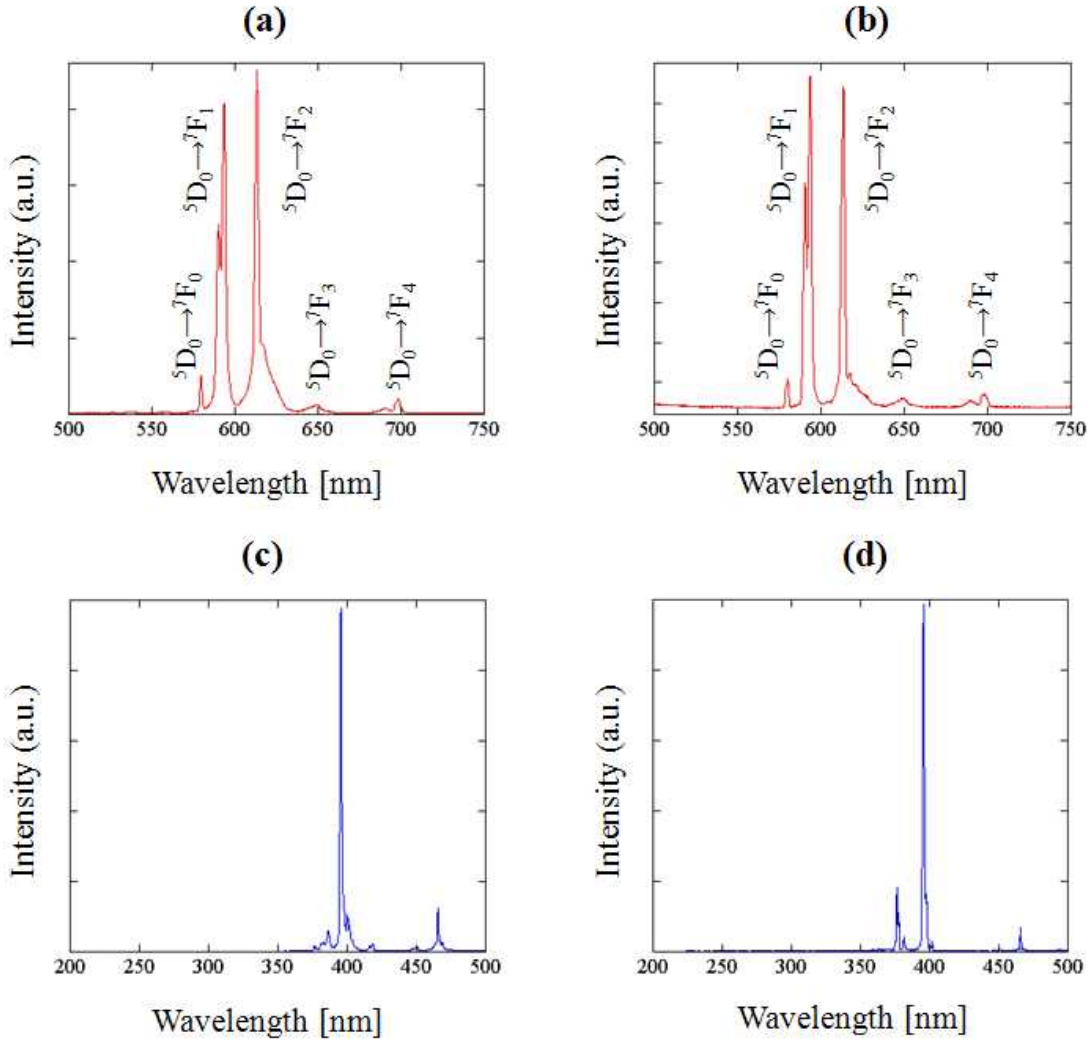

Figure 5-15. Emission (a, b) and excitation (c, d) spectra of the crystal of **Eu-L** at 298 K (a, c) and 77 K (b, d). The emission spectra were observed by Eu^{3+} excitation at 395 nm, while the excitation spectra were monitored at 613 nm ($^5D_0 \rightarrow {}^7F_2$) for (c) and 594 nm ($^5D_0 \rightarrow {}^7F_1$) for (d).

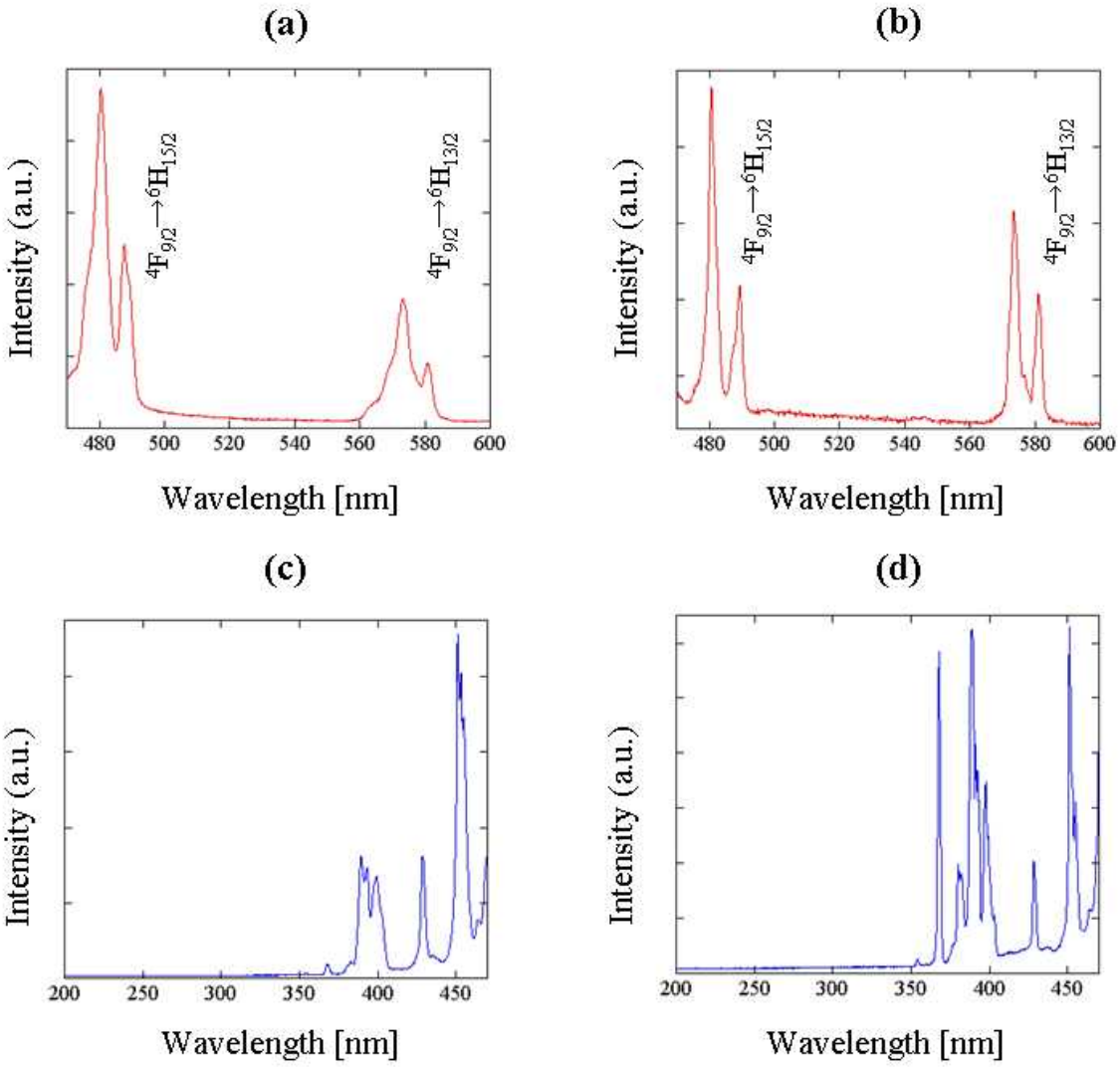

Figure 5-16. Emission (a, b) and excitation (c, d) spectra of the crystal of **Dy-L** at 298 K (a, c) and 77 K (b, d). The emission spectra were observed by Dy^{3+} excitation at 450 nm, while the excitation spectra were monitored at 480 nm ($^4F_{9/2}\rightarrow{}^6H_{15/2}$).

Chapter 6 The effects of lanthanide ion and molecular environments on the structure of the sandwich-type lanthanide-containing polyoxotungstates

6-1 Introduction

Variations of lanthanide ions (Ln) as linkers and lacunary polyoxometalate (POM) species as building blocks have produced numerous kinds of polyoxometallolanthanoates (Ln-POMs) [1-5]. In addition, synthetic conditions, such as stoichiometry, cation species as well as reaction pH and temperature strongly play an essential role in synthesizing Ln-POMs. Since the first discovery of the sandwich-type Ln-POMs containing $Ln^{3+/4+}$ coordinated by two mono-lacunary Keggin $[XM_{11}O_{39}]^{n-}$, Wells-Dawson $[X_2M_{17}O_{61}]^{n-}$, and Lindqvist $[X_5O_{18}]^{n-}$ units by Peacock and Weakley in 1971 [3], the intensive studies on the structural chemistry and physico and spectrochemical properties of Ln-POMs have been developed to date [6-24]. Especially for the $[Ln(\alpha\text{-}PW_{11}O_{39})_2]^{11-}$ and $[Ln(\alpha_2\text{-}P_2W_{17}O_{61})_2]^{17-}$ containing tetradentate mono-lacunary Keggin $[\alpha\text{-}PW_{11}O_{39}]^{7-}$ and Wells-Dawson $[\alpha_2\text{-}P_2W_{17}O_{61}]^{10-}$ units, respectively, the coordination mode of the central Ln^{3+} was studied by Fedotov and Francesconi using not only ^{31}P- and ^{183}W-NMR spectroscopy but also single crystal X-ray diffraction [6, 23]. In each of the $[Ln(\alpha\text{-}PW_{11}O_{39})_2]^{11-}$ and $[Ln(\alpha_2\text{-}P_2W_{17}O_{61})_2]^{17-}$ structures, the two mono-lacunary units have mirror planes, and the dihedral angle between the two mirror planes defines the molecular conformation and directs the coordination geometry of the central Ln ion. For example, ^{183}W-NMR studies of

$[Ln(\alpha\text{-}PW_{11}O_{39})_2]^{11-}$ in aqueous solutions suggested that the dihedral angle (ϕ) is dependent on the Ln species; 0º or 180º for Ln = La-Eu and 0º<ϕ<180º for Ln = Gd-Lu corresponding to cubic and square-antiprismatic (SA) conformation for Ln, respectively [6]. However, the past studies have been preoccupied with the effect of Ln species (i.e. ionic radius of Ln^{3+}), there has been little discussion about the effect of cationic environment and co-existing molecules on the detailed molecular conformation of Ln-POMs. It has been already demonstrated in Chapter 3 that both of counter-cationic environment and ionic size of Ln^{3+} are important factors for the conformation of $[Ln(\alpha\text{-}PW_{11}O_{39})_2]^{11-}$ and coordination mode of Ln^{3+}. Therefore, it is important to investigate molecular conformation of the $[Ln(\alpha\text{-}PW_{11}O_{39})_2]^{11-}$ and $[Ln(\alpha_2\text{-}P_2W_{17}O_{61})_2]^{17-}$ polyanions and its relationship with surrounding cations and co-existing molecules in greater detail. In this chapter, molecular structures of these polyanions described in Chapters 2-5 and in previous literatures are precisely analyzed and effects of environment on the polyanions are extracted. The result would contribute to molecular and functional design of Ln-POMs for practical applications to functional materials in future.

6-2 Structural evaluation of the sandwich-type $[M(\alpha\text{-}XW_{11}O_{39})_2]^{n-}$ and $[M(\beta_2\text{-}XW_{11}O_{39})_2]^{n-}$ polyanions

As described in Chapter1, there have been two types of the sandwich-type $[M(XW_{11}O_{39})_2]^{n-}$ polyanions to date, i.e. α-type and β_2-type of the mono-lacunary Keggin units. The coordination mode of Ln in the former $[M(\alpha\text{-}XW_{11}O_{39})_2]^{n-}$ polyanion has been expected to adopt cubic and SA coordination in aqueous solution by ^{183}W-NMR spectroscopy [6], however, all of the isolated $[M(\alpha\text{-}XW_{11}O_{39})_2]^{n-}$ polyanions

in the solid states held M^{n+} in a SA coordination environment. In this section, the molecular conformation of the well-known $[M(\alpha\text{-}PW_{11}O_{39})_2]^{n-}$ polyanions will be discussed preceding the recently reported $[Ln(\beta_2\text{-}SiW_{11}O_{39})_2]^{13-}$ polyanion. The effect of surroundings of $[M(\alpha\text{-}PW_{11}O_{39})_2]^{n-}$ is studied for (i) pure alkylammonium cations, (ii) mixed cations of alkylammonium and alkaline metals, and (iii) alkaline metal cations and amino acid (proline) hydrogen-bonded to the polyanion. Then, a constructive discussion will be made on the $[Ln(\beta_2\text{-}SiW_{11}O_{39})_2]^{13-}$ polyanion [24].

6-2-1 Definitions of the structural parameters in $[M(\alpha\text{-}PW_{11}O_{39})_2]^{n-}$

The mirror plane (*m*) which halves a C_s-symmetric $[\alpha\text{-}PW_{11}O_{39}]^{7-}$ unit in a $[M(\alpha\text{-}PW_{11}O_{39})_2]^{n-}$ polyanion is prescribed by the least-squares plane defined by M, one of the eleven W, P, and seven bridging O atoms. These atoms are numbered as [M, W(1), P(2), O(1, 2, 3, 4, 5, 6, 7)] and [M, W(2), P(2), O(8, 9, 10, 11, 12, 13, 14)] in **Fig. 6-1(top)**. The dihedral angle between the two least-squares planes defines the twist angle (ϕ) of the $[\alpha\text{-}PW_{11}O_{39}]^{7-}$ unit (**Fig. 6-1(bottom-left)**). Note that this ϕ also defines the geometry of 8-coordinate Ln center (**Fig. 6-1(bottom-right)**). The geometric parameters for structurally characterized $[M(\alpha\text{-}PW_{11}O_{39})]^{n-}$ polyanions in various compounds are collected in **Tables 6-1, 6-2, and 6-3**, which list ionic radius of M (R_M) [25], twist angle (ϕ), O···O contacts ($O_A\cdots O_{A'}$, $O_A\cdots O_{B'}$, and $O_{A'}\cdots O_B$) and P···P distance (d(P···P)). Positions of the O_A, $O_{A'}$, O_B, and $O_{B'}$ atoms are described in **Fig. 6-1(bottom-left).** Their O···O contacts are important for understanding the steric repulsion between the two $[\alpha\text{-}PW_{11}O_{39}]^{7-}$ units. The d(P···P) parameter describes the degree of separation between the two $[\alpha\text{-}PW_{11}O_{39}]^{7-}$ units.

6-2-2 Pure alkylammonium salts of $[M(\alpha\text{-}PW_{11}O_{39})_2]^{n-}$

Fig. 6-2 shows the relations between selected geometric parameters of $[Me_2NH_2]_{11}[Ce^{III}(\alpha\text{-}PW_{11}O_{39})_2]\cdot 14H_2O$ and $[Me_2NH_2]_{10}[Ce^{IV}(\alpha\text{-}PW_{11}O_{39})_2]\cdot 14H_2O$ described in Chapter 2 and of published compounds $[Me_2NH_2]_{10}[Hf^{IV}(\alpha\text{-}PW_{11}O_{39})_2]\cdot 8H_2O$ [26], $[Me_2NH_2]_{10}[Zr^{IV}(\alpha\text{-}PW_{11}O_{39})_2]\cdot 10H_2O$ [27], $[Et_2NH_2]_{10}[Hf^{IV}(\alpha\text{-}PW_{11}O_{39})_2]\cdot 2H_2O$ [28], and $[Et_2NH_2]_{10}[Zr^{IV}(\alpha\text{-}PW_{11}O_{39})_2]\cdot 7H_2O$ [28] (**Table 6-1)**. As shown in **Fig. 6-2(a)**, d(P···P) tends to increase with an increase in R_M due to lengthening of M–O bonds. **Fig. 6-2(b)** displays the correlation between d(P···P) and ϕ; the figure indicates that ϕ decreases as the two $[\alpha\text{-}PW_{11}O_{39}]^{7-}$ units approach each other. This behavior can reasonably be explained in terms of the repulsive interaction between O atoms in the $[\alpha\text{-}PW_{11}O_{39}]^{7-}$ units. **Fig. 6-3** schematically shows the $[M(\alpha\text{-}PW_{11}O_{39})_2]^{n-}$ molecule, in which the three short O···O contacts are denoted as $O_A\cdots O_{A'}$, $O_A\cdots O_{B'}$, and $O_{A'}\cdots O_B$. **Table 6-1** lists their distances – $d(O_A\cdots O_{A'})$, $d(O_A\cdots O_{B'})$, and $d(O_{A'}\cdots O_B)$ – of which $d(O_A\cdots O_{A'})$ is the shortest and decreases with decreasing d(P···P). For $[Hf^{IV}(\alpha\text{-}PW_{11}O_{39})_2]^{10-}$ polyanion containing the smallest Hf^{4+} (0.83 Å), the $d(O_A\cdots O_{A'})$ are short (2.77-2.93 Å) and about double of the ionic radius of O^{2-} ($1.35\times 2 = 2.70$ Å); this suggests a remarkable repulsion acting between the O_A and $O_{A'}$ atoms. **Fig. 6-3** describes how the approach of the $[\alpha\text{-}PW_{11}O_{39}]^{7-}$ units lowers ϕ through the $O_A\cdots O_{A'}$ repulsion, i.e. a decrease of R_M results in mutual approach of the $[\alpha\text{-}PW_{11}O_{39}]^{7-}$ units (**Fig. 6-2(a)**) and a remarkable repulsion between O_A and $O_{A'}$ atoms. This steric repulsion is reduced by the decrease of ϕ (**Fig. 6-2(b)**). Since the $[M(\alpha\text{-}PW_{11}O_{39})_2]^{n-}$ polyanions in these compounds are weakly hydrogen-bonded by alkylammonium cations and water molecules, it is suggested that their conformations are less influenced

by surroundings and follow mainly the repulsion within the molecule.

6-2-3 Tetramethylammonium(TMA^+)/Na^+-mixed salts of $[M(\alpha\text{-}PW_{11}O_{39})_2]^{n-}$

Fig. 6-4 shows the relation between structural parameters in $[Me_4N]_{5.5}Na_5H_{0.5}[Pr(\alpha\text{-}PW_{11}O_{39})_2]\cdot 21H_2O$, $[Me_4N]_{5.5}Na_5H_{0.5}[Eu(\alpha\text{-}PW_{11}O_{39})_2]\cdot 18H_2O$, $[Me_4N]_{5.5}Na_5H_{0.5}[Er(\alpha\text{-}PW_{11}O_{39})_2]\cdot 19H_2O$, and $[Me_4N]_{5.5}Na_3H_{2.5}[Y(\alpha\text{-}PW_{11}O_{39})_2]\cdot 22H_2O$, obtained in Chapter 3 and in published compounds, $[Me_4N]_4Na_3H_4[Pr(\alpha\text{-}PW_{11}O_{39})_2]\cdot 12H_2O$ [29] and $[Me_4N]_6Na_2(NH_4)_2[Ce(\alpha\text{-}PW_{11}O_{39})_2]\cdot 14H_2O$ [30] (**Table 6-2)**. As shown in **Fig. 6-4(a)**, d(P···P) tends to increase with an increase in R_M [25] due to lengthening of M–O bonds except for $[Me_4N]_6Na_2(NH_4)_2[Ce(\alpha\text{-}PW_{11}O_{39})_2]\cdot 14H_2O$ (**Na-Ce(IV)**). **Fig. 6-4(b)** displays the correlation between d(P···P) and ϕ, indicating that ϕ is considerably small and almost constant through d(P···P) except for **Na-Ce(IV)**. In contrast to the results of the pure alkylammonium salts, $d(O_A\cdots O_{A'})$ is large and almost invariable (3.21(2)–3.37(2) Å) throughout the compounds except for **Na-Ce(IV)** (**Table 6-1**). As shown in Chapter 3, the polyanions in **Pr-s**, **Eu-s**, **Er-s**, and **Y-s** are capped by Na^+ cations through the O_A and $O_{A'}$ atoms, forming $NaO_AO_{A'}O_{w4}$ octahedra. As a Na^+ cation generally tends to form a rigid NaO_6 octahedron, the constant $d(O_A\cdots O_{A'})$ may be due to this capping Na^+ cation, which seems to fix $d(O_A\cdots O_{A'})$ at relatively large values. This would result in the low and constant twist angle (ϕ) (**Table 6-2** and **Fig. 6-4(b)**). Note that the parameter in **Na-Ce(IV)** exceptionally deviates from this tendency. **Na-Ce(IV)** has no capping Na^+ linking the O_A and $O_{A'}$ atoms, instead, the polyanions are linked by Na^+ to form a *zigzag* chain running along the polyanion's longitudinal direction [30]. Such directional binding of Na^+ effectively elongates the distance between

$[\alpha\text{-}PW_{11}O_{39}]^{7-}$ units, as can be seen in the remarkably long d(P···P) (9.016(4) Å) (**Table 6-2**). In this case, the $O_A \cdots O_{A'}$ repulsion is reduced ($d(O_A \cdots O_{A'})$ = 3.480(4) Å), and ϕ is rather affected by the repulsion among all three O···O ($O_A \cdots O_{A'}$, $O_A \cdots O_{B'}$, and $O_{A'} \cdots O_B$) contacts. In fact, the three O···O contacts in **Na-Ce(IV)** are approximately equidistant (3.480(4)–3.539(6) Å) to minimize the overall O···O repulsion (**Table 6-2**).

6-2-4 Na^+/K^+-mixed salts of $[M(\alpha\text{-}PW_{11}O_{39})_2]^{n-}$ hydrogen-bonded by proline molecules

Fig. 6-5 shows the relation between selected geometric parameters of $K_{1.3}Na_{3.2}H_{6.5}[Ln(\alpha\text{-}PW_{11}O_{39})_2]\cdot 8.3(L\text{-/D-}C_5H_9NO_2)\cdot xH_2O$ (Ln = Pr, Nd, Sm, Gd, Tb, Dy, Er, Tm, Yb, and Y), and $K_{1.2}Na_2H_{7.8}[Ln(\alpha\text{-}PW_{11}O_{39})_2]\cdot 8.5(L\text{-}C_5H_9NO_2)\cdot xH_2O$ (Ln = La, Eu) analyzed in Chapter 4 (**Table 6-3)**. As shown in **Fig. 6-5(a)**, d(P···P) tends to increase with an increase in R_M due to lengthening of M–O bonds, which are similar to the tendency in alkylammonium and TMA^+/Na^+-mixed salts (**Figs. 6-2(a)** and **6-4(a)**). **Fig. 6-5(b)** displays the correlation between d(P···P) and ϕ, indicating that ϕ seems to have no correlation with d(P···P). This behavior can reasonably be explained when we consider the local structure of the polyanion. As stated in 4-3-4-1, there are two proline molecules around the LnO_8 center to form a complex like $[L\text{-/D-}Ln(\alpha\text{-}PW_{11}O_{39})_2]^{11-}\text{-}(L\text{-/D-proline})_2$ by hydrogen-bonding with stereoselective contacts between the surfaces of 'grooves' in the polyanion and proline molecules (see **Fig. 4-7** in Chapter 4). Four hydrogen-bondings from N atoms in proline to O atoms in LnO_8 stabilize the SA conformation and contribute to the chiral isolation. These proline molecules seem to prescribe ϕ rather than the Ln^{3+} species (**Table 6-3** and **Fig. 6-5**). Contribution of the $O_A \cdots O_{A'}$ repulsion in this series would be smaller because the

proline molecules fix ϕ at low value (34.5(1)-36.0(2)º), and this causes relatively large $d(O_A \cdots O_{A'})$ values (2.87(4)-3.063(2) Å) with a weak R_M dependence (**Table 6-3**).

6-2-5 Developmental application to the K^+ salts of $[Ln(\beta_2\text{-}SiW_{11}O_{39})_2]^{13-}$

As discussed above, intramolecular O···O repulsion between the $[\alpha\text{-}PW_{11}O_{39}]^{7-}$ units contributes to the twist angle (ϕ) in pure alkylammonium salts of $[M(\alpha\text{-}PW_{11}O_{39})_2]^{n-}$. Here, similar analysis is attempted for the compounds $K_{13}[Ln^{III}(\beta_2\text{-}SiW_{11}O_{39})_2]\cdot xH_2O$ (Ln = La, Ce, Sm, Eu, Gd, Tb, Er, Tm, Yb, and Lu), where the mono-lacunary $[\beta_2\text{-}SiW_{11}O_{39}]^{8-}$ is derived from $[\beta\text{-}SiW_{12}O_{40}]^{4-}$ by removing a WO_4 unit from the belt position. Although Coronado [22] and Kortz [24] have reported the geometric effect of R_M in $[Ln^{III}(\beta_2\text{-}SiW_{11}O_{39})_2]^{13-}$, they could not elucidate what controls ϕ. Note that ϕ (Kortz used the notation θ instead of ϕ) has been prescribed by different criteria [24] because $[\beta_2\text{-}SiW_{11}O_{39}]^{8-}$ is originally a chiral unit with no mirror plane. The geometric parameters for the $[Ln^{III}(\beta_2\text{-}SiW_{11}O_{39})_2]^{13-}$ polyanions are collected in **Table 6-4**. It should be noted that, in these compounds, there are K-O bonding between K^+ cations and a polyanion, which may cause unexpected distortions. However, unlike the anisotropic attachment of Na^+ in **Na-Ce(IV)**, the many K^+ cations surrounding a polyanion provide rather isotropic interaction that would cause only a small distortions. The decrease in ionic radius of Ln^{3+} (R_{Ln}) results in the reduction of Si···Si distance **(Fig. 6-6(a))**, i.e., the approach of the two $[\beta_2\text{-}SiW_{11}O_{39}]^{8-}$ units which is similar to $[M(\alpha\text{-}PW_{11}O_{39})]^{n-}$. However, ϕ has been reported to increase from 39.9° to 47.6° with decreasing d(Si···Si) owing to the decrease of R_{Ln}. (**Fig. 6-6(b)**) [22, 24], which seems antithetical to the R_M-ϕ relationship observed for $[M(\alpha\text{-}PW_{11}O_{39})_2]^{n-}$ (**Figs. 6-2(b)**, **6-4(b)** and **Tables 6-1** and **6-2**). Unlike $[M(\alpha\text{-}PW_{11}O_{39})_2]^{n-}$, the

$[Ln^{III}(\beta_2\text{-}SiW_{11}O_{39})_2]^{13-}$ polyanion has the two nearest intramolecular O···O contacts (< 4 Å) of O···O(A) and O···O(B) between the $[\beta_2\text{-}SiW_{11}O_{39}]^{8-}$ units (**Fig. 6-7**). The approach of the two $[\beta_2\text{-}SiW_{11}O_{39}]^{8-}$ units enhances O···O repulsion and induces relative rotation of the $[\beta_2\text{-}SiW_{11}O_{39}]^{8-}$ units in a ϕ-decreasing manner. Though these distances are relatively long, the existence of two different interactions would double the repulsion energy per a polyanion. Owing to the chirality in the $[\beta_2\text{-}SiW_{11}O_{39}]^{8-}$ unit, there are two diastereomers in $[Ln^{III}(\beta_2\text{-}SiW_{11}O_{39})_2]^{13-}$, namely, RR (or SS) and RS (or SR). It has been also reported that the decrease in R_{Ln} results in the gradual isomerization of the polyanion from RR (or SS) to RS (or SR) configurations for Ln = La-Ce and Er-Lu, respectively; there is also an intermediate mixture (disordering) region for Ln = Sm-Tb. The O···O(A) and O···O(B) distances are also plotted in **Fig. 6-7**, where O···O(A) is nearly constant throughout R_{Ln}, while the O···O(B) distance reduces with decreasing R_{Ln} but exhibits a significant increase in the Ln = Er-Lu region that corresponds to the RS (or SR) configuration. The lengthening of O···O(B) for RS (or SR) (**Fig. 6-8**) is caused by a structural change in one of the two $[\beta_2\text{-}SiW_{11}O_{39}]^{8-}$ moieties. The edge-sharing mode of the W_3O_{13} triad related to O···O(B) in the RR (or SS) anion (shaded polyhedra in **Fig. 6-8**) is changed to corner-sharing in the RS (or SR) anion (unshaded polyhedra in **Fig. 6-8**) through the edge/corner-disordering state (**Fig. 6-8)**. In other words, the $[Ln^{III}(\beta_2\text{-}SiW_{11}O_{39})_2]^{13-}$ polyanion with small R_{Ln} favors the RS (or SR) configuration to avoid repulsion acting on the O···O(B) contact.

6-2-6 Comparison of the molecular conformation for $[M(\alpha\text{-}PW_{11}O_{39})_2]^{n-}$ in cationic environment and co-existing materials

All of the above results are summarized in **Fig. 6-9**. As shown **Fig. 6-9(a)**, the

d(P···P) tends to increase with an increase in R_M for all series of the $[M(\alpha\text{-}PW_{11}O_{39})]^{n-}$ compounds irrespective to the cationic species and co-existing materials. This tendency indicates that the structural parameter *d*(P···P) is effectively ruled by the R_M due to the lanthanide contraction. On the other hand, the plots of *d*(P···P) vs. ϕ gave the two tendencies (**Fig. 6-9(b)**). For the pure alkylammonium salts, the ϕ decreases as the reduction of *d*(P···P) because of the $O_A \cdots O_{A'}$ steric repulsion produced by approaching of $[\alpha\text{-}PW_{11}O_{39}]^{7-}$ units. For the TMA^+/Na^+-mixed salts and Na^+/K^+-mixed salts containing proline, ϕ is low and almost constant or has no correlation with respect to *d*(P···P). This observation is attributable to the fixation of ϕ at small values by attachments of Na^+ and proline molecules to the $[\alpha\text{-}PW_{11}O_{39}]^{7-}$ units via Na–O and hydrogen-bonding, respectively (**Fig. 6-10**). Such external anisotropic forces are stronger than the isotropic hydrogen-bonding in pure alkylammonium cations, and precede the $O_A \cdots O_{A'}$ steric repulsion. In fact, the Na^+ linkage and proline insertion to the polyanions influence not only on ϕ but also on molecular bending. As shown in **Fig. 6-10**, the ∠P-Ln-P angle (φ) decreases as 167.9º and 161.7º, and 157.2º in the sequence of pure alkylammonium salts, TMA^+/Na^+-mixed salts, and Na^+/K^+-mixed salts crystallized with proline, respectively. The smaller φ in **Fig. 6-10(b)** can be interpreted by the strong Na-O bonding, while the smallest φ in **Fig. 6-10(c)** by insertion of the two proline molecules in the groove of the polyanion. In the latter case, other O···O interactions (with distances of 3.65(2) and 3.54(2) Å as represented by the light-blue broken lines in **Fig. 6-10(c)**) between the carboxylate O and polyanion's terminal may contribute to the distortion.

The plots of ϕ vs. φ is also shown in **Fig. 6-11(a)**. For the TMA^+/Na^+- and Na^+/K^+-mixed salts, both ϕ and φ are almost constant due to the immobilized

$[\alpha\text{-}PW_{11}O_{39}]^{7-}$ units by Na-O bonding and proline insertion, respectively. On the other hand, ϕ tends to decrease with a decrease of φ for the pure alkylammonium salts. This observation indicates that $[\alpha\text{-}PW_{11}O_{39}]^{7-}$ units are not effectively fixed by weak hydrogen-bonding involving alkylammonium cations and waters of crystallization.

Here, a geometrical relationship between ϕ and φ is estimated using a simple $[\alpha\text{-}PW_{11}O_{39}]^{7-}$-rotation model (**Fig. 6-11(b)**). The polyanion $[Ce^{III}(PW_{11}O_{39})_2]^{11-}$ with the cubic-coordinated CeO_8 center found in Chapter 3 is used as the starting model, which has the ideal geometry of ϕ = 180º and φ = 180º. The rotation axis of the $[\alpha\text{-}PW_{11}O_{39}]^{7-}$ unit is defined so that it passes through the Ce atom and is normal to the O_4-square plane of the CeO_8 center. In this case, the angle between the Ce···P vector and rotation axis was measured to be 8.52º. When ϕ is reduced from 180º to 0º, φ is also reduced from 180º to 162.96º according to an equation $\varphi = \cos^{-1}[-(a^2\cos\phi + b^2)]$ (a^2, b^2 = constant), which is drawn with a curve in **Fig. 6-11(c)**. This reveals that, in the range of *c.a.* 30º<ϕ<45º considered for the SA coordination, φ should exhibit only a small variation, from 163.5º to 164.3º. Thus, ϕ is not dominant to φ, when taking only the rotation effect of the $[\alpha\text{-}PW_{11}O_{39}]^{7-}$ units into account. Still, the plots for the pure alkylammonium salts have a remarkably wider range 159.1º<φ<167.93º (red plots in **Fig. 6-11**). This is attributable to both intrinsic and extrinsic factors acting to the flexible conformation of the pure alkylammonium salts. In summary, φ as well as ϕ is the geometrical parameter greatly affected by R_{Ln}, cationic environment, and interacting molecules, being almost independent on the rotation effect of $[\alpha\text{-}PW_{11}O_{39}]^{7-}$.

Again, these results demonstrate the rigidity of the $[\alpha\text{-}PW_{11}O_{39}]^{7-}$ unit and flexibility of the LnO_8 coordination. Such molecular bending would give a small effect on the $O_A\cdots O_{A'}$ contacts, and we cannot evaluate it irrespectively to other geometric

parameters.

6-3 Structural evaluation of the sandwich-type $[M(\alpha_2\text{-}P_2W_{17}O_{61})_2]^{n-}$ polyanion

For the sandwich-type Ln-POM coordinated by two mono-lacunary Wells-Dawson units, $[Ln(\alpha_1\text{-}P_2W_{17}O_{61})_2]^{n-}$ (α_1-α_1 type), $[Ln(\alpha_2\text{-}P_2W_{17}O_{61})_2]^{n-}$ (α_2-α_2 type), and $[Ln(\alpha_1\text{-}P_2W_{17}O_{61})(\alpha_2\text{-}P_2W_{17}O_{61})]^{n-}$ (α_1-α_2 type) have been isolated and structurally characterized as stated in 1-3-2-2. The expectation of coordination mode of Ln^{3+} in the $[Ln(\alpha_2\text{-}P_2W_{17}O_{61})_2]^{n-}$ polyanion has only been provided to adopt cubic and SA coordination in aqueous solution by ^{183}W-NMR spectroscopy like the $[Ln(\alpha\text{-}PW_{11}O_{39})_2]^{n-}$ polyanions [23]. However, all the isolated $[Ln(\alpha_2\text{-}P_2W_{17}O_{61})_2]^{n-}$ polyanion in the solid state held Ln^{3+} in a SA coordination environment. There are originally four examples of $[M(\alpha_2\text{-}P_2W_{17}O_{61})_2]^{n-}$ [28, 31, 32] which had been structurally characterized by single crystal X-ray diffraction analysis, but together with the successfully analyzed polyanions in Chapter 5, geometric variation over the Ln series has become possible. In this section, the molecular conformation of the $[M(\alpha_2\text{-}P_2W_{17}O_{61})_2]^{n-}$ polyanion coordinated by two mono-lacunary Wells-Dawson $[\alpha_2\text{-}P_2W_{17}O_{61}]^{10-}$ units will be discussed by using the similar structural parameters as $[M(\alpha\text{-}PW_{11}O_{39})_2]^{n-}$ polyanion.

6-3-1 Definition of the structural parameters

The $[\alpha_2\text{-}P_2W_{17}O_{61}]^{10-}$ unit has an ideal symmetry of C_s. The mirror plane (*m*) which halves the $[\alpha_2\text{-}P_2W_{17}O_{61}]^{10-}$ unit in $[M(\alpha_2\text{-}P_2W_{17}O_{61})_2]^{n-}$ prescribed by the least-squares plane defined by M, one of the seventeen W, two P atoms, and eleven bridging O atoms. These atoms correspond to [M, W(1), P(1, 2), O(1, 2, 3, 4, 5, 6, 7, 8, 9, 10, 11)] and [M,

W(2), P(3, 4), O(12, 13, 14, 15, 16, 17, 18, 19, 20, 21, 22)] sets for the polyanions (**Fig. 6-12**). The dihedral angle between the two least-squares planes defines the twist angle (ϕ). The geometric parameters for structural characterized $[M(\alpha_2\text{-}P_2W_{17}O_{61})_2]^{n-}$ polyanions are collected in **Tables 6-5**, which includes the ionic radius of M (R_M) [25], twist angle (ϕ), three O···O contacts ($O_A\cdots O_{A'}$, $O_A\cdots O_{B'}$, and $O_{A'}\cdots O_B$) and P···P distance (*d*(P1···P3)). Since the local structure around the LnO_8 center is identical to that in $[M(\alpha\text{-}PW_{11}O_{39})]^{n-}$, the definitions of $O_A\cdots O_{A'}$, $O_A\cdots O_{B'}$, and $O_{A'}\cdots O_B$ described in **Fig. 6-14** are similar to those in **Fig. 6-3**. Therefore, the O···O contacts can be used for an index to understand the steric repulsion between the two mono-lacunary Wells-Dawson units, and the *d*(P1···P3) parameter describes the degree of separation between the two $[\alpha_2\text{-}P_2W_{17}O_{61}]^{10-}$ units.

6-3-2 Application to the K^+ salts of $[M(\alpha_2\text{-}P_2W_{17}O_{61})_2]^{n-}$

Fig. 6-13 shows the relation between selected parameters of $K_{12}H_5[Ln(\alpha_2\text{-}P_2W_{17}O_{61})_2]\cdot 2(L\text{-}/D\text{-}C_5H_9NO_2)\cdot xH_2O$ (Ln = La, Eu, Gd, Tb, Dy, Er, Yb) described in Chapter 5 and $K_{16}H[Yb(\alpha_2\text{-}P_2W_{17}O_{61})_2]\cdot 44H_2O$ [31], $K_{17}[Lu(\alpha_2\text{-}P_2W_{17}O_{61})_2]$ [32], $K_{16}[Hf(\alpha_2\text{-}P_2W_{17}O_{61})_2]\cdot 19H_2O$ [28], and $K_{15}H[Zr(\alpha_2\text{-}P_2W_{17}O_{61})_2]\cdot 25H_2O$ [28] listed in **Table 6-5**. As shown in **Fig. 6-13(a)**, *d*(P1···P3) tends to increase with an increase in R_M due to lengthening of M-O bonds, which are similar to the corresponding relationship observed for the $[M(\alpha\text{-}PW_{11}O_{39})_2]^{n-}$ in section 6-2. **Fig. 6-13(b)** displays the correlation between *d*(P1···P3) and ϕ. The chiral crystals of compounds described in Chapter 5 exhibit low and nearly constant ϕ values (40.1(2)-40.3(3)°) irrespective to *d*(P1···P3), whereas the other racemate compounds show positive correlation with *d*(P1···P3). **Fig. 6-14** schematically shows the

$[M(\alpha_2\text{-}P_2W_{17}O_{61})_2]^{n-}$ molecule. Of the three short O···O contacts, $d(O_A\cdots O_{A'})$ is the shortest and decreases with decreasing d(P1···P3) (**Table 6-5**). For the chiral crystals, their behavior can be interpreted similarly to the Na^+/K^+-mixed chiral crystals of $[M(\alpha\text{-}PW_{11}O_{39})]^{n-}$ shown in the section 6-2-4. As shown in Chapter 5, there are also two proline molecules around the $[Ln(\alpha_2\text{-}P_2W_{17}O_{61})_2]^{17-}$ polyanion to form a $[Ln(\alpha_2\text{-}P_2W_{17}O_{61})_2]^{17-}$-$(proline)_2$ complex through O···H–N hydrogen-bonding. This complexation seems to stabilize the SA conformation and induce the chirality. Such two adjacent proline molecules fixed the $[\alpha_2\text{-}P_2W_{17}O_{61}]^{10-}$ position resulting in the relatively low and constant ϕ value. On the other hand, the tendency for the racemate crystals, although few cases, is consistent with that of alkylammonium salts of $[M(\alpha\text{-}PW_{11}O_{39})]^{n-}$. In the racemate crystals of $K_{16}H[Yb(\alpha_2\text{-}P_2W_{17}O_{61})_2]\cdot 44H_2O$, $K_{17}[Lu(\alpha_2\text{-}P_2W_{17}O_{61})_2]$, $K_{16}[Hf(\alpha_2\text{-}P_2W_{17}O_{61})_2]\cdot 19H_2O$, and $K_{15}H[Zr(\alpha_2\text{-}P_2W_{17}O_{61})_2]\cdot 25H_2O$, more than 50 K^+ cations are arranged around the $[M(\alpha_2\text{-}P_2W_{17}O_{61})_2]^{n-}$ polyanion, of which some are coordinating to the polyanion's O atoms. Such large number of K^+ cations would produce approximately an isotropic cationic potential to the polyanion, the geometry of which allows to an internal steric effect, i.e. the repulsion between the $O_A\cdots O_{A'}$ contact. **Fig. 6-14** shows the mechanism of how the decrease of d(P1···P3) results in the decrease of ϕ; the reduction of R_M results in the approach of $[\alpha_2\text{-}P_2W_{17}O_{61}]^{10-}$ units, and the enhanced steric repulsion acting between $O_A\cdots O_{A'}$ atoms makes ϕ small. This is similar to the mechanism in the pure alkylammonium salts of $[M(\alpha\text{-}PW_{11}O_{39})]^{n-}$ (**Fig. 6-3**).

6-4 Conclusion

The clear correlation between the ionic radius of the central metal (M) and twist angle of the two mono-lacunary $[\alpha\text{-}PW_{11}O_{39}]^{7-}$ and $[\alpha_2\text{-}P_2W_{17}O_{61}]^{10-}$ units was studied

for a series of $[M(\alpha\text{-}PW_{11}O_{39})_2]^{n-}$ and $[M(\alpha_2\text{-}P_2W_{17}O_{61})_2]^{n-}$ polyanion and could be explained in terms of not only steric repulsion of between O atoms in the mono-lacuanry units but also the molecular environment around the polyanion such as cation arrangement and co-existing materials. To discuss on the stable molecular geometries taking into account such intra- and intermolecular interactions, theoretical approaches based on quantum mechanics would be required. However, complete *ab initio* calculations of molecular scales of $[M(\alpha\text{-}PW_{11}O_{39})_2]^{n-}$ and $[M(\alpha_2\text{-}P_2W_{17}O_{61})_2]^{n-}$ and their cationic surroundings are still difficult.

6-5 References

[1] B. S. Bassil, M. H. Dickman, I. Rőmer, B. kammer, U. Kortz, *Angew. Chem. Int. ed.*, **46**, 6192 (2007).

[2] H. Naruke, T. Yamase, *Acta Crystallogr.*, **C52**, 2655, (1996).

[3] R. D. Peacock, T. J. R. Weakley, *J. Chem. Soc.*, **A**, 1836 (1971).

[4] K. Wassermann, M. H. Dickman, M. T. Pope, *Angew. Chem. Int. ed.*, **39**, 2914 (1997).

[5] K. Fukaya, T. Yamase, *Angew. Chem. Int. ed.*, **42**, 654 (2003).

[6] G. Xue, B. Lin, W. Wang, Q. Li, H. Li, *Hua Hsueh Hsueh Pao*, **60**, 2022 (2002).

[7] C. Rosu, T. J. R. Weakley, *Acta Crystallogr.*, **C54**, 2 (1998).

[8] T. Ozeki, T. Yamase, *Acta Crystallogr.*, **B50**, 128, (1994).

[9] M. Sugeta, T. Yamase, *Bull. Chem. Soc. Jpn.*, **66**, 444 (1993).

[10] M. A. AlDamen, S. Cardona-Serra, J. M. Clemente-Juan, E. Coronado, A. Gaita-Ariño, C. Martí-Gastaldo, F. Luis, O. Montero, *Inorg. Chem.*, **48**, 3467 (2009).

[11] C. Zhang, R. C. Howell, K. B. Scotland, F. G. Perez, L. Todaro, L. C. Francesconi, *Inorg. Chem.,* **43**, 7691 (2004).

[12] L. Fan, L. Xu, C. Zhang, F. Li, Z. Li, X. Liu, Structural Chemistry, **18**, 917 (2007).

[13] Y. H. Liu, G. L. guo, J. P. Wang, *J. Coord. Chem.*, **61**, 2428 (2008).

[14] R. Copping, A. J. Gaunt, I. May, M. J. Sarsfield, D. Collison, M. Helliwell, I. S. Denniss, D. C. Apperley, *Dalton Trans.,* 1256 (2005).

[15] R.-Q. Sun, H.-H Zhang, S.-L. Zhao, C.-C. Huang, X.-L. Zheng, *Jiegon Huaxue,* **20**, 413 (2001).

[16] P. Mialane, A. Dovecq, E. Riviere, J. Marrot, F. Secheresse, *Eur. J. Inorg. Chem.*, 33, 33 (2004).

[17] Y.-K. Shan, Z.-X. Liu, Z.-S. Jin, G.-C. Wei, Y.-S. Liu, E.-B. Wang, *Science in China.* B34, 513 (1991).

[18] Y.-K. Shan, Z.-X. Liu, E.-B. Wang, Z.-S. Jin, G.-C. Wei, Y.-S. Liu, *Jiegon Huaxue*, **9** 159 (1990).

[19] N. Jian, L. Xu, F. Li, G. Gao, L. Fan, *Inorg. Chem. Comm.,* **11**, 24 (2008).

[20] Y.-K. Shan, Z.-X. Liu, Z.-S. Jin, G.-C. Wei, *Hua Hsueh Hsueh Pao*, **50**, 357 (1992).

[21] M. A. Fedotov, B. Z. Pertsikov, D. K. Danovich, *Polyhedron*, **9**, 1249 (1990).

[22] R. Copping, L. Jonasson, A. J. Gaunt, D. Drennan, D. Collison, M. Helliwell, R. J. Pirttijarvi, C. J. Jones, A. Huguet, D. C. Apperley, N. Kaltsoyannis, I. May, *Inorg. Chem.,* **47**, 5787 (2008).

[23] J. Bartis, S. Sukal, M. Dankova, E. Kraft, R. Kronzon, M. Blumenstein, L. C. Francesconi, *J. Chem. Soc., Dalton Trans.*, 1937 (1997).

[24] B. S. Bassil, M. H. Dickman, B. Kammer, U. Kortz, *Inorg. Chem.*, **46**, 2452 (2007).

[25] R. D. Shannon, *Acta Crystallogr.*, **A32**, 751 (1976).

[26] Y. Hou, X. Fang, C.L. Hill, *Chem. Eur. J.*, **13**, 9442 (2007).

[27] L. Cai, Y. Li, C. Yu, H. Ji, Y. Liu, S. Liu, *Inorg. Chim. Acta*, **362** 2895 (2009).

[28] C. N. Kato, A. Shinohara, K. Hayashi, K. Nomiya, *Inorg. Chem.*, **45**, 8108 (2006).

[29] L. Fan, L. Xu, C. Zhang, F. Li, Z. Li, X. Liu, *Struct. Chem.*, **18**, 917 (2007).

[30] L. Fan, L. Xu, G. Gao, F. Li, Y. Qiu, *Inorg. Chem. Commun.*, **9** 1308 (2006).

[31] J.-Y. Niu, J. Zhao, D. Guo, J.-P. Wang, *J. Mol. Struct.*, **692**, 223 (2004).

[32] Q., Luo, R. C. Howell, M. Dankova, J. Bartis, C. W. Williams, J. Horrocks, W. Dew, J. V. G. Young, A. L. Rheingold, L. C. Francesconi, M. R. Antonio, *Inorg. Chem.*, **40**, 1894, (2001).

Table 6-1. Comparison of the structural parameters for the pure alkylammonium salts of the $[M(\alpha\text{-}PW_{11}O_{39})_2]^{n-}$.

M in $[M(\alpha\text{-}PW_{11}O_{39})_2]^{n-}$	Cation	R_M [Å][a]	d (P···P) [Å][b]	d (O_A···$O_{A'}$) [Å][c]	d (O_A···O_B) [Å][c]	d ($O_{A'}$···O_B) [Å][c]	[deg][d]	ref
Ce(**III**)	$[Me_2NH_2]^+$	1.143	9.067(6)	3.286(9)	4.501(9)	4.561(8)	42.9(1)	Chapter2
Ce(**IV**)	$[Me_2NH_2]^+$	0.97	8.743(8)	2.923(7)	3.747(7)	3.723(4)	40.2(2)	Chapter2
Hf(**IV**)	$[Me_2NH_2]^+$	0.83	8.511(4)	2.772(2)	3.200(2)	3.200(2)	37.5(1)	26
Zr(**IV**)-R	$[Me_2NH_2]^+$	0.84	8.558(2)	2.862(5)	3.284(6)	2.394(4)	38.1(3)	27
Zr(**IV**)-L	$[Me_2NH_2]^+$	0.84	8.550(9)	2.855(7)	3.315(9)	3.302(7)	37.8(2)	27
Hf(**IV**)-1	$[Et_2NH_2]^+$	0.83	8.514(1)	2.931(7)	3.137(9)	3.127(6)	35.9(2)	28
Hf(**IV**)-2	$[Et_2NH_2]^+$	0.83	8.595(9)	2.909(4)	3.423(3)	3.304(8)	38.2(2)	28
Zr(**IV**)-1	$[Et_2NH_2]^+$	0.84	8.558(5)	2.935(1)	3.253(0)	3.047(8)	35.9(3)	28
Zr(**IV**)-2	$[Et_2NH_2]^+$	0.84	8.612(1)	2.914(0)	3.268(4)	3.429(0)	37.9(2)	28

[a] R_M: ionic radius of M from ref [25].
[b] d(P···P): distance between P atoms belonging to two mono-lacunary Keggin units.
[c] d(O_A···$O_{A'}$), d(O_A···$O_{B'}$), d($O_{A'}$···O_B): distances between terminal O atoms represented in **Fig. 6-3**.
[d] ϕ: twist angle between the two mirror planes of mono-lacunary Keggin units.

Table 6-2. Comparison of the structural parameters for the TMA^+/Na^+-mixed salts of the $[M(\alpha\text{-}PW_{11}O_{39})_2]^{n-}$.

M in $[M(\alpha\text{-}PW_{11}O_{39})_2]^{n-}$	Cation	R_M [Å][a]	d(P···P) [Å][b]	d(O_A···$O_{A'}$) [Å][c]	d(O_A···$O_{B'}$) [Å][c]	d($O_{A'}$···O_B) [Å][c]	[deg][d]	ref
Pr(III)	Na^+, $[Me_4N]^+$, H^+	1.126	8.939(4)	3.40(2)	3.51(2)	3.51(2)	33.4(2)	29
Pr(III)-s	Na^+, $[Me_4N]^+$, H^+	1.126	8.986(4)	3.37(2)	3.62(2)	3.62(2)	33.4(2)	Chapter3
Eu(III)-s	Na^+, $[Me_4N]^+$, H^+	1.066	8.908(6)	3.34(2)	3.52(2)	3.52(2)	33.4(2)	Chapter3
Y(III)-s	Na^+, $[Me_4N]^+$, H^+	1.019	8.851(5)	3.21(2)	3.43(2)	3.43(2)	33.4(2)	Chapter3
Er(III)-s	Na^+, $[Me_4N]^+$, H^+	1.004	8.828(5)	3.25(2)	3.41(2)	3.41(2)	33.3(2)	Chapter3
Ce(**IV**)	Na^+, $[Me_4N]^+$, NH_4^+	0.97	9.016(4)	3.480(4)	3.539(6)	3.539(6)	32.1(1)	30

[a] R_M: ionic radius of M from ref [25].
[b] d(P···P): distance between P atoms belonging to two mono-lacunary Keggin units.
[c] d(O_A···$O_{A'}$), d(O_A···$O_{B'}$), d($O_{A'}$···O_B): distances between terminal O atoms represented in **Fig. 6-3**.
[d] ϕ: twist angle between the two mirror planes of mono-lacunary Keggin units.

Table 6-3. Comparison of the structural parameters for the chiral Na^+/K^+-mixed salts of the $[M(\alpha\text{-}PW_{11}O_{39})_2]^{n-}$.

M in $[M(\alpha\text{-}PW_{11}O_{39})_2]^{n-}$	Cation	R_M [Å][a]	d (P···P) [Å][b]	d (O_A···$O_{A'}$) [Å][c]	d (O_A···O_B) [Å][c]	d ($O_{A'}$···O_B) [Å][c]	[deg][d]	ref
La(III)-L	Na^+, K^+, H^+	1.160	8.91(2)	3.063(2)	3.543(2)	3.437(9)	36.0(2)	Chapter4
Pr(III)-L	Na^+, K^+, H^+	1.126	8.862(6)	3.00(2)	3.43(3)	3.48(2)	34.9(2)	Chapter4
Pr(III)-D	Na^+, K^+, H^+	1.126	8.851(6)	3.02(2)	3.40(2)	3.44(2)	34.5(1)	Chapter4
Nd(III)-L	Na^+, K^+, H^+	1.109	8.827(7)	3.02(2)	3.41(2)	3.45(2)	34.8(1)	Chapter4
Sm(III)-L	Na^+, K^+, H^+	1.079	8.798(6)	2.98(3)	3.39(3)	3.46(3)	35.0(1)	Chapter4
Eu(III)-L	Na^+, K^+, H^+	1.066	8.77(2)	2.983(1)	3.353(9)	3.400(1)	35.1(2)	Chapter4
Gd(III)-L	Na^+, K^+, H^+	1.053	8.780(9)	2.96(3)	3.39(2)	3.41(3)	36.0(2)	Chapter4
Tb(III)-L	Na^+, K^+, H^+	1.040	8.797(8)	2.96(3)	3.34(3)	3.42(3)	35.2(2)	Chapter4
Dy(III)-L	Na^+, K^+, H^+	1.027	8.77(1)	2.87(4)	3.38(4)	3.40(4)	35.0(3)	Chapter4
Y(III)-L	Na^+, K^+, H^+	1.019	8.731(7)	2.92(3)	3.34(3)	3.38(3)	35.2(1)	Chapter4
Er(III)-L	Na^+, K^+, H^+	1.004	8.731(8)	2.96(3)	3.32(3)	3.33(3)	35.5(1)	Chapter4
Er(III)-D	Na^+, K^+, H^+	1.004	8.724(7)	2.88(2)	3.37(2)	3.36(2)	34.7(1)	Chapter4
Tm(III)-L	Na^+, K^+, H^+	0.994	8.711(6)	2.89(2)	3.31(3)	3.30(2)	34.7(1)	Chapter4
Yb(III)-L	Na^+, K^+, H^+	0.985	8.735(6)	2.93(2)	3.33(2)	3.40(2)	34.9(1)	Chapter4

[a] R_M: ionic radius of M from ref [25].
[b] d(P···P): distance between P atoms belonging to two mono-lacunary Keggin units.
[c] d(O_A···$O_{A'}$), d(O_A···$O_{B'}$), d($O_{A'}$···O_B): distances between terminal O atoms represented in **Fig. 6-3**.
[d] ϕ: twist angle between the two mirror planes of mono-lacunary Keggin units.

Table 6-4. Comparison of the structural parameters for the K^+ salts of the $[Ln(\beta_2\text{-}SiW_{11}O_{39})_2]^{13-}$.

Ln in $[Ln(\beta_2\text{-}SiW_{11}O_{39})_2]^{13-}$	Cation	R_M [Å][a]	*d* (Si…Si) [Å][b]	*d* (O…O(A) [Å][c]	*d* (O…O(B)) [Å][c]	[deg][d]	ref
La(III)	K^+, H^+	1.160	8.976(6)	3.17(2)	3.56(2)	39.9	24
Ce(III)	K^+, H^+	1.143	8.930(9)	3.53(3)	3.11(3)	40.8	24
Sm(III)	K^+, H^+	1.079	8.874(9)	3.08(3)	3.42(3)	41.3	24
Eu(III)	K^+, H^+	1.066	8.870(7)	3.09(2)	3.46(2)	44.4	24
Gd(III)	K^+, H^+	1.053	8.834(9)	3.17(3)	3.36(3)	42.9	24
Tb(III)	K^+, H^+	1.040	8.831(7)	3.07(3)	3.43(3)	44.6	24
Er(III)	K^+, H^+	1.004	8.757(10)	3.03(3)	3.80(3)	47.5	22
Tm(III)	K^+, H^+	0.994	8.728(10)	3.05(3)	3.69(3)	48.0	22
Yb(III)	K^+, H^+	0.985	8.810(10)	3.21(3)	3.96(3)	48.3	24
Lu(III)	K^+, H^+	0.977	8.792(10)	3.18(3)	3.98(3)	47.6	24

[a] R_M: ionic radius of M from ref [25].
[b] *d*(Si···Si): distance between Si atoms belonging to two mono-lacunary Keggin units.
[c] *d*(O···O(A)), *d*(O···O(B)): distances between terminal O atoms represented in **Fig. 6-7**.
[d] ϕ: twist angle between the two mirror planes of mono-lacunary Keggin units.

Table 6-5. Comparison of the structural parameters for the K^+ salts of the $[M(\alpha_2\text{-}P_2W_{17}O_{61})_2]^{n-}$.

M in $[M(\alpha_2\text{-}P_2W_{17}O_{61})_2]^{n-}$	Cation	R_M [Å][a]	d (P1···P3) [Å][b]	d (O_A···$O_{A'}$) [Å][c]	d (O_A···$O_{B'}$) [Å][c]	d ($O_{A'}$···O_B) [Å][c]	[deg][d]	ref
La(III)-L	K^+, H^+	1.160	8.925(4)	2.936(14)	3.814(13)	3.814(13)	40.3(3)	Chapter5
Eu(III)-L	K^+, H^+	1.066	8.810(4)	2.857(12)	3.687(12)	3.687(12)	40.1(3)	Chapter5
Gd(III)-L	K^+, H^+	1.053	8.817(4)	2.846(12)	3.666(12)	3.666(12)	40.1(3)	Chapter5
Tb(III)-L	K^+, H^+	1.040	8.806(6)	2.90(2)	3.67(2)	3.67(2)	40.2(4)	Chapter5
Dy(III)-L	K^+, H^+	1.027	8.797(4)	2.856(14)	3.644(12)	3.644(12)	40.2(3)	Chapter5
Er(III)-L	K^+, H^+	1.004	8.775(3)	2.825(10)	3.591(10)	3.591(10)	40.1(2)	Chapter5
Er(III)-D	K^+, H^+	1.004	8.779(4)	2.818(12)	3.594(12)	3.594(12)	40.2(3)	Chapter5
Yb(III)-L	K^+, H^+	0.985	8.754(4)	2.810(14)	3.556(13)	3.556(13)	40.2(3)	Chapter5
Yb(III)	K^+, H^+	0.985	8.705(7)	2.89(2)	3.675(15)	3.470(14)	42.1(5)	31
Lu(III)	K^+, H^+	0.977	8.699(7)	2.87(2)	3.44(2)	3.59(2)	41.8(5)	32
Hf(IV)	K^+, H^+	0.830	8.555(6)	2.76(2)	3.38(2)	3.38(2)	40.7(4)	28
Zr(IV)	K^+, H^+	0.840	8.563(4)	2.787(13)	3.363(12)	3.363(12)	40.6(3)	28

[a] R_M: ionic radius of M from ref [25].
[b] d(P···P): distance between P atoms closest to the substitution site belonging to two mono-lacunary Wells-Dawson units.
[c] d(O_A···$O_{A'}$), d(O_A···$O_{B'}$), d($O_{A'}$···O_B): distances between terminal O atoms represented in **Fig. 6-14**.
[d] ϕ: twist angle between the two mirror planes of mono-lacunary Wells-Dawson units.

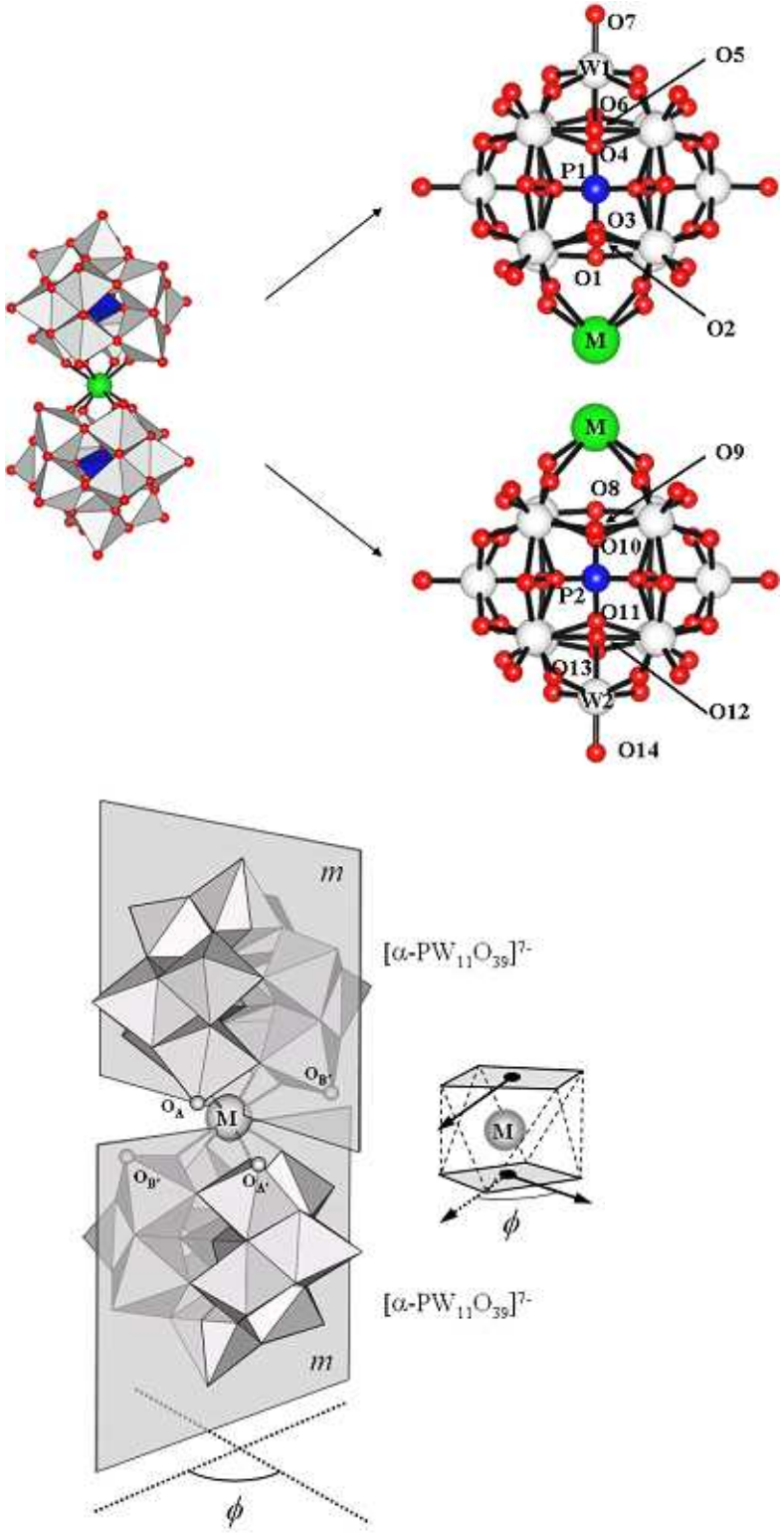

Figure 6-1. Labeling of the defining the mirror planes of the mono-lacunary $[\alpha\text{-}PW_{11}O_{39}]^{7-}$ units (top). Definition of the dihedral angle (ϕ) between the two least-squares planes in $[\alpha\text{-}PW_{11}O_{39}]^{7-}$ units (bottom).

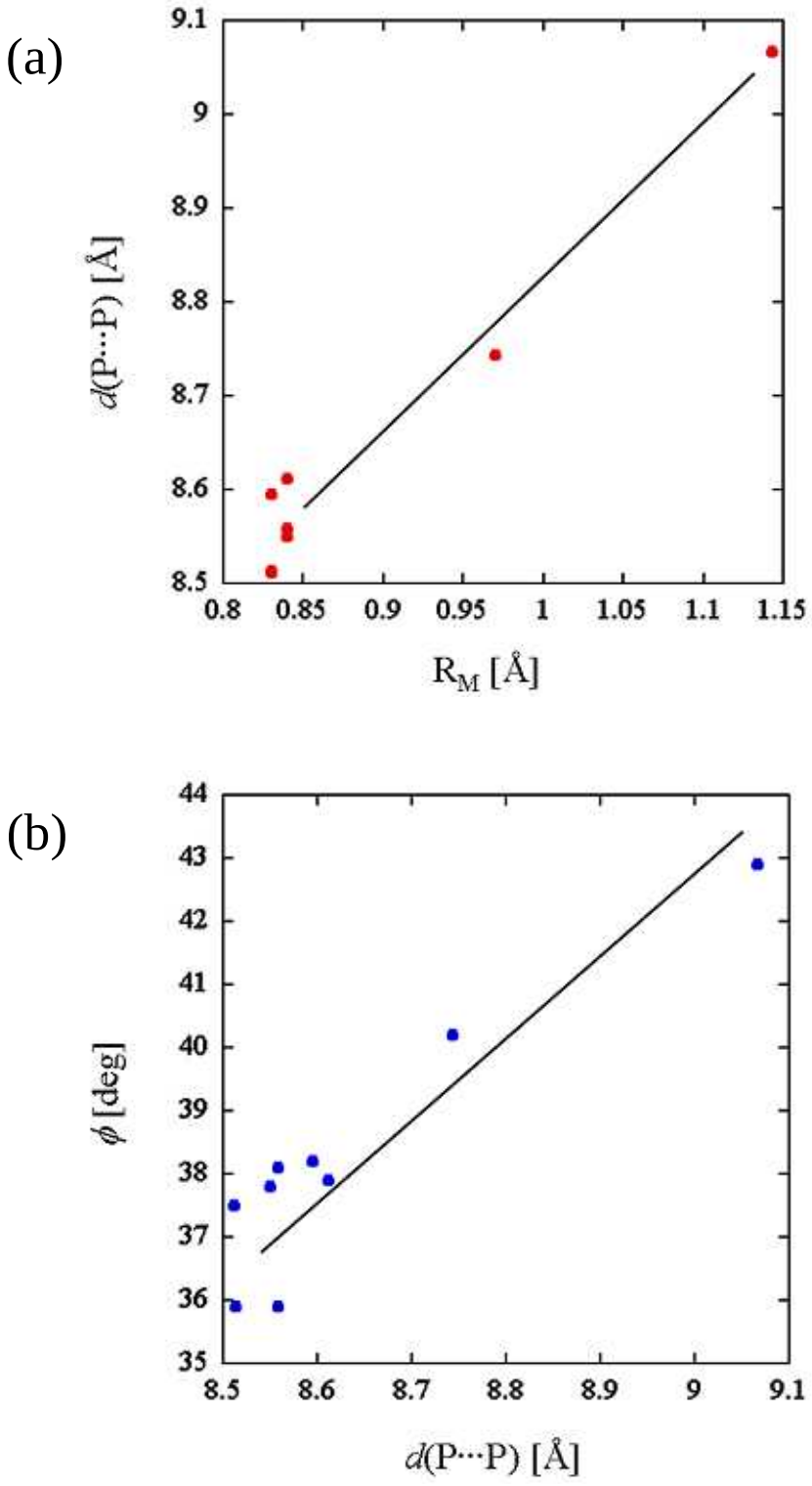

Figure 6-2. Plots of the (a) ionic radius of M (R_M) versus P···P distance (d(P···P)) and (b) d(P···P) versus twist angle (ϕ) for the $[M(\alpha\text{-}PW_{11}O_{39})_2]^{n-}$ polyanion in the pure ammonium salts in listed in **Table 6-1**. The solid line in each plot is drawn to guide the correlation.

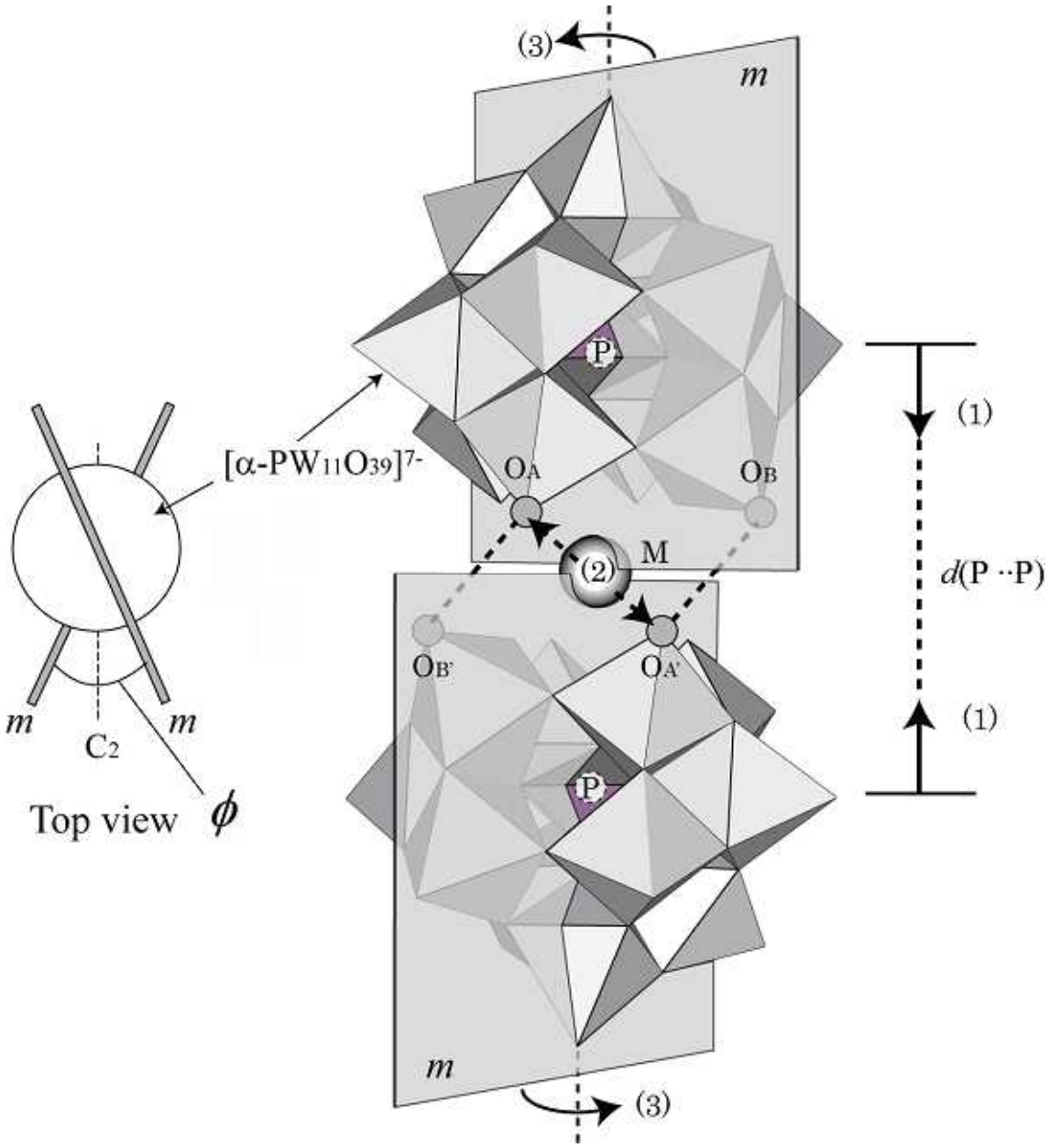

Figure 6-3. Schematic drawing of the $[M(\alpha\text{-}PW_{11}O_{39})_2]^{n-}$ polyanion viewed along the polyanion's C_2 axis, exhibiting the relation between the ionic radius of M (R_M) and twist angle (ϕ). (1) The P···P distance (d(P···P)) decreases with decreasing R_M. (2) The $O_A \cdots O_{A'}$ distance $d(O_A \cdots O_{A'})$ decreases with decreasing d(P···P). (3) The two mirror planes (m) in the $[\alpha\text{-}PW_{11}O_{39}]^{7-}$ units rotate in the ϕ-decreasing direction to diminish the $O_A \cdots O_{A'}$ repulsion.

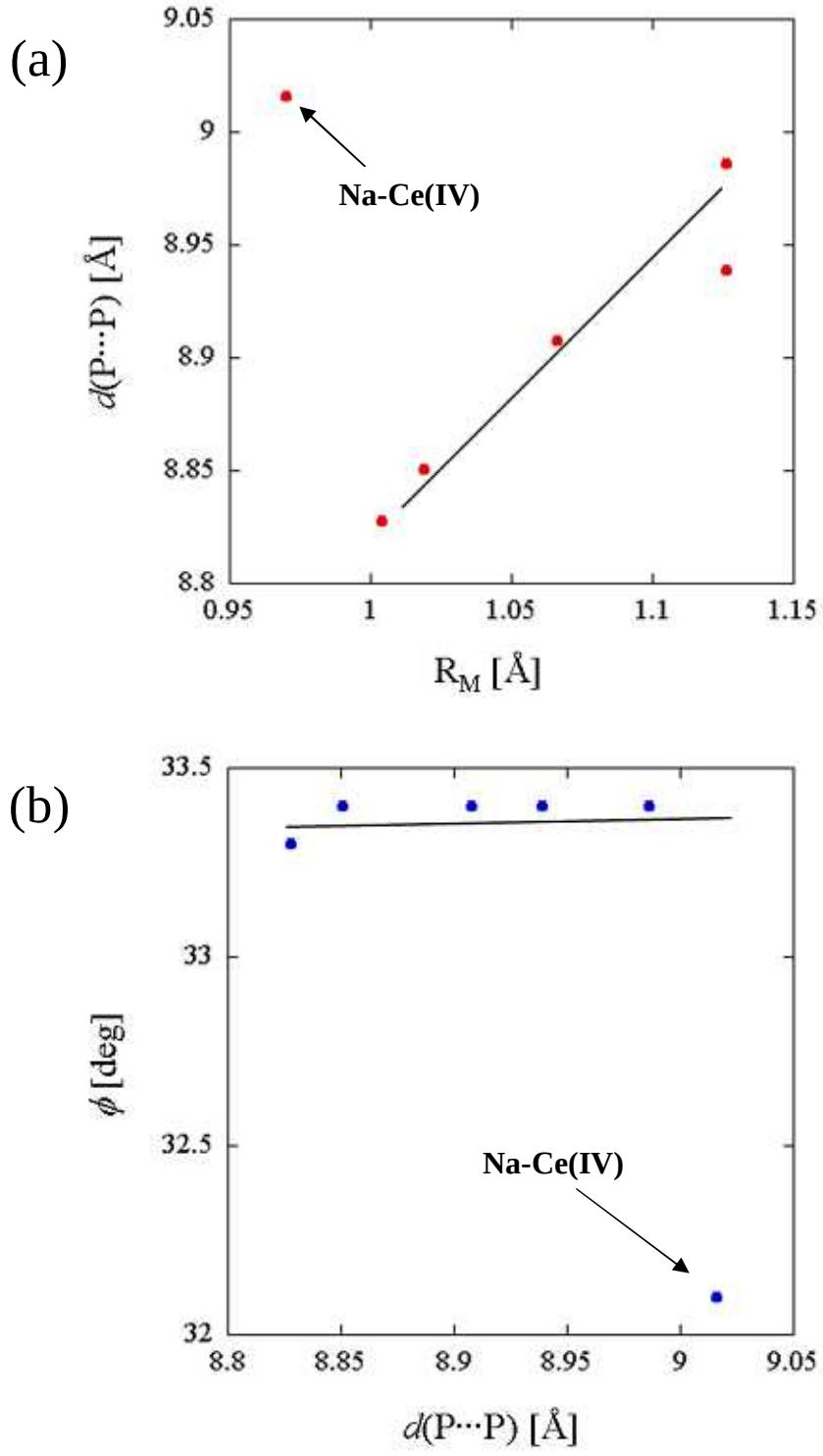

Figure 6-4. Plots of the (a) ionic radius of M (R_M) versus P···P distance (d(P···P)), (b) d(P···P) versus twist angle (ϕ) for the $[M(\alpha\text{-}PW_{11}O_{39})_2]^{n-}$ polyanion in the TMA^+/Na^+-mixed salts in listed in **Table 6-2**. The solid line in each plot is drawn to guide the correlation.

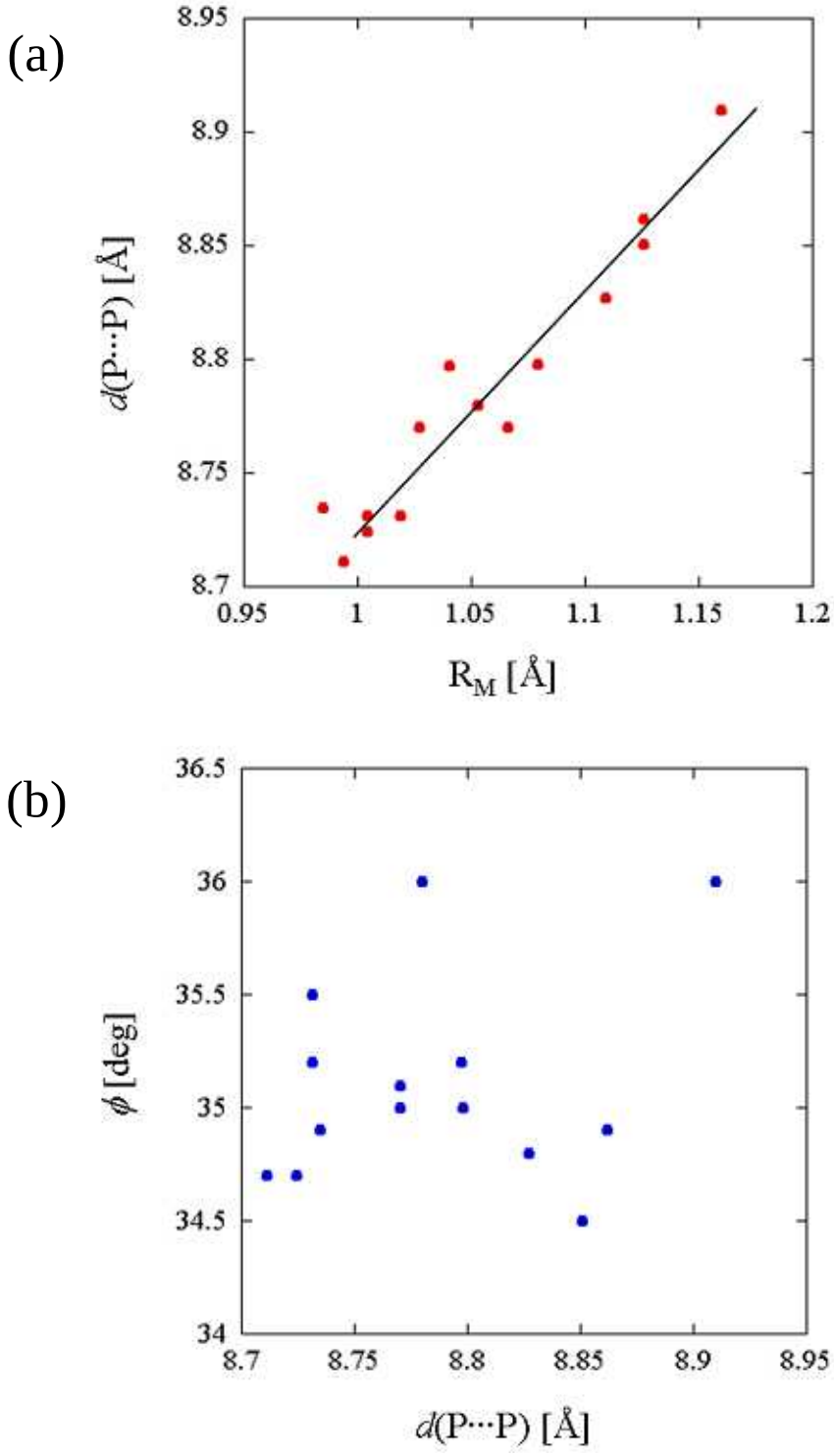

Figure 6-5. Plots of the (a) ionic radius of M (R_M) versus P···P distance (d(P···P)), (b) d(P···P) versus twist angle (ϕ) for the $[M(\alpha\text{-}PW_{11}O_{39})_2]^{n-}$ polyanion in the chiral Na^+/K^+-mixed salts in listed in **Table 6-3**. The solid line in each plot is drawn to guide the correlation.

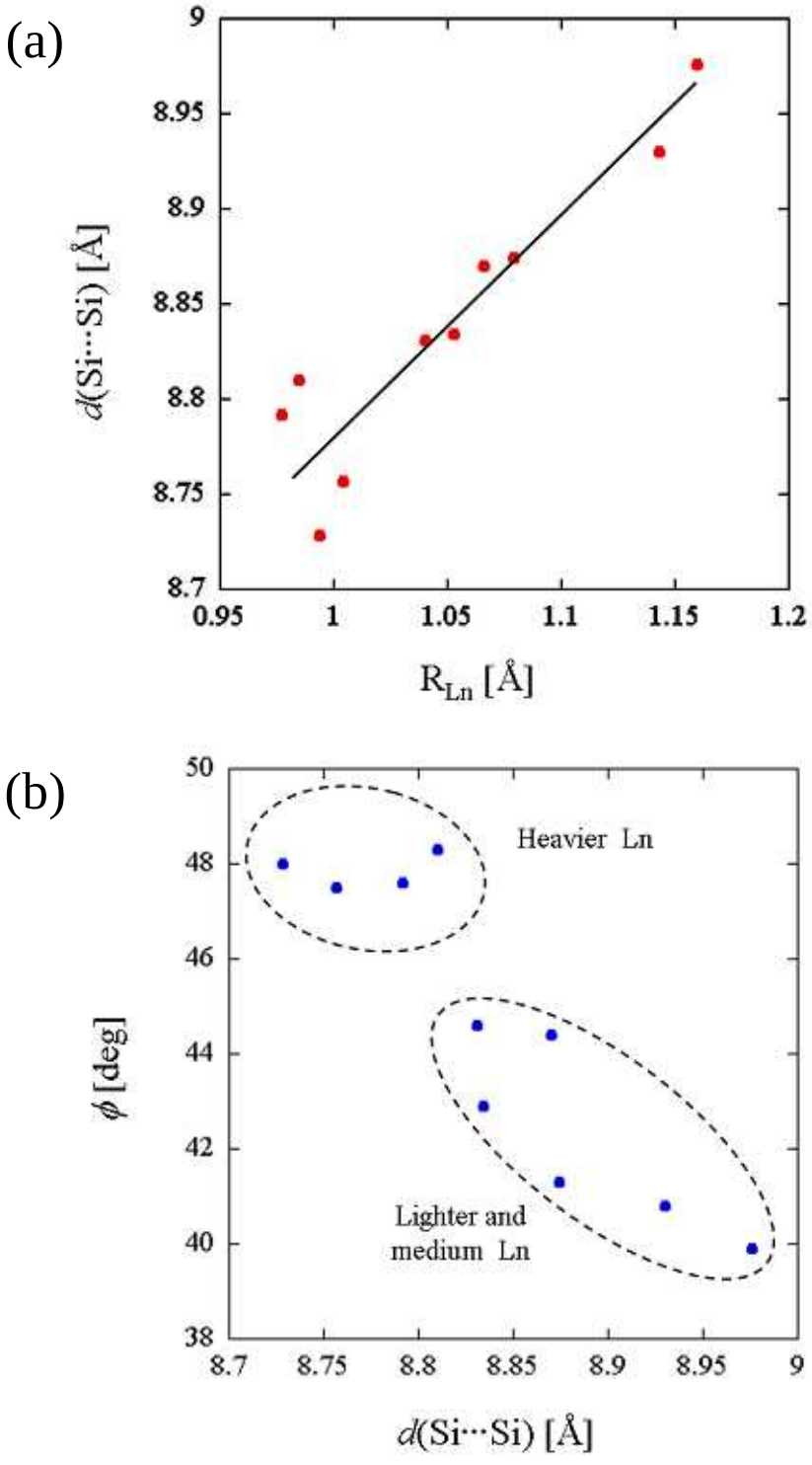

Figure 6-6. Plots of the (a) ionic radius of M (R_M) versus Si···Si distance (*d*(Si···Si)), (b) *d*(Si···Si) versus twist angle (ϕ) for the $[Ln(\beta_2\text{-}SiW_{11}O_{39})_2]^{13-}$ polyanion in the K salts in listed in **Table 6-4**. The solid line in each plot is drawn to guide the correlation.

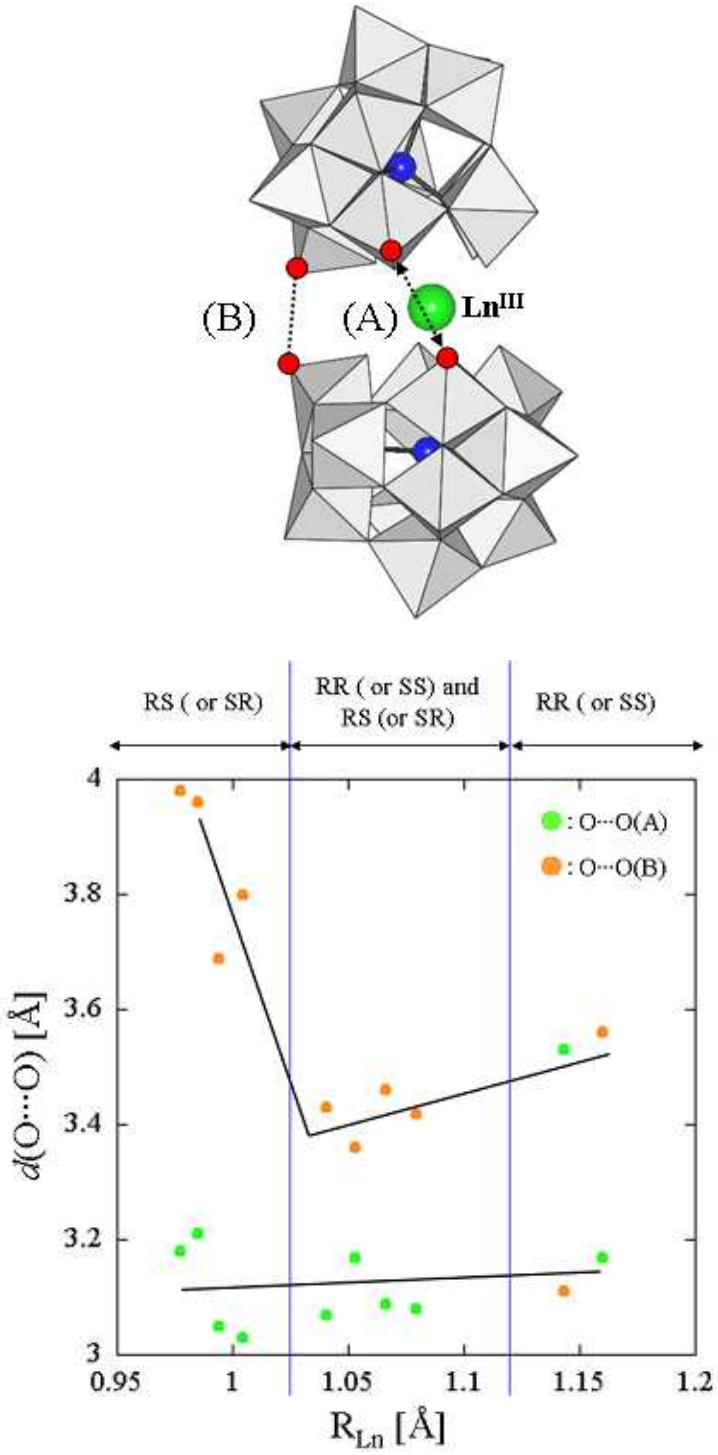

Figure 6-7. The definition of O···O(A) and O···O(B) in the $[Ln(\beta_2\text{-}SiW_{11}O_{39})_2]^{13-}$ polyanion (above). The plots of R_{Ln} vs. O···O(A) and O···O(B) distances based on structural data of $[Ln(\beta_2\text{-}SiW_{11}O_{39})_2]^{13-}$ (Ln = La-Lu) [22, 24] (below). The solid line in each plot is drawn to guide the correlation.

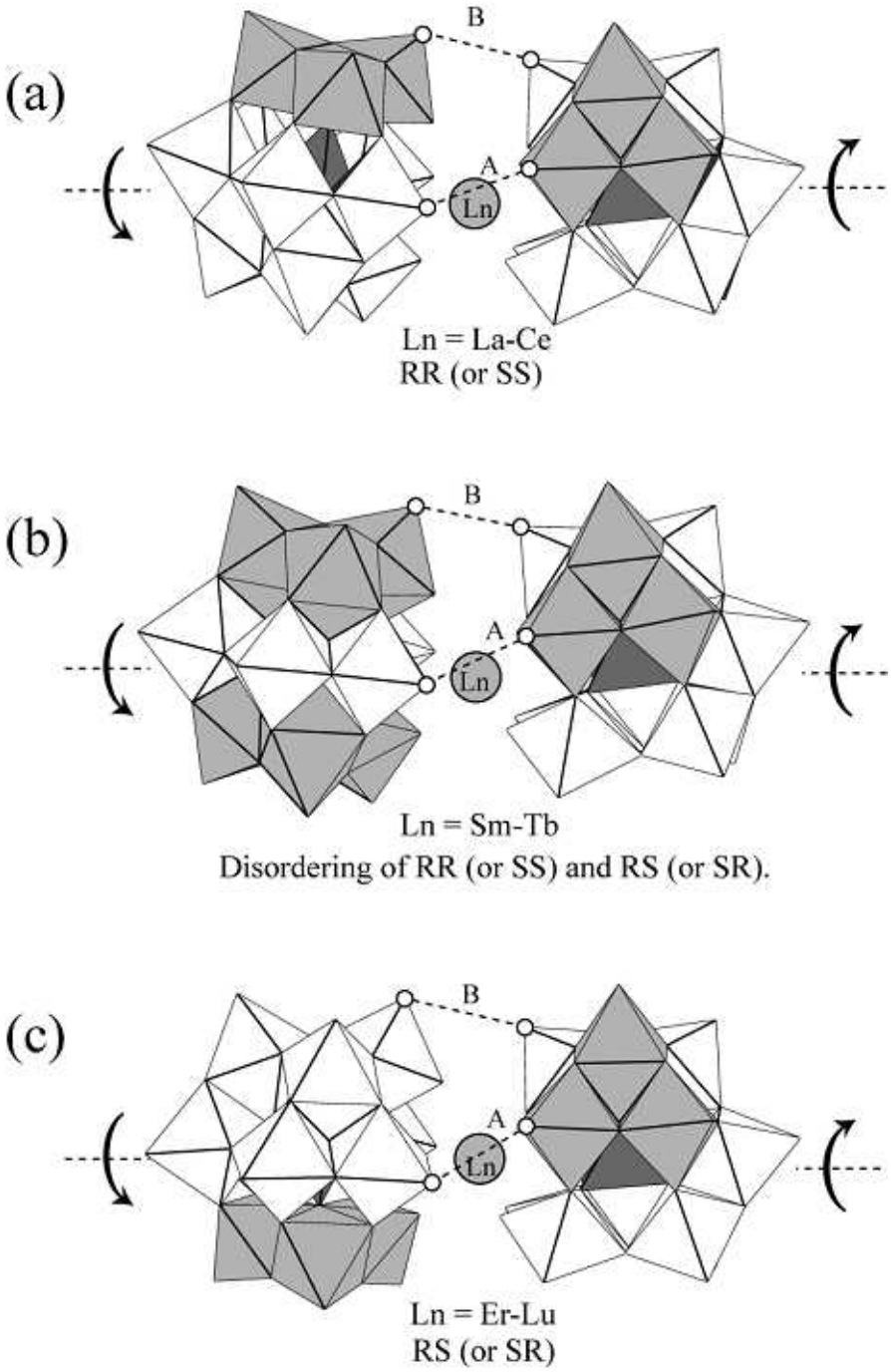

Figure 6-8. Explanation of the correlation between ionic radius of Ln (R_{Ln}) and twist angle (ϕ) of $[\beta_2\text{-}SiW_{11}O_{39}]^{8-}$ together with relation to absolute configuration in the series of $[Ln(\beta_2\text{-}SiW_{11}O_{39})_2]^{13-}$ (Ln = La-Lu) [22, 24]. The rotated W_3O_{13} triad of β structure is denoted with shaded polyhedra. (a): RR (or SS) for Ln = La-Ce. (b): disordering between RR (or SS) and RS (or SR) for Ln = Sm-Tb. (c): RS (or SR) for Ln = Er-Lu. There are two short O···O contacts (O···O(A) and O···O(B)) between the $[\beta_2\text{-}SiW_{11}O_{39}]^{8-}$ units. A decrease of R_{Ln} induces repulsion of both A and B, which gives rise to relative rotation of the $[\beta_2\text{-}SiW_{11}O_{39}]^{8-}$ units to ϕ- increasing directions (indicated with arrows).

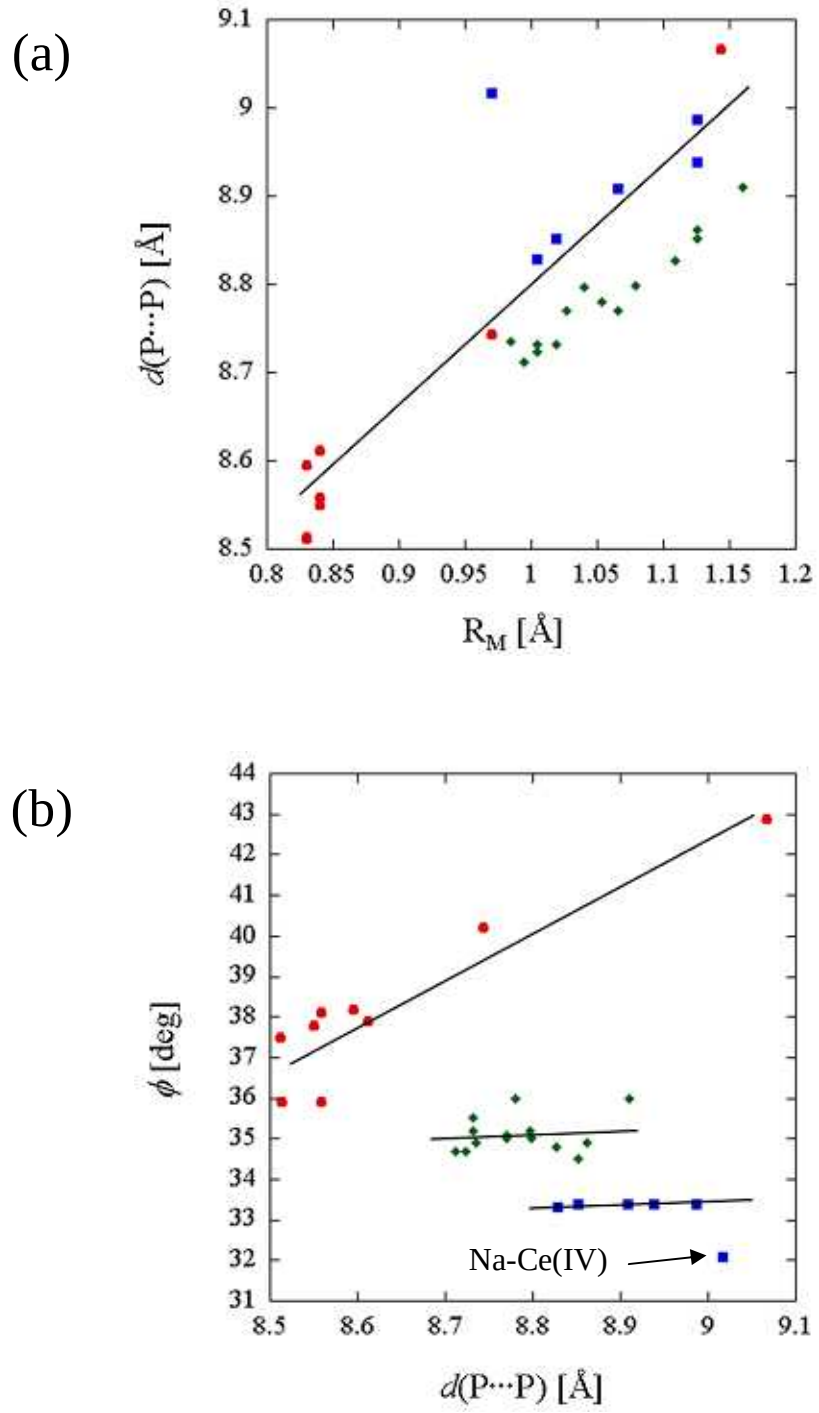

Figure 6-9. Plots of the (a) ionic radius of M (R_M) versus P···P distance (d(P···P)) and (b) d(P···P) versus twist angle (ϕ) for all of the $[M(\alpha\text{-}PW_{11}O_{39})_2]^{n-}$ polyanion in listed in **Tables 6-1, 2, 3**. The solid line in each plot is drawn to guide the correlation. The red spheres, green rhombuses, and blue squares are the plots corresponding to the pure alkylammonium salts, chiral Na^+/K^+-mixed salts, and TMA^+/Na^+-mixed salts, respectively.

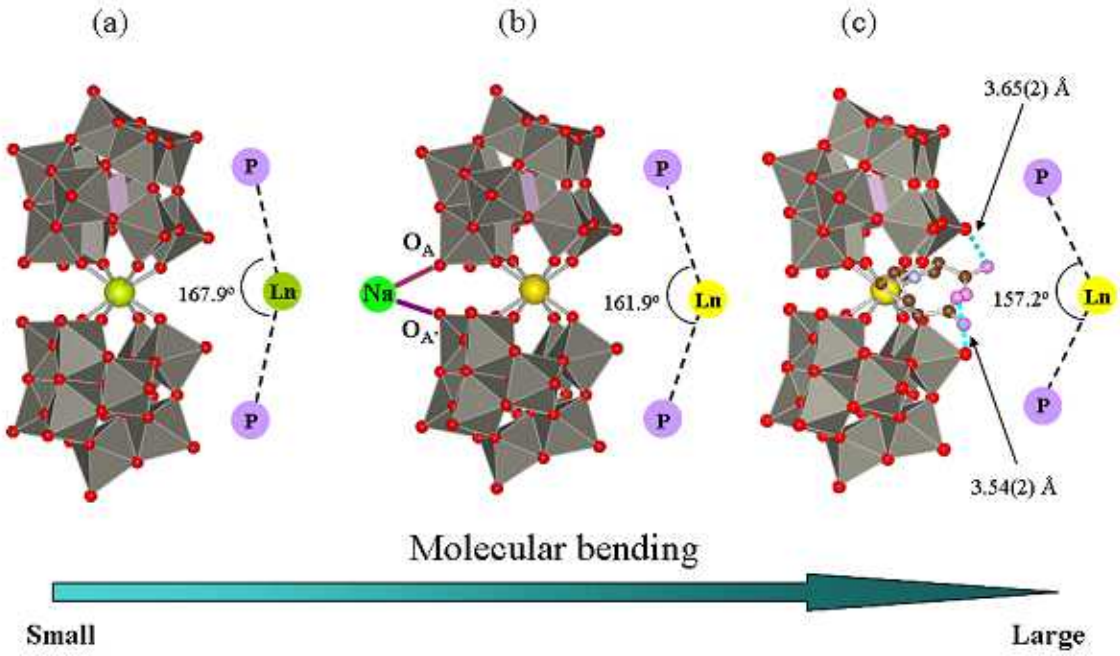

Figure 6-10. The difference in the molecular bending (∠P-Ln-P = φ) in the polyanion. (a) pure alkylammonium salt, (b) TMA^+/Na^+-mixed salts, (c) chiral Na^+/K^+-mixed salts. The polyanions are represented by the combined polyhedral and ball-and-stick representation method. Color code: WO_6 octahedra (gray), PO_4 tetrahedra (purple), Ln atoms (light green and yellow spheres), O atom in the polyanion (red spheres), Na atom (green sphere), N atoms (light blue spheres), C atoms (brown spheres), O atoms in the proline molecule (pink spheres). The Na-O bondings and O···O steric repulsion between $[\alpha\text{-}PW_{11}O_{39}]^{7-}$ and carboxyl group in proline are denoted by bold purple line and dashed blue line, respectively.

(a)

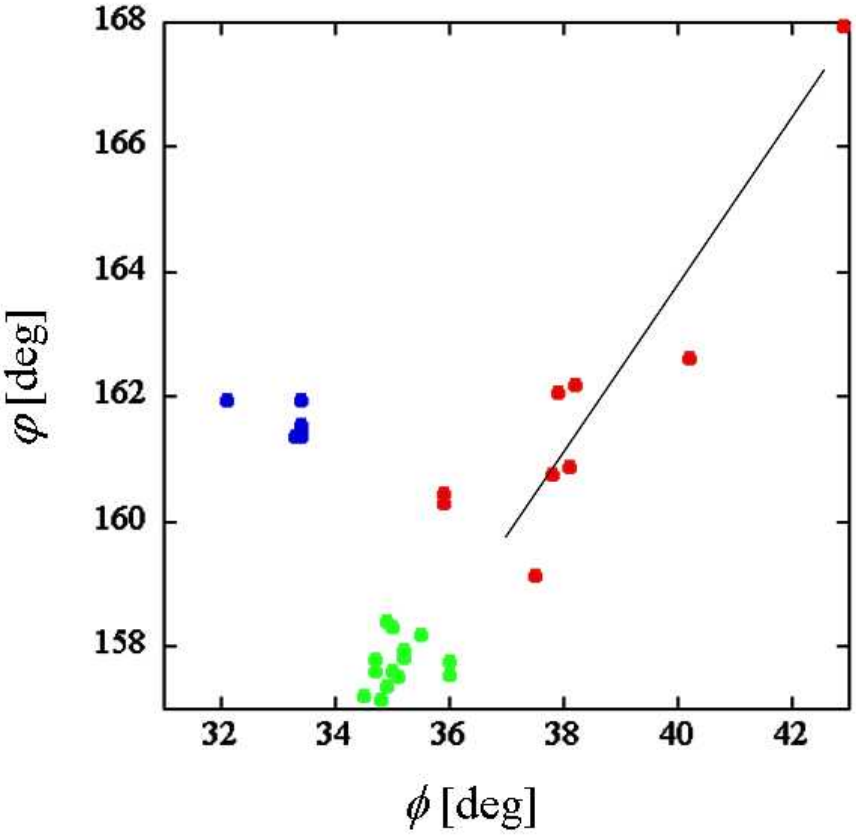

Figure 6-11. (a) Plots of the molecular bending ∠P-M-P' (φ) versus twist angle (ϕ) for all of the $[M(\alpha\text{-}PW_{11}O_{39})_2]^{n-}$ polyanion in listed in **Tables 6-1, 2, 3**. The red, blue, green plots correspond to the pure alkylammonium ammonium salts, TMA^+/Na^+-mixed salts, and chiral Na^+/K^+-mixed salts, respectively.

(b)

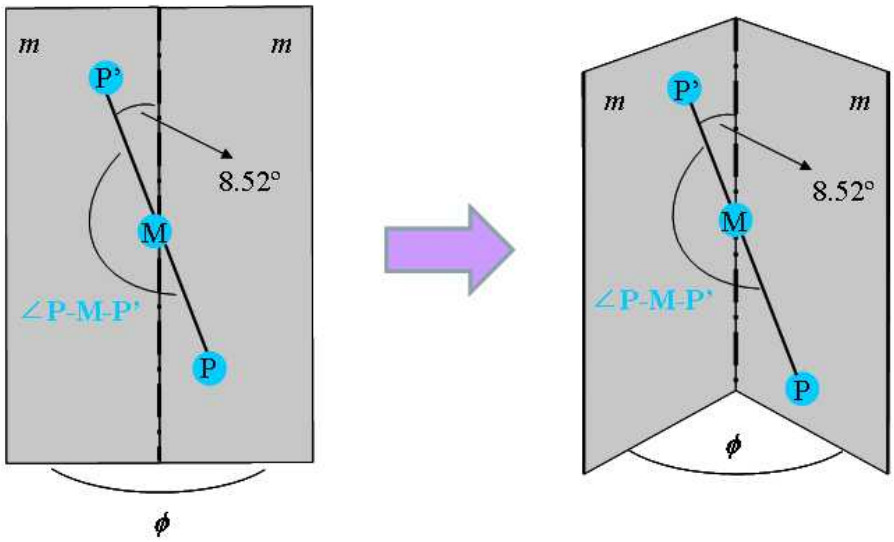

ϕ = 180°
φ = 180°

0°<ϕ<180°
162.96°<φ< 180°

(c)

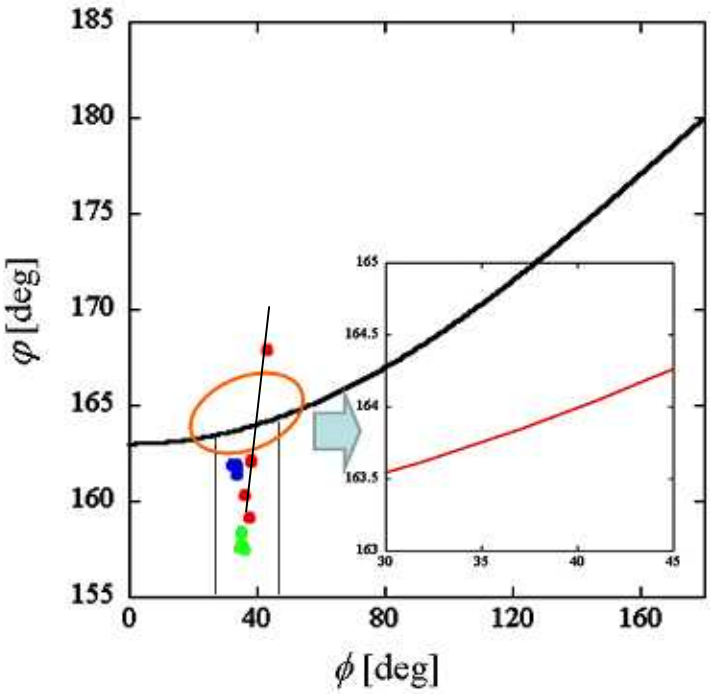

Figure 6-11. (b) Definition of ϕ and φ based on the geometrical modeling considering the genuine rotation effect of $[\alpha\text{-}PW_{11}O_{39}]^{7-}$. (c) Plots of φ versus ϕ based on the geometrical modeling demonstrated above. The inset is demonstrated by expanding the orange circled region. The red, blue, green spheres are the plots corresponding to the pure alkylammonium salts, TMA^+/Na^+-mixed salts, and chiral Na^+/K^+-mixed salts, respectively.

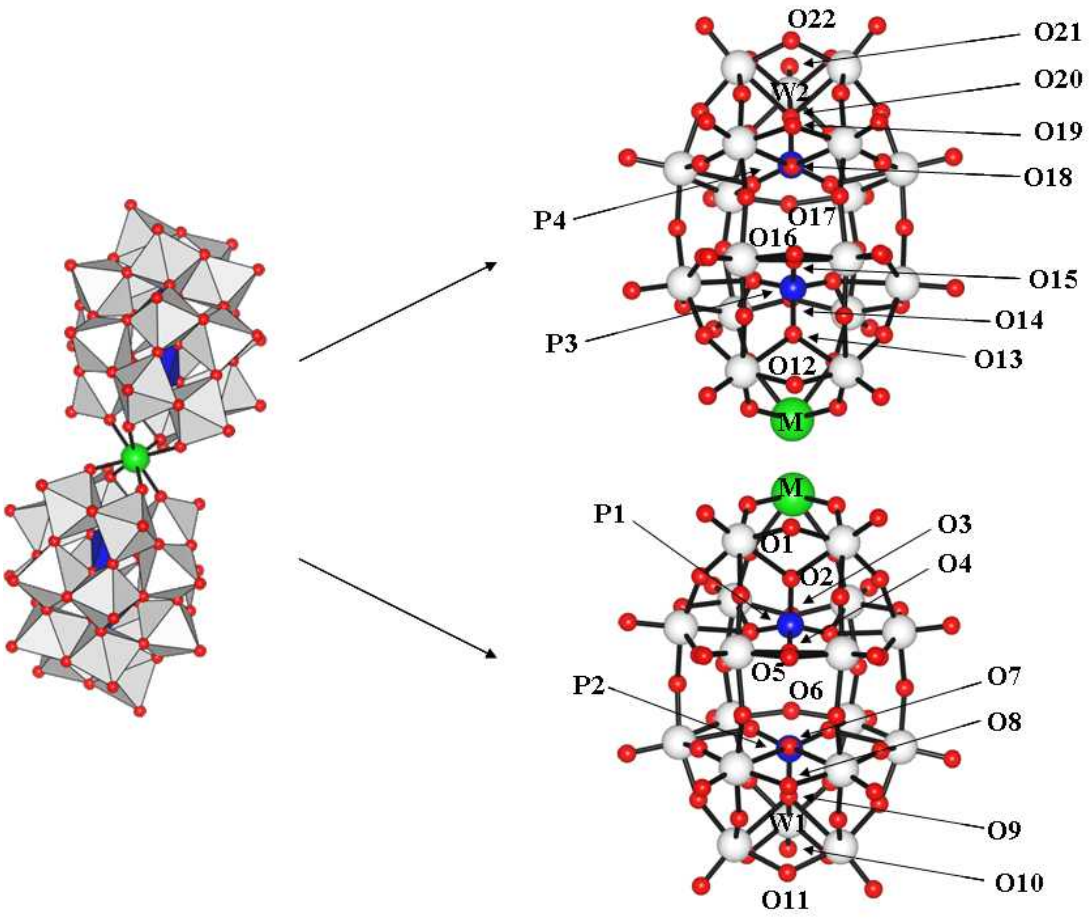

Figure 6-12. Labeling of the defining the mirror planes of the mono-lacunary $[\alpha_2\text{-}P_2W_{17}O_{61}]^{10-}$ units.

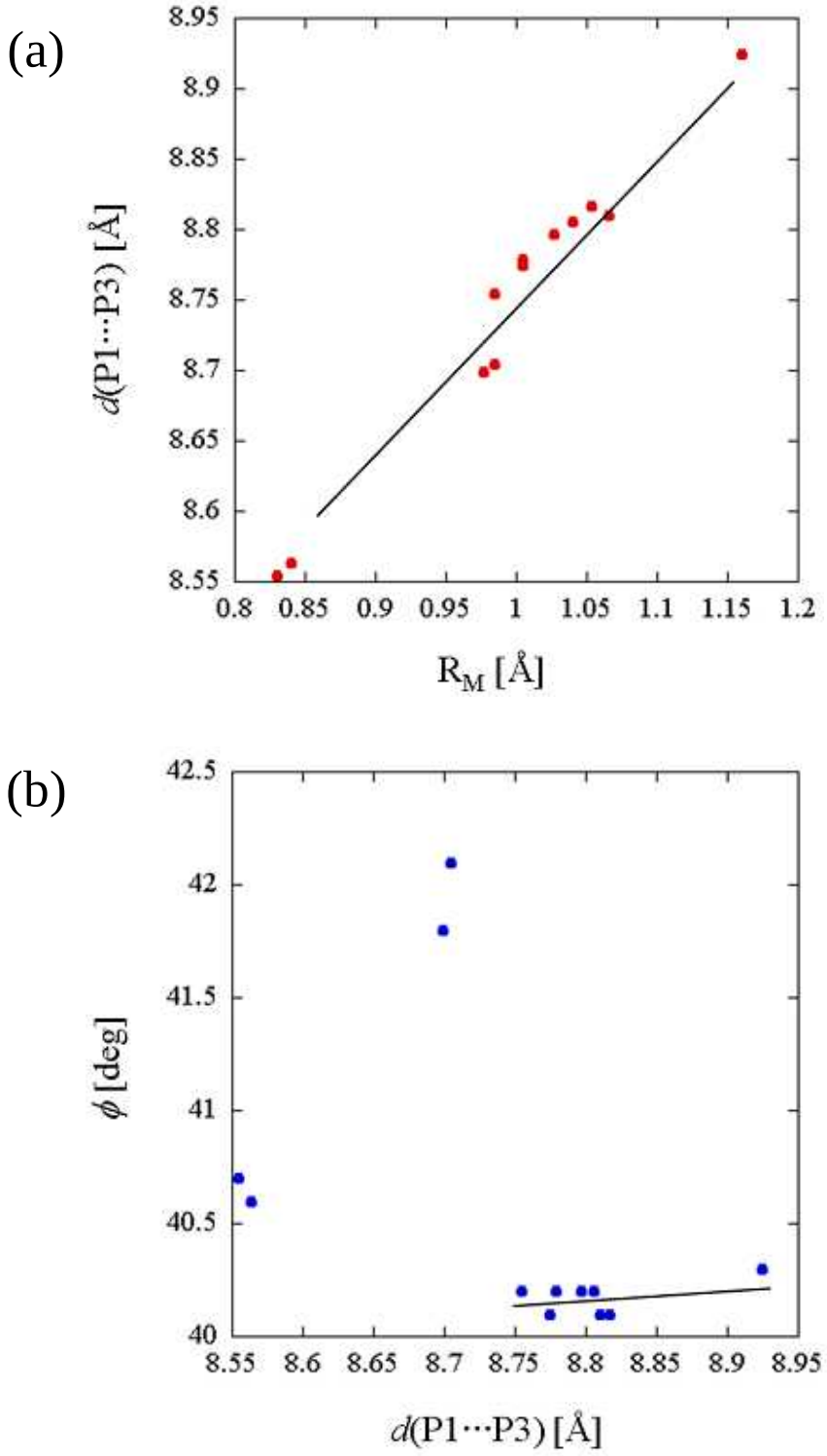

Figure 6-13. Plots of the (a) ionic radius of M (R_M) versus P1···P3 distance (*d*(P1···P3)) and (b) *d*(P1···P3) versus twist angle (ϕ) for the $[M(\alpha_2\text{-}P_2W_{17}O_{61})_2]^{n-}$ polyanion in listed in **Table 6-5**. The solid line in each plot is drawn to guide the correlation.

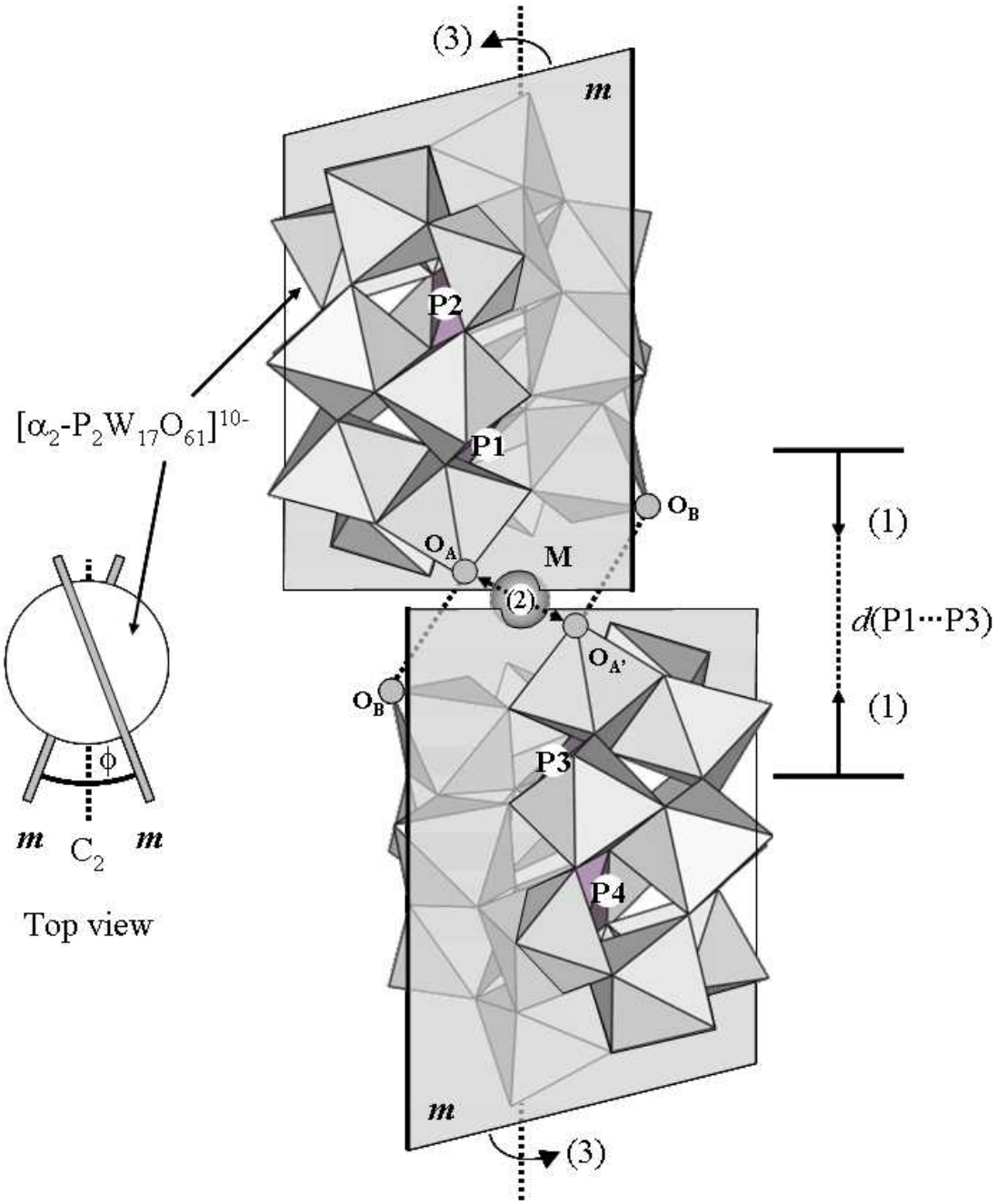

Figure 6-14. Schematic drawing of the $[M(\alpha_2\text{-}P_2W_{17}O_{61})_2]^{n-}$ polyanion viewed along the polyanion's C_2 axis, exhibiting the relation between the ionic radius of M (R_M) and twist angle (ϕ). (1) The P1···P3 distance (d(P1···P3)) decreases with decreasing R_M. (2) The $O_A\cdots O_{A'}$ distance $d(O_A\cdots O_{A'})$ decreases with decreasing d(P1···P3). (3) The two mirror planes (m) in the $[\alpha_2\text{-}P_2W_{17}O_{61}]^{10-}$ units rotate in the ϕ-decreasing direction to diminish the $O_A\cdots O_{A'}$ repulsion.

Chapter 7 Summary

This study is related to two Ln-containing polyoxotungstates $[Ln(\alpha\text{-}XM_{11}O_{39})_2]^{n-}$ and $[Ln(\alpha_2\text{-}X_2M_{17}O_{61})_2]^{n-}$, which have been synthesized by Peacock and Weakley for the first time [1]. Mono-lacunary units of $[\alpha\text{-}XM_{11}O_{39}]^{n-}$ and $[\alpha_2\text{-}X_2M_{17}O_{61}]^{n-}$ have tetradentate coordination position with square-shape, the coordination geometry of Ln center, which is coordinated by two mono-lacunary units, is possible to adopt cubic or square-antiprism (SA). On the development of fundamental and application studies about the $[Ln(\alpha\text{-}XM_{11}O_{39})_2]^{n-}$ and $[Ln(\alpha_2\text{-}X_2M_{17}O_{61})_2]^{n-}$ polyanions, the challenging problem to be conquered has been confronted to POM chemists for a long time. This is the one about the coordination geometry of Ln in the polyanion. In the past studies, all the coordination environment of Ln is SA regardless of the kind of Ln and POM units in the solid states. However, in aqueous solution, a cubic coordination has been presumed for the early lanthanides, La-Eu [2]. Thus, little has been known about what regulates the coordination geometry of Ln in $[Ln(\alpha\text{-}XM_{11}O_{39})_2]^{n-}$ and $[Ln(\alpha_2\text{-}X_2M_{17}O_{61})_2]^{n-}$ and their molecular conformations in the solid states. This problem can be replaced by what rules the twist angle ϕ, which is defined by the dihedral angle between the mirror planes of the C_s-symmetrical mono-lacunary $[\alpha\text{-}XM_{11}O_{39}]^{n-}$ or $[\alpha_2\text{-}X_2M_{17}O_{61}]^{n-}$ units. The ϕ = 0° and 180° corresponds to C_{2v} and C_{2h} symmetries, in which Ln adopts cubic coordination. On the other hand, $0° < \phi < 180°$ corresponds to a C_2 symmetry, in which an ideal SA coordination is achieved for ϕ = ~45° and ~135° [2, 3]. Therefore, polyanion with ϕ = 0° and 180° is achiral, while the one with $0° < \phi < 180°$ is chiral. Thus, to regulate ϕ means to control the chirality of the polyanion. All of the isolated crystalline solids of $[Ln(\alpha\text{-}XM_{11}O_{39})_2]^{n-}$ and $[Ln(\alpha_2\text{-}X_2M_{17}O_{61})_2]^{n-}$ polyanions are racemic mixture of the polyanions with ϕ = ~ ±45°. To unify the ϕ = ~ -45° or ~ +45° in all polyanions in

aqueous solution and in the solid state corresponds to a selective synthesis of each enantiomer. Then, to control of the molecular conformation of the $[Ln(\alpha\text{-}XM_{11}O_{39})_2]^{n-}$ and $[Ln(\alpha_2\text{-}X_2M_{17}O_{61})_2]^{n-}$ polyanions in aqueous solution and in the solid state, and to elucidate the controlling factors are set as the final goal in this study. The research strategies are to investigate the molecular conformation and chirality expression of the polyanions with controlling ionic radius of $Ln^{3+/4+}$, and symmetry, arrangement, and chirality of countercations and co-existing materials.

7-1 The effects of the external factors

7-1-1 The effect of the countercation

The use of simple and high symmetric tetramethylammonium (TMA) cation resulted in weak, isotropic, and averaged potential around the $[Ln(\alpha\text{-}PW_{11}O_{39})_2]^{11-}$ polyanion. The resultant symmetric molecular environment leads to the isolation of the $[Ln(\alpha\text{-}PW_{11}O_{39})_2]^{11-}$ polyanions with cubic coordination in $[Me_4N]_{10}H[Ln(\alpha\text{-}PW_{11}O_{39})_2]\cdot xH_2O$ (Ln = La and Ce) for the first time. The Ln^{3+} in the polyanion is imposed on the crystallographic inversion center, and the polyanion is approximated to C_{2h} symmetry corresponding to $\phi = 180^o$. As for the cubic coordination species of the $[Ln(\alpha\text{-}PW_{11}O_{39})_2]^{11-}$ polyanion in aqueous solution, ϕ has long been undetermined to date, 0^o (C_{2v}) or 180^o (C_{2h}). The isolation of the cubic coordination species in this study delivered the answer that 180^o is favorable, probably due to a steric hindrance between the $[\alpha\text{-}PW_{11}O_{39}]^{7-}$ units for $\phi = 0^o$.

While, a partial anisotropic potential produced from the isotropic disruption by Na^+ uptake prompted a formation of SA coordination in $[Me_4N]_{5.5}Na_5H_{0.5}[Ln(\alpha\text{-}PW_{11}O_{39})_2]\cdot xH_2O$ (Ln = Pr, Eu, Er) and

$[Me_4N]_{5.5}Na_3H_{2.5}[Y(\alpha\text{-}PW_{11}O_{39})_2]\cdot 22H_2O$, which had been primitively observed in the solid state. Until now, the $[Ln(\alpha\text{-}PW_{11}O_{39})_2]^{11-}$ polyanions possessing the early lanthanides (La-Eu) have been believed to adopt a cubic coordination in aqueous solutions. However, in TMA salts, cubic coordination species are limited for La and Ce analogues, and a SA coordination are observed for the Pr, Eu, Er, and Y analogues with unexpected partial replacement of TMA^+ with Na^+. These facts suggest that the cationic environment dominantly affects the coordination geometry rather than the ionic radius of Ln^{3+}. Also, one of the Na^+ ions in **Pr-s**, **Eu-s**, **Er-s**, and **Y-s** links the two $[\alpha\text{-}PW_{11}O_{39}]^{7-}$ units through Na-O bonding, which makes ϕ low and constant in a series of SA coordination species.

It is known that physicochemical properties such as magnetism and luminescence for Ln-POM are sensitive to ligand–field of Ln. The first isolation of cubic coordination species in Ln-POM would give us the opportunity to produce novel molecular materials. Appropriate choices of cation and preparation precursor of the mono-lacunary species with different hetero atom probably spread the range of cubic coordination species up to mid-lanthanide of Eu, which have been presumed by Fedotov in previous report [2].

7-1-2 The effect of the co-existing chiral materials

The enantioselective synthesis of the $[Ln(\alpha\text{-}PW_{11}O_{39})_2]^{11-}$ and $[Ln(\alpha_2\text{-}P_2W_{17}O_{61})_2]^{17-}$ polyanions was achieved in $K_{1.3}Na_{3.2}H_{6.5}[Ln(\alpha\text{-}PW_{11}O_{39})_2]\cdot 8.3(C_5H_9NO_2)\cdot xH_2O$ (Ln = Pr, Nd, Sm, Gd, Tb, Dy, Er, Tm, Yb, and Y), $K_{1.2}Na_2H_{7.8}[Ln(\alpha\text{-}PW_{11}O_{39})_2]\cdot 8.5(C_5H_9NO_2)\cdot xH_2O$ (Ln = La, Eu), and $K_{12}H_5[Ln(\alpha_2\text{-}P_2W_{17}O_{61})_2]\cdot 2(C_5H_9NO_2)\cdot xH_2O$ (Ln = La, Sm, Eu, Gd, Tb, Dy, Er, Yb) by using proline as chiral auxiliary agent for the first time. In the solid state, chirality of the

polyanion was induced by the stereo- and enantioselective hydrogen-bonded interaction from proline molecules to the polyanion. The proline molecules are inserted to 'grooves' of the $[Ln(\alpha\text{-}PW_{11}O_{39})_2]^{11-}$ and $[Ln(\alpha_2\text{-}P_2W_{17}O_{61})_2]^{17-}$ polyanions, this leads to constant ϕ values throughout the Ln series. On the other hand, the chirality induction due to the addition of proline into the racemic aqueous solution of $[Ln(\alpha\text{-}PW_{11}O_{39})_2]^{11-}$ was confirmed by monitoring CD spectroscopy. The polyanion containing paramagnetic Ln is promising for a numerous application such as optical isolator or magneto-optical memory. Also, the analogues having luminescent Ln are candidates for optical detecting of chiral materials.

7-2 The effects of the internal factors

7-2-1 The effect of the ionic radius of $Ln^{3+/4+}$

In the DMA salts of the $[Ce^{III/IV}(\alpha\text{-}PW_{11}O_{39})_2]^{11-/10-}$ polyanions, $[Me_2NH_2]_{11}[Ce^{III}(\alpha\text{-}PW_{11}O_{39})_2]\cdot 14H_2O$ and $[Me_2NH_2]_{10}[Ce^{IV}(\alpha\text{-}PW_{11}O_{39})_2]\cdot 14H_2O$, the Ce(III) containing analogue crystallized in racemate, while the spontaneous resolution of the Ce(IV) analogue was achieved without chiral auxiliaries. The spontaneous resolution of the sandwich-type $[M^{IV}(\alpha\text{-}PW_{11}O_{39})_2]^{10-}$ analogues was observed for M^{IV} = Hf^{IV} and or Zr^{IV} in DMA salts [4, 5], whereas all the Ln^{III} analogues were isolated as racemate containing two enantiomers. This study revealed that valence of M(IV) (i.e. anion charge 10-) and countercation are both essential for achievement of spontaneous resolution of $[M^{IV}(\alpha\text{-}PW_{11}O_{39})_2]^{10-}$.

Besides, the ionic radius of Ln largely affects some geometrical properties of $[Ln^{III}(\alpha\text{-}PW_{11}O_{39})_2]^{11-}$. For the molecular conformation, a cubic coordination is adopted for larger Ln, while a SA coordination is for smaller Ln. For the racemization

mechanism, enantiomeric conversion between L-form and D-form occurs rapidly for the polyanion with larger Ln and slowly for the one with smaller Ln, respectively. These properties may be explained in terms of lower barrier to rotation of $[\alpha\text{-}PW_{11}O_{39}]^{7-}$ for larger Ln ions as suggested previously [6]. In all series of compounds in this study, the *d*(P···P) values linearly increase with increasing of the ionic radius of Ln, meaning that the distance between two $[\alpha\text{-}PW_{11}O_{39}]^{7-}$ units are controlled.

7-2-2 Steric repulsion between mono-lacunary units within a molecule

Based on the interaction of the cation and co-existing material on the polyanion, the correlation between the ionic radius of the central metal and twist angle ϕ of the two mono-lacunary Keggin and Wells-Dawson units was clearly found.

For the $[M(\alpha\text{-}PW_{11}O_{39})_2]^{n-}$ polyanion, in the series of DMA salts ($[Me_2NH_2]_{11}[Ce^{III}(\alpha\text{-}PW_{11}O_{39})_2]\cdot 14H_2O$ and $[Me_2NH_2]_{10}[Ce^{IV}(\alpha\text{-}PW_{11}O_{39})_2]\cdot 14H_2O$) with weak hydrogen bonded interaction to the polyanion, the ϕ deviates from 45º for an ideal SA coordination to avoid the approaching of $[\alpha\text{-}PW_{11}O_{39}]^{7-}$ units. In the case of TMA^+/Na^+-mixed salts ($[Me_4N]_{5.5}Na_5H_{0.5}[Ln(\alpha\text{-}PW_{11}O_{39})_2]\cdot xH_2O$, $[Me_4N]_{5.5}Na_3H_{2.5}[Ln(\alpha\text{-}PW_{11}O_{39})_2]\cdot xH_2O$), the introduced Na^+ bridging across the two $[\alpha\text{-}PW_{11}O_{39}]^{7-}$ units inhibits their mutual twist to give constant ϕ independently on the kind of Ln. As shown above, in the series of chiral Na^+/K^+-mixed salts ($K_{1.3}Na_{3.2}H_{6.5}[Ln(\alpha\text{-}PW_{11}O_{39})_2]\cdot 8.3(C_5H_9NO_2)\cdot xH_2O$ and $K_{1.2}Na_2H_{7.8}[Ln(\alpha\text{-}PW_{11}O_{39})_2]\cdot 8.5(C_5H_9NO_2)\cdot xH_2O$), two proline molecules acting as chirality inducer for the polyanion, disturb the twist of $[\alpha\text{-}PW_{11}O_{39}]^{7-}$ units by hydrogen-bonded interaction to similarly produce the constant ϕ to the TMA^+/Na^+-mixed salts. For the $[M(\alpha_2\text{-}P_2W_{17}O_{61})_2]^{n-}$ polyanion in

$K_{12}H_5[Ln(\alpha_2\text{-}P_2W_{17}O_{61})_2]\cdot 2(C_5H_9NO_2)\cdot xH_2O$, the hydrogen-bonding interaction between the polyanion and proline molecules is similar to that in $K_{1.3}Na_{3.2}H_{6.5}[Ln(\alpha\text{-}PW_{11}O_{39})_2]\cdot 8.3(C_5H_9NO_2)\cdot xH_2O$ and $K_{1.2}Na_2H_{7.8}[Ln(\alpha\text{-}PW_{11}O_{39})_2]\cdot 8.5(C_5H_9NO_2)\cdot xH_2O$, and delivered constant ϕ. On the other hand, in the racemate crystals of $K_{16}H[Yb(\alpha_2\text{-}P_2W_{17}O_{61})_2]\cdot 44H_2O$, $K_{17}[Lu(\alpha_2\text{-}P_2W_{17}O_{61})_2]$, $K_{16}[Hf(\alpha_2\text{-}P_2W_{17}O_{61})_2]\cdot 19H_2O$, and $K_{15}H[Zr(\alpha_2\text{-}P_2W_{17}O_{61})_2]\cdot 25H_2O$, the isotropic cationic environment around the polyanion seems to be produced by a large number of crystallized K^+ like pure alkylammonium salts of $[M(\alpha\text{-}PW_{11}O_{39})_2]^{n-}$. Then, the ϕ deviates from 45º for an ideal SA coordination to avoid the approaching of $[\alpha_2\text{-}P_2W_{17}O_{61}]^{10-}$ units. These observations were discussed in detail in Chapter 6 by focusing on the steric repulsion between two mono-lacunary Keggin or Wells-Dawson units via terminal O atoms. The $[M(\alpha\text{-}PW_{11}O_{39})_2]^{n-}$ and $[M(\alpha_2\text{-}P_2W_{17}O_{61})_2]^{n-}$ polyanions hold similar three short O···O contacts between two $[\alpha\text{-}PW_{11}O_{39}]^{7-}$ and $[\alpha_2\text{-}P_2W_{17}O_{61}]^{10-}$ units (**Figs. 6-3** and **14**), so all the steric repulsion ascribed to their contacts should be considered in order to comprehensively interpret the overall molecular conformation of the polyanion.

Two tendencies have been sequentially found between the O···O contacts and the molecular conformation. One is that the steric instability due to the more shortened contacts between one pair of O atoms retains the ϕ close to an ideal SA coordination (ϕ = 45º). Another is that the small ϕ, which are severely deviated from the ϕ = 45º, keeps three contacts of O atoms nearly equal so that the steric repulsion looming over the terminal O atoms is delocalized. Which ways the polyanion is stabilized by is determined, depending on the interaction of cation and co-existing material to the polaynion.

In the case of pure alkylammonium salts of $[M(\alpha\text{-}PW_{11}O_{39})_2]^{n-}$ ($[Me_2NH_2]_{11}[Ce^{III}(\alpha\text{-}PW_{11}O_{39})_2]\cdot 14H_2O$ and $[Me_2NH_2]_{10}[Ce^{IV}(\alpha\text{-}PW_{11}O_{39})_2]\cdot 14H_2O$ in Chapter 2 and related compounds in the literature) and racemate K^+ salts of $[M(\alpha_2\text{-}P_2W_{17}O_{61})_2]^{n-}$ ($K_{16}H[Yb(\alpha_2\text{-}P_2W_{17}O_{61})_2]\cdot 44H_2O$, $K_{17}[Lu(\alpha_2\text{-}P_2W_{17}O_{61})_2]$, $K_{16}[Hf(\alpha_2\text{-}P_2W_{17}O_{61})_2]\cdot 19H_2O$, and $K_{15}H[Zr(\alpha_2\text{-}P_2W_{17}O_{61})_2]\cdot 25H_2O$), the distance between one pair of O atoms becomes much shorter than those of the other contacts, giving the ϕ close to an ideal SA coordination. On the other hand, for the TMA^+/Na^+-mixed salts ($[Me_4N]_{5.5}Na_5H_{0.5}[Ln(\alpha\text{-}PW_{11}O_{39})_2]\cdot xH_2O$, and $[Me_4N]_{5.5}Na_3H_{2.5}[Ln(\alpha\text{-}PW_{11}O_{39})_2]\cdot xH_2O$) and the chiral Na^+/K^+-mixed salts of $[M(\alpha\text{-}PW_{11}O_{39})_2]^{n-}$ ($K_{1.3}Na_{3.2}H_{6.5}[Ln(\alpha\text{-}PW_{11}O_{39})_2]\cdot 8.3(C_5H_9NO_2)\cdot xH_2O$, and $K_{1.2}Na_2H_{7.8}[Ln(\alpha\text{-}PW_{11}O_{39})_2]\cdot 8.5(C_5H_9NO_2)\cdot xH_2O$) and chiral K^+ salts of $[M(\alpha_2\text{-}P_2W_{17}O_{61})_2]^{n-}$ ($K_{12}H_5[Ln(\alpha_2\text{-}P_2W_{17}O_{61})_2]\cdot 2(C_5H_9NO_2)\cdot xH_2O$), their ϕs left from an ideal SA coordination, which are much smaller than those of the pure alkylammonium salts of $[M(\alpha\text{-}PW_{11}O_{39})_2]^{n-}$ and racemate K^+ salts of $[M(\alpha_2\text{-}P_2W_{17}O_{61})_2]^{n-}$, and they hold the three O atoms contact to be nearly equal. However, from the results of single crystal X-ray diffraction analysis, the molecular conformation of their salts' polyanion is supported by intramolecular Na^+ bridging across the two $[\alpha\text{-}PW_{11}O_{39}]^{7-}$ units and the hydrogen bonded interaction from proline to the polyanion, respectively.

7-3 Scope of the future studies on $[Ln(\alpha\text{-}XM_{11}O_{39})_2]^{n-}$ and $[Ln(\alpha_2\text{-}X_2M_{17}O_{61})_2]^{n-}$

In this study, based on the effects of ionic radius, cationic environment, and co-existing materials on the sandwich-type Ln-containing polyoxotungstates

$[Ln(\alpha\text{-}XM_{11}O_{39})_2]^{n-}$ and $[Ln(\alpha_2\text{-}X_2M_{17}O_{61})_2]^{n-}$, to regulate the molecular conformation and to induce the chirality for the polyanion were tackled. When the contents for Chapters 2, 3, 4, and 5 are extracted into the chemical phenomenon, they are named to be spontaneous resolution, transformation of coordination geometry, and enantioselective synthesis, respectively.

In Chapter 2, the first example of spontaneous resolution was achieved for sandwich-type Ln-containing polyoxotungstate. However, the main cause for the spontaneous resolution was not identified. This phenomenon is sometimes turned up based on the past studies and experience, but cannot be helped saying an accidental case, because definitive reason why the spontaneous resolution occurs is not fundamentally cleared. In the case of sandwich-type $[Ln(\alpha\text{-}XM_{11}O_{39})_2]^{n-}$, it is expected that further variations of the kind of hetero atom, valence of Ln, and the charge of the polyanion in combination with the choice of countercation would provide more information on how the spontaneous resolution occurs. The isolated crystalline solids from spontaneous resolution are enantiopure in each of single crystals, but are still racemic mixture in overall product. Therefore, it is probably difficult to obtain enantiopure compounds for application into functional materials.

For transformation of coordination geometry, cubic coordination species were successfully isolated for La and Ce, while SA coordination was achieved for the heavier Ln from Pr. It seems that SA coordination is caused by the anisotropic potential by Na^+ accidentally incorporated to the crystals despite the same synthesis method. In this study, it is presumed that attachment of alkaline metals such as Na, K, and Cs to polyanions seems to induce the SA coordination. To prove this, cubic coordination species in heavier Ln region should be demonstrated in Na-free compounds isostructural with La

and Ce analogues. When the $[PW_{11}O_{39}]^{7-}$ unit is led from $H_3[PW_{12}O_{40}]\cdot nH_2O$, it would be possible to extend the cubic coordination species from Pr to mid-lanthanide such as Eu. This attempt is in progress. If this is achieved, the expectation in aqueous solutions by Fedotov and Francesconi is realized in solid states [1, 2]. Furthermore, the resulting Pr, Nd, and Eu-centered polyanions will provide specific magnetism or luminescence characterized by cubic coordination.

For enantioselective synthesis, enantiopure crystals of $[Ln(\alpha\text{-}PW_{11}O_{39})_2]^{11-}$ were isolated by utilizing a proline molecule as chiral inducer, so it is probably concluded that enantioselective synthesis was achieved. However, from the results of ^{31}P-NMR spectroscopy and CD spectroscopy, since the racemization equilibrium between L-form and D-form is delivered, which is caused through 'on-site' rotation of $[\alpha\text{-}PW_{11}O_{39}]^{7-}$ or dissociation of the polyanion, at least, it is likely that enantiopure crystals are obtained from the synthetic solution containing a unique enantiomer. Thus, if the position of the two $[\alpha\text{-}PW_{11}O_{39}]^{7-}$ units can be retained in $[Ln(\alpha\text{-}PW_{11}O_{39})_2]^{11-}$, i.e. the polyanions' chirality with ϕ = ~ -45º or +45º (L-form or D-form) is fixed in aqueous solutions, more idealized enantioselective synthesis of $[Ln(\alpha\text{-}PW_{11}O_{39})_2]^{11-}$ will be completed. This requires new synthetic strategy; for example, linkage of the two $[\alpha\text{-}PW_{11}O_{39}]^{7-}$ units by organic chains, and inhibition of the mutual rotation of $[\alpha\text{-}PW_{11}O_{39}]^{7-}$ units under magnetic or electric field.

Chiral sandwich-type Ln-containing polyoxotungstates are possible to be used in a various kinds of applications. For example, polyoxometalates are originally anions, so it is possible to use for asymmetric catalysis in organic synthesis related to carbocation reaction. Although a large number of reports about potent polyoxometalate to realize inorganic medicine have been already delivered, the studies using chiral

polyoxometalate have never been carried out. Additionally, chiral magnetic $[Ln(\alpha\text{-}PW_{11}O_{39})_2]^{11-}$ with Ln = Pr or Nd or Er, might be available for optical isolator, signal branching filter, super high density magnetic optical recorder, which may support our IT industry in future. Also, as well as the CD activities, circular polarized luminescent (CPL) activities of the $[Ln(\alpha\text{-}PW_{11}O_{39})_2]^{11-}$ and $[Ln(\alpha_2\text{-}P_2W_{17}O_{61})_2]^{17-}$ with Ln = Sm, Eu, Tb, Dy in the enantiopure compounds are also expected. This CPL technique is usable for molecular optical memory, in which information is stored as a sequential array of molecules with opposite chirality. The $[Ln(\alpha\text{-}PW_{11}O_{39})_2]^{11-}$ polyanion with the flexible coordination of Ln centers may be suitable material for this purpose.

I hope that knowledge obtained in this thesis would provide useful information on the progress of fundamental and application researches of not only $[Ln(\alpha\text{-}XM_{11}O_{39})_2]^{n-}$ and $[Ln(\alpha_2\text{-}X_2M_{17}O_{61})_2]^{n-}$ polyanions but also the other Ln-containing POMs.

7-4 References

[1] R. D. Peacock, T. J. R. Weakley, *J. Chem. Soc.*, **A**, 1836 (1971).

[2] M. A. Fedotov, B. Z. Pertsikov, D. K. Danovich, *Polyhedron*, **9**, 1249 (1990).

[3] J. Bartis, S. Sukal, M. Dankova, E. Kraft, R. Kronzon, M. Blumenstein, L. C. Francesconi, *J. Chem. Soc., Dalton Trans.*, 1937 (1997).

[4] Y. Hou, X. Fang, C.L. Hill, *Chem. Eur. J.*, **13**, 9442 (2007).

[5] L. Cai, Y. Li, C. Yu, H. Ji, Y. Liu, S. Liu, *Inorg. Chim. Acta,* **362**, 2895 (2009).

[6] A. Müller, F. Perters, M. T. Pope, D. Gatteschi, *Chem. Rev.,* 239 (1998).

Acknowledgment

The author wishes to express his deepest appreciation to Associate Professor Haruo Naruke for his expert guidance and constant warm encouragement during the course of this study. He is also grateful to Associate Professor Eri Ishikawa at Chubu University for measuring the reflection data of single crystal X-ray diffraction. He would also like to say thanks to Associate Professor Takanobu Sanji for measuring the CD spectra and his cooperation. He is thankful to Assistant Professor Takeru Itoh at Tokai University and Dr. Keisuke Fukaya at the University of Tokyo for their helpful advices. He is also grad to get a lot of help and advices from everyone belonging to Naruke laboratory. Finally I would like to express my thanks to my parents and friends. This thesis is devoted to them.

July, 2011

Jun Iijima

List of Publications

(The related papers)

1. Synthesis and structural investigation of sandwich polyoxotungstates containing cerium (III/IV) and mono-lacunary Keggin tungstophosphate.

   Inorg. Chim. Acta, **363**, 1500-1506 (2010).

   J. Iijima, E, Ishikawa, Y. Nakamura, H. Naruke.

2. Structures of square-antiprismatic and cubic coordination of Ln^{3+} in sandwich-type $[Ln(\alpha\text{-}PW_{11}O_{39})_2]^{11-}$ anions conducted by cationic environment.

   Inorg. Chim. Acta, submitted.

   J. Iijima, H. Naruke

3. Enantioselective resolutions and circular dichroism studies of lanthanide-containing Keggin-type $[Ln(PW_{11}O_{39})_2]^{11-}$ polyoxometalates.

   Inorg. Chem., **50**, 7535-7539 (2011).

   H. Naruke, J. Iijima, T. Sanji

4. Synthesis and crystal structure of sandwich-type polyoxotungstate containing cerium (IV) and mono-lacunary Wells-Dawson tungstophosphate.

   In preparation.

   J. Iijima, H. Naruke

5. Isolation of the enantiopure crystals of $[Ln(\alpha_2\text{-}P_2W_{17}O_{61})_2]^{17-}$ (Ln = La, Sm, Eu, Gd, Tb, Dy, Er, and Yb) containing amino acid proline.

   In preparation.

   J. Iijima, H. Naruke

(Miscellaneous)

1. Hybrid inorganic-organic crystals composed of octamolybdate isomers and pyridinium surfactant.

   Chem. lett., **39(12)**, 1323-1325 (2010).

   T. Itoh, K. Mikurube, Y. Abe, T. Koroki, M. Saito, J. Iijima, H. Naruke, T. Ozeki.